12-2020

A high resolution study of long-term vertebrate decomposition in human and animal model systems

Lois S. Taylor

To the Graduate Council:

I am submitting herewith a dissertation written by Lois S. Taylor entitled "A high resolution study of long-term vertebrate decomposition in human and animal model systems." I have examined the final electronic copy of this dissertation for form and content and recommend that it be accepted in partial fulfillment of the requirements for the degree of Doctor of Philosophy, with a major in Plant, Soil and Environmental Sciences.

Jennifer DeBruyn, Major Professor

We have read this dissertation and recommend its acceptance:

Michael Essington, Ernest C. Bernard, Dawnie Steadman

Accepted for the Council:

Dixie L. Thompson

Vice Provost and Dean of the Graduate School

(Original signatures are on file with official student records.)

A high-resolution study of long-term vertebrate decomposition in human and animal model systems

A Dissertation Presented for the

Doctor of Philosophy

Degree

The University of Tennessee, Knoxville

Lois Stacy Taylor

December 2020

This resource was prepared by the author(s) using Federal funds provided by the U.S. Department of Justice. Opinions or points of view expressed are those of the author(s) and do not necessarily reflect the official position or policies of the U.S. Department of Justice.

Acknowledgments

I would like to thank my advisor and mentor, Dr. Jennifer DeBruyn, and my committee members, Dr. Ernest Bernard, Dr. Michael Essington, and Dr. Dawnie Steadman, for their invaluable guidance and contributions to this project. Thank you for your time, enthusiasm, and hours of assistance!

I am indebted to the members of our lab and the Bernard lab, past and present: Dr. Sarah Keenan, Dr. Sreejata Bandopadhyay, Kelsey Henderson, Allison Mason, Mallari Starrett, Victoria Beard, Morgan White, Dr. Gary Phillips, and Dr. Satyendra Pothula, for advice, assistance, friendship, support, and the baked goods necessary to make this journey possible. Thank you so much—I couldn't have done it without you!

A special thank you to Rachel Ford and Mark Tucker, dear friends who have made this possible. And last but by no means least, thank you to my father, Dr. Houston Taylor, and my husband, Sean Claire, who have actively encouraged and supported me every step of the way!

Chapter 1: Acknowledgments are listed in the text as published.

Chapter 2: We would like to thank the Oak Ridge Arboretum for providing space and facilities used in this study. We would also like to thank the USDA wildlife services of East Tennessee for providing subject materials. Sarah W. Keenan assisted with site setup, and Satyendra Pothula assisted with sample collection. Chauncey Whitlock provided assistance with nematode extraction.

Chapter 3: We would like to thank the University of Tennessee Anthropology Research Facility, Dr. Dawnie Steadman, and Mary Davis for providing space in the facility for this project, as well as site setup assistance. Allison Mason, Mallari Starrett, and Victoria Beard for site setup, sample collection, and sample processing assistance.

We would like to thank the donors and their families for their very generous gifts to the Forensic Anthropology Center donation program.

Financial support: funding for the materials in Chapter 3 were provided by a National Institute of Justice Graduate Research Fellowship in Science, Technology, Engineering, and Mathematics (GRF-STEM) Award number 2017-R2-CX-0008.

Abstract

The effects of vertebrate decomposition are wide-ranging across multiple foodwebs, and have been shown to persist in the environment, however there is a lack of systematic assessment of these changes over long periods of time or in sufficiently high resolution as to resolve seasonal flux patterns. The ultimate aim of this body of research was to explore nematode systematics in decomposition environments, culminating in a pair of long-term human decomposition seasonal trials, in high resolution, with the specific intent of integrating the fields of soil chemistry, microbial ecology, and nematology in order to assess the relationships of cross-disciplinary impacts. Of these three fields, soil chemistry has the largest body of literature dedicated to its study. Microbial ecology, for forensic purposes, is still an emerging field, and primarily focuses on bacterial successional characteristics in the early phases of decomposition. Nematology as a forensic tool has had very little study dedicated to it, however initial results are promising. Therefore, prior to performing a fully integrated study, further examination of nematode community systematics was required in order to ascertain the nature of their responses to the decomposition environment. Our body of work consisted of three objectives: (1) evaluation of nematode communities in a multi-individual grave, (2) evaluation of longitudinal patterns in nematode diversity in an animal model system, and (3) evaluation of seasonal differences in decomposition patterns across the disciplines of soil chemistry, microbial ecology, and nematology, in high resolution and long-term. Overall, nematode communities were shown to exhibit persistent modification after four years in a grave, and successional patterns in a vertebrate surface-decomposition model system. The human seasonal study demonstrated that soil chemistry and fungal beta diversity were inextricably interlinked, as were nematode abundances and thermal effects, and that seasonal rates of change in decomposition progression

are mirrored across all three disciplines. This suite of simultaneous changes is sufficiently compelling for us to recommend that it is absolutely crucial to broaden decomposition soil research into an interdisciplinary study in order to fully and accurately contextualize these processes in future work.

Table of Contents

List of Tables

List of Figures

Introduction

The terrestrial decomposition of vertebrate remains is a dynamic process, and is dependent upon an array of environmental variables; to date, most forensically focused decomposition studies have been driven by an attempt to quantify those factors that affect estimates of the post-mortem interval (PMI) [1]. The environmental and ecological effects of vertebrate decomposition, particularly those involving human subjects, are challenging to study *in situ*. Very few human decomposition facilities exist, and fewer still are equipped to study this process in high volume due to myriad complexities involving human donor acquisition, and the necessities of mutually satisfying experimental design criteria with facility spatial constraints (but see: [1-13]). Human decomposition facilities have two limiting factors that often control experimental design: physical space within the facility, and availability of the deceased human subjects (donors). Since these facilities are reliant upon volunteer donations, there is no control over age, sex, size, body composition, medical history, pharmaceutical history, or trauma. Individual facilities vary as to how many donors they may accept per year, and what types of storage are available for those donors upon acquisition.

As a result, the forensically-focused literature using human subjects is composed of an assortment of study frameworks that attempt to balance the trade-offs associated between achieving robust replication with acquiring environmentally meaningful data. For example, case studies fall on the extreme end of low replication but often provide a broad and meticulous characterization of the local environment and ecosystem [9, 10, 14-16]. Case studies have been used to detail a variety of parameters associated with graves and remains, including: vertical and lateral profiles of soil biogeochemistry [9, 10, 16], soil enzymes [9], microbial and microfaunal communities [9, 16], fatty acids [14], steroids [15], and cholesterol [10]. However, these types of studies typically only characterize conditions at single time points unless the site can be visited

later, and in the instance of ongoing forensic investigations this may not be possible. Overall, case studies are of considerable value for hypothesis generation, however, they are limited in empirical robustness and predictive scope, requiring comparison with other longitudinal or cross-sectional supporting studies in order for their data to be appropriately contextualized. These supporting cross-sectional and longitudinal studies are, in turn, limited in their potential empirical and predictive utility by choice of experiment design parameters, which include such elements as: temporal resolution, replication, and lack of inclusion of supplementary data (e.g. soil chemistry data to accompany microbial data, or environmental data to accompany soil chemistry or microbial data, etc.).

Another experimental design, not commonly used, employs simultaneously-placed replicates in an effort to ensure similar environmental characteristics throughout the course of the study [11, 17-19]. This usually requires some manner of donor storage and preservation (often freezing) prior to their placement in the field, which then may influence decomposition progression patterns at the beginning of the study as temperatures equilibrate. Other experimental designs call for higher numbers of donors, placed in the field as they are acquired, thus eliminating the need for donor storage [2, 3, 5, 6, 8, 12, 13]. However, this does not assess data resolution stemming from seasonal variability, which is known to influence decomposition progression [17, 18]. Donors in this type of study design may constitute individual replicates unless they are binned in some manner (e.g. by decomposition stage or by accumulated degree days/hours (ADD/ADH), etc.), thus creating potentially complex statistical evaluation. In contrast to the longitudinal frameworks described above, one of the more unique experimental designs involves a one-time sampling across a large number of donors that have been deployed in the field at disparate times, ranging from months to years apart [7, 20]. This compilation of

individual donor results is then used to construct a chronosequence of decomposition progression. While this compiled approach certainly overcomes the problems associated with low replication, it suppresses environmental or seasonal variability while simultaneously amplifying individual donor variability when presenting data trends. Alternatively, experiments using animal models have been designed to address both the issues of statistical power and similarity of replicates; these have used pigs [17, 18, 20-35], rabbits [17, 18, 36], mice [11, 37], kangaroos [38, 39], beavers [40], and occasional other vertebrates as subjects [41-43]. However, in the case of rabbits and pigs, it has been shown that their decomposition patterns vary from those of humans, thus there is some question as to the scope of their utility as human analogs [17, 18, 20, 31].

Decomposition soil studies, both human and animal, can be divided into two areas: those dedicated to the study of buried remains [9, 33, 34, 44-53] or surface-decomposed remains [2, 3, 6, 7, 10-16, 21-23, 26-30, 32, 36-38, 40, 41, 53-55]. Throughout the surface-decomposition literature the temporal spectrum of decomposition progression has been surveyed to varying degrees. However, most high-resolution studies have focused on the very early period of decomposition through active decay when the majority of mass has been lost and decomposition progression begins to slow [3, 5, 8, 11, 19, 22, 23, 27, 28]. As a result, very little is known about progressively later time periods associated with decomposition progression except in a general sense; data accompanying those time periods is sparse, often with the implicit assumption that with the absence of visibly decaying mass very little is occurring elsewhere. Exacerbating this issue, the two primary fields of inquiry into decomposition processes in the soil, those of soil chemistry and microbial ecology, have largely evolved separately. There has been minor

experimental intersection between the two, however given that the chemical environment is a strong driver of microbial function, absence of this overlap is notable [44, 56, 57].

Research in soil chemistry generally focuses on temporal [3, 11, 13, 23, 26, 28, 29, 38, 40, 46, 49, 55] and spatial [10, 29, 40] exploration of gravesoil biogeochemistry and nutrient cycling, and has characterized both short-term and long-term decomposition impaction over a wide range of chemical parameters, however with markedly varying degrees both in sampling resolution and choice of parameters explored. Decompostion processes create a biogeochemical hotspot [40], sometime termed a cadaver decompostion island [1], resulting from decomposition-derived fluids and other materials moving into the soil beneath decomposing remains; these hotspots extend some distance from decomposing remains and are chemically active, exhibiting changes in soil pH [2, 7, 13, 26-30, 36, 38-41], electrical conductivity [2, 7, 36, 38-40], organic and inorganic C and N pools [2, 3, 7, 13, 26-28, 30, 36, 38, 40, 41], as well as exhibiting briefly reduced soil oxygen levels and elevated respiration rates [3, 12, 40]. However, while it is generally acknowledged that these parameters change, the magnitude and patterns associated with these changes, and the specific timing of their responses during decomposition is not well-described. Furthermore, recent study arising from several fields has independently documented evidence of seasonal effects on decomposition patterns, notably caused by warmer or cooler weather, and thus by extension, with or without the presence of insects [11, 17, 23, 25, 27, 29, 35, 42]. While this body of work provides a general sense of mammalian decomposition biogeochemistry, little work has been focused on a systematic, long-term, and high-resolution exploration of these environmental impacts, and less still for human decomposition specifically.

Fungi have often been reported associated with gravesoils, however their specific relationships with decomposition-derived soil inputs stemming from vertebrate sources is

unknown. Soil fungi are primarily saprobes involved with the degradation of plant residues, having enzymes that degrade lignin, cellulose, and hemicellulose [58]. In contrast, vertebrate tissues are constructed primarily of proteins and fats, have a lower C:N ratio, and thus their decomposition has differing requirements, resulting in large deposits of nitrogen-rich organic compounds into the soil [1, 44]. Previous work focusing on fungi associated with gravesoil has concentrated on taxa that fruit when exposed to nitrogen [59-62]. These fungi have been shown to fruit in two groupings: “early stage” fungi, deuteromycetes, ascomycetes, and basidiomycetes that fruit generally within ten months of nitrogen deposition, and are associated with ammonia but not nitrate; and “late stage” fungi that typically fruit after a year or more and that are associated with both ammonium and nitrate [59-62]. It has been suggested that fungal successional patterns within these nitrogen-based classifications might have utility for forensic science, however, discrepancies over specific taxon associations with decomposing remains in conjunction with ecosystem differences has complicated this as a practical pursuit, and research into potential application as a forensic tool had not flourished prior to the development of culture-independent (molecular) techniques for assessing microbial community composition [59-63]. To date, the probing of decomposition-induced microbial community changes via molecular techniques has been heavily focused on evaluating bacterial communities via 16S rRNA amplicon sequencing [3, 5, 8, 11, 12, 24, 25, 33, 37, 53, 64]. Far fewer studies have probed eukaryotic successional patterns via 18S rRNA, [11, 22, 23, 37], however, there is a growing body of work specifically focused on fungal communities [11, 32, 34, 43, 64]. This body of fungal literature has explored changes in soil underneath pigs [32, 34], mice [11] humans [11, 64], and bison and elk [43] however amplicon-based sequencing exploration of human decomposition is extremely limited [11]. The human fungal microbiome is well described for

living subjects [65, 66], however, data from human decomposition studies differs from these results. For example, *Malassezia* is a mammalian (including human) commensal yeast that consumes lipids from skin secretions. Theoretically, tracking *Malassezia* in the soil would be possible, however, this organism has only been identified in one ITS non-human mammalian decomposition survey to date [32]. Currently a significant knowledge gap exists in characterizing the responses of fungi in soil to vertebrate-derived decomposition products; fungal successional patterns associated with observed changes in soil nitrogen pools, in conjunction with tracking of human commensals introduced into the soil, may prove uniquely useful as a manner of establishing decomposition progression.

While existing research has begun evaluating microbial community succession and diversity occurring in soil during decomposition, only nominal attention has been allocated to eukaryotic members of the soil decomposer food web. Nematodes are central members of the microfaunal soil food web, and of their five most important trophic groups, bacterial feeders and fungal feeders serve as channel indicators of nutrient availability and flow. It is estimated that nematodes constitute 80% of all multicellular organisms on earth [67]. Free-living nematodes are diverse members of the soil food web, and exhibit r/K selection behavior. Yeates et al. (1993) devised a system whereby nematodes could be classified by feeding habits into a series of trophic guilds [68]. Further refinements to this system occurred by dividing r/K strategists into discrete colonizer and persister groups based upon resource utilization, and subsequently led to the creation of a series of structural and enrichment indices unique to nematology that function not only as a characterization of taxa but of their habitat as well [69-71]. In practice, as resource availability changes, nematode communities undergo successional shifts whereby enrichment opportunists quickly yield to general opportunists, and ultimately resource cascading effects

create opportunities for omnivorous and predaceous genera in higher trophic levels [67, 69, 70]. Further, it has been shown in agricultural systems that trophic groups produce varying responses to nitrogen loading: ammonium concentration has been negatively correlated with overall abundance and diversity as well as displaying suppressive effects upon plant-parasitic taxa, while on the other hand ammonium concentration has been shown to momentarily stimulate responses of bacterial feeders, presumably in response to increased bacterial activity [72]. From a community ecology perspective, nematode resource requirements have been described for agricultural and forest systems and while successional and diversity patterns are broadly recognized [73, 74] these qualities have not been fully harnessed for use in characterizing the nature and progression of vertebrate/human decomposition events which constitute much higher quality resources and present far lower C:N ratios [75]. Nematodes have been reported in vertebrate decomposition sites as members of the soil community as well as arriving via phoretic transfer by other insects [16, 21-23, 37, 69]. However, they are not traditionally considered as part of the decomposition insect succession, and they have received little direct study during decomposition [16, 21], therefore there is the possibility for highly specific contributions from this sector of the eukaryotic decomposer community. Population densities of nematodes in soils can vary from 1-50 million per square meter, and they can be readily identified to genus level, and often species, by microscope. Populations are directly representative of bacterial and fungal availability [76], and enrichment opportunists (cp-1 taxa, Rhabditidae in particular) will accumulate quickly and in great number when bacterial populations increase [69, 77]. This is consistent with observations from decomposition studies during the soft tissue mass-loss time period, where it was initially found that approximately three families (Rhabditidae, Neodiplogasteridae and Diplogasteridae) tended to dominate the soil environment [11, 21].

Taken together, early evidence of nematode activity is highly suggestive that their community changes in response to altered chemical environments and food supply could function as an indicator of decomposition progress.

While the majority of studies focused on decomposition soil hotspots originates from the disciplines of soil chemistry and microbial ecology, these disciplines seldom overlap, and nematology as a potential forensic tool is not yet sufficiently developed for comparisons with other fields. The overarching goal of this body of research is to integrate these three currently diverse areas of study in decomposition (soil chemistry, fungal microbial ecology, and nematode ecology); this integrated approach would then be used to characterize long-term human decomposition progression with fine temporal resolution in order to address knowledge gaps in temporal resolution and environmental persistence, as well as to cross-examine the effects of impacts derived from different disciplines on each other. To accomplish this research project, preliminary data regarding nematode successional patterns during decomposition was required to ensure that a working knowledge of their response was commensurate with what is currently known in the areas of soil chemistry and microbial ecology. To this end, a series of three experiments were performed. The first of these (Chapter 1) was designed to evaluate what nematode taxa were present in a grave (human) after 4 years, and how these communities compared with those of controls. The second of these experiments (Chapter 2) consisted of an animal model decomposition designed to track nematode community successional patterns from carcass placement through skeletonization (one year). The first two experiments served to create a more robust body of knowledge regarding nematode community response in decomposition environments, as well as to explore and refine elements of the experimental design of a human decomposition study (Chapter 3). This human study was designed to characterize the progression

of decomposition impacts in soil at high resolution for the period of one year, encompassing two different seasonal trials (spring and winter). This characterization was to consist of a fully integrated approach, reporting simultaneous changes in environmental conditions, soil chemistry, microbial ecology (fungal, in this case), and nematode community assemblages. A brief explanation of each chapter follows.

Chapter 1: Spatial impacts of a multi-individual grave on microbial and microfaunal communities and soil biogeochemistry

The goals of this study were to evaluate nematode communities along a vertical gradient within a grave, as well as along laterally radiating transects in order to determine both degree and spread of disturbance. Nematode communities were characterized vertically within, and horizontally radiating away from a multi-individual grave. Three human donors were interred, comingling, in a grave and allowed to remain for a period of four years. Upon disinterment, sampling was performed at depths of 0-5 cm, 30-35 cm (burial depth), 70-75 cm, 80-85 cm, and included an additional sample of decomposing material from within a ribcage at a depth of 40 cm. Transects radiating away from the grave were sampled at depths of 0-5 cm and 30-35 cm. In total, a full suite of soil chemical analyses was performed, bacterial and fungal abundances (including human-associated *Bacteroides*) were assayed via qPCR, and nematode assemblages were characterized. My portion of this study was restricted to nematode ecology. Nematode communities were found to differ significantly between grave soils and controls, and two taxa of interest emerged based upon their abundances in impacted soil: the fungal-feeder *Filenchus*, and the bacterial-feeder *Plectus*. *Filenchus*, common in control soils, exhibited unusually low abundances in grave soils, and *Plectus*, which typically demonstrates only moderate abundances in controls, was enriched in grave soils.

Chapter 2: Soil nematode functional diversity, successional patterns, and indicator taxa associated with vertebrate decomposition hotspots

The goal of this study was to describe nematode successional patterns throughout a long-term vertebrate decomposition experiment at fine taxonomic resolution, and to identify taxa that could be used as indicators to assess decomposition progression. Nematode communities were characterized in two soil depths (0-1 cm) and (0-30 cm) underneath six decomposing beaver carcasses for the period of a year. Environmental sensors were deployed to record soil moisture, conductivity, and temperature, and well as internal carcass and ambient temperatures. The successional patterns of nematodes were described for both soil depths. Abundances and alpha diversity were shown to have largely recovered after one year, however beta and functional diversity remained altered at the end of the study. Four unique decomposition-induced response patterns were described for nematodes: B1 bacterial-feeder enrichment during active and advanced decay, general suppression, general enrichment (non-B1 related), and early suppression during active decay followed by enrichment during skeletonization. From these groupings, criteria for indicator taxa were determined based upon enrichment response patterns, and eight taxa were proposed as possible indicators for tracking decomposition progression.

Chapter 3: Soil fungal and nematode community changes as a methodology for determining long-term postmortem interval after cadaver mass loss

In this human decomposition study, our goals were to describe long-term human decomposition in high resolution, fully integrating the disciplines of soil chemistry, microbial (fungal) ecology, and nematode ecology. The second of these goals was to examine the effects of seasonal differences in decomposition to characterize long-term decomposition progression. These changes were tracked over the course of two year-long seasonal studies (spring and winter) of

human donors and at high resolution throughout each year-long study. A total of six human donors were allowed to decompose, three in the spring, and three in the winter for a full year. A suite of soil chemical parameters (pH, conductivity, dissolved oxygen, respiration rates, ammonium, and nitrate) and environmental parameters (soil moisture, conductivity, as well as temperature measurements for the soil, ambient air, and donors) were measured. DNA sequencing was performed using the ITS2 region to assess fungal successional patterns in the soil. Nematode community successional patterns and diversity were determined. Soil chemistry, fungal ecology, and nematode ecology were shown to be interlinked across all parameters measured, and to vary seasonally. Larval thermogenesis effects were shown to partially drive seasonal effects.

References

1. Carter DO, Yellowlees D, Tibbett M. Cadaver decomposition in terrestrial ecosystems. Naturwissenschaften. 2007;94(1):12-24. doi: 10.1007/s00114-006-0159-1.

2. Aitkenhead-Peterson JA, Owings CG, Alexander MB, Larison N, Bytheway JA. Mapping the lateral extent of human cadaver decomposition with soil chemistry. Forensic Science International. 2012;216(1-3):127-34. doi: 10.1016/j.forsciint.2011.09.007.

3. Cobaugh KL, Schaeffer SM, DeBruyn JM. Functional and Structural Succession of Soil Microbial Communities below Decomposing Human Cadavers. Plos One. 2015;10(6):20. doi: 10.1371/journal.pone.0130201.

4. Damann FE, Tanittaisong A, Carter DO. Potential carcass enrichment of the University of Tennessee Anthropology Research Facility: A baseline survey of edaphic features. Forensic Science International. 2012;222(1-3):4-10. doi: 10.1016/j.forsciint.2012.04.028.

5. DeBruyn JM, Hauther KA. Postmortem succession of gut microbial communities in deceased human subjects. PeerJ. 2017;5:14. doi: 10.7717/peerj.3437.

6. Emmons AL, DeBruyn JM, Mundorff AZ, Cobaugh KL, Cabana GS. The persistence of human DNA in soil following surface decomposition. Science & Justice. 2017;57(5):341-8. doi: 10.1016/j.scijus.2017.05.002.

7. Fancher JP, Aitkenhead-Peterson JA, Farris T, Mix K, Schwab AP, Wescott DJ, et al. An evaluation of soil chemistry in human cadaver decomposition islands: Potential for estimating postmortem interval (PMI). Forensic Science International. 2017;279:130-9. doi: 10.1016/j.forsciint.2017.08.002.

8. Hauther KA, Cobaugh KL, Jantz LM, Sparer TE, DeBruyn JM. Estimating Time Since Death from Postmortem Human Gut Microbial Communities. Journal of Forensic Sciences.

2015;60(5):1234-40. doi: 10.1111/1556-4029.12828.

9. Keenan SW, Emmons AL, Taylor LS, Phillips G, Mason AR, Mundorff AZ, et al. Spatial impacts of a multi-individual grave on microbial and microfaunal communities and soil biogeochemistry. PloS one. 2018;13(12):e0208845-e. doi: 10.1371/journal.pone.0208845.
10. Luong S, Forbes SL, Wallman JF, Roberts RG. Monitoring the extent of vertical and lateral movement of human decomposition products through sediment using cholesterol as a biomarker. Forensic Science International. 2018;285:93-104. doi: 10.1016/j.forsciint.2018.01.026.
11. Metcalf JL, Xu ZZ, Weiss S, Lax S, Van Treuren W, Hyde ER, et al. Microbial community assembly and metabolic function during mammalian corpse decomposition. Science. 2016;351(6269):158-62. doi: 10.1126/science.aad2646.
12. Singh B, Minick KJ, Strickland MS, Wickings KG, Crippen TL, Tarone AM, et al. Temporal and Spatial Impact of Human Cadaver Decomposition on Soil Bacterial and Arthropod Community Structure and Function. Frontiers in Microbiology. 2018;8:12. doi: 10.3389/fmicb.2017.02616.
13. Vass AA, Bass WM, Wolt JD, Foss JE, Ammons JT. Time since death determinations of human cadavers using soil solution. Journal of Forensic Sciences. 1992;37(5):1236-53.
14. Lühe B, Fiedler S, Mayes RW, Dawson L. Temporal fatty acid profiles of human decomposition fluid in soil. Organic Geochemistry. 2017;111:26-33. doi: 10.1016/j.orggeochem.2017.06.004.
15. Lühe B, Birk JJ, Dawson L, Mayes RW, Fiedler S. Steroid fingerprints: Efficient biomarkers of human decomposition fluids in soil. Organic Geochemistry. 2018;124:228-37. doi: 10.1016/j.orggeochem.2018.07.016.

16. Szelecz I, Losch S, Seppey CVW, Lara E, Singer D, Sorge F, et al. Comparative analysis of bones, mites, soil chemistry, nematodes and soil micro-eukaryotes from a suspected homicide to estimate the post-mortem interval. Scientific reports. 2018;8(1):25-. doi: 10.1038/s41598-017-18179-z.
17. Dautartas A, Kenyhercz MW, Vidoli GM, Meadows Jantz L, Mundorff A, Steadman DW. Differential Decomposition Among Pig, Rabbit, and Human Remains. Journal of forensic sciences. 2018. doi: 10.1111/1556-4029.13784.
18. Steadman DW, Dautartas A, Kenyhercz MW, Jantz LM, Mundorff A, Vidoli GM. Differential Scavenging Among Pig, Rabbit, and Human Subjects. Journal of forensic sciences. 2018. doi: 10.1111/1556-4029.13786.
19. Hyde ER, Haarmann DP, Petrosino JF, Lynne AM, Bucheli SR. Initial insights into bacterial succession during human decomposition. International Journal of Legal Medicine. 2015;129(3):661-71. doi: 10.1007/s00414-014-1128-4.
20. Barton PS, Reboldi A, Dawson BM, Ueland M, Strong C, Wallman JF. Soil chemical markers distinguishing human and pig decomposition islands: a preliminary study. Forensic science, medicine, and pathology. 2020. doi: 10.1007/s12024-020-00297-2.
21. Szelecz I, Sorge F, Seppey CVW, Mulot M, Steel H, Neilson R, et al. Effects of decomposing cadavers on soil nematode communities over a one-year period. Soil Biology & Biochemistry. 2016;103:405-16. doi: 10.1016/j.soilbio.2016.09.011.
22. Weiss S, Carter DO, Metcalf JL, Knight R. Carcass mass has little influence on the structure of gravesoil microbial communities. International Journal of Legal Medicine. 2016;130(1):253-63. doi: 10.1007/s00414-015-1206-2.
23. Carter DO, Metcalf JL, Bibat A, Knight R. Seasonal variation of postmortem microbial

communities. Forensic Science Medicine and Pathology. 2015;11(2):202-7. doi: 10.1007/s12024-015-9667-7.

24. Pechal JL, Crippen TL, Benbow ME, Tarone AM, Dowd S, Tomberlin JK. The potential use of bacterial community succession in forensics as described by high throughput metagenomic sequencing. International Journal of Legal Medicine. 2014;128(1):193-205. doi: 10.1007/s00414-013-0872-1.
25. Pechal JL, Crippen TL, Tarone AM, Lewis AJ, Tomberlin JK, Benbow ME. Microbial Community Functional Change during Vertebrate Carrion Decomposition. PLoS ONE. 2013;8(11):e79035. doi: 10.1371/journal.pone.0079035.
26. Szelecz I, Koenig I, Seppey CVW, Le Bayon R-C, Mitchell EAD. Soil chemistry changes beneath decomposing cadavers over a one-year period. Forensic Science International. 2018;286:155-65. doi: 10.1016/j.forsciint.2018.02.031.
27. Meyer J, Anderson B, Carter DO. Seasonal Variation of Carcass Decomposition and Gravesoil Chemistry in a Cold (Dfa) Climate. Journal of Forensic Sciences. 2013;58(5):1175-82. doi: 10.1111/1556-4029.12169.
28. Benninger LA, Carter DO, Forbes SL. The biochemical alteration of soil beneath a decomposing carcass. Forensic Science International. 2008;180(2-3):70-5. doi: 10.1016/j.forsciint.2008.07.001.
29. Perrault KA, Forbes SL. Elemental analysis of soil and vegetation surrounding decomposing human analogues. Canadian Society of Forensic Science Journal. 2016;49(3):138-51. doi: 10.1080/00085030.2016.1184840.
30. Anderson B, Meyer J, Carter DO. Dynamics of Ninhydrin-Reactive Nitrogen and pH in Gravesoil During the Extended Postmortem Interval. Journal of Forensic Sciences.

2013;58(5):1348-52. doi: 10.1111/1556-4029.12230.

31. Notter SJ, Stuart BH, Rowe R, Langlois N. The initial changes of fat deposits during the decomposition of human and pig remains. Journal of Forensic Sciences. 2009;54(1):195-201. doi: 10.1111/j.1556-4029.2008.00911.x.
32. Fu X, Guo J, Finkelbergs D, He J, Zha L, Guo Y, et al. Fungal succession during mammalian cadaver decomposition and potential forensic implications. Scientific Reports. 2019;9. doi: 10.1038/s41598-019-49361-0.
33. Procopio N, Ghignone S, Williams A, Chamberlain A, Mello A, Buckley M. Metabarcoding to investigate changes in soil microbial communities within forensic burial contexts. Forensic Science International-Genetics. 2019;39:73-85. doi: 10.1016/j.fsigen.2018.12.002.
34. Procopio N, Ghignone S, Voyron S, Chiapello M, Williams A, Chamberlain A, et al. Soil Fungal Communities Investigated by Metabarcoding Within Simulated Forensic Burial Contexts. Frontiers in Microbiology. 2020;11. doi: 10.3389/fmicb.2020.01686.
35. Breton H, Kirkwood AE, Carter DO, Forbes SL. The impact of carrion decomposition on the fatty acid methyl ester (FAME) profiles of soil microbial communities in southern Canada. Can Soc Forensic Sci J. 2016;49(1):1-18. doi: 10.1080/00085030.2015.1108036.
36. Quaggiotto MM, Evans MJ, Higgins A, Strong C, Barton PS. Dynamic soil nutrient and moisture changes under decomposing vertebrate carcasses. Biogeochemistry. 2019;146(1):71-82. doi: 10.1007/s10533-019-00611-3.
37. Metcalf JL, Parfrey LW, Gonzalez A, Lauber CL, Knights D, Ackermann G, et al. A microbial clock provides an accurate estimate of the postmortem interval in a mouse model system. Elife. 2013;2:19. doi: 10.7554/eLife.01104.
38. Macdonald BCT, Farrell M, Tuomi S, Barton PS, Cunningham SA, Manning AD. Carrion

decomposition causes large and lasting effects on soil amino acid and peptide flux. Soil Biology & Biochemistry. 2014;69:132-40. doi: 10.1016/j.soilbio.2013.10.042.

39. Barton PS, McIntyre S, Evans MJ, Bump JK, Cunningham SA, Manning AD. Substantial long-term effects of carcass addition on soil and plants in a grassy eucalypt woodland. Ecosphere. 2016;7(10). doi: 10.1002/ecs2.1537.
40. Keenan SW, Schaeffer SM, Jin VL, DeBruyn JM. Mortality hotspots: Nitrogen cycling in forest soils during vertebrate decomposition. Soil Biology & Biochemistry. 2018;121:165-76. doi: 10.1016/j.soilbio.2018.03.005.
41. Towne EG. Prairie vegetation and soil nutrient responses to ungulate carcasses. Oecologia. 2000;122(2):232-9. doi: 10.1007/pl00008851.
42. Parmenter RR, MacMahon JA. Carrion decomposition and nutrient cycling in a semiarid shrub-steppe ecosystem. Ecological Monographs. 2009;79(4):637-61. doi: 10.1890/08-0972.1.
43. Risch AC, Frossard A, Schuetz M, Frey B, Morris AW, Bump JK. Effects of elk and bison carcasses on soil microbial communities and ecosystem functions in Yellowstone, USA. Functional Ecology. 2020. doi: 10.1111/1365-2435.13611.
44. Dent BB, Forbes SL, Stuart BH. Review of human decomposition processes in soil. Environmental Geology. 2004;45(4):576-85. doi: 10.1007/s00254-003-0913-z.
45. Carter DO, Tibbett M. Microbial decomposition of skeletal muscle tissue (Ovis aries) in a sandy loam soil at different temperatures. Soil Biology & Biochemistry. 2006;38(5):1139-45. doi: 10.1016/j.soilbio.2005.09.014.
46. Stokes KL, Forbes SL, Tibbett M. Human Versus Animal: Contrasting Decomposition Dynamics of Mammalian Analogues in Experimental Taphonomy. Journal of Forensic

Sciences. 2013;58(3):583-91. doi: 10.1111/1556-4029.12115.

47. Wilson AS, Janaway RC, Holland AD, Dodson HI, Baran E, Pollard AM, et al. Modelling the buried human body environment in upland climes using three contrasting field sites. Forensic Science International. 2007;169(1):6-18. doi: 10.1016/j.forsciint.2006.07.023.
48. Carter DO, Yellowlees D, Tibbett M. Moisture can be the dominant environmental parameter governing cadaver decomposition in soil. Forensic Science International. 2010;200(1-3):60-6. doi: 10.1016/j.forsciint.2010.03.031.
49. Haslam TCF, Tibbett M. Soils of Contrasting pH Affect the Decomposition of Buried Mammalian (Ovis aries) Skeletal Muscle Tissue. Journal of Forensic Sciences. 2009;54(4):900-4. doi: 10.1111/j.1556-4029.2009.01070.x.
50. Hopkins DW, Wiltshire PEJ, Turner BD. Microbial characteristics of soils from graves: arm investigation at the interface of soil microbiology and forensic science. Applied Soil Ecology. 2000;14(3):283-8. doi: 10.1016/s0929-1393(00)00063-9.
51. Forbes SL. Decomposition chemistry in a burial environment. Soil Analysis in Forensic Taphonomy. 2008:203-23. doi: 10.1201/9781420069921.ch8.
52. Chimutsa M, Olakanye AO, Thompson TJU, Ralebitso-Senior TK. Soil fungal community shift evaluation as a potential cadaver decomposition indicator. Forensic Science International. 2015;257:155-9. doi: 10.1016/j.forsciint.2015.08.005.
53. Finley SJ, Pechal JL, Benbow ME, Robertson BK, Javan GT. Microbial Signatures of Cadaver Gravesoil During Decomposition. Microbial Ecology. 2016;71(3):524-9. doi: 10.1007/s00248-015-0725-1.
54. Lauber CL, Metcalf JL, Keepers K, Ackermann G, Carter DO, Knight R. Vertebrate Decomposition Is Accelerated by Soil Microbes. Applied and Environmental Microbiology.

2014;80(16):4920-9. doi: 10.1128/aem.00957-14.

55. Payne JA. A SUMMER CARRION STUDY OF THE BABY PIG SUS-SCROFA LINNAEUS. Ecology. 1965;46(5):592-602. doi: 10.2307/1934999. PubMed PMID: WOS:A1965CLA5200002.

56. Rath KM, Fierer N, Murphy DV, Rousk J. Linking bacterial community composition to soil salinity along environmental gradients. Isme Journal. 2019;13(3):836-46. doi: 10.1038/s41396-018-0313-8.

57. Rousk J, Baath E, Brookes PC, Lauber CL, Lozupone C, Caporaso JG, et al. Soil bacterial and fungal communities across a pH gradient in an arable soil. Isme Journal. 2010;4(10):1340-51. doi: 10.1038/ismej.2010.58.

58. De Boer W, Folman LB, Summerbell RC, Boddy L. Living in a fungal world: impact of fungi on soil bacterial niche development. Fems Microbiology Reviews. 2005;29(4):795-811. doi: 10.1016/j.femsre.2004.11.005.

59. Sagara N. PRESENCE OF A BURIED MAMMALIAN CARCASS INDICATED BY FUNGAL FRUITING BODIES. Nature. 1976;262(5571):816-. doi: 10.1038/262816a0.

60. Carter DO, Tibbett M. Taphonomic mycota: Fungi with forensic potential. Journal of Forensic Sciences. 2003;48(1):168-71.

61. Tibbett M, Carter DO. Mushrooms and taphonomy: The fungi that mark woodland graves. Mycologist. 2003;17(1):20-4. doi: 10.1017/s0269915x03001150.

62. Sagara N, Yamanaka T, Tibbett M. Soil fungi associated with graves and latrines: Toward a forensic mycology. Soil Analysis in Forensic Taphonomy. 2008:67-107. doi: 10.1201/9781420069921.ch4.

63. Hawksworth DL, Wiltshire PEJ. Forensic mycology: the use of fungi in criminal

investigations. Forensic Science International. 2011;206(1-3):1-11. doi: 10.1016/j.forsciint.2010.06.012.

64. Parkinson RA, Dias K-R, Horswell J, Greenwood P, Banning N, Tibbett M, et al. Microbial Community Analysis of Human Decomposition on Soil. In: Ritz K, Dawson L, Miller D, editors. Criminal and Environmental Soil Forensics. Berlin, Springer; 2009, pp. 379-394.
65. Wu GX, Zhao H, Li CH, Rajapakse MP, Wong WC, Xu J, et al. Genus-Wide Comparative Genomics of Malassezia Delineates Its Phylogeny, Physiology, and Niche Adaptation on Human Skin. Plos Genetics. 2015;11(11):26. doi: 10.1371/journal.pgen.1005614.
66. Grice EA, Kong HH, Conlan S, Deming CB, Davis J, Young AC, et al. Topographical and temporal diversity of the human skin microbiome. Science. 2009;324(5931):1190-2. doi: 10.1126/science.1171700.
67. Bongers T, Ferris H. Nematode community structure as a bioindicator in environmental monitoring. Trends in Ecology & Evolution. 1999;14(6):224-8. doi: 10.1016/s0169-5347(98)01583-3.
68. Yeates GW, Bongers T, Degoede RGM, Freckman DW, Georgieva SS. FEEDING-HABITS IN SOIL NEMATODE FAMILIES AND GENERA - AN OUTLINE FOR SOIL ECOLOGISTS. Journal of Nematology. 1993;25(3):315-31.
69. Bongers T, Bongers M. Functional diversity of nematodes. Applied Soil Ecology. 1998;10(3):239-51. doi: 10.1016/s0929-1393(98)00123-1.
70. Ferris H, Bongers T. Nematode indicators of organic enrichment. Journal of Nematology. 2006;38(1):3-12.
71. Ferris H, Bongers T, de Goede RGM. A framework for soil food web diagnostics: extension of the nematode faunal analysis concept. Applied Soil Ecology. 2001;18(1):13-29. doi:

10.1016/s0929-1393(01)00152-4.

72. Wei C, Zheng H, Li Q, Lu X, Yu Q, Zhang H, et al. Nitrogen Addition Regulates Soil Nematode Community Composition through Ammonium Suppression. Plos One. 2012;7(8). doi: 10.1371/journal.pone.0043384.
73. Neher, D. Ecology of Plant and Free-Living Nematodes in Natural and Agricultural Soil. Annual Review of Phytopathology. 2010;48:371-94.
74. Ruess L. Nematode soil faunal analysis of decomposition pathways in different ecosystems. Nematology. 2003;5:179-81. doi: 10.1163/156854103767139662.
75. Carter DO, Tibbett M. Cadaver decomposition and soil: Processes. Soil Analysis in Forensic Taphonomy. 2008:29-51. doi: 10.1201/9781420069921.ch2.
76. Ritz K, Black HIJ, Campbell CD, Harris JA, Wood C. Selecting biological indicators for monitoring soils: A framework for balancing scientific and technical opinion to assist policy development. Ecological Indicators. 2009;9(6):1212-21. doi: 10.1016/j.ecolind.2009.02.009.
77. Todd TC, Powers TO, Mullin PG. Sentinel nematodes of land-use change and restoration in tallgrass prairie. Journal of Nematology. 2006;38(1):20-7.

Chapter 1: Spatial impacts of a multi-individual grave on microbial and microfaunal communities and soil biogeochemistry

This chapter is a reformatted version of a manuscript published in PLoS ONE under the same name (citation follows). Permission for the use of this manuscript has been obtained in writing from Dr. Sarah Keenan, the copyright holder, and from the Journal, PLoS ONE. My contribution to this chapter was limited exclusively to nematode systematics and ecology, and I can claim no other material as my own.

Citation: Keenan SW, Emmons AL, Taylor LS, Phillips G, Mason AR, Mundorff AZ, Bernard EC, Davore J, DeBruyn, JM (2018) Spatial impacts of a multi-individual grave on microbial and microfaunal communities and soil biogeochemistry. PLoS ONE 13(12):e0208845. DOI: 10.1371/journal.pone.0208845

Abstract

Decomposing vertebrates, including humans, result in pronounced changes in surrounding soil biogeochemistry, particularly nitrogen (N) and carbon (C) availability, and alter soil micro- and macrofauna. However, the impacts of subsurface human decomposition, where oxygen becomes limited and microbial biomass is generally lower, are far less understood. The goals of this study were to evaluate the impact of human decomposition in a multi-individual, shallow (~70 cm depth) grave on soil biogeochemistry and soil microbial and nematode communities. Three individuals were interred and allowed to decay for four years. Soils were collected from two depths (0–5 and 30–35 cm) along linear transects radiating from the grave as well as from within and below (85–90 cm depth) the grave during excavation to assess how decomposition affects soil properties. Along radiating surface transects, several extracellular enzymes rates and nematode richness increased with increasing distance from the grave, and likely reflect physical site disruption due to grave excavation and infill. There was no evidence of carcass-sourced C and N lateral migration from the grave, at least at 30–35 cm depth. Within the grave, soils

exhibited significant N-enrichment (e.g., ammonium, dissolved organic N), elevated electrical conductivity, and elevated respiration rates with depth. Soil biogeochemistry within the grave, particularly in the middle (30–35 cm) and base (70–75 cm depth), was significantly altered by human decomposition. Mean microbial gene abundances changed with depth in the grave, demonstrating increased microbial presence in response to ongoing decomposition. Human-associated *Bacteroides* were only detected at the base of the grave where anoxic conditions prevailed. Nematode community abundance and richness were reduced at 70–75 cm and not detectable below 85–90 cm. Further, we identified certain *Plectus* spp. as potential indicators of enrichment due to decomposition. Here we demonstrate that human decomposition influences soil biogeochemistry, microbes, and microfauna up to four years after burial.

Introduction

Decomposing vertebrates transform their surrounding environment by releasing compounds, particularly carbon (C) and nitrogen (N), [1-4] that stimulate invertebrate [5,6] and vertebrate scavengers [7], and alter surrounding physiochemistry and biological communities [2,8-11]. When carcasses decay in terrestrial ecosystems, the soil beneath exhibits a wide range of chemical changes, including increased concentrations of ammonium, dissolved organic carbon, dissolved organic nitrogen, phosphate, and calcium [4,10,12-15]. The lateral and vertical extent to which carcasses influence their surrounding environment depends on a variety of factors, including size of the animal and soil physical properties [16,17]. At the far end of the spectrum, for example, elevated soil nitrogen was detected up to 2 m away from decomposed muskox carcasses [18]. Prior studies of surface human decomposition have demonstrated that decomposition products migrate laterally through soil up to approximately 1 m away [12,19].

Changes in macro- and micro-fauna generally accompany the soil chemical changes in

decomposition islands. Numerous insect and arthropod taxa change in response to carcass decomposition, with changes in community membership diagnostic of specific decay stages [20-22]. Soil microbial communities, both bacteria and fungi, also change during decay [9,10,23-25]: microbial activity peaks during active decomposition, and communities shift towards a higher proportion of anaerobic taxa such as Bacteroidetes and Firmicutes [10,24,26]. Such changes generally coincide with an overall decrease in diversity over time [27].

The majority of vertebrate decomposition studies in terrestrial ecosystems have focused on surface decomposition, over timescales ranging from days to years [12,18,28,29]. Surface decay rates are influenced by a range of variables that change on diurnal and seasonal scales, including temperature and precipitation or moisture [30-33]. In contrast, buried remains experience rapidly developing anaerobic conditions, limited gas and fluid exchange with surrounding soil, and greatly reduced insect and scavenger activity [34], resulting in a closed system relative to surface decomposition [14]. Additionally, the variable decomposition rates observed in burials [16,34] result in long periods before soft tissues are completely degraded. The contrast between surface and burial decomposition has also been noted in terms of impacts on microbial communities. For example, burial resulted in consistent measures of diversity with increases in richness and decreases in evenness compared to surface systems during decay [27].

The effects of buried carcass decomposition are more difficult to study, particularly with respect to identifying time-resolved changes, resulting in significant gaps in our understanding of subsurface decay processes in soil systems. Despite several prior studies of interred carcass decomposition [14,21,27,35,36], the potential for decomposing carcasses to influence soil physiochemistry and biology within and outside of a grave has not been fully explored. Additionally, the temporal duration that soils retain physiochemical indicators of decomposition

is largely unknown. Several studies have examined changes to soil physiochemistry and microbial ecology after 1 to 1.2 years [35,36], and in both studies carcasses were still actively degrading. Assessing the impact of buried remains on soil chemistry and biology, and whether soils maintain chemical or biotic signatures of decay years post-deposition, after soft tissues have largely decomposed, may have applications in several areas: for example, insight into nutrient pulse or 'hot spot' dynamics in terrestrial ecosystems; a better understanding of taphonomy *i.e.* the interplay between environment and decomposing remains as they relate to long term preservation of remains; and/or determining the age of human graves and guiding recovery or discovery of clandestine graves.

Decomposition environments are host to multi-trophic level food webs, which are influenced by changes in soil physiochemistry [37-40]. Of the microfauna, free-living soil nematodes are of particular interest; nematodes are ubiquitous across all known ecosystems, comprising an estimated 80% of all multicellular organisms in the soil environment [41]. Differentiated feeding habits and successional patterns have rendered them useful as soil enrichment indicators [42-44]. Nematode enrichment has been observed in association with decaying carcasses [45], however limited work has been done to date in terms of a systematic description of nematode community responses to vertebrate decomposition [38,46]. At present, studies of microfaunal communities associated with decomposing vertebrate remains have been restricted to cataloging taxa of nematodes [38], testate amoeba [37,39], and arthropods [40,46] in surface soils. The effects of buried remains on subsurface microfaunal communities are poorly understood. Nematode community composition is sensitive to soil resource availability in agricultural systems [47-54] as well as physical or chemical disturbances [54-56]. Given the dynamic nature and high flux of nutrients to the soil during decay, it was expected that vertebrate

decomposition would select for nematodes feeding on the bloom of decomposer bacteria and fungi associated with the carcass and/or tolerating the extreme physiochemical changes.

The goals of this study were to evaluate the spatial (vertical and lateral) changes in soil chemistry and biological communities, including microbes and nematodes, associated with a multi-individual grave, four years after burial of three human subjects. We expected to observe physiochemical indicators of decay in the soils within and immediately adjacent to the gravesite, including decreased pH, elevated electrical conductivity, elevated soil respiration rates, and elevated total C and N. In addition, we expected to observe enrichment of microbes and nematodes within the grave. Given the dense and clay-rich soil at the experimental site, lateral migration of porewater fluids transporting grave-derived organics was expected to be minimal and restricted to downward movement. The results provided novel insights into the impact of interred remains on soil biogeochemistry, and microbial and nematode ecology.

Materials and methods

Field location and multi-individual interment

The University of Tennessee Anthropological Research Facility (ARF) is the longest running human decomposition laboratory [2,57]. The ARF is located in Knoxville, Tennessee, United States on 2 acres of temperate mixed deciduous forest, with varying densities of understory and groundcover. The soil type consists of decomposed plant material and loam in the O-A horizons (0–10 cm), underlain by clay loam and channery clay loam extending to bedrock (limestone, shale, and sandstone) [58]. In February 2013 two graves (~2 m x 2 m x 0.7 m) were excavated at the facility in an area that had not previously hosted decomposition experiments (Figure 1.1). On 14 February 2013, three deceased human subjects (two white males and one

white female, Table 1) donated to the University of Tennessee Forensic Anthropology Center for the W. M. Bass Donated Skeletal Collection (http://web.utk.edu/~fac/collection.html) were placed into one of the graves. Individuals were stacked in the grave; the first individual placed (Individual A) was positioned in a W-E orientation, with the superior position in the W. The second individual, Individual B, was oriented N-S, and Individual C, the individual closest to the surface, was oriented W-E. The grave was backfilled and left undisturbed until March 2017. The second grave (referred to as the control grave) was excavated and backfilled at the same time as body placement and used as a negative control to simulate the effects of excavation in the absence of human decomposition. Because no living human subjects were involved in this research and no personally identifiable information was collected, the project was exempt from review by the University of Tennessee Institutional Review Board.

Soil collection and chemical analyses

The graves were excavated and human remains were removed in March 2017. At the time of disinterment, the individuals were in disparate states of decomposition. Skeletal elements from a single individual spanned multiple depths due to the nature of placement within the grave, and the grave was saturated with water, especially in the NW section. Individual C was skeletonized with essentially no adipocere or soft tissue present, while Individual B was partially skeletonized but with greater amounts of adipocere and some large portions of skin and soft tissue present, especially in the upper torso, hands, and feet. Conversely, individual A was nearly intact but in a suspended state of decomposition due to extensive adipocere formation, with pink muscle tissue and skin still present on most of the body. The torso (upper and lower) was encased in an outer shell of adipocere, which protected the underlying decomposing muscle and tissue. Soil samples were collected from three linear transects radiating from the grave, from

inside the grave (Figure 1.2), and from below the grave once remains were recovered. The transect soils were collected on 14 February 2017, exactly 4 years after the bodies were interred and prior to grave excavation. The three linear transects (Figure 2) radiating 2 m from the grave were subsampled at 0.5 m intervals from the O/A horizon (0–5 cm) and B horizon (30–35 cm). Transects were selected based on logistical constraints (i.e., limestone boulders, fallen or live trees) and avoided any nearby gravesites. All transects were a minimum of 3 m from any nearby graves, and there are no records of previous surface vertebrate decomposition in these areas. Soil samples were collected using a 10 cm-diameter auger. Holes from O/A horizon surface samples were extended to 30 cm depth to allow collection of B horizon samples from 30–35 cm with a 3 cm-diameter auger. Two O/A horizon, pre-excavation soil samples were collected from the top of the grave. Control soils were also collected from two regions prior to grave excavations. Three cores were obtained and composited from 0–5 cm and 30–35 cm from the control grave. Additional off-grave control cores (n = 3) were collected from the same depths at three undisturbed locations approximately 5 m from the grave.

During excavation (8–9 March 2017), four additional O/A horizon samples were collected from the grave surface. Once excavations reached the human remains, three soil samples were collected immediately adjacent to the bodies at 30–35 cm. An additional soil sample containing adipocere and other partially decomposed organic material was obtained from within the rib cage of Individual C (~40 cm depth). Following the complete removal of skeletal remains (14 March 2017), four soil samples were collected at the base of the grave (70–75 cm) and three samples were collected from the 85 cm depth (15 cm below the base of the grave; the deepest sample possible due to the dense clay and proximity to the underlying bedrock). All samples (n = 45) were homogenized by hand in the field to remove rocks or vegetation greater

than 2 mm prior to transport to the lab. Approximately 10 g of soil was flash-frozen in liquid nitrogen and stored at -80°C for DNA extraction. Soils for enzyme assays were weighed into sterile 15 mL tubes and frozen at -20°C until analysis.

All soil biogeochemical analyses were conducted within 24 hours after storing soils under field conditions overnight. Soil pH and electrical conductivity were measured using a 1:2 soil to deionized water slurry and an Orion Star A329 multiparameter meter (ThermoScientific). Soil gravimetric moisture was assessed in triplicate by oven-drying soil aliquots for at least 48 hours at 105°C. Respiration rates were measured using field-moist soils sealed in 60 mL serum bottles. Measurements immediately after capping (time 0) and after 24 hours of incubation at room temperature were conducted in duplicate using a LI-820 CO_2 analyzer (LI-COR) with manual injection (0.5 mL volume). For soil extracts, field moist soils were incubated at room temperature on a shaking platform (150 rpm) in 0.5 M K_2SO_4 for four hours (soil:solution ratio of 1:4). Jars were allowed to sit for one hour to allow sediment to settle from solution. Soil slurries were then vacuum filtered (Ahlstrom, glass microfiber filters, 1 μm), and filtered extracts were stored at -20°C.

Ammonium concentrations in soil extracts were quantified following a microplate protocol after 2 hours of incubation, with minor modifications [59]. The ammonium standard [$(NH_4)_2SO_4$] was dissolved in 0.5 M K_2SO_4 instead of deionized water to account for potential matrix effects. In addition, 70 μL (instead of 50 μL) of each soil extract or standard were pipetted into the microplate, and 50 μL of deionized water was used (instead of 100 μL) [59].

Soil nitrification potential was determined with a modified chlorate block method designed for a microplate reader [60-62]. The nitrification potential medium contained: 4 mL of 0.2 M K_2HPO_4, 0.5 mL of 0.2 M KH_2PO_4, 2.5 mL of 0.2 M $(NH_4)_2SO_4$, and 10 mL of 1 M

$NaClO_3$, diluted up to 1 L with sterile deionized water. The color reagent consisted of 87.6 mL of sterile deionized water, 17 mL of 85% H_3PO_4, 4 g of sulfanilamide, and 0.1 g of N-(1-Naphthyl) ethylenediamine). A 100 ppm-N as NO_2^- standard was made using $NaNO_2$. Soils (2 g) were frozen at -20°C prior to beginning nitrification potential assays, which may underestimate the total amount of nitrite in the soil by 27% [61]. Nitrification potential medium (2 g soil: 14 mL medium) was added to each 50 mL tube after allowing the soil to fully thaw to room temperature [60]. Samples were vortexed (10 seconds) to break up soil aggregates. Tubes containing the chlorate-soil slurry were placed horizontally on a shaking incubator set to temperatures that corresponded to ambient conditions in the field and were allowed to shake for 5 minutes (120 rpm) before transferring 1 mL aliquot of slurry (T_0) to sterile 1.5 mL microcentrifuge tubes. Tubes were placed back on the shaking platform, and subsampled again after 2.5 (T_1) and 5 hours (T_2). The tubes containing solution aliquots were immediately centrifuged for 2 minutes at 10,000 × g. Nitrite concentrations were determined (in triplicate) colorimetrically using 50 µL of the NO_2^- color reagent and 200 µL of the supernatant from centrifuged samples in a 96-well plate. Absorbance values were measured with a plate reader at 543 nm after incubating for at least 10 minutes at room temperature.

Extracts were oxidized to quantify dissolved organic carbon (DOC) and dissolved organic nitrogen (DON) following the persulfate method [63]. DOC was measured as the amount of CO_2 released after overnight incubation at 80°C. Nitrate concentrations of soil extracts and persulfate oxidized extracts (DON) were determined colorimetrically in triplicate for each sample after 5 hours of incubation at room temperature [64].

Soils previously frozen at -20°C were allowed to thaw to room temperature and were then used to assay extracellular enzyme activity. Potential activity of leucine aminopeptidase (LAP),

N-acetyl-β-glucoseaminidase (NAG), and β-D-cellulobiosidase (CB) [65], as well as phosphodiesterase (PDE) [66] and collagenase (COL) were assayed using a 50 mM Tris buffer at pH 6.7, optimized based on average soil pH. The COL assay was developed from the EnzChek gelatinase/collagenase kit (Molecular Probes) and optimized for soils. The same soil slurry used to measure LAP, NAG, CB, and PDE was used to measure COL. A ratio of 20 µL soil slurry: 20 µL fluorescence substrate: 160 µL 1X reaction buffer was found to work best in this soil type for the COL assay. The fluorescence substrate, DQ gelatin, was diluted to a final working concentration of 80 µg/mL. Standard curves were generated for each soil sample by spiking the soil with the kit-supplied *Clostridium histolyticum*, which has a known collagenase activity, with standard curves ranging from 0.01 to 1.0 U mL^{-1}. Each standard contained 20 µL soil slurry: 20 µL standard: 20 µL fluorescence substrate: 140 µL 1× reaction buffer. Samples were loaded directly into an opaque 96 well plate, and fluorescence was measured on a Synergy H1plate reader (BioTek) after 3 hours.

Soil biological community assessment methods

DNA was extracted from soils that had been stored at -80ºC using the DNeasy Powerlyzer Powersoil kit (QIAGEN Inc.) per manufacturer's instructions, following recommendations for clay soils. 250 mg of soil were used for each extraction. Soil DNA extracts were stored at -20°C. All soil DNA extracts were quantified for total DNA concentration using the Quant-iT™ PicoGreen™ dsDNA Assay Kit (Invitrogen) on a 96-well microplate reader using reduced assay volumes of 200 µL. Samples were quantified in duplicate while standards were run in triplicate. Five standards were included in each plate ranging from 0 µg mL^{-1} to 0.5 µg mL^{-1}.

As a proxy for bacterial and fungal abundances, qPCR was used to quantify 16S rRNA

and ITS gene abundances in soil using the Femto™ Bacterial DNA Quantification Kit and the Femto™ Fungal DNA Quantification Kit, respectively. Assays were performed in accordance with the manufacturer's instructions using a CFX Connect™ Real-Time PCR Detection System (BioRad). Samples were quantified in triplicate, while standards were quantified in duplicate. A minimum of three no-template controls were included in each 96-well plate. Data are presented as copy number per gram of dry weight soil (copy gdw^{-1}).

Human-associated *Bacteroides* are common gut microbes that have been found to enter the soil and persist during decomposition [10]. DNA extracts from all samples were used to test for the presence of human-associated *Bacteroides* (HuBac) via a qPCR assay developed by Layton et al. [67]. A dilution series of plasmid DNA containing the human-associated *Bacteroides* 16 rRNA gene [67] ranging from 10^7 to 10^2 copies per µL was used to generate a standard curve. Each 25 µl reaction contained 12.5 µl 2X TaqMan™ Universal PCR master mix (ThermoFisher), 6.5 µl nuclease-free water (ThermoFisher), 1.5 µl each of HuBac566f primer (10 µM) and HuBac692r primer (10 µM), 0.5 µl of HuBac594Bhqf probe (10 µM) (synthesized by Eurofins), and 2.5 µl of template DNA. The reactions were run on a CFX Connect (BioRad) using the following amplification conditions: 50°C for 2 minutes, 95°C for 10 minutes, and 40 cycles of 95°C for 30 seconds and 60°C for 45 seconds. Data are presented as copies per gram dry weight soil.

Nematodes were extracted from fresh soil using a sugar flotation-centrifugation method [68]. Total abundances (N) were expressed as nematodes per 100 cm^3 soil. Nematodes were counted and identified to genus with the aid of a differential interference contrast (DIC) microscope. For uncertain identifications, Bongers [42], Geraert [69], Siddiqi [70] and various recently published keys and revisions were consulted. *Anaplectus* and *Plectus* spp. were

identified according to Allen & Noffsinger [71], Andrassy [72], and Zell [73]. Nematodes were assigned trophic classifications based on identification: bacterial feeders (B), fungal feeders (F), plant parasites (Pp), predators (Pr), and omnivores (O) [74]. They were also assigned colonizer-persister (c-p) values, ranging from 1 through 5, representing a range between quickly reproducing enrichment opportunists associated with ephemeral nutrient sources or disturbed environments, to those that reproduce slowly and in low density, found most often in mature, stable environments [42]. Trophic groups and c-p classes were combined into functional guilds according to Bongers and Bongers [75]. Community richness was defined as the number of unique genera. Shannon diversity (H) and equitability (evenness, EH) were calculated using equations (1) and (2), respectively.

$$H = -\sum p_i (ln\ p_i) \quad (1)$$

$$EH = H/Hmax \quad (2)$$

Where p_i is the proportion of the i^{th} genus in the sample community, and $Hmax = ln(n)$, where n consists of the total number of genera in a sample [76]. Faunal indices were calculated according to [77], and consist of an enrichment index (EI) (3) and structure index (SI) (4), designed to characterize nematode communities based upon community structure and prevailing food web conditions.

$$EI = 100(e/(e+b)) \quad (3)$$

$$SI = 100(s/(s+b)) \quad (4)$$

Where $b = \sum k_b n_b$, k_b is the weighting constant assigned to functional guilds B2 and F2, indicators of basal soil states, and n_b is the number of nematodes present in those guilds. Similarly, e is calculated with weighting constants assigned to functional guilds B1 and F2, indicators of enrichment, and s is calculated with weighting constants assigned to structure (B3–

5, F3–5, O3–5, Pr3–5). EI (3) and SI (4) values are plotted on a faunal ordination diagram [77]. The Maturity Index (MI) (5) [42] consists of the weighted mean of all c-p values, excluding plant-parasitic taxa, and serves as a general indicator of soil enrichment status.

$$MI = \sum v_i \ ^*f_i \quad (5)$$

Where v_i is the c-p value (1–5), and f_i is the frequency of each c-p class represented in the sample.

Grave aqueous geochemistry

A perched water lens formed along the base of the grave. Cores from the 85-cm depth were collected from areas without standing water. A water sample was collected during excavation, stored overnight at 4°C, and filtered to 0.2 μm into Nalgene bottles. A subsample was filtered into an HCl-washed Nalgene bottle, and preserved by the addition of trace grade nitric acid for cation analyses. Anions and cations were analyzed using Ion Chromatography (Dionex ICS-2000 and 2100, respectively) at the University of Tennessee. Total alkalinity (as bicarbonate, HCO_3^-) was measured by titration with 0.1 N H_2SO_4 to pH 4.3 [78].

Data analyses and statistics

To assess potential for lateral transport, soils collected along linear transects radiating from the grave at 0–5 and 30–35 cm depths were compared with soils collected from these same depths within the grave to evaluate potential changes in soil chemistry and biology. To determine the potential for vertical changes in soil chemistry within the grave, soils collected from 0–5, 30–35, 70–75, and 85–90 cm within the grave were compared. Soil chemical and biological data are presented on a gram dry weight (gdw) basis when appropriate. Significant differences between samples at depth and along transects were based on a one-way analysis of variance (ANOVA) followed by a Holm-Sidak post hoc test using SigmaPlot (version 14, Systat Software, Inc.). To

evaluate the effects of depth and distance along the transect, two-way ANOVAs were also computed. For all ANOVAs, significance was set at $p < 0.05$.

Nematode community analyses were performed using the basic statistical functions in R (version 3.3.2), along with the "car" statistical package (version 2.1-4) [79-80]. For transect samples, in order to evaluate the effects of depth, transect distance, and interactions between factors, a two-way ANOVA was performed followed by a Tukey HSD posthoc test to identify differences.

To visualize the overall differences in soil biogeochemistry between all samples, a principal components analysis (PCA) was run on a Euclidean distance matrix of all samples (except for the rib cage sample which was a strong outlier), including all physicochemical parameters measured along with biological parameters of activity (respiration, enzyme activities) and microbial gene abundances. The PCA was done in Primer 7 v 7.0.13 (PRIMER-e, Quest Research Ltd.).

Results

Lateral changes in soil biogeochemistry

In soils radiating laterally from the grave, gravimetric moisture was significantly elevated in surface samples (0–5 cm) compared to their depth equivalent (30–35 cm) along the transects ($p < 0.001$; $F = 36.600$), and gravimetric moisture significantly increased with distance from the grave ($p < 0.001$; $F = 12.480$). Surface soil pH (6.68 to 6.82) was not significantly different from soil pH at depth (6.05 to 6.74) (Tables 1.2-1.3), and there were no significant differences in pH with proximity to the grave (Table 4). Conductivity was significantly elevated in surface soils compared to samples at depth ($p < 0.001$; $F = 18.995$). In surface soils, conductivity ranged from

18.26 to 30.75 μS cm^{-1}, with lowest conductivity values observed in the top of the grave. At depth, values ranged from 10.91 to 20.75 μS cm^{-1}, with highest conductivity values observed inside the grave (Tables 1.2-1.3).

In general, nitrogen pools were elevated in surface soils compared to their depth equivalents along transects (Figure 3). Mean ammonium concentrations were 6.03 ± 2.7 μg NH_4-N gdw^{-1} in surface soils and decreased to 2.80 ± 1.2 μg NH_4-N gdw^{-1} at depth ($p < 0.001$; $F = 24.326$). Interestingly, we did not observe a significant enrichment of NH_4^+ closer to the grave. The highest ammonium concentrations were measured in surface soils at 1.5 m and 2.0 m from the grave, but these differences were non-significant. Nitrate decreased from a mean of 2.92 ± 1.5 to 1.17 ± 1.4 μg NO_3^--N gdw^{-1} ($p < 0.001$; $F = 14.6$) between surface samples and those collected at depth. Nitrate was significantly elevated in surface soils compared to their depth equivalents at 1.0, 1.5, and 2.0 m along transects. At 0 and 0.5 m, [NO_3^-] was similar in surface and subsurface samples. Soils collected from the grave had greater [NO_3^-] at 30–35 cm depth compared to grave surface soils. In contrast, the opposite trend was observed in transect soils, where [NO_3^-] was greater in surface soils and comparatively depleted at 30–35 cm depth (Tables 2 and 4). Dissolved organic nitrogen (DON) increased with distance from the grave ($P < 0.001$; $F = 15.290$) and was elevated in surface compared to subsurface soils ($p = 0.009$; $F = 8.130$) along the transects. Similar to NO_3^-, DON was elevated at the 30–35 cm depth and relatively depleted in the grave surface soils. Nitrification potential rates decreased with depth ($p = 0.008$; $F = 9.194$), except for soils collected from the grave, which exhibited greater nitrification potential rates in the 30–35 cm soils compared to the grave surface soil (Tables 1.2 and 1.4).

Lateral changes in soil microbial and microfaunal communities

Microbial respiration rates, measured as CO_2 produced during a 24 hour incubation at

ambient temperature, were three times lower in deep samples compared to surface soils along the transects ($p < 0.001$; $F = 32.2$). Within the grave, respiration rates were highly variable at 30–35 cm depth, ranging from 7.2 to 45.1 μg CO_2-C released gdw^{-1} day^{-1}. At 0 and 0.5 m along the transects, there was no significant difference between respiration rates in surface and 30–35 cm soils. Respiration rates were significantly higher further from the grave (1.0, 1.5, and 2.0 m), however DOC did not significantly differ in surface and subsurface soil along the transects or as a function of distance from the grave (Tables 1.2 and 1.4).

The potential rates of several extracellular enzymes changed along the transects. Leucine amino peptidase (LAP), N–acetylglucoseaminidase (NAG), and cellulobiosidase (CB) activities were higher in surface compared to depth (Table 1.4, Table 1.5). CB and LAP activity increased with increasing distance from the grave (Figure 4). Phosphodiesterase (PDE) and collagenase (COL) did not differ significantly between depths or with distance from the grave (Table 1.4).

As a proxy for bacterial and fungal abundances, 16S rRNA and ITS gene copy numbers were quantified using qPCR assays. Bacterial gene copy numbers were elevated in surface soils compared to deep soils, and gene copy numbers increased in surface soils with distance from the grave relative to copy numbers observed within grave surface soils ($p = 0.039$, Tables 1.2 and 1.4). Within the grave, bacterial copy numbers significantly varied ($p<0.001$) with a significant decrease in the 85–90 cm layer (Table 1.2). Fungal copy numbers did not change significantly as a function of depth or distance along transects (Table 1.2). Using the qPCR assay specifically targeting human-associated *Bacteroides*, no human-associated *Bacteroides* were detected in any of the soils along the transects.

Along the transects, nematode abundances, richness and diversity were higher in surface soils compared to those at depth (Table 1.6). In surface soils along the transects, diversity,

evenness, and MI did not significantly change with distance from the grave; however, richness increased with distance from the grave: samples from 1, 1.5, and 2.0 m had significantly higher richness than those collected from the surface of the grave. Evenness increased with distance from the grave in the subsurface (30 cm soils). Subsurface soils also exhibited significantly higher richness at distances of 1 and 1.5 m from the surface of the grave.

All surface transect soil samples contained the F2 fungal feeder *Filenchus* (mean of 28% relative abundance) and the B2 bacterial feeder *Plectus* (5%), with additional representation from bacterial feeding c-p classes 1–3 (Rhabditidae, 18%; *Acrobeloides,* 2%; *Prismatolaimus,*1%) and plant parasites (*Xenocriconemella*, 10%; *Gracilacus,* 8%; *Helicotylenchus,* 10%; *Meloidogyne,* 2%; *Xiphinema,* 2%) (Figure 5A). At the 30–35 cm depth, *Filenchus* was reduced to 20%, but was present in all samples. *Meloidogyne* (11%), Rhabditidae (8%), *Gracilacus* (8%), *Helicotylenchus* (8%) and *Plectus* (3%) were also present at depth (Figure 5A). Between surface samples and those at depth, there was an overall shift from bacterial feeding (B) to plant-parasitic (Pp) taxa (Figure 1.5B, Tables 1.7 and 1.8).

Changes in soil biogeochemistry within the grave

The base of the grave contained a perched water lens that accumulated within and surrounded the bodies. As a result, soil gravimetric moisture differed significantly with depth ($p < 0.001$; $F = 33.511$); soil moisture increased with depth from the surface (0.321 ± 0.01) to the base of the grave (0.464 ± 0.04) where soils were saturated. Below the grave, soils were unsaturated with gravimetric soil moisture of 0.335 ± 0.02. Compared to the transects and control grave and off-grave controls, gravimetric moisture at 30–35 cm was higher within the grave (Table 2). Soil pH was elevated at depth compared to surface samples, reaching a maximum of 7.66 ± 0.36 at 85–90 cm depth. A similar pattern was observed with electrical

conductivity, which was greatest in soils collected from 85–90 cm (139.9 ± 16.4 μS cm^{-1}) (Table 1.2, Figure 1.6).

Ammonium concentrations increased several orders of magnitude with depth, reaching maximum concentrations at the 85–90 cm depth (1075 ± 390 μg NH_4-N gdw^{-1}) ($p < 0.001$; $F = 17.105$) (Figure 1.2, Table 1.4). A similar pattern was observed with DON and DOC, both of which were elevated in the 70–75 cm and 85–90 cm samples (Figure 1.3, Table 1.2). Within the grave, nitrate concentrations were elevated but not significantly different at the 30–35 cm depth (Figure 1.3). Nitrification potential rates decreased with depth ($p = 0.009$, $F = 6.192$) (Figure 1.3).

A single sample of partially decomposed organic material mixed with mineral soil was recovered from within the ribcage of Individual C at ~40 cm depth. The material had elevated conductivity and gravimetric moisture compared to soils collected adjacent to the body at 30–35 cm depth (Table 1.2). Ammonium, nitrification potential rates, DOC, and DON were elevated in this sample as well. Respiration rates were an order of magnitude greater compared to soils collected anywhere else in the grave or along the linear transects.

The water sample collected from the perched groundwater at the base of the grave was pH 6.23 (at 11.5°C) with an electrical conductivity of 778.5 μS cm^{-1}. The water contained: 17.48 mg L^{-1} Na^+, 3.78 mg L^{-1} K^+, 38.91 mg L^{-1} NH_4^+, 85.57 mg L^{-1} Ca^{2+}, 6.43 mg L^{-1} Mg^{2+}, 7.87 mg L^{-1} Cl^{-1}, 11.67 SO_4^{2-}, and an alkalinity of 302.8 mg L^{-1} (as HCO_3^-). The grave water chemistry was similar to surface water in East Tennessee (Figure 1.7), but contained significantly more ammonium than typical surface water, which ranged from 0.01 to 0.13 mg L^{-1}.

Changes in biological communities within the grave

Microbial enzymatic activity did not significantly change with depth in the grave, except

for NAG, which was an order of magnitude greater in the 70–75 cm samples ($p = 0.01$, $F = 5.002$) (Figure 1.8).

Bacterial and fungal rRNA gene copy abundances were not significantly different through the grave; below the grave (85–90 cm), abundances were significantly reduced. Human-associated *Bacteroides* were only detected in four of the 45 soil samples tested. These four samples were collected at the base of the grave (70–75 cm), where *Bacteroides* gene abundances ranged from $4.9 \times 10^4 \pm 1.9 \times 10^4$ to $2.9 \times 10^6 \pm 1.7 \times 10^6$ copies gdw^{-1} (Figure 1.9). It should be noted that this was not simply due to the amount of DNA extracted from soil (which could affect detection limits), as DNA extracted decreased significantly with depth, with less than 1 ng gdw^{-1} recovered at 85–90 cm depth (Figure 1.9).

Nematode abundances within the grave were similar between surface and 30–35 cm depth soils, but were reduced in abundance at 70–75 cm and not detectable below the base of the grave (85–90 cm) (Table 1.6). Nematode community richness was significantly reduced at 70–75 cm (Table 1.6). No significant differences in diversity, evenness or MI were detected within the grave (Table 1.6). Nematode community composition at the surface of the grave was similar to that found along transects (Figure 1.5). Taxa present in surface grave soils included: F2 fungal feeder *Filenchus* (35% of total abundance), B1-2 bacterial feeders Rhabditidae (15%) and *Plectus* (5%), and plant parasites *Helicotylenchus* (14%) and *Xenocriconemella* (11%) (Figure 1.5A). The plant parasite *Gracilacus* (10%) was present in most samples. A marked shift in community composition was observed at 30–35 cm, where fungal-feeding taxa were present in lower proportions (*Filenchus,* 6%), and plant parasites were more abundant (*Gracilicus,* 42%; *Xenocriconemella,* 18%). Within bacterial feeding groups, B1 taxa predominated (Rhabditidae, 18%) in surface samples, and B2 taxa were more abundant at 30–35 cm (*Plectus* 29%). One

Plectus species identified was only found in grave samples. At 70–75 cm depth, community membership decreased to only a few genera (Table 1.6, Table 1.9) largely composed of B1–2 (Rhabditidae, *Acrobeloides*, and *Plectus*), and F2 (*Filenchus*) taxa. The plectid component consisted of five species, according to Allen and Noffsinger [71], Andrassy [72], and Zell [73]. *Anaplectus granulosus* (Bastian), *Plectus cirratus* Bastian and *P. parietinu*s Bastian were commonly collected from most surface samples but were scarce or absent from deeper cores. *Plectus longicaudatus* Bütschli was frequently collected from the 30–35 and 70–cm samples, and was particularly abundant (80% of total nematodes) in soil associated with the 30-cm-deep water lens sample and in the ribcage sample. *Plectus aquatilis* Andrassy was collected only from the water lens sample. Tardigrades (*Hypsibius* sp.) were abundant in the water lens sample but infrequent in most other samples.

Nematode communities were examined using a faunal profile analysis, which shows nematode functional group responses (Figure 1.10). Communities in quadrant A are indicative of a response to a highly enriched and/or disturbed environment, with an increased relative abundance of B1 bacterial feeders. Communities within quadrant B also indicate enrichment, but with a more balanced ratio of bacterial and fungal feeders, as well as increased predatory and omnivorous taxa characteristic of a more stable environment. Quadrant C represents mature communities with a greater abundance of fungal feeders, often found in soils with low disturbance and high carbon:nitrogen ratios. Quadrant D is indicative of a community dominated by fungal feeders, often found in soils with depleted resources [77]. The faunal profile of this study shows that within 0–5 and 30–35 cm depths, both grave and transect communities largely occupy quadrants A and B, exhibiting similar degrees of enrichment but variable community structures, as shown on the structure index (SI) axis (Figure 1.10).

The organic matter-rich sample collected within the ribcage had elevated respiration, PDE and LAP activity compared to any other sample within the grave, and indicates elevated microbial activity. While LAP activity was comparable to activities measured in surface control grave and off-grave samples, PDE activity was higher than controls and bacterial and fungal gene copy numbers were higher than any other soil samples. Surprisingly, despite the fact that this sample was recovered from within the body cavity, human-associated *Bacteroides* were not detected. Nematode communities in this sample were not comparable to surrounding soil samples in all metrics (Table 1.6). The community was dominated by B1 and B2 bacterial feeders, primarily *Plectus* (36%), Rhabditidae (26%), and Diplogasteridae (15%); the last of which was not observed in any of the other samples in this study (Figure 1.5, Table 1.9).

When taken all together, the combination of soil physical, chemical, and biological data shows some overall patterns in these grave soils (Figure 1.11). The most impacted soils in this system were the within-grave samples at 30–35, 70–75 cm, and 85–90 cm. While differences were expected between surface and deep samples along transects, these differences were not dissimilar from control sites and therefore we did not detect an overall impact of human decomposition on soils radiating laterally from the grave.

Discussion

One of the goals of this study was to evaluate the potential for chemical inputs released by decomposing human subjects within a grave to influence soil biogeochemistry and biology within and outside of the grave four years post-burial. There are two processes that may explain the observed changes in soil properties in and around graves: (1) physical mixing and compaction of the soil during grave infill, and (2) human decomposition. In surface soils along lateral transects as well as within the grave, some of the observed physiochemical and biological

changes may have been due to physical mixing and compaction. In particular, LAP and CB activities were lower in control grave samples compared to off-grave controls, suggesting that physical disruption of the soil has the potential to influence microbial enzymatic activity. Additionally, conductivity, ammonium, and nitrification potential rates were all lower in surface soils on the control grave compared to the off-grave control soils. This suggests that physical processes explain some of the observed differences, and four years after grave excavation and infill, surface soils have not returned to native conditions.

Despite some influence from physical processes, the overwhelming majority of changes observed within the grave at 30–35 cm, 70–75 cm, and 85–90 cm depth were due to human decomposition. At 30–35 cm depth, elevated nitrate and nitrification potential within the grave contrasted with soil collected outside of the grave (Figure 1.3), and indicates that soils contain enough oxygen to support nitrification. Fungal abundances were also elevated at the 30–35 cm depth indicative of a microbial 'bloom'. The presence of water-saturated soils from ~60 to 75 cm depth at the base of the grave resulted in suboxic to anoxic conditions; therefore it was not surprising to observe inhibited nitrification and a reduction in nematode abundances at these depths. At the base of the grave, ammonium, DON, DOC, and respiration rates were elevated, reflecting C and N compounds sourced from the bodies. Carcass-sourced organics were still present four years after burial, including soft tissue and adipocere formation on two of the donors. Adipocere is often observed in wet and anoxic environments with low gas diffusivity and low oxidation–reduction potentials [16,81,82] and was therefore not a surprise in this environment. Moreover, reduced rates of LAP and PDE activity at depth, indicators of protein and nucleic acid degradation, suggest that oxygen limitation may be controlling microbial enzymatic activity despite the presence of labile C and N resources (i.e., remnant soft tissues).

Elevated NAG activity at the base of the grave, an enzyme specific to chitin or fungal degradation, suggests that microbes are able to utilize a more recalcitrant C and N pool, and this activity is likely driven by anaerobic microbial communities. It is also notable that the saturated base of the grave was the only location where human-associated *Bacteroides* were detected, suggesting that the anoxic conditions and/or the presence of remaining soft tissue on the lowest body were conducive to long-term preservation of these obligate anaerobes. Our previous work showed that human-associated *Bacteroides* persisted for over a year in surface soils below decomposing donors, preserved by soft tissue remains that restricted oxygen flow to the soils [10]. Here we have added to this observation by showing that in saturated subsurface conditions, human-associated microflora can persist at least four years post-mortem.

We examined nematode communities associated with this multi–individual grave in order to determine whether there was an influence of human decomposition on soil microfauna. Nematode communities are often used as indicators of disturbance or enrichment because of their successional patterns. For example, manure addition to agricultural fields causes initial blooms of enrichment opportunists followed by taxa less affected by chemical disturbance [83]. In this study, a minor increase in nematode richness was observed > 0.5 m away from the grave in surface soils. Grave surface soil richness was consistent with that found in grave controls. Since the grave was completely excavated to a depth of 70 cm prior to donor interment and infilling, the observed differences in richness along transects and with respect to both the top of the grave and the grave controls suggests that physical processes and mixing may be partly responsible for the observed community change. Indeed, studies of agricultural soils show that cultivation can reduce nematode abundance and diversity [54].

With few exceptions [84-86], most field studies of nematodes focus on a single depth

range, usually within the top 30 cm of the soil profile [38,47,49,52,53,56,87]. Our study compared multiple depths, and revealed that abundance, richness, and diversity decreased with depth both within and outside the grave. Within the grave, there was an overall reduction in nematode abundance and richness with depth. Previous studies have reported that approximately 70% of nematodes exist in the top 20 cm of soil and their distributions are associated with available food sources [85,86]. Our findings of elevated abundances at 30–35 cm, in conjunction with high variation in samples at those depths, is likely due to elevated bacterial and fungal abundances in these areas. The lowest abundance, richness, and diversity were observed at the base of the grave (70–75 cm). Nematodes were not detected below the grave (85–90 cm), which is consistent with observations of nematode abundances found in deep agricultural and forest soils [85].

The faunal profile of the nematode communities provided some insight to their response to physical disturbance and decomposition products (Figure 1.10). Transect surface soils largely fall within quadrant A, indicative of enrichment by opportunistic taxa. Transect soils from 30–35 cm are shifted toward quadrant B, indicative of increasing community maturity with undisturbed depth. Surface grave soils also fall within quadrant A; however, they are clustered below 40 on the SI, indicating that severe physical disruption caused by excavation and infilling influenced nematode populations. Similarly, 30–35 cm soils within the grave are shifted lower on the SI compared to transect soils of the same depth. The observation that soils in close proximity to decomposition products display a difference in community structure is consistent with observations by Szelecz et al. [38]. Meng et al. [85] reported that most enrichment opportunists (B1 taxa) were found to inhabit the upper 20 cm of the soil profile, but that the location of nematodes in a vertical profile was dependent upon food source location. In our study, the

location of decomposition products and associated microbial blooms clearly influenced nematode communities below 20 cm.

Interestingly, within 30–35 cm grave soils, one sample was strongly enriched with a unique (unidentified) species of *Plectus* (B2) that was found only within the grave. Modest increases in bacterial abundances can stimulate some B2 taxa without exceeding threshold stimulation for enrichment opportunist response (B1 taxa) [88]. This may account for the surprisingly low abundances of bacterial feeding enrichment opportunists (notably Rhabditidae). Samples from 70–75 cm depths within the perched water table had extremely low SI values and highly variable EI values, indicating a wide range in enrichment and disturbance status of these soils. These samples were low in abundance ($n = 25 \pm 26$) and richness ($n = 4 \pm 4$), resulting in high variation in EI. Members of c-p classes 3–5, which include K-selected taxa, were not observed, thus accounting for the low SI. It is possible that decomposition products and anaerobic conditions may have created sufficient chemical disturbance to inhibit nematodes sensitive to environmental change, and thus skew these communities in favor of taxa in c-p classes 1 and 2.

Plectus has been proposed as a potential indicator taxon for chemical disturbances. It has been shown to negatively correlate to chemical fertilization; however, it positively correlates with organic amendments [54,89]. We found *Plectus* to be enriched within the grave (both 30–35 cm and ribcage samples) with a concomitant depletion of *Filenchus* abundances. This was in contrast to all other soils where *Filenchus* was more abundant than *Plectus*. *Plectus* and *Filenchus* are both classified as general opportunists (c-p 2), but occupy different trophic groups and so do not compete for resources. To our knowledge, this is the first observation of a potential inverse relationship between *Filenchus* and *Plectus,* suggesting either a potential interaction

between them or contrasting sensitivities. Further study is warranted as these taxa may be useful as indicator taxa for determining decomposition progress.

The mixed soil and adipocere sample collected within the ribcage of one donor contrasted sharply with nearby soil biogeochemistry and microbial ecology. In particular, total DNA, bacterial and fungal copy numbers, and microbial respiration rates were higher than any other soil collected within or outside of the grave. Microbial LAP and PDE enzymatic activity was also elevated, contrasting with the soils collected above and below the donors. Interestingly, despite the sample coming from inside a body cavity, there were no human-associated *Bacteroides* gene copies detected. Nematodes from the genus *Plectus* were also enriched in this sample compared with transect soils. The elevated respiration, abundant bacterial-feeding *Plectus*, and elevated enzymatic activity specific for protein and nucleic acid degradation suggests that C and N breakdown from carcass-derived organics was still actively occurring four years post-burial.

Conclusions

Subsurface human decomposition physically and chemically altered the surrounding soils in this system. After four years of burial in clay-rich sediments at the ARF, soils still preserved several physiochemical and biological indicators of interment and decay. At the base of the grave, elevated respiration rates and microbial gene abundances demonstrated that microbial communities were still present and active – likely because decomposition was active and on-going. Human-associated *Bacteroides* persisted at the base of the grave and demonstrated the potential for these microbes to serve as markers of human decomposition in the subsurface environment, at least in a system with protracted decay. Extracellular enzyme activity specific for chitin degradation (NAG) was elevated. The microbial communities persisting at the base of

the grave are able to utilize more recalcitrant C and N pools, likely driven by low oxygen availability. Soils were also elevated in DON, DOC, and ammonium, demonstrating that indicators of decomposition persisted. Nematode communities were affected by the presence of decomposing remains, supporting the idea that they may be potential indicators of carcass-derived nutrient enrichment in soil.

Given the constraints associated with human taphonomy research, and the destructive nature of the sampling (i.e. excavation), this study was not replicated (i.e. included only one test grave and one control grave) and does not include a time series examination of these changes. Future work on the repeatability of these results and the temporal dynamics will be needed to extrapolate beyond this system and build a consensus of the impacts of buried remains on soils.

Acknowledgments

Emily Grimes assisted with soil sample processing. Annette S. Engel provided access to IC equipment, and Audrey Paterson conducted grave water geochemical analyses. Thanks to DeBruyn and Mundorff Lab members and to graduate students in the Department of Anthropology for assisting with internment, excavation, and data collection. The authors would also like to thank the Forensic Anthropology Center at the University of Tennessee for their support and assistance facilitating this research.

Funding

This project was supported by Award No. 2016-DN-BX-0178, awarded by the National Institute of Justice, Office of Justice Programs, U.S. Department of Justice to AZM, JMD, JD, and ALE. The opinions, findings, and conclusions or recommendations expressed in this presentation are those of the authors and do not necessarily reflect those of the Department of Justice. The

funders had no role in study design, data collection and analysis, decision to publish, or preparation of the manuscript.

References

1. Bump JK, Webster CR, Vucetich JA, Peterson RO, Shields JM, Powers MD. Ungulate carcasses perforate ecological filters and create biogeochemical hotspots in forest herbaceous layers allowing trees a competitive advantage. Ecosystems. 2009; 12: 996-1007.
2. Damann FE, Tanittaisong A, Carter DO. Potential carcass enrichment of the University of Tennessee Anthropology Research Facility: a baseline survey of edaphic features. Forensic Science International. 2012; 222: 4-10.
3. Subalusky AL, Dutton CL, Rosi EJ, Post DM. Annual mass drownings of the Serengeti wildebeest migration influence nutrient cycling and storage in the Mara River. Proceedings of the National Academy of Sciences of the United States of America. 2017; 114: 7647-7652.
4. Keenan SW, Schaeffer SM, Jin VL, DeBruyn JM. Mortality hotspots: nitrogen cycling in forest soils during vertebrate decomposition. Soil Biology & Biochemistry. 2018; 121: 165-176.
5. Tomberlin JK, Barton BT, Lashley MA, Jordan HR. Mass mortality events and the role of necrophagous invertebrates. Current Opinion in Insect Science. 2017; 23: 7-12.
6. Smith CR, Glover AG, Treude T, Higgs ND, Amon DJ. Whale-fall ecosystems: recent insights into ecology, paleoecology, and evolution. Annual Review of Marine Science. 2015; 7: 571-506.
7. Bump JK, Peterson RO, Vucetich JA. Wolves modulate soil nutrient heterogeneity and foliar nitrogen by configuring the distribution of ungulate carcasses. Ecology. 2009; 90: 3159-3167.
8. DeBruyn JM, Hauther KA. Postmortem succession of gut microbial communities in diseased human subjects. PeerJ. 2017; doi.org/10.7717/peerj.3437.
9. Hauther KA, Cobaugh KL, Jantz LM, Sparer TE, DeBruyn JM. Estimating time since death

from postmortem human gut microbial communities. Journal of Forensic Sciences. 2015; 60: 1234-1240.

10. Cobaugh KL, Schaeffer SM, DeBruyn JM. Functional and structural succession of soil microbial communities below decomposing human cadavers. PLoS One. 2015; doi.org/10.1371/journal.pone.0130201.
11. Fonseca G, Hutchings P, Vieira DC, Gallucci F. Meiobenthic community underneath the carcass of a stingray: a snapshot after natural death. Aquatic Biology. 2011; 13: 27-33.
12. Aitkenhead-Peterson JA, Owings CG, Alexander MB, Larison N, Bytheway JA. Mapping the lateral extent of human cadaver decomposition with soil chemistry. Forensic Science International. 2012; 216: 127-134.
13. Vass AA, Bass WM, Wolt JD, Foss JE, Ammons JT. Time since death determinations of human cadavers using soil solution. Journal of Forensic Sciences. 1992;37: 1236-1253.
14. Dent BB, Forbes SL, Stuart BH. Review of human decomposition processes in soil. Environmental Geology. 2004; 45: 576-585.
15. Wheeler TA, Kavanagh KL. Soil biogeochemical responses to the deposition of anadromous fish carcasses in inland riparian forests of the Pacific Northwest, USA. Canadian Journal of Forest Research. 2017; 47: 1506-1516.
16. Carter DO, Yellowlees D, Tibbett M. Cadaver decomposition in terrestrial ecosystems. Naturwissenschaften. 2007; 94: 12-24.
17. Towne EG. Prairie vegetation and soil nutrient responses to ungulate carcasses. Oecologia. 2000; 122: 232-239.
18. Danell K, Berteaux D, Brathen KA. Effect of muskox carcasses on nitrogen concentration in tundra vegetation. Arctic. 2002; 55: 389-392.

19. Singh B, Minick KJ, Strickland MS, Wickings KG, Crippen TL, Tarone AM, et al. Temporal and spatial impact of human cadaver decomposition on soil bacterial and arthropod community structure and function. Frontiers in Microbiology. 2018; doi.org/10.3389/fmicb.2017.02616.
20. Rodriguez WC, Bass WM. Insect activity and its relationship to decay-rates of human cadavers in East Tennessee. Journal of Forensic Sciences. 1983;28: 423-432.
21. Payne JA, King EW, Beinhart G. Arthropod succession and decomposition of buried pigs. Nature. 1968; 219: 1180-1181.
22. Benbow ME, Lewis AJ, Tomberlin JK, Pechal JL. Seasonal necrophagous insect community assembly during vertebrate carrion decomposition. Journal of Medical Entomology. 2013; 50: 440-450.
23. Damann FE, Williams DE, Layton AC. Potential use of bacterial community succession in decaying human bone for estimating postmortem interval. Journal of Forensic Sciences. 2015; 60: 844-850.
24. Pechal JL, Crippen TL, Tarone AM, Lewis AJ, Tomberlin JK, Benbow ME. Microbial community functional change during vertebrate carrion decomposition. PLoS One. 2013; doi.org/10.1371/journal.pone.0079035.
25. Carter DO, Tibbett M. Taphonomic mycota: fungi with forensic potential. Journal of Forensic Sciences. 2003; 48: 168-171.
26. Metcalf JL, Xu ZZ, Weiss S, Lax S, Van Treuren W, Hyde ER, et al. Microbial community assembly and metabolic function during mammalian corpse decomposition. Science. 2016; 351: 158-162.
27. Finley SJ, Pechal JL, Benbow ME, Robertson BK, Javan GT. Microbial signatures of

cadaver gravesoil during decomposition. Microbial Ecology. 2016; 71: 524-529.

28. Lauber CL, Metcalf JL, Keepers K, Ackermann G, Carter DO, Knight R. Vertebrate decomposition is accelerated by soil microbes. Applied and Environmental Microbiology. 2014; 80: 4920-4929.
29. Lashley MA, Jordan HR, Tomberlin JK, Barton BT (2017) Indirect effects of larval dispersal following mass mortality events. Ecology. 2017; 99: 491-493.
30. Janaway RC, Percival SL, Wilson AS. Decomposition of human remains. In: Percival SL, editor. Microbioloy and aging. Humana Press; 2009. pp. 313-334.
31. Carter DO, Yellowlees D, Tibbett M. Moisture can be the dominant environmental parameter governing cadaver decomposition in soil. Forensic Science International. 2010; 200: 60-66.
32. Carter DO, Yellowlees D, Tibbett M. Temperature affects microbial decomposition of cadavers (*Rattus rattus*) in contrasting soils. Applied Soil Ecology. 2008; 40: 129-137.
33. Tibbett M, Carter DO, Haslam T, Major R, Haslam R. A laboratory incubation method for determining the rate of microbiological degradation of skeletal muscle tissue in soil. Journal of Forensic Sciences. 2004; 49: 560-565.
34. Rodriguez WC, Bass WM. Decomposition of buried bodies and methods that may aid in their location. Journal of Forensic Sciences. 1985; 30: 836-852.
35. Hopkins DW, Wiltshire PEJ, Turner BD. Microbial characteristics of soils from graves: an investigation at the interface of soil microbiology and forensic science. Applied Soil Ecology. 2000; 14: 283-288.
36. Wilson AS, Janaway RC, Holland AD, Dodson HI, Baran E, Pollard AM, et al. Modelling the buried human body environment in upland climes using three contrasting field sites. Forensic Science International. 2007; 169: 6-18.

37. Szelecz I, Fournier B, Seppey C, Amendt J, Mitchell E. Can soil testate amoebae be used for estimating the time since death? A field experiment in a deciduous forest. Forensic Science International. 2014; 236: 90-98.

38. Szelecz I, Sorge F, Seppey CVW, Mulot M, Steel H, Neilson R, et al. Effects of decomposing cadavers on soil nematode communities over a one-year period. Soil Biology & Biochemistry. 2016; 103: 405-416.

39. Seppey CVW, Fournier B, Szelecz I, Singer D, Mitchell EAD, Lara E. Response of forest soil euglyphid testate amoebae (Rhizaria: Cercozoa) to pig cadavers assessed by high-throughput sequencing. International Journal of Legal Medicine. 2016; 130: 551-562.

40. Braig HR, Perotti MA. Carcases and mites. Experimental and Applied Acarology. 2009; 49: 45-84.

41. Bongers T, Ferris H. Nematode community structure as a bioindicator in environmental monitoring. Trends in Ecology & Evolution. 1999; 14: 224-228.

42. Bongers T. The maturity index: an ecological measure of environmental disturbance based on nematode species composition. Oecologia. 1990; 83: 14-19.

43. Neher DA. Role of nematodes in soil health and their use as indicators. Journal of Nematology. 2001; 33: 161-168.

44. Ferris H, Bongers T. Nematode indicators of organic enrichment. Journal of Nematology. 2006; 38: 3-12.

45. Metcalf JL, Parfrey LW, Gonzalez A, Lauber CL, Knights D, Ackermann G, et al. (2013) A microbial clock provides an accurate estimate of the postmortem interval in a mouse model system. Elife. 2013; doi/org/10.7554/eLife.01104.

46. Szelecz I, Losch S, Seppey CVW, Lara E, Singer D, Sorge F, et al. Comparative analysis of

bones, mites, soil chemistry, nematodes and soil micro-eukaryotes from a suspected homicide to estimate the post-mortem interval. Scientific Reports. 2018; doi.org/10.1038/s41598-017-18179-z.

47. Briar S, Tenuta M, Barker C, Entz M. Soil nematode community response to long-term crop rotation, organic management and prairie restoration in the Red River Valley of central North America. Journal of Nematology. 2009; 41: 313-313.
48. Briar SS, Barker C, Tenuta M, Entz MH. Soil nematode responses to crop management and conversion to native grasses. Journal of Nematology. 2012; 44: 245-254.
49. Crotty FV, Fychan R, Sanderson R, Rhymes JR, Bourdin F, Scullion J, et al. Understanding the legacy effect of previous forage crop and tillage management on soil biology, after conversion to an arable crop rotation. Soil Biology & Biochemistry. 2016; 103: 241-252.
50. Höss S, Nguyen HT, Menzel R, Pagel-Wieder S, Miethling-Graf R, Tebbe CC, et al. Assessing the risk posed to free-living soil nematodes by a genetically modified maize expressing the insecticidal Cry3Bb1 protein. Science of the Total Environment. 2011; 409: 2674-2684.
51. Ortiz V, Phelan S, Mullins E. A temporal assessment of nematode community structure and diversity in the rhizosphere of cisgenic *Phytophthora infestans*-resistant potatoes. BMC Ecology. 2016; doi.org/10.1186/s12898-016-0109-5.
52. Porazinska DL, McSorley R, Duncan LW, Graham JH, Wheaton TA, Parsons LR. Nematode community composition under various irrigation schemes in a citrus soil ecosystem. Journal of Nematology. 1998; 30: 170-178.
53. Porazinska DL, Duncan LW, McSorley R, Graham JH. Nematode communities as indicators of status and processes of a soil ecosystem influenced by agricultural management practices.

Applied Soil Ecology. 1999; 13: 69-86.

54. Zhao J, Neher DA. Soil nematode genera that predict specific types of disturbance. Applied Soil Ecology. 2013; 64: 135-141.

55. Althoff PS, Todd TC, Thien SJ, Callaham MA. Response of soil microbial and invertebrate communities to tracked vehicle disturbance in tallgrass prairie. Applied Soil Ecology. 2009; 43: 122-130.

56. Blakely JK, Neher DA, Spongberg AL. Soil invertebrate and microbial communities, and decomposition as indicators of polycyclic aromatic hydrocarbon contamination. Applied Soil Ecology. 2002; 21: 71-88.

57. Jantz LM, Jantz RL. The Anthropology Research Facility: the outdoor laboratory of the Forensic Anthropology Center, University of Tennessee. In: Warren MW, Walsh-Haney HA, Freas LE, editors. The forensic anthropology laboratory. Boca Raton, FL: CRC Press; 2008. pp. 7-21.

58. Web Soil Survey. Natural Resources Conservation Service, United States Department of Agriculture. https://websoilsurvey.sc.egov.usda.gov/. Cited 13 February 2018.

59. Rhine ED, Sims GK, Mulvaney RL, Pratt EJ. Improving the Berthelot reaction for determining ammonium in soil extracts and water. Soil Science Society of America Journal. 1998; 62: 473-480.

60. Belser LW, Mays EL. Specific inhibition of nitrite oxidation by chlorate and its use in assessing nitrification in soils and sediments. Applied and Environmental Microbiology. 1980; 39: 505-510.

61. Hart SC, Stark JM, Davidson EA, Firestone MK. Nitrogen mineralization, immobilization, and nitrification. In: Weaver RW, Angle, S., Bottomley, P., Bezdicek, D., Smith, S.,

Tabatabai, A., Wollum, A., editors. Methods of soil analysis, part 2: microbiological and biochemical properties. Madison, Wisconsin: Soil Science Society of America; 1994. pp. 985-1018.

62. Keeney DR, Nelson MH. Nitrogen—inorganic forms. In: Page AL, Miller DR, Keeney DR, editors. Methods of soil analysis, part 2: chemical and microbiological methods. Madison, WI: American Society of Agronomy and the Soil Science Society of America; 1982. pp. 643-698.
63. Doyle A, Weintraub MN, Schimel JP. Persulfate digestion and simultaneous colorimetric analysis of carbon and nitrogen in soil extracts. Soil Science Society of America Journal. 2004; 68: 669-676.
64. Doane TA, Horwath WR. Spectrophotometric determination of nitrate with a single reagent. Analytical Letters. 2003; 36: 2713-2722.
65. Bell CW, Fricks BE, Rocca JD, Steinweg JM, McMahon SK, Wallenstein MD. High-throughput fluorometric measurement of potential soil extracellular enzyme activities. Journal of Visualized Experiments. 2013; doi.org/10.3791/50961.
66. Nannipieri P, Giagnoni L, Landi L, Renella G. Role of phosphatase enzymes in soil. In: Bunemann EK, Oberson A, Frossard E, editors. Phosphorus in action: biological processes in soil phosphorus cycling. Berlin: Springer-Verlag; 2011. pp. 215-243.
67. Layton A, McKay L, Williams D, Garrett V, Gentry R, Saylor G. Development of *Bacteroides* 16S rRNA gene TaqMan-based real-time PCR assays for estimation of total, human, and bovine fecal pollution in water. Applied and Environmental Microbiology. 2006; 72: 4214-4224.
68. Jenkins WR. A rapid centrifugal-flotation technique for separating nematodes from soil.

Plant Disease Reporter. 1964; 48: 692-692.

69. Geraert E. The Tylenchidae of the World. Ghent: Academia Press; 2008.
70. Siddiqi MR. Tylenchida, Parasites of Plants and Insects. 2nd Ed. Wallingford, UK: CABI Publishing; 2000.
71. Allen MW, Noffsinger EM. Revision of the genus *Anaplectus* (Nematoda: Plectidae). Proceedings of the Helminthological Society of Washington. 1968; 35: 77-91.
72. Andrassy I. The genus *Plectus* Bastian, 1865 and its nearest relatives (Nematoda: Plectidae). Acta Zoologica Hungarica. 1985; 31: 1-52.
73. Zell H. Die gattung *Plectus* Bastian, 1865 *sensu lato* (Nematoda, Plectidae): ein betrag zur ökologie, biogeographie, phylogenie und taxonomie der Plectidae. Andrias. 1993; 11: 3-171.
74. Yeates GW, Bongers T, Degoede RGM, Freckman DW, Georgieva SS. Feeding habits in soil nematode families and genera—an outline for soil ecologists. Journal of Nematology. 1993; 25: 315-331.
75. Bongers T, Bongers M. Functional diversity of nematodes. Applied Soil Ecology. 1998; 10: 239-251.
76. Pepper IL, Gerba CP, Gentry TJ, editors. Environmental Microbiology. Third edition; 2015.
77. Ferris H, Bongers T, de Goede RGM. A framework for soil food web diagnostics: extension of the nematode faunal analysis concept. Applied Soil Ecology. 2001; 18: 13-29.
78. American Public Health Association. Standard methods for the examination of water and wastewater. http://www.standard-methods.org. Cited 13 March 2017.
79. Team RC. R: A language and environment for statistical computing. Vienna, Austria. 2018. Available from: https://www.R-project.org/
80. Fox J, Weisberg S. An (R) Companion to Applied Regression. Second Edition. Thousand

Oaks CA: Sage; 2011. Available from: http://socserv.socsci.mcmaster.ca/jfox/Books/companion

81. Gill-King H. Chemical and ultrastructural aspects of decomposition. In: Haglund WD, Sorg MH, editors. Forensic taphonomy: the postmortem fate of human remains. Boca Raton, Florida: CRC Press; 1997. pp. 93-108.
82. Fiedler S, Graw M. Decomposition of buried corpses, with special reference to the formation of adipocere. Naturwissenschaften. 2003; 90: 291-300.
83. Ettema CH, Bongers T. Characterization of nematode colonization and succession in disturbed soil using the Maturity Index. Biology and Fertility of Soils. 1993; 16: 79-85.
84. Ruess L. Nematode soil faunal analysis of decomposition pathways in different ecosystems. Nematology. 2003; 5: 179-181.
85. Meng FX, Ou W, Li Q, Jiang Y, Wen DZ. Vertical distribution and seasonal fluctuation of nematode trophic groups as affected by land use. Pedosphere. 2006; 16: 169-176.
86. Arieira GD, Santiago DC, Franchini JC, Guimaraes MD. Depth-stratified soil sampling for assessing nematode communities. Semina: Ciências Agrárias. 2016; 37: 715-727.
87. Ferris H, Matute MM. Structural and functional succession in the nematode fauna of a soil food web. Applied Soil Ecology. 2003; 23: 93-110.
88. Bongers T, De Goede RGN, Korthals GW, Yeates GW. Proposed changes of c-p classification for nematodes. Russian Journal of Nematology. 1995; 3: 61-62.
89. Fiscus DA, Neher DA. Distinguishing sensitivity of free-living soil nematode genera to physical and chemical disturbances. Ecological Applications. 2002; 12: 565-575.

Appendix 1

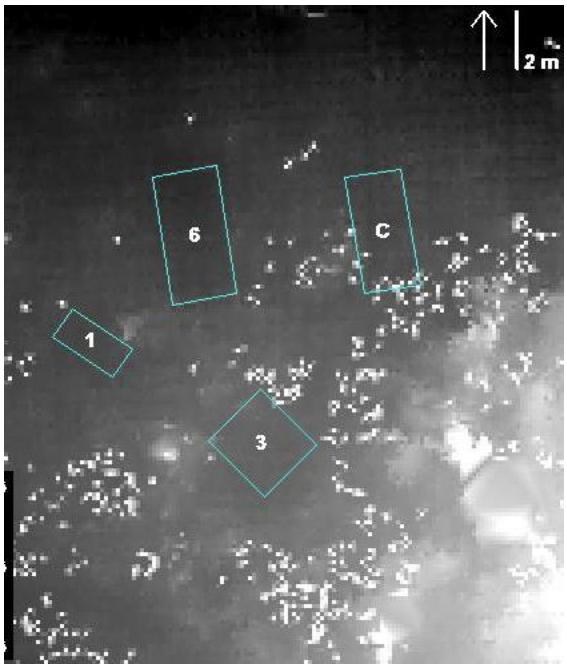

Figure 1.1: Aerial image of study site. The multi-individual grave is indicated by "3", and the control grave by "C". The other two boxes (6 and 1) represent other graves not used in this study. Arrow indicates North. Figure adapted from: Corcoran, K. A., et al. (2018). "A novel application of terrestrial LIDAR to characterize elevation change at human grave surfaces in support of narrowing down possible unmarked grave locations." Forensic Science International 289: 320-328.

Table 1.1: Biometric data of deceased human subject donors used in the study.

Individual	Sex	Age at Death	Weight (kg)	Stature (cm)
A	Female	68	60	164
B	Male	63	71	166
C	Male	63	52	168

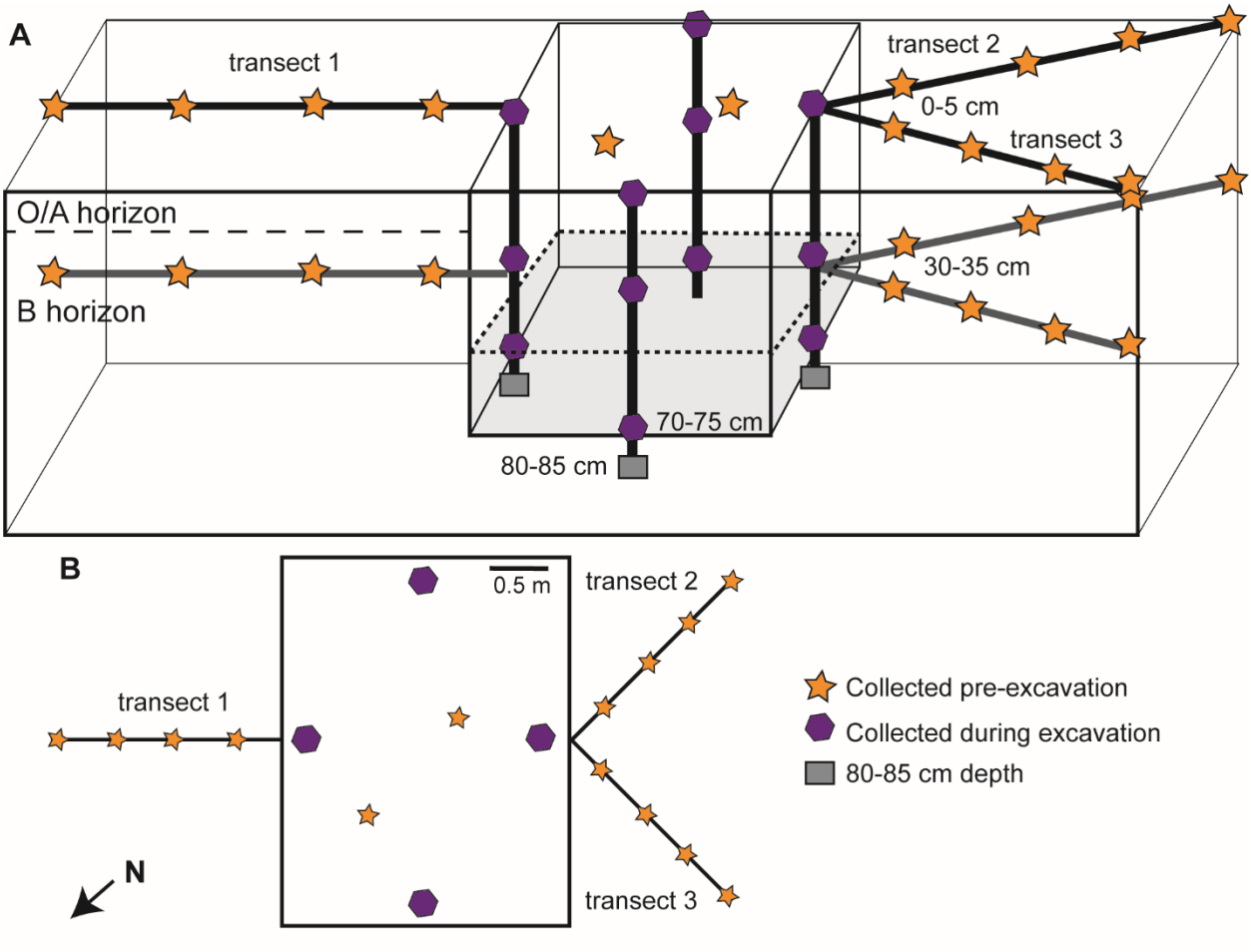

Figure 1.2: Soil sample locations within and outside of the multi-individual grave. (A) Cross-sectional view of sample locations. Samples were collected along three lateral transects (orange stars), within the disturbed grave soils (purple hexagons), and below the grave floor (gray squares) during excavation. Shading within the grave indicates the approximate depth of donor placement. Soils along lateral transects were collected from surface (0–5 cm) and subsurface (30–35 cm) soils. Soils within the grave were also collected at the base of the grave (70–75 cm) and below the grave (85–90 cm). (B) Top down map view of sampling locations and transect orientations.

Table 1.2: Measured soil physicochemical parameters, presented as means and standard deviations of transects (distances of 0.5, 1, 1.5, 2 m) and grave soils (distance of 0 m). n = 3 samples from three independent transects or 3 grave soil samples. DON = dissolved organic nitrogen; DOC = dissolved organic carbon. * = sample collected from the ribcage.

Distance from grave (m)	Depth (cm)	Gravimetric moisture	pH	Conductivity ($\mu S\ cm^{-1}$)	Ammonium ($\mu g\ N\ gdw^{-1}$)	Nitrification potential ($mg\ NO_2\ gdw^{-1}\ d^{-1}$)	Respiration ($CO_2\ gdw^{-1}\ d^{-1}$)	DOC ($\mu g\ C\ gdw^{-1}$)	Nitrate ($\mu g\ N\ gdw^{-1}$)	DON ($\mu g\ N\ gdw^{-1}$)	Bacterial gene copies ($x\ 10^8$) gdw^{-1}	Fungal gene copies ($x\ 10^8$) gdw^{-1}
2	0-5	0.377 ± 0.03	6.75 ± 0.25	29.92 ± 9.75	7.39 ± 1.8	0.126 ± 0.10	30.9 ± 5.6	2.94 ± 0.6	3.31 ± 2.5	11.31 ± 0.8	125 ± 19	5.3 ± 3.8
	30-35	0.309 ± 0.02	6.05 ± 0.77	10.91 ± 2.83	2.54 ± 1.2	0.039 ± 0.03	6.18 ± 1.2	5.26 ± 6.2	0.451 ± 0.21	12.69 ± 8.3	28.5 ± 39	3.5 ± 3.0
1.5	0-5	0.397 ± 0.04	6.82 ± 0.19	28.37 ± 9.83	9.00 ± 4.7	0.174 ± 0.14	37.6 ± 6.9	3.09 ± 0.9	3.34 ± 1.3	16.41 ± 6.3	134 ± 76	5.5 ± 3.9
	30-35	0.335 ± 0.03	6.28 ± 0.73	13.3 ± 7.15	2.86 ± 0.6	0.038 ± 0.03	10.1 ± 0.8	3.52 ± 2.0	0.606 ± 0.35	8.14 ± 2.1	57.2 ± 43	4.1 ± 4.9
1	0-5	0.374 ± 0.02	6.68 ± 0.22	30.75 ± 12.05	5.75 ± 0.5	0.120 ± 0.05	31.0 ± 8.9	2.16 ± 0.5	3.74 ± 2.3	10.19 ± 1.2	123 ± 64	5.8 ± 2.7
	30-35	0.267 ± 0.03	6.60 ± 0.67	20.75 ± 1.36	2.75 ± 0.3	0.023 ± 0.01	6.78 ± 2.5	2.42 ± 1.8	0.708 ± 0.23	5.09 ± 0.3	37.1 ± 14	2.2 ± 0.56
0.5	0-5	0.315 ± 0.02	6.77 ± 0.22	27.04 ± 9.61	5.57 ± 2.0	0.053 ± 0.03	22.6 ± 8.7	1.54 ± 0.5	2.65 ± 1.1	10.03 ± 3.6	127 ± 32	8.3 ± 1.3
	30-35	0.236 ± 0.01	6.74 ± 0.48	12.74 ± 1.75	2.99 ± 1.3	0.036 ± 0.03	8.39 ± 3.2	0.99 ± 0.5	0.943 ± 0.48	5.02 ± 1.0	25.6 ± 17	2.3 ± 1.8
0	0-5	0.321 ± 0.01	6.40 ± 0.38	18.26 ± 7.35	4.23 ± 1.8	0.011 ± 0.04	20.0 ± 7.7	2.18 ± 0.6	2.23 ± 0.6	7.51 ± 1.4	40.2 ± 19	5.9 ± 2.1
	30-35	0.375 ± 0.02	6.21 ± 0.13	19.48 ± 10.7	3.84 ± 1.4	0.040 ± 0.01	21.0 ± 21	1.93 ± 0.8	3.55 ± 2.1	9.98 ± 2.3	21.0 ± 26	21 ± 35
	40*	0.974	6.36	48.57	14.181	0.227	273	5.50 ± 0.6	0.839	22.62	629 ± 12	796 ± 18
	70-75	0.464 ± 0.04	7.20 ± 0.51	134.8 ± 38.1	742 ± 389	-0.061 ± 0.03	83.5 ± 29	6.96 ± 4.6	1.04 ± 1.1	126.1 ± 37	26.2 ± 17	20 ± 13
	85-90	0.335 ± 0.02	7.66 ± 0.36	139.9 ± 16.4	1075 ± 390	0.006 ± 0.03	23.6 ± 2.9	5.19 ± 2.5	3.22 ± 3.0	110.4 ± 13	0.51 ± 0.7	0.02 ± 0.03
Control off-grave	0-5	0.476	7.04	40.40	8.043	0.569	38.4	4.43	5.530	16.490	234 ± 2.4	79 ± 0.42
	30-35	0.312	7.47	21.06	2.636	0.048	7.72	1.09	0.851	6.174	29 ± 0.32	1.9 ± 0.061
Control grave	0-5	0.342	6.66	14.19	4.956	0.040	31.7	1.60	0.949	7.632	101 ± 1.2	6.0 ± 0.23
	30-35	0.309	6.30	4.316	2.099	0.054	5.56	2.13	0.947	7.016	16 ± 0.096	1.7 ± 0.009

Table 1.3: Measured soil physicochemical and biogeochemical parameters for all samples taken during the study. Summary statistics of the data are presented in Table 2. Off-grave control samples from an undisturbed location are indicated with *; Samples from the control grave (excavated but no donors interred) are indicated with ł. DON=dissolved organic nitrogen; DOC=dissolved organic carbon.

Sample	Depth (cm)	Distance from grave (m)	Collection date	pH	Conductivity (µS cm^{-1})	Ammonium (µg N gdw^{-1})	% soil moisture	Nitrate (µg N gdw^{-1})	DON (µg N gdw^{-1})	DOC (µg C gdw^{-1})	Nitrification potential (mg NO_2 gdw^{-1} d^{-1})	Respiration (CO_2 gdw^{-1} d^{-1})
MGS_001_0*	0	5	2/14/2017	7.04	40.40	8.04	0.48	5.53	16.49	4.43	0.57	38.44
MGS_001_30*	30	5	2/14/2017	7.47	21.06	2.64	0.31	0.85	6.17	1.09	0.05	7.72
MGS_002_0ł	0	5	2/14/2017	6.66	14.19	4.96	0.34	0.95	7.63	1.60	0.04	31.73
MGS_002_30ł	30	5	2/14/2017	6.30	4.316	2.10	0.31	0.95	7.02	2.13	0.05	5.56
MGS_003_0	0	2	2/14/2017	6.97	22.08	9.41	0.37	1.14	11.42	3.58	0.08	28.11
MGS_003_30	30	2	2/14/2017	6.23	8.429	1.26	0.28	0.31	3.47	0.87	0.07	5.64
MGS_004_0	0	1.5	2/14/2017	7.01	32.05	14.30	0.41	2.43	16.65	3.70	0.09	39.76
MGS_004_30	30	1.5	2/14/2017	5.92	9.206	2.28	0.37	0.52	7.24	4.44	0.06	9.60
MGS_005_0	0	1	2/14/2017	6.52	17.76	5.12	0.37	1.08	8.92	1.53	0.07	24.09
MGS_005_30	30	1	2/14/2017	5.83	21.94	2.43	0.25	0.69	5.33	4.49	0.02	5.90
MGS_006_0	0	0.5	2/14/2017	6.55	21.94	7.65	0.32	1.43	9.41	1.54	0.03	21.03
MGS_006_30	30	0.5	2/14/2017	6.22	11.34	2.60	0.24	0.84	5.43	1.56	0.03	4.68
MGS_007_0	0	1.5	2/14/2017	6.82	44.00	5.59	0.44	4.81	22.56	3.56	0.34	45.75
MGS_007_30	30	1.5	2/14/2017	7.12	21.51	3.45	0.31	1.00	10.57	1.23	0.05	11.27
MGS_008_0	0	2	2/14/2017	6.80	40.83	5.83	0.41	6.07	12.01	2.85	0.24	37.35
MGS_008_30	30	2	2/14/2017	6.71	10.32	2.80	0.32	0.69	19.51	2.52	0.04	7.56
MGS_009_0	0	1	2/14/2017	6.93	41.56	6.14	0.36	5.38	10.32	2.42	0.18	41.08
MGS_009_30	30	1	2/14/2017	6.94	21.05	3.00	0.30	0.49	5.21	1.53	0.01	9.84
MGS_010_0	0	0.5	2/14/2017	6.77	21.05	3.57	0.29	2.85	6.81	0.99	0.03	14.85
MGS_010_30	30	0.5	2/14/2017	6.86	12.19	4.40	0.24	1.46	5.72	0.77	0.07	10.21
MGS_011_0	0	2	2/14/2017	6.48	26.84	6.93	0.35	2.71	10.52	2.39	0.06	27.22
MGS_011_30	30	2	2/14/2017	5.2	13.99	3.56	0.32	0.35	15.08	12.40	0.01	5.35
MGS_012_0	0	1.5	2/14/2017	6.63	24.50	7.10	0.35	2.79	10.02	2.01	0.09	27.26
MGS_012_30	30	1.5	2/14/2017	5.79	9.063	2.85	0.33	0.31	6.60	4.89	0.01	9.47
MGS_013_0	0	1	2/14/2017	6.59	32.94	5.98	0.39	4.74	11.33	2.53	0.11	27.72
MGS_013_30	30	1	2/14/2017	7.03	19.27	2.80	0.25	0.94	4.74	1.24	0.04	5.20
MGS_014_0	0	0.5	2/14/2017	6.99	38.13	5.49	0.34	3.68	13.87	2.09	0.09	32.03
MGS_014_30	30	0.5	2/14/2017	7.16	14.70	1.97	0.23	0.52	3.91	0.65	0.01	10.26
MGS_015_0	0	0	2/14/2017	6.39	13.08	3.00	0.31	1.94	6.81	2.75	0.02	12.06
MGS_016_0	0	0	2/14/2017	5.73	10.26	5.35	0.31	2.58	7.88	3.00	0.00	12.61
MGS_017_0	0	0	3/8/2017	6.39	16.28	2.69	0.33	1.95	6.35	1.68	0.02	27.34
MGS_018_0	0	0	3/8/2017	6.37	21.99	7.36	0.33	2.85	10.03	2.42	0.00	188.93
MGS_019_0	0	0	3/8/2017	6.68	17.07	3.43	0.31	1.32	6.23	1.64	-0.05	19.93
MGS_020_0	0	0	3/8/2017	6.83	30.90	3.55	0.34	2.74	7.73	1.60	0.07	28.02
MGS_017_30	30	0	3/9/2017	6.06	31.14	5.47	0.40	5.58	10.92	2.89	0.04	45.13
MGS_017_40	40	0	3/9/2017	6.36	48.57	14.18	0.97	0.84	22.62	5.50	0.23	273.29
MGS_019_30	30	0	3/9/2017	6.31	17.24	2.77	0.36	3.63	11.66	1.55	0.05	10.52
MGS_020_30	30	0	3/9/2017	6.26	10.06	3.27	0.37	1.46	7.37	1.35	0.03	7.20
MGS_017_70	70	0	3/14/2017	6.55	96.31	664.81	0.51	0.33	134.53	7.24	-0.04	93.03
MGS_017_85	85	0	3/14/2017	7.3	151.1	821.85	0.31	1.89	95.86	2.35	-0.03	26.73
MGS_018_70	70	0	3/14/2017	7.36	164	999.74	0.46	0.26	122.26	5.65	-0.09	98.14
MGS_018_85	85	0	3/14/2017	7.65	147.4	1525.02	0.33	6.61	116.62	6.92	0.04	21.10
MGS_019_70	70	0	3/14/2017	7.11	107.9	224.02	0.46	1.82	78.65	1.96	-0.03	40.62
MGS_020_70	70	0	3/14/2017	7.78	170.8	1078.47	0.42	0.23	169.11	13.00	-0.09	102.06
MGS_020_85	85	0	3/14/2017	8.02	121.1	879.42	0.36	1.14	118.71	6.30	0.00	23.01

Table 1.4: The effects of depth and distance on soil physiochemistry and biology. Results of ANOVAs comparing depths or five distances (0, 0.5, 1.0, 1.5, and 2.0 m), as well as interaction effects. Significant differences as a function of depth or distance from the grave are bolded (based on one-way ANOVAs; $p < 0.05$). Rates are presented per gram dry weight (gdw). PDE = phosphodiesterase activity; NAG = N-acetyl-β-glucoseaminidase activity; CB = β-D-cellulobiosidase activity; LAP = leucine aminopeptidase activity; COL = collagenase activity.

	Depth		Distance		Depth*Distance	
	p	F	p	F	P	F
Gravimetric moisture	**<0.001**	36.6	**<0.001**	12.48	**<0.001**	16.45
pH	0.07	3.61	0.39	1.08	**<0.001**	14.47
Conductivity (μS cm^{-1})	**<0.001**	19.00	0.535	0.80	**<0.001**	38.57
Ammonium (μg NH_4-N gdw^{-1})	**<0.001**	24.33	0.417	1.02	**<0.001**	16.06
Nitrification potential rate (mg NO_2^--N gdw^{-1} day^{-1})	**0.008**	8.47	0.14	1.93	**0.010**	7.34
Respiration (μg C gdw^{-1} day^{-1})	**<0.001**	32.20	0.588	0.72	0.081	3.24
Dissolved organic carbon (DOC) (mg CO_2 gdw^{-1})	0.557	0.36	0.177	1.73	0.620	0.25
Nitrate (μg NO_3^--N gdw^{-1})	**<0.001**	14.55	0.528	0.82	**0.002**	12.05
Dissolved organic nitrogen (DON) (μg N gdw^{-1})	**0.009**	8.13	**<0.001**	15.29	**<0.001**	22.13
PDE (nmols hr^{-1} gdw^{-1})	0.243	1.438	0.838	0.354	0.211	1.62
NAG (nmols hr^{-1} gdw^{-1})	**0.014**	7.089	0.078	2.417	**0.003**	9.80
CB (nmols hr^{-1} gdw^{-1})	**<0.001**	24.336	**0.031**	3.225	**<0.001**	23.52
LAP (μmols hr^{-1} gdw^{-1})	**<0.001**	61.319	**0.016**	3.833	**<0.001**	44.95
COL (U hr^{-1} gdw^{-1})	0.386	0.779	0.136	1.953	0.648	7.22
Bacterial copy numbers gdw^{-1}	**<0.001**	31.278	**0.039**	3.005	**<0.001**	15.15
Fungal copy numbers gdw^{-1}	0.901	0.0159	0.393	1.071	0.520	0.422
Total DNA (ng gdw^{-1})	**<0.001**	30.334	0.053	2.738	**<0.001**	18.93

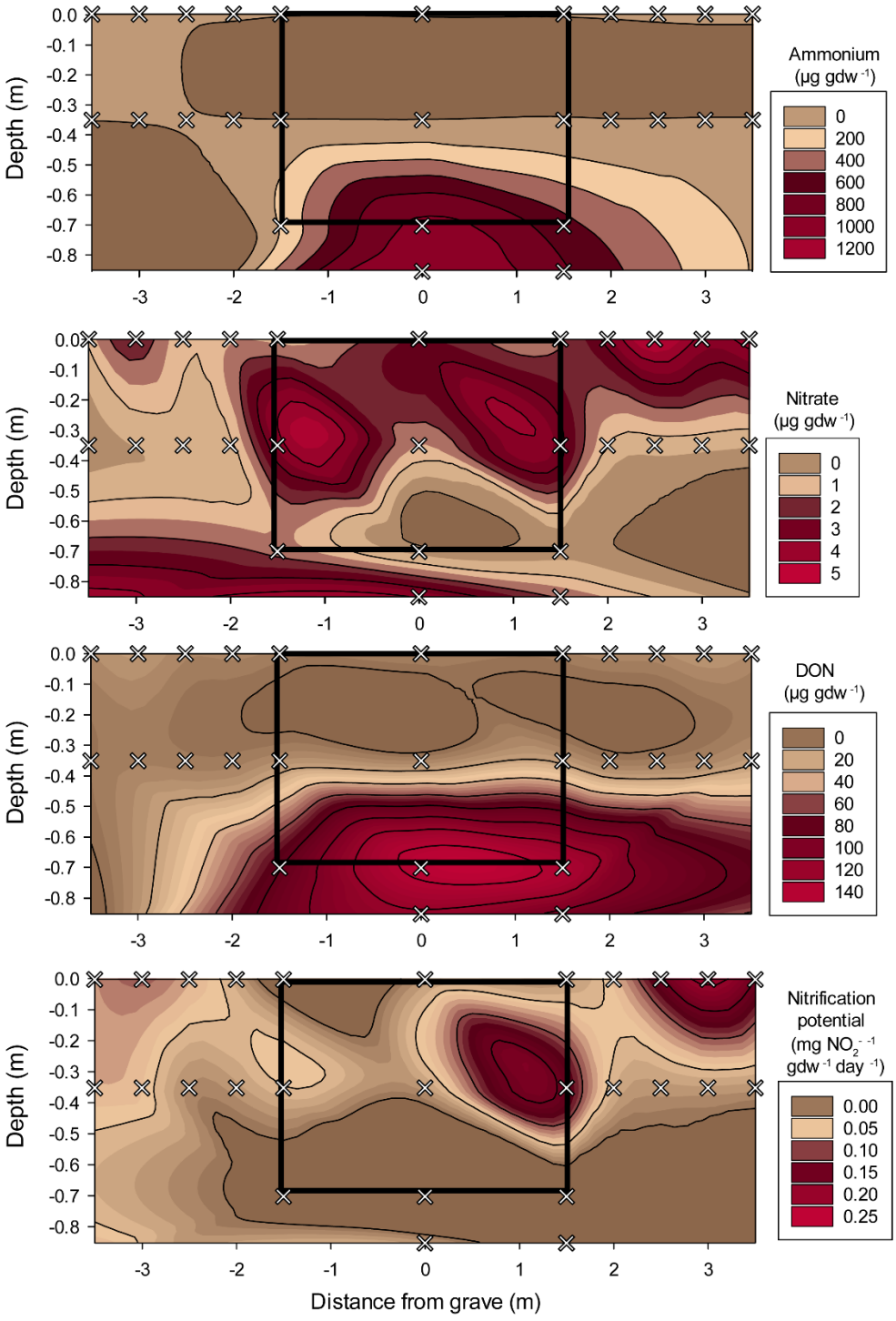

Figure 1.3: Cross-sectional contour maps of nitrogen concentrations or flux rates measured along lateral transects and within the multi–individual grave. Grey x indicate soil sampling locations. The black box in each figure outlines the excavated area of the grave.

This resource was prepared by the author(s) using Federal funds provided by the U.S. Department of Justice. Opinions or points of view expressed are those of the author(s) and do not necessarily reflect the official position or policies of the U.S. Department of Justice.

Table 1.5: Measured soil enzyme activities for all samples taken during the study. Sample descriptions (location and collection date) are provided in Table 3. Mean and standard deviations of these data are shown in Table 2 and Figure 4. Off-grave control samples from an undisturbed location are indicated with *; Samples from the control grave (excavated but no donors interred) are indicated with ǂ. PDE = phosphodiesterase activity; NAG = N-acetyl-β-glucoseaminidase activity; CB = β-D-cellulobiosidase activity; LAP = leucine aminopeptidase activity; COL = collagenase activity.

Sample	PDE (nmol gdw^{-1} hr^{-1})	NAG (nmol gdw^{-1} hr^{-1})	CB (nmol gdw^{-1} hr^{-1})	LAP µmol gdw^{-1} hr^{-1})	COL (U gdw^{-1} hr^{-1})	Fungal gene copies gdw^{-1}	Bacterial gene copies gdw^{-1}
MGS_001_0*	38.18	103.97	106.51	1.31	-2.90	7.91E+08	2.34E+10
MGS_001_30*	14.87	26.10	6.23	0.19	-1.25	1.93E+08	2.95E+09
MGS_002_0ǂ	15.18	111.46	48.34	0.61	3.88	5.96E+08	1.01E+10
MGS_002_30ǂ	4.23	80.49	5.96	0.10	0.39	1.65E+08	1.65E+09
MGS_003_0	17.59	220.65	46.19	0.57	1.96	4.88E+08	1.05E+10
MGS_003_30	4.02	71.62	7.70	0.07	0.64	1.33E+08	6.07E+08
MGS_004_0	19.79	162.33	58.98	0.77	-7.18	9.96E+08	2.23E+10
MGS_004_30	9.46	21.93	3.91	0.13	-4.29	8.73E+07	3.49E+09
MGS_005_0	18.15	55.25	15.78	0.84	3.20	4.93E+08	1.96E+10
MGS_005_30	4.70	10.63	1.22	0.11	-0.30	1.64E+08	2.93E+09
MGS_006_0	15.18	47.85	13.30	0.76	2.22	8.68E+08	1.55E+10
MGS_006_30	6.10	11.68	0.42	0.12	6.19	1.72E+08	3.13E+09
MGS_007_0	24.43	67.10	31.00	1.56	-3.47	4.17E+08	9.03E+09
MGS_007_30	21.57	19.16	5.30	0.40	1.26	9.75E+08	1.07E+10
MGS_008_0	23.48	71.20	28.16	1.33	4.55	5.62E+08	1.26E+10
MGS_008_30	18.85	15.32	7.12	0.21	3.25	6.92E+08	7.32E+09
MGS_009_0	33.87	16.09	12.43	0.73	0.64	3.59E+08	8.03E+09
MGS_009_30	20.84	13.52	2.36	0.25	2.54	2.19E+08	5.34E+09
MGS_010_0	20.74	16.54	6.70	0.48	5.92	6.77E+08	1.34E+10
MGS_010_30	15.91	12.25	3.91	0.24	-2.03	4.26E+08	3.94E+09
MGS_011_0	28.11	29.04	10.34	1.18	-0.87	5.36E+08	1.43E+10
MGS_011_30	8.13	6.77	1.71	0.04	-5.55	2.11E+08	6.27E+08
MGS_012_0	23.86	27.16	11.20	0.80	1.70	2.45E+08	9.03E+09
MGS_012_30	10.33	8.86	2.59	0.12	-2.60	1.69E+08	3.03E+09
MGS_013_0	30.34	25.59	17.74	1.27	0.34	8.84E+08	9.23E+09
MGS_013_30	16.24	12.78	3.50	0.28	-0.15	2.75E+08	2.87E+09
MGS_014_0	31.69	25.49	19.43	1.11	1.16	9.33E+08	9.22E+09
MGS_014_30	11.98	14.10	4.06	0.24	1.19	9.02E+07	6.09E+08
MGS_015_0	14.49	20.25	10.83	0.41	0.00	2.39E+08	9.06E+08
MGS_016_0	12.70	17.16	5.46	0.28	2.38	7.73E+08	4.58E+09
MGS_017_0	16.77	19.53	12.04	0.48	-9.59	4.87E+08	4.16E+09
MGS_018_0	18.09	8.29	2.52	0.22	-1.00	7.13E+08	6.86E+09
MGS_019_0	13.55	8.22	2.42	0.16	0.52	5.81E+08	3.22E+09
MGS_020_0	18.96	8.46	5.53	0.29	0.74	7.69E+08	4.40E+09
MGS_017_30	81.94	23.56	1.81	0.18	10.11	6.15E+09	5.10E+09
MGS_017_40	112.39	46.54	5.66	1.05	7.20	7.96E+10	6.29E+10
MGS_019_30	8.16	6.31	-1.33	0.08	-0.99	9.83E+07	8.36E+08
MGS_020_30	7.25	8.55	-0.22	0.05	18.14	8.71E+07	3.70E+08
MGS_017_70	11.59	15.00	-1.07	0.14	0.42	2.98E+09	2.54E+09
MGS_017_85	3.58	27.11	1.37	0.08	0.76	0.00E+00	1.13E+07
MGS_018_70	14.12	215.95	13.52	0.41	-0.27	1.77E+09	4.61E+09
MGS_018_85	3.35	20.79	1.24	0.06	-11.87	5.36E+06	1.28E+08
MGS_019_70	4.44	81.76	8.90	0.15	-9.19	2.68E+08	5.65E+08
MGS_020_70	28.27	256.95	25.02	0.40	-18.29	2.96E+09	2.78E+09
MGS_020_85	6.53	15.85	0.67	0.21	-0.46	0.00E+00	1.48E+07

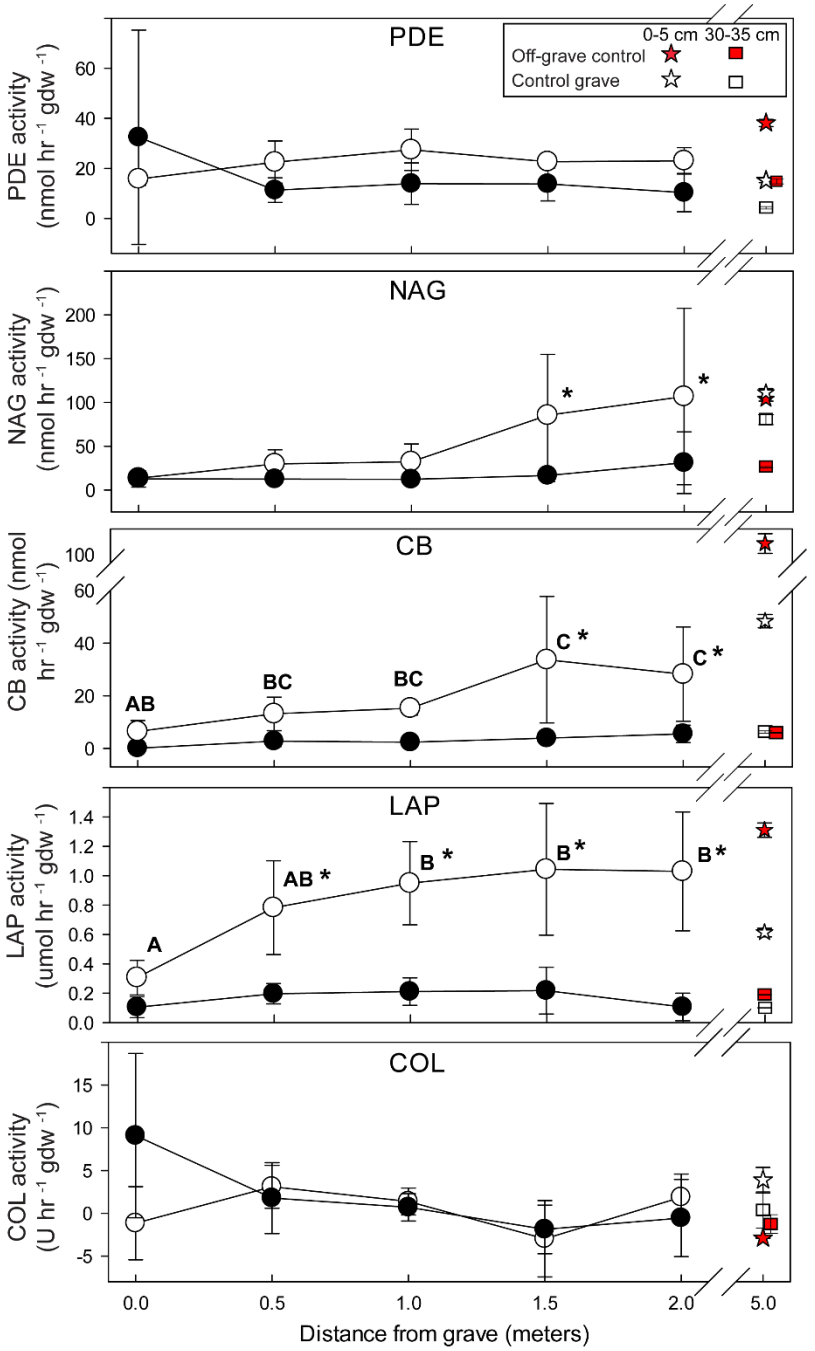

Figure 1.4: Potential extracellular enzyme rates along linear transects from the grave. Points are means of n=3 samples from three independent transects. Significant changes in enzyme activity between distances are denoted by letters. Significant differences between surface soils (0–5 cm, open circles) and soils collected at 30–35 cm depth (filled circles) are indicated by asterisks. Measurements from off-grave site and control grave are included for reference. PDE = phosphodiesterase activity; NAG = N-acetyl-β-glucoseaminidase activity; CB = β-D-cellulobiosidase activity; LAP = leucine aminopeptidase activity; COL = collagenase activity.

This resource was prepared by the author(s) using Federal funds provided by the U.S. Department of Justice. Opinions or points of view expressed are those of the author(s) and do not necessarily reflect the official position or policies of the U.S. Department of Justice.

Table 1.6: Mean nematode abundance and diversity indices by depth (± standard deviation). Significant differences between depths are indicated in bold and superscript letters designate groups that are not significantly different from each other (within either transects or grave) based on the Tukey HSD post hoc test.

Location	Depth (cm)	Abundance	Richness (Genera)	Evenness	Shannon diversity	Maturity index (MI)
Transects (0.5-2 m distance)	0–5*	**445.5 ± 191.0** ^{A}	**14.4 ± 3.6** ^{A}	0.7 ± 0.1	1.9 ± 0.3	**1.9 ± 0.2** ^{A}
	30–35*	**148.3 ± 209.7** ^{B}	**8.9 ± 2.9** ^{B}	0.8 ± 0.2	1.6 ± 0.6	**2.3 ± 0.4** ^{B}
Grave (0 m distance)	0–5	**480.6 ± 191.9** ^{A}	**10.3 ± 2.0** ^{A}	0.7 ± 0.1	1.7 ± 0.2	1.8 ± 0.2
	30–35	**480.0 ± 306.2** ^{A}	**7.7 ± 2.1** ^{AB}	0.4 ± 0.2	0.8 ± 0.4	2.1 ± 0.1
	40–45	**352.0**	**8.0**	0.8	1.7	1.5
	70–75	**25.0 ± 26.1** ^{B}	**4.0 ± 4.1** ^{B}	0.7 ± 0.5	0.9 ± 0.9	1.7 ± 0.5
	85–90	**0.0**	**0.0**	0.0	0.0	n/a

*Data for transects represent the mean of samples from all distances (0.5, 1.0, 1.5 and 2.0 m) in all three transects (n=18: 0–5 cm, n=15: 30–35 cm), as there was no statistically significant difference with distance from grave.

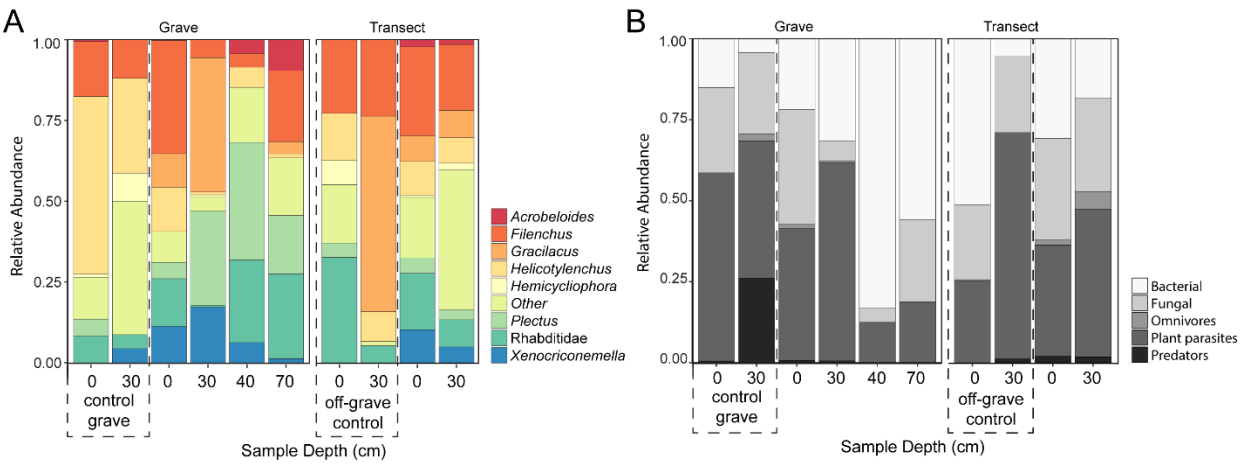

Figure 1.5: Nematode relative abundance and trophic groups by depth. (A) Relative abundances are based on taxa found in at least 50% of all soil samples. (B) Relative abundances of trophic groups are presented for all nematode taxa. Control grave (excavated, but no donors) and off–grave controls (undisturbed site) are included for comparison. No taxa were recovered from the 85–90 cm depth soils below the grave.

Table 1.7: Counts of nematode genera from soils collected along transects at the surface (0 cm depth). Columns represent samples along transects at 0.5, 1.0, 1.5, and 2.0m from grave. *Off-grave control samples.

	5 m*	2 m	2 m	2 m	1.5 m	1.5 m	1.5 m	1 m	1 m	1 m	0.5 m	0.5 m	0.5 m
Achromadora	0	0	0	0	0	4	2	0	8	0	0	0	4
Acrobeles	0	0	0	16	0	0	31	0	32	16	0	5	0
Acrobeloides	0	5	2	0	5	0	3	22	0	28	0	31	9
Alaimus	0	2	0	0	0	0	0	0	0	11	1	0	4
Anaplectus	29	0	6	0	0	17	0	0	0	0	0	0	0
Aphanolaimus	0	0	0	0	0	0	0	0	0	0	1	0	9
Aphelenchoides	0	2	3	0	5	9	0	0	0	0	3	0	0
Aporcelaimellus	0	2	0	0	5	0	1	0	0	0	0	0	0
Basiria	0	0	0	0	10	0	0	7	24	0	0	0	0
Bunonema	0	0	2	0	5	0	0	0	0	0	0	0	0
Cephalenchus	0	0	2	0	0	0	0	0	0	5	0	0	0
Cervidellus	0	0	0	0	0	4	0	4	8	0	0	0	4
Clarkus	0	0	2	0	0	0	1	0	0	0	0	0	0
Coslenchus	0	0	2	0	5	0	0	7	0	0	3	0	0
Diphtherophora	1	7	2	23	0	4	8	4	8	5	5	5	0
Discotylenchus	0	0	0	0	0	0	0	0	0	0	0	0	0
Ditylenchus	0	0	0	0	5	0	5	0	0	0	0	0	0
Dorylaimida (j)	0	0	2	8	0	4	5	0	1	0	0	0	4
Dorylaimus	0	1	0	1	0	0	0	0	1	1	0	0	0
Enchodelus	1	0	0	0	0	0	0	0	0	0	1	0	0
Eudorylaimus	0	0	2	0	5	0	0	7	0	0	1	0	0
Filenchus	72	145	43	309	57	86	95	75	179	109	13	94	251
Gracilacus	0	36	0	0	92	4	0	38	57	30	5	151	9
Helicotylenchus	46	20	5	38	57	4	44	0	0	93	3	62	349
Hemicycliophora	24	0	5	23	0	9	0	0	0	0	0	0	0
Heterocephalobus	2	0	5	31	0	0	3	0	8	0	5	0	0
Heteroderidae	0	0	0	0	0	0	3	0	0	0	0	0	0
Leptolaimidae	0	0	0	0	0	0	0	0	0	0	0	0	0
Leptonchidae	0	0	0	0	0	0	0	0	0	0	0	0	0
Meloidogyne	0	7	0	9	10	0	3	0	0	31	0	62	4
Mesocriconema	0	0	0	0	0	0	0	0	0	5	0	0	0
Miconchus	0	0	0	0	24	0	0	7	0	0	1	0	0
Mononchoides	0	0	0	0	5	0	0	0	0	0	0	0	0
Mylonchulus	0	0	0	0	10	9	0	4	0	0	1	0	4
Nygolaimidae	0	0	0	0	0	0	0	0	0	0	0	26	4
Panagrolaimus	0	2	0	0	0	0	0	0	0	0	0	0	0
Paratylenchus	8	0	6	0	0	0	3	0	0	0	0	0	0
Plectus	14	18	6	39	19	30	3	15	32	23	13	16	21
Prionchulus	0	0	0	0	0	0	0	0	1	0	1	0	0
Prismatolaimus	14	0	0	23	5	9	0	0	8	11	3	0	21
Rhabditidae	103	27	51	62	63	265	13	26	113	130	0	203	21
Teratocephalus	0	0	0	0	0	0	0	4	0	0	0	0	0
Tripyla	0	0	0	2	0	0	1	0	0	5	0	0	0
Tylencholaimus	0	0	2	0	0	0	3	0	16	0	0	0	0
Tylenchorhynchus	0	0	0	0	0	0	0	0	0	0	0	0	0
Tylocephalus	0	0	0	0	0	0	0	0	0	0	0	0	0
Xenocriconemella	0	52	12	8	5	73	48	0	24	0	95	0	4
Xiphinema	2	10	2	0	0	17	1	4	40	5	0	5	0
Total count	316	336	162	592	392	548	276	224	560	508	155	660	722

This resource was prepared by the author(s) using Federal funds provided by the U.S. Department of Justice. Opinions or points of view expressed are those of the author(s) and do not necessarily reflect the official position or policies of the U.S. Department of Justice.

Table 1.8: Counts of nematode genera from soils collected along transects at the surface (30 cm depth). Columns represent samples along transects at 0.5, 1.0, 1.5, and 2.0m from grave. *Off-grave control samples.

	5 m*	2 m	2 m	2 m	1.5 m	1.5 m	1.5 m	1 m	1 m	1 m	0.5 m	0.5 m	0.5 m
Achromadora	0	0	0	0	0	0	0	0	0	0	0	0	0
Acrobeles	0	0	0	0	0	1	0	0	0	0	0	0	0
Acrobeloides	0	0	0	2	2	0	2	0	0	0	0	0	7
Alaimus	0	0	0	0	0	0	0	0	3	0	0	0	0
Anaplectus	0	0	0	0	0	0	0	0	0	0	0	0	0
Aphanolaimus	0	0	0	0	0	0	0	0	0	4	0	0	0
Aphelenchoides	0	0	0	0	0	0	2	0	0	0	0	0	0
Aporcelaimellus	0	0	0	0	0	0	0	0	0	0	0	0	0
Basiria	0	0	5	0	0	0	0	0	0	0	0	0	0
Bunonema	0	0	0	0	0	0	0	0	0	0	0	0	0
Cephalenchus	0	0	0	0	0	0	0	0	0	0	0	5	0
Cervidellus	0	0	0	0	0	0	0	0	0	0	0	5	0
Clarkus	0	0	0	0	0	0	0	0	0	0	0	0	0
Coslenchus	0	0	7	0	2	0	0	0	0	4	0	0	0
Diphtherophora	0	0	7	0	0	1	2	0	3	19	0	0	10
Discotylenchus	0	0	0	0	0	1	0	0	0	0	0	0	0
Ditylenchus	0	0	0	0	2	0	0	0	0	13	0	0	0
Dorylaimida (j)	0	0	0	4	2	0	7	9	0	4	0	0	0
Dorylaimus	0	0	0	0	0	0	0	0	0	0	0	0	1
Enchodelus	0	0	0	0	0	0	0	0	0	0	0	0	0
Eudorylaimus	0	0	0	0	0	1	0	0	0	0	0	8	0
Filenchus	18	7	18	2	18	10	9	2	29	28	4	10	25
Gracilacus	46	0	0	0	4	7	0	9	20	23	0	10	0
Helicotylenchus	7	0	2	2	4	1	2	0	0	4	4	4	67
Hemicycliophora	0	0	0	0	0	0	0	0	0	0	0	28	4
Heterocephalobus	0	0	0	0	0	0	2	0	3	0	0	0	0
Heteroderidae	0	0	0	0	0	0	0	0	0	0	0	0	0
Leptolaimidae	0	0	2	0	0	0	0	0	0	0	0	0	0
Leptonchidae	0	0	0	0	0	3	0	0	0	0	0	0	0
Meloidogyne	0	7	0	20	2	0	0	12	3	0	0	24	0
Mesocriconema	0	0	0	0	0	0	0	0	3	0	4	0	0
Miconchus	0	0	0	0	0	0	1	0	0	0	0	0	0
Mononchoides	0	0	0	0	0	0	0	0	0	0	0	0	0
Mylonchulus	0	0	0	0	0	0	0	0	0	0	0	5	0
Nygolaimidae	1	2	0	0	0	0	0	0	3	0	0	0	1
Panagrolaimus	0	0	0	0	0	0	0	0	0	0	0	0	0
Paratylenchus	0	0	0	0	0	0	0	0	0	0	20	0	0
Plectus	0	0	5	0	6	2	2	2	0	4	0	0	0
Prionchulus	0	0	0	0	0	0	0	0	0	0	0	0	0
Prismatolaimus	0	5	0	2	6	0	0	0	0	4	0	0	0
Rhabditidae	4	5	0	4	14	2	5	0	9	13	0	10	7
Teratocephalus	0	0	0	0	0	0	0	0	0	0	0	0	0
Tripyla	0	0	0	0	2	0	0	0	0	0	0	0	0
Tylencholaimus	0	0	0	0	0	7	0	0	0	0	0	0	0
Tylenchorhynchus	0	0	0	0	0	0	0	0	0	0	0	10	0
Tylocephalus	0	0	0	0	0	1	0	0	0	0	0	0	0
Xenocriconemella	0	2	2	2	4	3	14	0	0	0	0	0	0
Xiphinema	0	0	0	0	0	1	0	2	0	0	0	5	4
Total count	76	28	48	38	68	41	48	36	76	120	32	124	126

This resource was prepared by the author(s) using Federal funds provided by the U.S. Department of Justice. Opinions or points of view expressed are those of the author(s) and do not necessarily reflect the official position or policies of the U.S. Department of Justice.

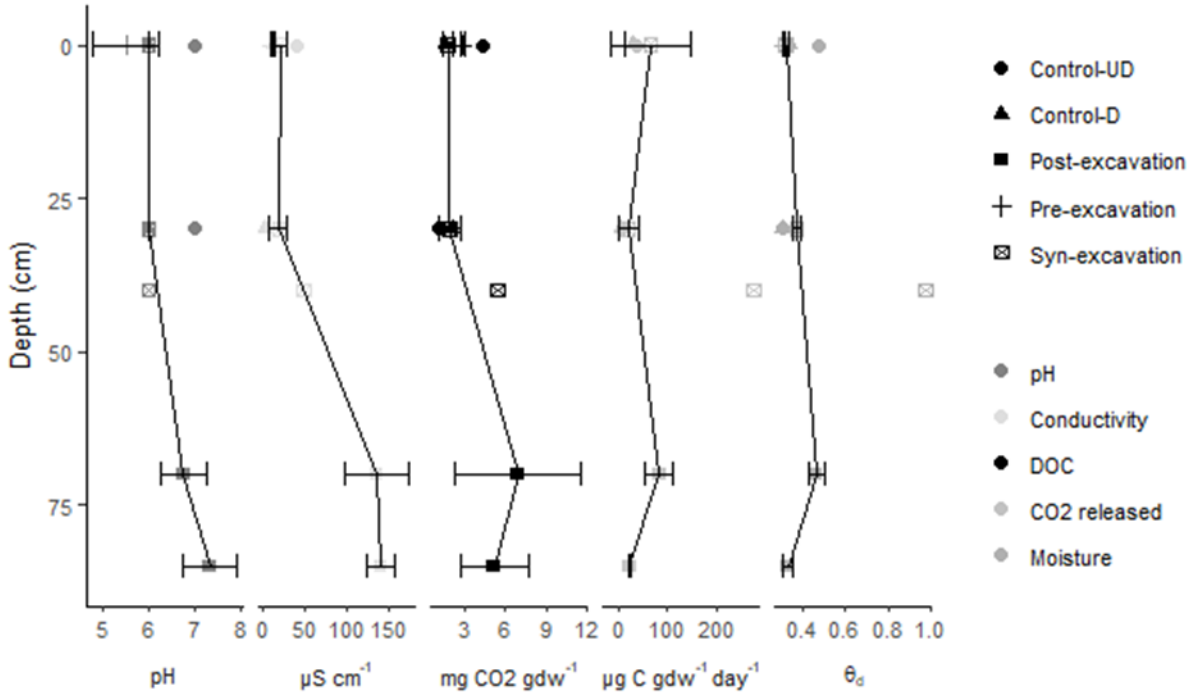

Figure 1.6: Changes in soil physicochemical parameters within the grave. Points are mean and standard deviation of n=3 samples.

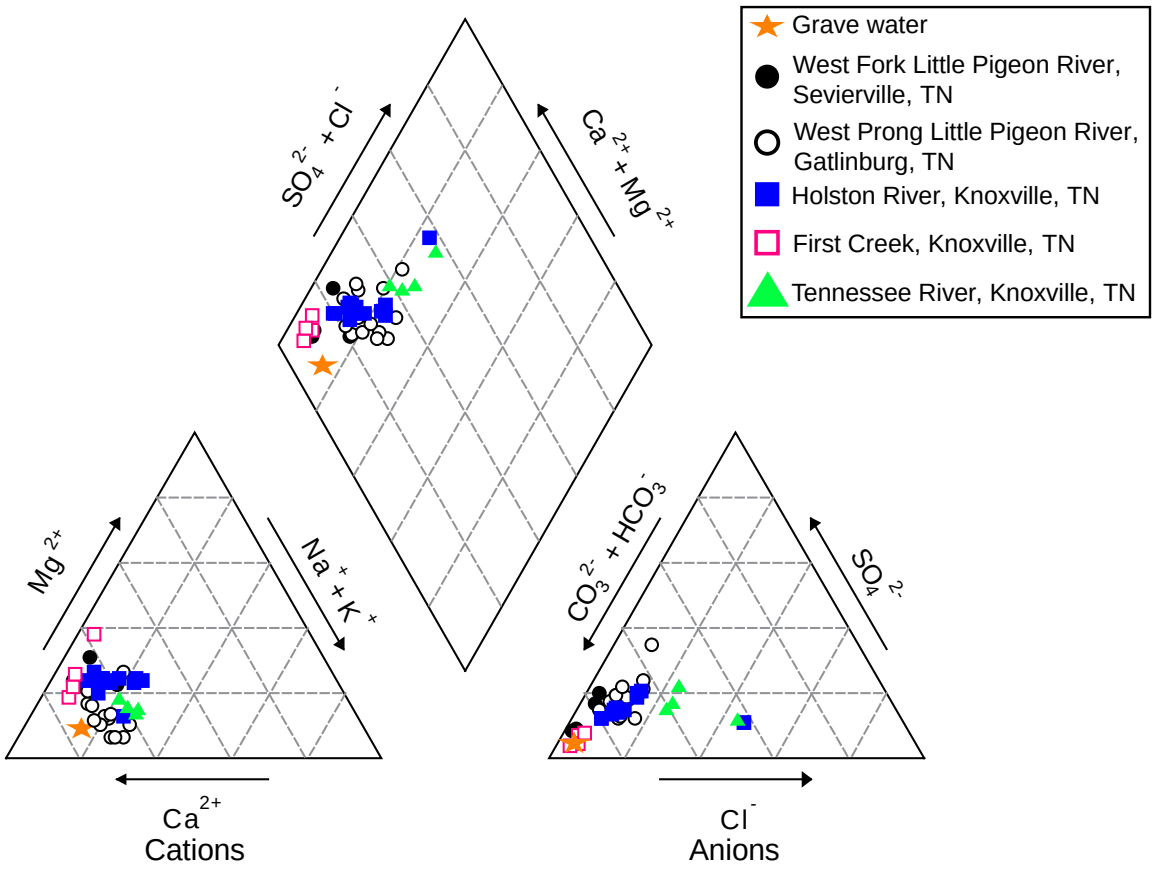

Figure 1.7: Piper diagram for grave water and nearby surface water geochemistry. Water samples from five East Tennessee rivers and the grave water are geochemically similar, and are predominantly Ca-Na-K-HCO_3^- type waters. Surface water geochemistry was obtained through the USGS (Water for the Nation, https://waterdata.usgs.gov/nwis), selecting samples from nearby rivers (less than 50 miles away), with complete water geochemistry provided (including pH, temperature, total dissolved solids, bicarbonate), and ionic charge balance of +/- 17%. The resulting dataset included 40 surface samples plus the grave water.

Reference

USGS Water for the Nation, US Department of the Interior, US Geological Survey. https://waterdata.usgs.gov/nwis. Accessed 13 February 2018.

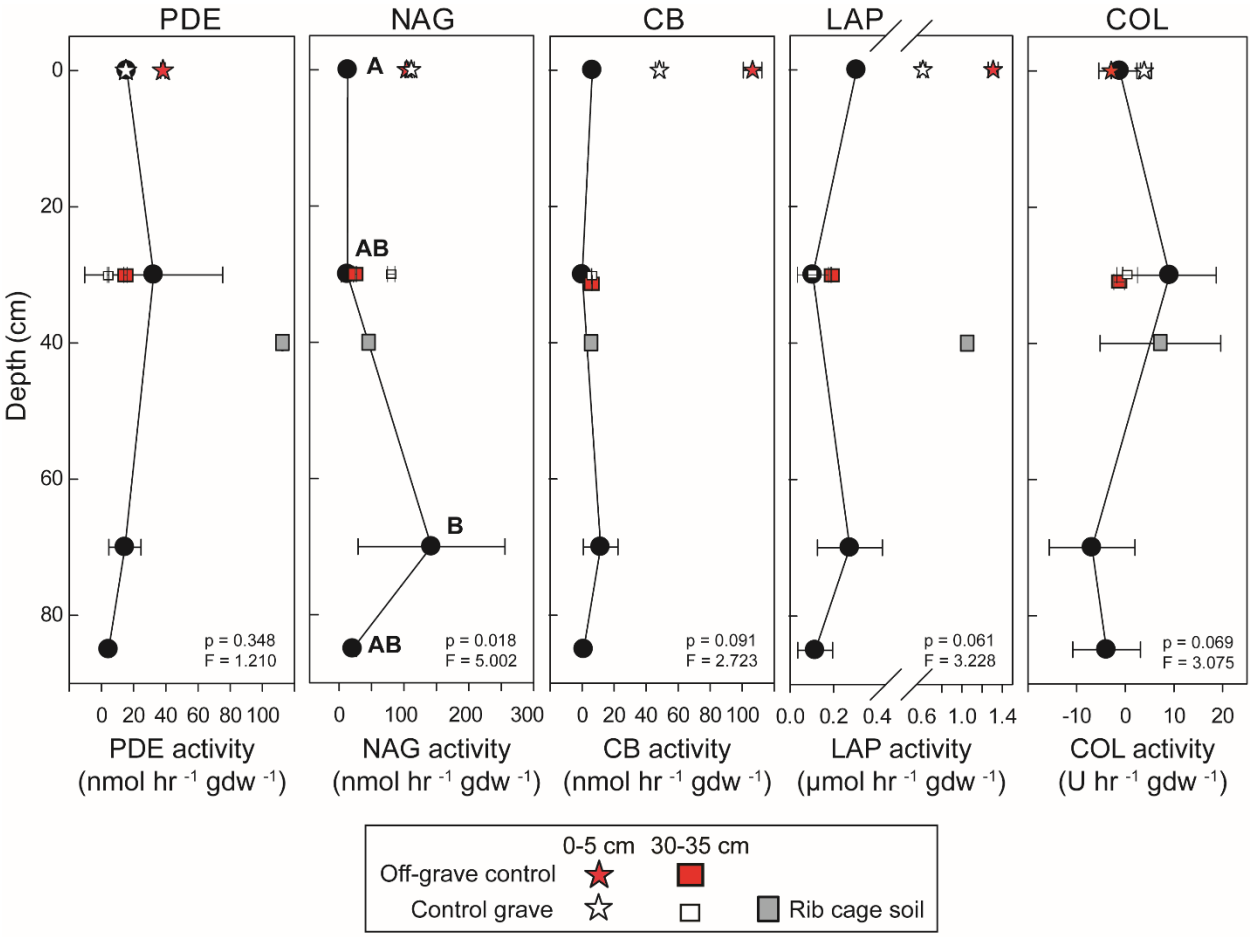

Figure 1.8: Extracellular enzyme activities within the multi-individual grave. Control grave and off-grave samples are included for reference. Significant differences in enzyme activity with depth are denoted by letters. PDE = phosphodiesterase activity; NAG = N-acetyl-β-glucoseaminidase activity; CB = β-D-cellulobiosidase activity; LAP = leucine aminopeptidase activity; COL = collagenase activity.

This resource was prepared by the author(s) using Federal funds provided by the U.S. Department of Justice. Opinions or points of view expressed are those of the author(s) and do not necessarily reflect the official position or policies of the U.S. Department of Justice.

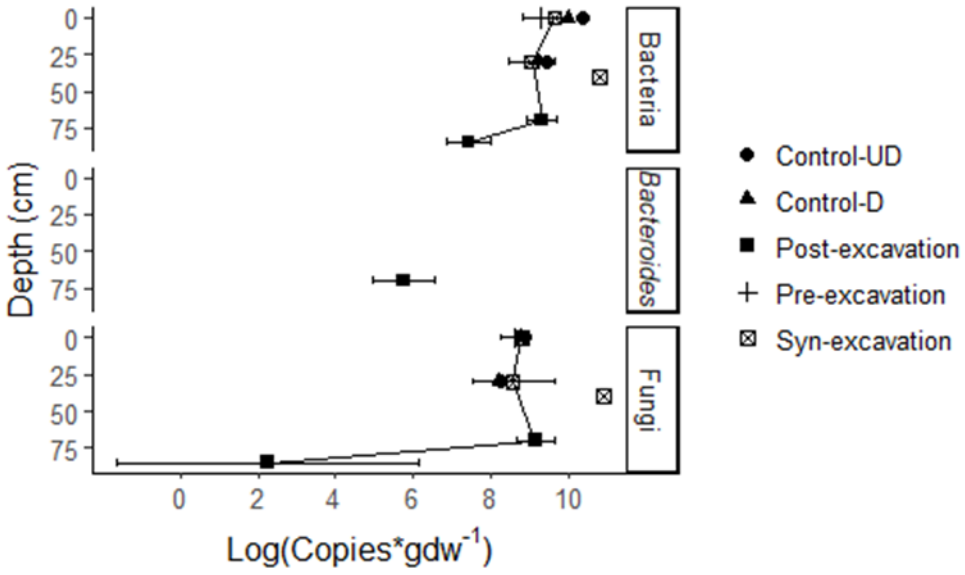

Figure 1.9: Gene copy abundances of Total 16S rRNA (Bacteria), *Bacteroides* 16S rRNA (*Bacteroides*), and ITS (Fungi) within the grave. *Bacteroides* were below detection in all but the 70-75 cm samples.

Table 1.9: Counts of nematode genera from soils collected within the grave. Columns represent samples from different depths within the grave. *Control grave samples.

	0 cm*	30 cm*	0 cm						30 cm			40 cm	70 cm				85 cm		
Achromadora	0	0	0	0	0	0	4	0	0	4	0	0	0	0	0	0	0	0	0
Acrobeles	0	0	5	0	0	0	0	0	0	0	0	0	0	0	0	0	0	0	0
Acrobeloides	5	0	0	0	0	7	0	0	0	0	0	15	2	0	0	18	0	0	0
Aphelenchoides	0	4	0	0	0	0	0	0	10	0	0	0	4	0	0	2	0	0	0
Aporcelaimellus	0	0	0	0	0	0	0	0	0	0	0	0	0	0	0	0	0	0	0
Basiria	0	4	0	0	0	0	0	5	0	0	0	0	0	0	0	0	0	0	0
Boleodorus	84	0	0	0	0	0	0	0	0	0	0	0	0	0	0	0	0	0	0
Cephalobus	0	0	0	0	0	0	0	5	39	4	0	0	0	0	0	0	0	0	0
Clarkus	0	0	0	0	0	0	0	5	0	0	0	0	0	0	0	0	0	0	0
Coslenchus	19	0	0	0	0	0	0	9	0	0	0	0	0	0	0	0	0	0	0
Diphtherophora	0	4	5	0	0	0	0	0	0	0	0	0	0	0	0	0	0	0	0
Diplogasteridae	0	0	0	0	0	0	0	0	0	0	0	52	0	0	0	0	0	0	0
Dorylaimida (j)	0	1	0	4	0	0	0	0	0	0	0	0	0	0	0	0	0	0	0
Dorylaimus	0	0	0	0	5	0	0	14	0	4	0	0	0	0	0	0	0	0	0
Eudorylaimus	0	1	0	0	0	0	0	0	0	0	0	0	0	0	0	0	0	0	0
Filenchus	154	11	162	55	177	163	256	139	49	8	15	15	10	0	0	34	0	0	0
Gracilacus	0	0	32	20	41	201	0	5	10	440	57	0	6	0	0	0	0	0	0
Helicotylenchus	497	27	108	8	25	13	60	214	0	4	3	22	2	0	0	0	0	0	0
Hemicycliophora	9	8	0	0	0	0	0	0	0	0	3	0	0	0	0	0	0	0	0
Heterocephalobus	0	0	5	4	10	7	4	5	0	0	0	8	0	0	0	0	0	0	0
Meloidogyne	0	0	0	0	85	0	0	0	0	0	0	0	0	2	0	0	0	0	0
Mesocriconema	0	0	54	0	5	0	0	14	10	8	0	0	0	0	0	0	0	0	0
Miconchus	0	4	0	0	0	0	0	0	0	0	0	0	0	0	0	0	0	0	0
Mononchoides	0	0	0	0	0	0	0	0	0	0	0	0	0	0	0	0	0	0	0
Mylonchulus	5	0	11	0	0	0	0	0	0	0	3	0	0	0	0	0	0	0	0
Nygolaimidae	0	20	0	0	0	0	8	0	0	0	0	0	0	0	0	0	0	0	0
Panagrolaimus	0	0	0	0	0	0	0	0	0	0	0	0	3	0	0	0	0	0	0
Plectus	47	0	11	11	25	26	24	28	0	0	0	128	3	2	0	0	0	0	0
Plectus (spp. 2)	0	0	0	0	0	0	4	0	662	4	3	0	6	0	0	0	0	0	0
Prismatolaimus	9	0	0	0	5	0	0	0	0	0	0	0	0	0	0	0	0	0	0
Rhabditidae	75	4	238	11	90	59	48	47	0	8	0	90	2	0	2	0	0	0	0
Tylencholaimus	0	0	5	0	0	0	0	0	0	0	0	0	0	0	0	0	0	0	0
Xenocriconemella	0	4	108	43	20	72	4	42	0	8	84	22	2	0	0	0	0	0	0
Xiphinema	0	0	0	4	0	0	0	0	0	0	0	0	0	0	0	0	0	0	0
Total count	904	92	744	160	488	548	412	532	780	492	168	352	40	4	2	54	0	0	0

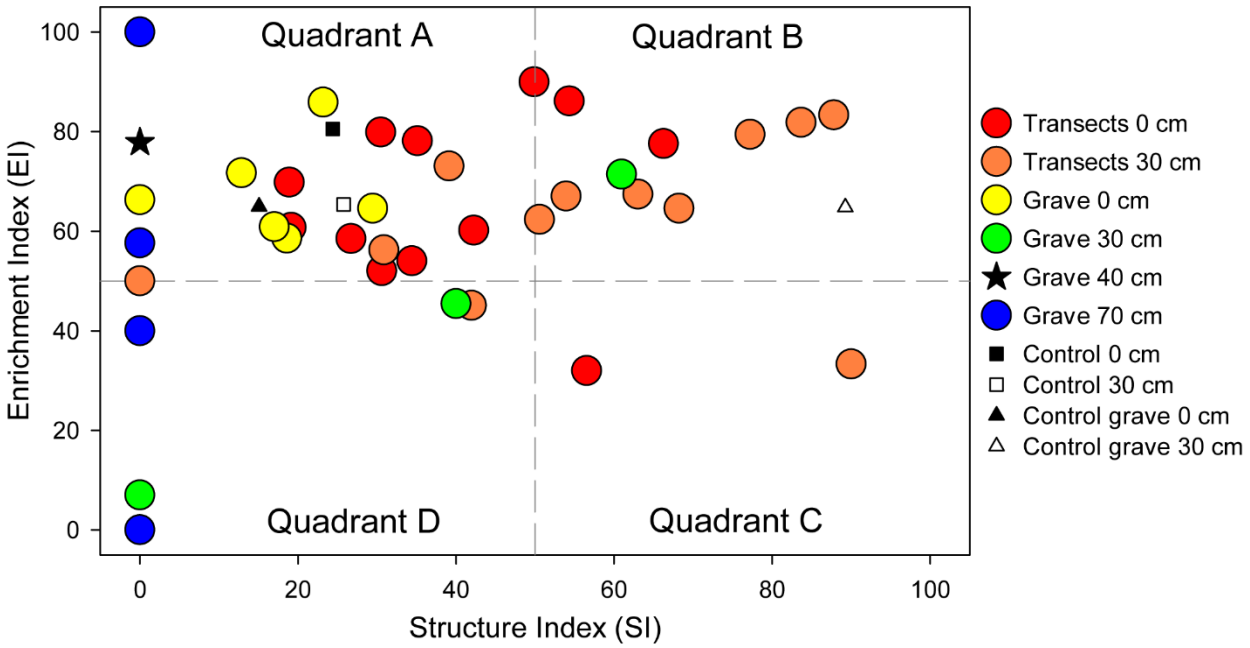

Figure 1.10: Faunal profiles representing the structure (SI) and enrichment (EI) conditions of the soil food web within the grave, along transects, and in control soils.

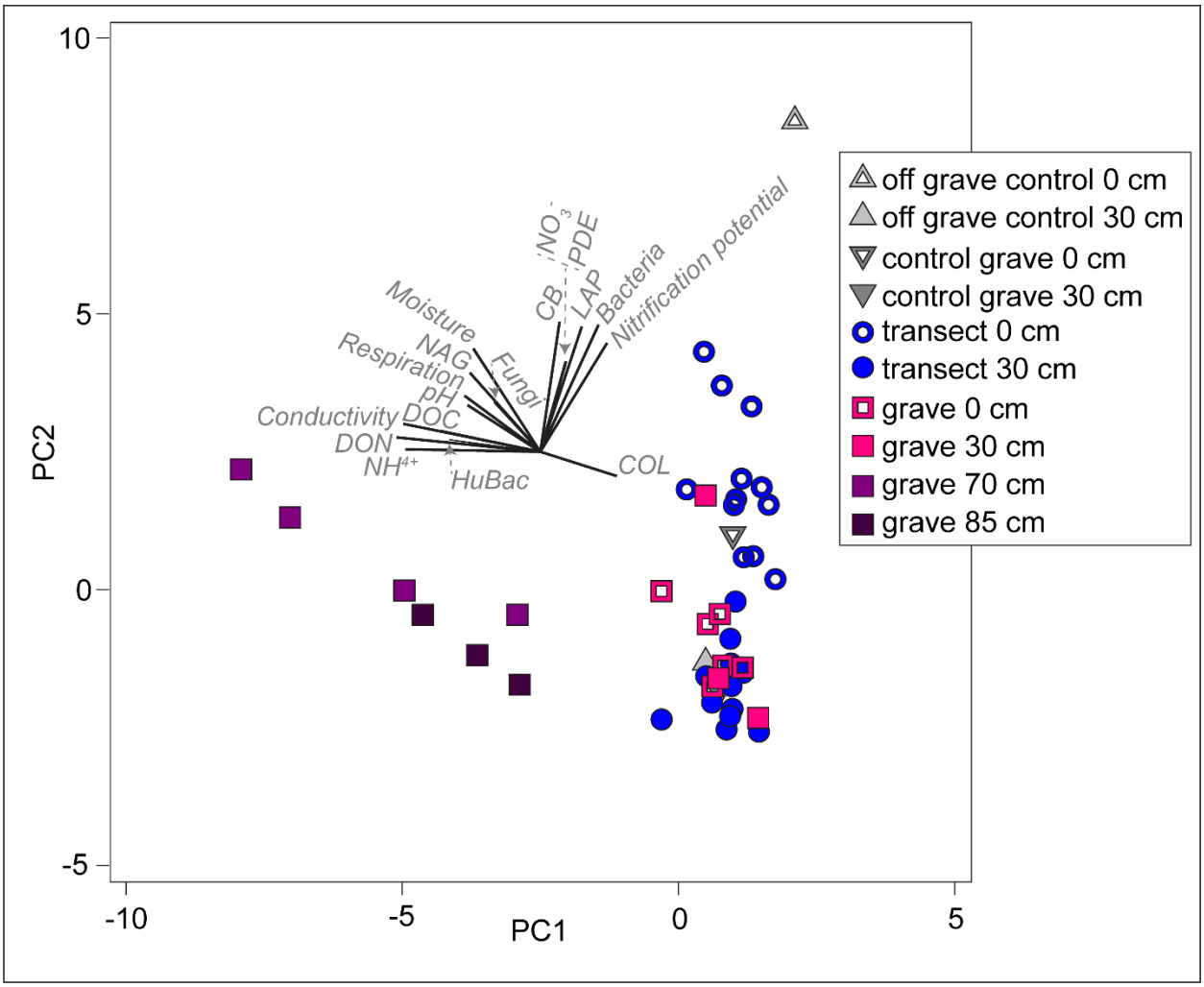

Figure 1.11: Principal components analysis of grave soils showing a clear difference in soil chemistry in samples from the bottom and below the grave. PC1 accounted for 33% of the variation; PC2 accounted for an additional 28.4%, for a cumulative variation explained of 61.4%.

Chapter 2: Soil nematode functional diversity, successional patterns, and indicator taxa associated with vertebrate decomposition hotspots

This chapter is a reformatted version of a manuscript under the same name that is published in PLoS ONE. My contribution to this manuscript included: conceptualization, data curation, formal analysis, investigation, methodology, project administration, visualization, writing, review, and editing.

The citation is: Taylor LS, Phillips G, Bernard EC, DeBruyn, JM (2020) Soil nematode functional diversity, successional patterns, and indicator taxa associated with vertebrate decomposition hotspots. PLoS ONE 15(11):e0241777. DOI: 10.1371/journal.pone.0241777

Abstract

Decomposition of vertebrate remains is a dynamic process that creates localized soil enrichment zones. A growing body of literature has documented effects of vertebrate decomposition on soil pH, electrical conductivity, oxygen levels, nitrogen and carbon speciation, microbial biomass, and microbial successional patterns. However, relatively few studies have examined the microfaunal members of the soil food web that function as secondary consumers, specifically nematodes. Nematodes are often used as indicators of enrichment in other systems, and initial observations from vertebrate decomposition zones have indicated there is an effect on nematode communities. Our goal was to catalog decomposition-induced nematode succession and changes to alpha, beta, and functional diversity, and identify potential indicator taxa associated with decomposition progression. Six adult beaver (*Castor canadensis*) carcasses were allowed to decompose in a forest ecosystem for one year. During this period soil temperature, moisture, and electrical conductivity were monitored. Soils samples were taken at two depths in order to assess nematode community dynamics: 30-cm cores and 1-cm interface samples. Nematode abundance, alpha, beta, and functional diversity all responded to soil enrichment at the onset of active decay, and impacts persisted through skeletonization. After one year, nematode

abundances and alpha diversity had recovered to original levels, however both community membership and functional diversity remained significantly altered. We identified seven indicator taxa that marked major transitions in decomposition progression. Enrichment of Rhabditidae (B1) and Diplogasteridae (B1) coupled with depletion in *Filenchus* (F2) characterized active and advanced decay prior to skeletonization in both cores and interface soils. Enrichment of *Acrobeloides* (B2), *Aphelenchoides* (F2), Tylencholaimidae (F4) and *Seinura* (P2) occurred during a narrow period in mid-skeletonization (day 153). Our study has revealed soil nematode successional patterns during vertebrate decomposition and has identified organisms that may function as indicator taxa for certain periods during decomposition.

Introduction

Decomposition of vertebrate remains is a dynamic process that creates localized soil enrichment zones. These biogeochemical hotspots exhibit increased rates of nutrient cycling which are short-lived in comparison with surrounding areas [1, 2]. There is a growing body of literature documenting the effects of vertebrate decomposition on soil in these hotspots, which include a wide range of abiotic, biotic, and biotically-induced parameters. Soil chemistry studies have revealed temporally-associated changes in pH [2-11], electrical conductivity [5, 8, 10, 11], soil oxygen levels [2], enzyme profiles [2], fatty acid residues [12], steroid fingerprints [13], and fluxes in carbon and nitrogen speciation pools [2, 3, 5-8, 10, 11]. High-throughput sequencing has been used to examine bacterial (and to a lesser extent, fungal) community composition and successional patterns [6, 7, 14-19]. However, in comparison with soil chemistry and microbial studies, targeted examination of multicellular soil faunas, particularly microfaunal members of the soil food web that function as secondary consumers of these resources, have received the least attention [but see 20, 21-24].

Microscopic soil animals, or microfauna, is a designation that includes tardigrades, mites, rotifers, and nematodes, among others. Of these microfauna, nematodes are estimated to comprise some 80% of all multicellular organisms found in the soil environment [25]. Nematodes are well-studied across a wide range of environments, ecosystems, and biomes, at scales ranging from local to global [26-28]. They can be divided into morphologically distinct trophic groups (bacterial feeders, fungal feeders, plant feeders, omnivores, and predators), and thus exhibit functionally-partitioned responses to environmental changes [29]. These trophic groups can be further subdivided according to colonizer-persister (cp-) classifications, based upon an *r*- and *K*-selection continuum [30]. Thus, nematode community diversity and

successional patterns have been shown to be sensitive indicators of soil enrichment and disturbance in agricultural systems [31-43] and composting processes [44, 45]. Many field studies of nematodes focus on the upper 30 cm of soil, where the majority of free-living nematodes reside [24, 31, 35-41, 43, 46-49]. Vertical and horizontal distributions of soil nematodes are most commonly driven by food source location [47, 48]; nematode density, particularly those of bacterivores, correlates with areas enriched in soil organic carbon (SOC), and therefore higher densities of bacterial biomass [28].

Nematode community dynamics resulting from soil enrichment during vertebrate decomposition have been only initially explored [24]. Szelecz et al. (2016) observed successional patterns of nematode community diversity during pig carcass decomposition which were similar to patterns observed in composting and amended agricultural soils. While the study by Szelecz et al. (2016) showed changes in community membership at the family level, they did not report changes in taxa absolute abundance. Given the substantial differences in ecological responses between cp classes to ecosystem disturbances, it is likely that a finer, or perhaps mixed, taxonomic resolution is needed to document patterns and identify potential marker taxa linked with decomposition progress. Data derived from human and animal vertebrate decomposition studies have demonstrated that seasonality, climate, and choice of decomposing organism all affect the rates and patterns of decomposition progression [4, 50, 51]. Taken together, these studies highlight both the potential for using nematode community changes as temporal markers to track decomposition progress, as well as a critical need to better characterize nematode successional and functional diversity dynamics during decomposition across a wide range of decomposing organisms as well as environmental and edaphic conditions.

Our study was designed to build upon existing findings and fill a gap in our

understanding of microfaunal dynamics associated with vertebrate decomposition. Our goal was to catalog decomposition-induced nematode succession and changes to functional diversity with fine resolution, both temporally and taxonomically, in soils beneath decomposing vertebrate carcasses. We expected to observe successional and functional diversity changes in nematode community composition through time commensurate with the progression of decomposition of vertebrate carcasses. We expected to detect potential indicator taxa that were both positively and negatively correlated to the conditions present in these hotspot environments over extended time periods. Lastly, we hypothesized that the interface between the decomposing vertebrate material and the top-most organic layer of soil would harbor a more distinctive nematode community succession than deeper in the soil profile.

Materials and methods

Experimental site

This study took place over the course of 11 months, spanning March 2017 through February 2018, and was conducted at the Oak Ridge Arboretum, part of the University of Tennessee Forest Resources AgResearch and Education facilities, located in Oak Ridge, TN, USA (35º 59' 36.28" N, 84º 13' 12.34" W). The climate is categorized as *Cfa* (Humid subtropical) according to the Köppen classification system. Mean annual precipitation is 143 cm; mean annual air temperature is 13.6ºC. Temperatures during this study ranged between 3ºC and 35ºC, with a mean of 19.7ºC [52]. Soils belong to the Fullerton-Pailo complex, comprised of approximately 60% Fullerton and 30% Pailo soils, with a parent material of cherty limestone. The ecological site listing is: thermic cherty dolomite upland oak-hickory forest [53]. Beavers were selected for this experiment as a model of a local, mid-sized, wild vertebrate. Nuisance

beaver carcasses (*Castor canadensis*) were obtained from East Tennessee USDA. All animals used in this study were salvaged carcasses, therefore IACUC approval was not required. Carcasses were stored at -20^{o}C and placed frozen at the experimental site at the start of the experiment. Six mature adult beavers were used for this study, approximately 20 to 23 kg each. Beavers were placed in wire cages to allow contact with soil and access by insect scavengers, while eliminating animal and avian scavenging. Cages were placed 3 m apart. Sensors were placed in the soil underneath each carcass to measure soil temperature, moisture, and electrical conductivity (Decagon Devices, GS3). Temperature probes were inserted rectally into each carcass 1 day after placement (Decagon Devices, RT-1). Soil and internal sensors were removed late in the decay process after temperatures returned to ambient (day 100 of the study).

Soil sampling and nematode extraction

Soil samples were taken at twelve time points throughout decomposition. The first six samples corresponded to visual assessments of decomposition stages after Payne (1965) and Cobaugh et al. (2015) [6, 54]: Placement, day 0; fresh, day 2; bloat, day 6; active decay, day 15; advanced decay 1, day 21; advanced decay 2, day 40. After skeletonization, sampling continued on a monthly basis for four months (days 78, 110, 153, 188), and at roughly two-month intervals thereafter (days 250, 317). At each sampling time point three 30-cm cores were removed from underneath each of the six carcasses with a 1.9 cm (¾-inch) diameter soil probe, and composited to generate one sample per carcass, for a total of six samples per time point. Soils were also sampled from paired control sites located approximately 4 m from each carcass that were unimpacted by decomposition, for a total of six control soil samples at each sampling time point. Early results of nematode response to cadaver-enrichment suggested stratification in the soil column. Therefore, starting at day 15, we additionally collected the top 1 cm of soil from directly

underneath carcasses. This 0-1 cm sample was referred to as an interface sample and was included to explore hotspot effects in immediate proximity to decomposing material. Care was taken in order not to sample the same areas twice. Samples were immediately transferred to the laboratory and stored at 4^{o}C until nematode extraction.

Nematodes were extracted from soil by means of a sugar-flotation centrifugation technique as described by Jenkins (1964)[55]. All extractions were performed by the same person. Total abundances were expressed as nematodes per 100 cm^3 soil. Nematodes were counted and identified from live samples by differential interference contrast (DIC) microscopy. Taxa were identified primarily to genus level, and to family or order level where appropriate.

Alpha, beta, and functional diversity

Nematode communities were characterized as described in Keenan et al. (2018) [56]. Briefly, nematodes were assigned trophic groups, colonizer-persister (cp) classifications, and functional guilds using methods described previously [29, 30, 33]. *Filenchus* was classified as an F2 fungivore according to Okada et al. (2005) [57]. The family Tylenchidae is very large and currently not well studied, and frequently Tylenchidae ecology is based upon observations of resource proximity rather than cultured studies [58, 59]. *Filenchus*, *Lelenchus*, and *Malenchus* have recently been shown to be closely related and thus for the purposes of this study both *Lelenchus* and *Malenchus* have been classified as F2 fungivores [58]. *Ecphyadophora* has no clearly defined ecological function in the literature, however it also has been shown to be closely related to *Malenchus*; according to similar classification and behavioral characteristics *Ecphyadophora* has thus been classified as an F4 fungivore [58, 59]. Richness was defined as the number of unique taxa at family and genus levels. Shannon diversity was calculated as described in Keenan et al. (2018). Functional diversity indices were calculated according to Ferris et al.

(2001) and Keenan et al. (2018) [56, 60]. All visualizations were created in R (version 3.6.1) using the ggplot2 (version 3.2.1), RColorBrewer (version 1.1-2), and pheatmap (version 1.0.12) packages [61-64].

Statistical analysis

The six carcass sites in this study were treated as experimental replicates. Six paired control sites, one associated with each carcass, were treated as control replicates. Two-way ANOVA ($p < 0.05$) was conducted to test for significant differences between the effects of decomposition products and sampling time point. This was followed by paired T-tests at each sampling time point to determine if decomposition-impacted soils significantly differed from control soils. Redundancy analysis (RDA) on Euclidean distances was performed in order to visualize community differences by decomposition stage, as well as between core and interface soils as a whole. Ellipses represent standard deviations from decay stage centroids. Analyses were conducted in R (version 3.6.1) using the tidyverse (version 1.2.1), car (version 3.0-7), and vegan packages [63, 65-67].

Identification of indicator taxa

Due to ranges in r- and *K*-selection characteristics present in each trophic group, variations in taxonomic composition of cp-classes, and acknowledging the limitations of cp-class designations (whereby membership of the same cp-class consists of multiple organisms whose life-histories are not always well-documented), care must be taken in assigning indicator taxa in order to avoid inferring cross-taxonomic or life-history relationships that might not exist. To assess candidacy of an individual taxon as an indicator, both positive (enrichment) and negative (suppression) response patterns were determined using the following criteria. Nematode taxa were identified as exhibiting enrichment if they satisfied two criteria: 1) a minimum mean

abundance of five at any sampling time point (study day); and 2) increase above a threshold, which was calculated by multiplying the mean abundance in the control soils by a scaling factor (10 for B1 organisms, two for all others). The satisfaction of both criteria screened for well-represented taxa that exhibit a substantial increase and eliminated rare taxa whose overall sample representation would be low regardless of enrichment. Nematode taxa exhibiting suppression were also required to satisfy two simultaneous criteria: 1) a minimum mean abundance of five in controls, and 2) sample decrease to below a threshold, which was calculated by dividing the control mean by the same scaling factor as used for enrichment criteria (10 for B1 organisms, two for all others). The satisfaction of both criteria screened for initially well-represented taxa that exhibited a substantial decrease, and eliminated rare taxa that exhibited uneven sample representation, and therefore would not be considered robust indicators. Scaling factors of 10 for B1 enrichment opportunists and two for all other taxa were selected based upon ecological patterns. Thresholds of five were chosen in order to exclude rare taxa whose appearance in samples could not be consistently observed or demonstrate robust response patterns. Core (0-30 cm) and interface (0.1 cm) soils were assessed separately.

In order to visualize overall response patterns as well as indicator taxon patterns, heatmaps were constructed for both core (0-30 cm) and interface (0-1 cm) soils and subdivided by trophic group (bacterivores, fungivores, omnivores, and predators). Each trophic group heatmap was then organized according to functional guilds (cp-class) (B1, B2, etc.) in descending order from greatest r-selection to greatest K-selection. Within each cp-class taxa were alphabetized. All taxa within the above trophic categories are included regardless of numerical contribution.

Results

Decomposition stages

Six frozen beaver carcasses were placed at the experimental site on day 0. By day 1 carcasses had thawed sufficiently that internal temperature probes could be inserted rectally; external temperatures of carcasses had equilibrated by this time; however, core body temperatures remained below ambient air temperature. By day 2 internal temperatures had equilibrated with ambient air temperature, and carcasses were considered to be at the fresh stage. Fly egg masses were visible in the eyes. Early bloating occurred by day 6. Bloating continued for nine days, in part due to a period of colder weather (Figure 2.1A). During the bloat period the main body portion of the carcasses was swollen and skin surfaces could not be depressed when touched. Maggot masses were present in the facial and rectal areas, with no visible seepage of fluids from those areas. Active decay, day 15, was marked by an increase in maggot activity in the torso area, the movement of decomposition fluid into the soil and the initial formation of visible cadaver decomposition islands (CDIs). Advanced decay began at day 21, after the majority of tissue mass was gone and maggot activity had decreased. Sampling occurred twice during advanced decay: Upon decrease of maggot activity at day 21 (advanced decay 1), and again as greater amounts of remaining tissue were lost but prior to dry and skeletonized remains at day 40 (advanced decay 21). Early skeletonization consisted of bone with some greasy or dry tissue; this stage was sampled twice at monthly intervals: Day 78 (early skeletonization 1) and day 110 (early skeletonization 2). After this period only fully skeletonized remains were left; these were sampled every two months at four time points: Days 153, 188, 250, and 317 (late skeletonization 1-4, respectively) (Table 1).

Internal carcass temperature, soil temperature, moisture, and electrical conductivity

The temperatures of the carcass and decomposition-impacted soils began to increase above ambient air and control soil temperatures during the transition from bloat to active decay (day 13) and remained elevated until day 25, corresponding to the periods of active and early advanced decay and peak maggot activity (Figure 2.1A). Maximum internal temperatures ranged from 28.0 to 42.4ºC with a mean of 31.6ºC. Maximum temperatures of impacted soils underneath carcasses ranged from 25.3 to 34.5ºC with a mean maximum of 25.8ºC. Soil temperatures at control sites did not appreciably deviate from ambient air temperature; however, as expected for soils, the range of diurnal variation in soil was attenuated compared to ambient air temperatures. The maximum temperature of control soils ranged from 26.1 to 27.5ºC with a mean maximum of 25.8ºC; in comparison, ambient air reached a temperature maximum of 35ºC.

Soil moisture rapidly increased following day 21 (primarily in in carcasses 1 and 6), and remained elevated until day 95, corresponding to advanced decay and early skeletonization. During this period, the soil was covered with tissue and fur, and small pockets of adipocere developed. As tissue and fur continued to degrade during the latter portion of advanced decay, soil surfaces were gradually uncovered and soil moisture content decreased. During this period of enhanced soil moisture the mean moisture maximum in impacted soils reached 48.2 percent volumetric water content (%VWC) and individual maxima ranged from 45.2 to 60.0 %VWC, whereas control soil maxima ranged from 46.3 to 51.0 with a mean maximum of 48.9 %VWC (Figure 2.1B).

Electrical conductivity began to increase between days 10-20, during bloat (carcass 1) and active decay (all others) as purge decomposition fluids moved into the soil. Conductivity in

impacted soils remained elevated throughout early skeletonization, reaching a mean maximum of 2.0 mS cm^{-1} during advanced decay, with individual maxima ranging from 1.3-3.9 mS cm^{-1}. Control soil maxima ranged from 0.1-0.2 with a mean maximum of 0.1 mS cm^{-1} (Figure 2.1C).

Nematode total abundances and alpha diversity in core (0-30 cm) samples

In decomposition-impacted soils, all nematode indices (abundances, richness, diversity) differed significantly from control soils ($p < 0.001$) over the course of the study (Figure 2.2). At the onset of active decay (day 15), nematode abundances began to increase while both richness and diversity decreased. Mean abundances tripled in affected soils between bloat and active decay (days 6-15), while mean richness and diversity decreased by 26.5% and 12.5% respectively. All three indices exhibited mean maxima (abundance) or minima (richness and diversity) on day 40 (advanced decay 2); mean abundances were enriched by 13 times those of control means, whereas richness and diversity had decreased by 38.2% and 60.1%, respectively, compared to their respective controls. Changes in nematode abundance and diversity continued through day 153 (late skeletonization 1) before returning to initial levels, whereas richness remained depressed to the end of the study (Figures 2.2A, C, E, and Tables 2.2-2.3).

Nematode total abundances and alpha diversity in interface (0-1 cm) samples

Interface soils were collected starting in active decay (day 15) in order to ascertain the degree of nematode activity in the upper-most layer of soil directly in contact with decomposing remains. As with 0-30 cm core samples, all interface (0-1 cm) indices (abundances, richness, and diversity) were observed to significantly differ from controls ($p < 0.001$) over the course of the

entire study.

On days 15 and 21, corresponding to active decay and advanced decay 1, mean nematode abundances in impacted interfaces (0-1 cm) were 3 and 8.6 times higher than found in deeper soil (0-30 cm) samples. Similar to the pattern seen in cores, mean interface maxima (abundances) and minima (richness) occurred on day 40 (advanced decay 2). Mean abundances in interface soils from day 40 were enriched 20.8 times that found in interface controls, and 10.7 times core abundance maxima from the same sampling date. Richness in interfaces on day 40 decreased 79.8% with respect to controls, and 60.1% with respect to the richness minimum found in cores on the same date. Diversity reached a minimum on day 21 (advanced decay1). Overall, interface soils were observed to have increased abundances between days 40-110 (advanced decay through early skeletonization) before returning to initial levels, whereas the impact upon richness and diversity remained throughout the end of the study (Figures 2.2B, D, F, and Tables 2.2-2.3).

Nematode beta diversity - community structure in core (0-30 cm) samples

Fungivores were the primary trophic group found initially in soils at this site. At the onset of active decay (day 15), bacterivores began to proliferate in decomposition-impacted soils, peaking in abundance during advanced decay (day 40), concurrent with the changes observed in abundances, richness, and diversity. After day 40, relative abundances of bacterivores decreased, although not to initial levels: soils were still shifted toward a bacterivore-dominated community after one year (Figure 2.3A). Temporal changes in colonizer-persister (cp) class composition mirrored patterns found in trophic group succession, shifting from a mixture of largely cp-2 class taxa, to communities dominated by select cp-1 class taxa (an exclusively bacterial feeding

designation) at day 15. After day 40 a gradual decrease in cp-1 and concomitant increase in cp-2 through cp-5 class taxa was observed during skeletonization; however, by the end of the study soils were still moderately enriched with cp-1 bacterivores, indicating that communities continued to be impacted by decomposition products (Figure 2.3B). These shifts in functional diversity were reflected in the faunal profile (Figure 2.3C). Samples from controls, initial, and bloat decomposition stages populate the centerline of the Enrichment Index (EI), indicative of a mixed bacterial and fungal community composed primarily of cp-2 class taxa with low representation of cp-1 bacterial feeders. During advanced decay, and continuing through early skeletonization, communities populate the upper regions of the EI, indicative of a strong shift towards bacterial-feeding dominance, and the large abundances of those constituents when stimulated to reproduce. By late skeletonization (day 188) community composition, in terms of relative proportions of trophic classes and cp constituencies, had partially recovered to previous levels but still exhibited some enrichment response when compared with initial communities (Figure 2.3C). It should be noted that by convention, the faunal profile does not include herbivorous taxa in calculations of enrichment or structure indices (EI or SI), as these organisms, while free-living, are plant feeders and therefore not directly subject to fluctuations in microbial food sources [68]. Redundancy analysis (RDA) showed that decomposition stages differed in community membership during decomposition progression, and that community composition at the end of the study (day 317) was fundamentally different from both initial conditions and controls (Figure 2.4A).

During the community composition shift occurring on day 15 (active decay) as bacterial feeding populations changed from general representation across B1-4 taxa to a dominance by B1 taxa, a succession of B1 enrichment opportunists were observed. Of the seven B1 taxa present,

representing five families, only three taxa, representing two families, responded strongly to decomposition enrichment. Diplogasteridae exhibited a sharp and distinct maximum abundance on day 15. Following that, Rhabditidae, of which approximately 30% belonged to the genus *Pelodera*, peaked on day 40. Rhabditidae (and *Pelodera*) enrichment markedly decreased by day 188. No other B1 taxa responded appreciably to enrichment products (Figure 2.5). After day 40, *Acrobeloides* (B2), which did not exhibit early response to decomposition enrichment, began to increase in abundance, and this enrichment trend continued to the end of the study. *Pseudacrobeles* (B2), *Plectus* (B2), and *Prismatolaimus* (B3), all taxa with notable abundances in control and initially unimpacted soils, were not appreciably affected by decomposition products or microbial fluctuations throughout the study (Figure 2.5).

Fungal-feeding populations, with the exception of *Filenchus* (F2), were notably absent in core soils during the early phases of decay (days 0-6). *Aphelenchoides* (F2), *Boleodorus* (F2), *Ditylenchus* (F2), and Tylencholaimidae (F4) all increased in abundance beginning on day 15 and continuing for the remainder of the study, with final sample enrichments surpassing those of controls. In contrast, *Filenchus* (F2) abundances decreased on day 15 with the deposition of decomposition products, and with the exception of day 21, remained suppressed for the duration of the study. *Diphtherophora* (F3) and *Ecphyadophora* (F4) remained largely unaffected throughout the study (Figure 2.5).

Omnivorous taxa were generally found in low abundance in core soils and demonstrated varied response to nutrient enrichment. Of the more *r*-selected taxa in this group, *Achromadora* (O3), mixed Dorylaimida (O4), and *Eudorylaimus* (O4) all exhibited suppression at the onset of active and advanced decay (days 15-21) and dropped below detection by day 78 at the beginning of skeletonization. *Achromadora* abundances recovered by day 110, remaining enriched with

respect to control abundances for the remainder of the study. Dorylaimida was enriched at the very end of skeletonization. *Eudorylaimus* peaked in days 153-188 in late skeletonization. All other taxa exhibited no distinct trends other than generalized suppression throughout day 78, and reappearance beginning in day 110 (Figure 2.5).

Predators, with the exception of *Seinura* (P2), *Tripyla* (P3), *Clarkus* (P4), and Nygolaimidae (P5), were low in abundance and no overall response to decomposition products was observed. *Seinura*, uncommon in controls, increased by an order of magnitude in late-decomposition soils on days 153 and 317. *Tripyla* was suppressed between days 40–188, spanning late advanced decay through mid-skeletonization, and recovered by day 250. *Clarkus* increased in abundance between days 6-21 (bloat through early advanced decay) and again on day 153 in skeletonization. *Nygolaimidae* abundances fluctuated beginning on day 15, remaining suppressed from days 110-250, and increasing by day 317 (Figure 2.5).

Nematode beta diversity - community structure in interface (0-1 cm) samples

Interface soils from control sites were dominated by fungivores. While composition of decomposition-impacted soils from initial and bloat stages were unknown for interfaces, samples from the onset of active decay (day 15) contained high relative abundances of bacterial feeding taxa that subsequently increased, reaching maximal abundances in late advanced decay through early skeletonization (days 40-110). After day 110, relative abundances of bacterivores decreased. In contrast with 0-30 cm cores, interface community composition at study day 317 generally resembled those of control samples from a trophic standpoint (Figure 2.6A). Analogous to patterns observed in deeper soils, fluctuations in cp-class composition mirrored those found in trophic groups; a shift occurred from control communities predominantly

composed of bacterial and fungal representatives of cp-2 class taxa, to one composed almost entirely of cp-1 class taxa in days 15-110. This was followed by an increase in cp-2 through cp-5 class taxa during the skeletonization process (Figure 2.6B). Compared to core samples, interface communities exhibited higher relative abundances of bacterial feeders, principally cp-1 taxa, during active decay through late skeletonization (days 15-110). The communities remained enriched in the faunal profile (EI=100, SI=0) from advanced decay 2 (day 40) through late skeletonization 1 (day 153) corresponding to the reduction of alpha diversity. Similar to cores, by late skeletonization (day 188) interface communities had only partially recovered to previous levels (Figure 2.6C, Figure 2.4B). Overall community change contribution in core and interface throughout the entire decomposition process shows that degree of impact is larger in interfaces than in cores (Figure 2.4C).

Beginning in active decay (day 15) populations of Rhabditidae and Diplogastridae (B1) began to increase. Rhabditidae abundances peaked twice, first on day 21 and secondly on day 78, corresponding to early advanced decay and early skeletonization. Both peak abundances exceeded those observed in cores by at least an order of magnitude. *Pelodera* were exceptionally abundant in interfaces, twice that of the remainder of the members of family Rhabditidae, which was opposite of the pattern observed in core samples. As with core samples, no other notable enrichment or suppression was observed for any other B1 taxa. Of the B2- taxa, *Acrobeloides* and *Plectus* exhibited suppression between days 40-110, corresponding to the transition between late advanced decay and through early skeletonization. All other bacterial-feeding taxa were suppressed between days 15-153 corresponding to the onset of active decay through late skeletonization (Figure 2.7).

Aphelenchoides (F2), *Boleodorus* (F2), *Ditylenchus* (F2), Tylencholaimidae (F4), *Lelenchus* (F2) and *Nothotylenchus* (F2) were suppressed to undetectable levels beginning on or shortly after day 15 and recovered between days 78-153 during the early part of skeletonization. This pattern was similar to those observed in core soils; however, cores on days 0-6 exhibited undetectable or near-undetectable abundances prior to an increase on day 15; day 0-6 data is not available for interface soils. *Filenchus* (F2) dropped below control abundances by day 21 and below detectable levels for days 78-110 and remained below control abundances for the duration of the study (Figure 2.7).

In contrast to core samples, community shifts observed in omnivores in the interfaces was sharply delineated with strong suppression evident from day 15 through 110 in all taxa except *Thorneella* (O4), *Thornia* (O4), and *Ecumenicus* (O5); these latter constituted rare taxa, observed only in controls or in one impacted sample. General community recovery began by day 153, marking the beginning of late skeletonization, with variable abundances in all taxa except Dorylaimida which increased in abundance until the end of the study (Figure 2.7).

Predators, with the exception of *Seinura* (P2), *Clarkus* (P4), and Nygolaimidae (P5), were found in low abundance and exhibited no overall response to decomposition products in interface soils. As seen in cores, *Seinura* enrichment occurred in interfaces as well; here the enrichment occurred on day 110, and the enrichment factor was by two orders of magnitude with respect to controls. *Clarkus*, the most abundant predator in control samples, was suppressed between days 15-110 and exhibited recovery to roughly half of control abundances by the end of the study. Nygolaimidae abundances were suppressed in days 40-78, after which recovery occurred (Figure 2.7).

Nematode indicator taxa

The partitioning of long cores into shorter segments for depth-stratified studies has been shown to select against rare taxa, and in assessing any given taxon for indicator status, rare taxa, while of interest, are not necessarily of primary concern, especially due to potentially low shifts in abundance with high statistical variability. Taxa that exhibited clear patterns of change in both core and interface soils that may be useful as indicators of decomposition stages were identified. These candidate indicator taxa largely fell into four distinct categories: B1 enrichment only, early decay suppression with late decay enrichment, suppression only, and non-B1 enrichment only.

Three taxa were identified as B1 enrichment indictors in both core and interface soils. Diplogastridae exceeded threshold values on days 15 and 40 in cores, and days 15 through 110 in interfaces. Both *Pelodera* and Rhabditidae exceeded threshold values on days 40 through 110 in both cores and interfaces. Rhabditidae additionally exceeded threshold values beginning in day 15. Two taxa met indicator criteria in one soil depth but not in both: Bunonematidae and *Diploscapter* both met enrichment criteria in interfaces on single dates, days 79 and 188, respectively, but did not meet those criteria in cores. No B1 taxa demonstrated suppression at any point in the study.

Taxa that exhibited early decay suppression followed by late decay enrichment in both cores and interfaces included *Acrobeloides* (B2) and *Aphelenchoides* (F2), and *Boleodorus* (F2). *Acrobeloides* met suppression criteria on day 40 in cores; this period began earlier and was extended in interfaces (days 15, and 40-110). Enrichment occurred on day 78 in cores, day 21 in interfaces, and days 153 through 317 in both depths. *Aphelenchoides* suppression occurred in cores between days 0 through 6 and 21 through 40, and in interfaces for an extended period, days 15 through 110. Enrichment occurred on day 78 in cores, day 21 in interfaces, and throughout

days 153-371 in both depths. *Boleodorus* exhibited suppression intermittently until day 188 in cores, and from days 15 through 153 in interfaces. Enrichment occurred only on study day 317. Both *Prismatolaimus* (B3) and Tylencholaimidae (F4) met criteria for suppression (days 0 through 78) and subsequent enrichment (day 153) in cores, but general suppression and only enrichment to recovery levels in interfaces. *Plectus* (B2) satisfied initial suppression criteria in both cores (days 78 through 110) and interfaces (days 15 and 40 through 188), however satisfied subsequent enrichment criteria only in cores on day 153, and could thus be considered to belong to two separate indicator categories based on sampling depth.

Filenchus (F2), which had the largest resident population in control soils, was the only taxon to exhibit suppression-only behavior in both soil depths, falling below threshold values on days 40, 110, and 188 in cores, and throughout days 15-188 in interfaces. *Filenchus* did not exhibit enrichment but did partially recover to background levels by the end of the study. Both *Ceratoplectus* (B2) and *Pseudacrobeles* (B2) satisfied suppression-only criteria for the entire study in interfaces but not in cores. Conversely, *Lelenchus* (F2) satisfied suppression criteria in interfaces only.

The dorylaimids (*K*-selected organisms) were the only group to exhibit non-B1 enrichment in both cores and interfaces, this occurring after day 250. Seven taxa from a variety of cp-classes met criteria as indicators in specific soil depths, however, most did so for very brief periods. Three taxa exhibited single-day enrichment in cores: *Ditylenchus* (day 317), *Ecphyadophora* (day 78), and *Eudorylaimus* (day 188). Two others met single-day enrichment criteria in interfaces: *Aporcelinus* (day 317) and *Chiloplacus* (day 78). The two taxa that met enrichment criteria for multiple consecutive sampling time points were both found in interfaces: *Nothotylenchus* between days 78 and 110, and *Seinura* with abundance increases by an order of

magnitude between days 110 and 153.

Discussion

The decomposition of vertebrate remains is a unique process in comparison with the decomposition and nutrient cycling associated with plant material. Vertebrate remains are composed of protein-rich tissues, have a low C:N ratio, and are considered a high-quality resource, thus the breakdown of these products has shown to differ considerably in pattern and resource inputs into the soil creating a “hotspot” pulse event rather than the sustained release of nutrients characteristic of decaying plant matter [69]. While nematode community composition has been evaluated over a variety of agricultural and field conditions, few studies have explored responses associated with vertebrate hotspots [24,26-28,35-43].

Our study investigated temporal changes of nematode communities underneath decomposing vertebrate carcasses in order to discern successional characteristics and functional diversity changes associated with hotspot enrichment. We additionally identified potential indicator taxa associated with decomposition progress. During the course of this experiment, we elected to add a second sampling depth consisting of soil interfaces: The 0-1 cm upper-most layer of soil in immediate contact with decomposition products. This allowed for direct comparison between nematode community responses resulting from close proximity to the enrichment source (i.e. the decomposing carcass), and those deeper in the soil that would be responding to changes in the soil environment due to the enrichment. We focused on the upper layers of soil because it has been demonstrated that approximately 70% of nematodes exist in the top 20 cm of soil. Nematode community composition at a local scale is most commonly associated with available food sources, both horizontally and vertically [28, 47, 48]. Therefore, we hypothesized that the highly enriched interface soils and deeper soils might harbor unique

nematode community assemblages and/or successional patterns. Indeed, we found that enrichment response was more pronounced in interface samples than in deeper soils by an order of magnitude, and that both trophic response and cp-classes mirrored each other within respective strata. This mirroring is partly based upon the manner in which cp-classes are constructed (B1=bacterial feeder with high enrichment response, B2=bacterial feeder with moderate enrichment response, and so forth). We also found that as succession progressed, a limited number of taxa exhibited unique enrichment or suppression patterns.

General successional patterns

Our study demonstrated that nematode abundances, alpha and beta diversity, and functional diversity responded immediately to the introduction of decomposition products into the soil during active decay (day 15) in both cores and interfaces, with the strongest effects observed in interface samples (Figures 2.2, 2.3-2.4, 2.6, Table 2.2). Overall, there do not appear to be markedly different community compositions between the two soil depths, and taxa that are present in each depth appear to be positively or negatively affected by decomposition products in a consistent manner (Figures 2.5 and 2.7). The greatest differences in response between the soil depths appear to arise from the abundance magnitudes, particularly those of the cp1/B1 bacterial feeders. This is readily apparent by contrasting the consistency found between beta and functional diversity response (Figures 2.3C and 2.6C) with the variability observed in the RDA composite that compares the response of the two soil depths (Figure 2.4C). Figure 2.4C illustrates that while community composition between the two depths overlaps throughout the study, the magnitude of response within those depths, as evidenced by distance from centroids, indicates that the response to decomposition products is exaggerated in interfaces in comparison with cores (Figures 2.3A-B, 2.4C, 2.6A-B). This exaggerated response in interfaces likely

originates from a particularly high concentration of microbial abundances in the uppermost soil layer. In comparison, a 30 cm soil column would require infiltration of decomposition products and food sources, some of which could be lost in the soil aggregate structure.

The nematode community during active decay was dominated by bacterial-feeding enrichment opportunists (cp-1/B1) composed almost exclusively of two families, Rhabditidae and Diplogasteridae, which was consistent both in terms of general behavior and composition with previous reports assessing the effects of vertebrate pig decomposition on nematode community structure in a temperate forest in Switzerland [24]. Elevated abundances in both cores and interfaces in our study persisted throughout late skeletonization (day 153) for a total period of 138 days. In agricultural systems, the addition of organic amendments is typically associated with an increased abundance of *r*-selected bacterial-feeding nematodes (cp-1/B1) as a result of stimulated bacterial growth [32].

In our study, internal carcass temperatures diverged from ambient air temperatures immediately prior the onset of active decay (day 13) and remain elevated until early advanced decay (day 254). Thermogenesis associated with decomposing carcasses is well-known, and is considered primarily attributable to the large maggot masses that develop during active decay [70]. This generates maximum temperatures that can range from (27- 50°C) based upon size and density of the maggot mass that is present [70]. Elevated internal carcass temperatures were also reported by Payne (1965), as well as from a similar experiment performed by Keenan et al. (2018) at a site located approximately 500 m from our study [2, 54]. Keenan et al. (2018) found that internal core temperatures and soil temperatures exceeded ambient temperatures for a period of 4 days during active decomposition. Payne (1965) performed a decomposition experiment using baby pigs and reported that during bloat throughout advanced decay, internal carcass and

soil temperature means all exceeded ambient air temperatures. In another pig decomposition study, Szelecz et al. (2016) reported elevated nematode abundances beginning on day 15 of their study followed by a sharp reduction in abundances beginning on day 22; they did not measure temperature, but proposed that this might be related to thermal stress due to decomposition processes. In composting systems, Steel et al. (2010) and (2013) found sharp reductions in nematode abundances when compost temperatures exceeded 70°C, but they demonstrated that Rhabditidae and *Aphelenchoides* spp. could survive during this period and proliferate once the heat peak passed and temperatures fell below 30°C [71]. Temperatures exceeding 25°C have adverse reproductive effects upon many rhabditids, and temperatures of 24.6°C exceed the thermal tolerance of *Rhabditis cucumeris*, specifically [72]. We observed elevated internal and soil temperatures associated with maggot proliferation but did not see discernible evidence of temperature-induced suppression of nematode abundance. Evidence from compost systems (Steel et al., 2010, 2013) suggests that the duration or magnitude of high temperatures in our study was not long enough to affect nematode reproduction. Another possible contributing factor to the lack of temperature suppression may be due to the fact that the beavers in this study weighed approximately 20 to 23 kg, whereas the pigs in Szelecz et al. (2016) were larger (28 kg) and may have hosted a larger maggot mass that contributed to enhanced heating.

Cp-1 response patterns

Not all taxa in the cp-1 class responded to enriched soil conditions at the same time or with similar abundances. For the purposes of this discussion it should be noted that *Pelodera*, a genus within the family Rhabditidae, was counted as an individual taxon due to its prominent presence in these samples. No other genera within the family of Rhabditidae displayed conspicuous abundances, and therefore the remainder were simply combined under the general

heading of Rhabditidae. Interface samples exhibited a sequential response to enrichment in which Rhabditidae spp. reacted the most quickly (day 15), followed by *Pelodera* (day 40), with abundances almost double those of the other collective Rhabditidae. Members of Diplogastridae were present throughout this period but with unremarkable abundances in comparison with Rhabditidae. Soil cores, on the other hand, exhibited distinct maxima beginning with a brief spike in Diplogastridae (day 15), followed by simultaneous maxima of *Pelodera* and Rhabditidae (day 40), and in contrast to interface samples, Rhabditidae abundances were approximately twice those of *Pelodera*. Of the seven cp-1 taxa present in these samples, only three (Rhabditidae, *Pelodera*, and Diplogastridae) were found in quantity, and met the criteria for consideration as enrichment indicator taxa across both sampling depths. These findings are consistent with results reported by nematode-specific experiments involving decomposing pigs, compost development, and agricultural systems, as well as generalized eukaryotic sequencing surveys of decomposition that have noted the presence of nematodes amongst other taxa [7, 14, 15, 18, 24, 44, 68]. Szelecz et al. (2016) reported that in pigs decomposing on the ground, the three nematode families with enriched abundances were Rhabditidae, Diplogasteroididae, and Neodiplogasteridae. In organically-enriched agricultural soils and cow dung the three nematode families most often reported in largest abundance are Rhabditidae, Panagrolaimidae, and Diplogastridae [30, 32, 41]. Amplicon sequencing has consistently reported a robust presence of Rhabditidae in broad 18S surveys. Metcalf et al. (2016) additionally noted the presence of Monhysteridae associated with decomposing humans and Panagrolaimidae with decomposing mice, although in both instances absolute abundances were not reported. It is notable that in all cases members of the family Rhabditidae are consistently associated with a range of organic enrichment types and are found in high abundance on these occasions. The order Diplogastrida (which includes the families

Diplogastridae, Diplogasteroididae, and Neodiplogasteridae) are consistently found in studies that involve manual extraction and also exhibit high abundances, suggesting the possibility that molecular studies may be less-sensitive to this particular group of taxa. Interestingly, some Diplogastrids, notably *Pristionchus* spp., have recently been observed enriched in rotting vegetal material (including fruit), expanding on previous reports of their necromenic association with beetles [73]. Thus, there is the possibility that Diplogastrids may be found to be general enrichment opportunists transferred between enrichment patches via phoresy, which could explain our observed Diplogastrid blooms from very low soil control densities. Panagrolaimidae abundances were found to be negligible both in this study and in Szelecz (2016) and its presence was reported intermittently in molecular studies. Taken together this suggests that the family Rhabditidae and the order Diplogastrida offer the most consistently robust response in decomposition hotspot environments.

We also observed that while Rhabditidae was enriched to varying degrees over much of the decomposition process (through day 188), enrichment of other B1 taxa was more short-lived in comparison. For example, *Pelodera* and Diplogastridae abundances were elevated between days 15-110. This result suggests that the presence of Diplogastridae enrichment is constrained to a window (in this case approximately 100 days) representing active decay through early skeletonization. *Pelodera* abundances peak very distinctly on day 40, congruent with peak abundance and diversity impacts in both core and interface soils, thus potentially functioning as a genus-level indicator for this narrow period of time. At family-level taxonomic rank Rhabditidae does not appear to provide further resolution than *Pelodera*, simply due to generalized long-term enrichment. Other free-living Rhabditidae genera, notably *Oscheius tipulae*, have been reported in amplicon sequencing surveys during the period of advanced decomposition [18]. While our

study did not differentiate Rhabditidae at the genus level beyond that of documenting the outstanding representation from the genus *Pelodera*, it is worth noting that enrichment responses of genera found within Rhabditidae have varied between studies, decomposing organism, and extraction methodologies, whereas the family Rhabditidae as a whole has been shown over multiple studies to respond very strongly and consistently to decomposition, thus suggesting that the application of genus-level resolution to cp 1 enrichment-opportunistic taxa when tracking decomposition progression is not advisable.

Cp-2 response patterns

Nematodes occupying the cp-2 class, which includes both bacterial and fungal feeders, generally became more dominant as the populations of cp-1 opportunists declined due to dwindling microbial food supply. In our study, cp-2 taxa displayed mixed reactions to decomposition enrichment. The general opportunists *Aphelenchoides* (F2) and *Acrobeloides* (B2) exhibited maximum abundances during late skeletonization (day 153) in cores, and in interfaces a month later (day 188), increasing in abundance throughout skeletonization. This *Aphelenchoides* enrichment was also observed post-heating in compost systems [70]. *Aphelenchoides* and *Acrobeloides* both satisfy criteria for consideration as suppression indicator taxa at the onset of active decay and through the early phases of skeletonization (days 15-110). Additionally, *Aphelenchoides* and *Acrobeloides* also satisfy enrichment criteria as indicators to frame the transition from early to late skeletonization, so it is possible that this pair of nematodes might be used in tandem to describe a midpoint in the skeletonization process around day 153. While suppression is suggestive of either environmental sensitivity or competition for resources, and conversely an enrichment response is suggestive of increased food availability, further study needs to be done comparing microbial quantities and changes in soil chemistry to see what these

decomposition periods directly correspond to.

Filenchus (F2) was the most abundant fungivore found in both interface and core control samples. During the early stages of decomposition *Filenchus* abundances sharply decreased in both cores and interface samples, and upon reappearance remained below control levels. This suppression of *Filenchus* in close temporal proximity with Rhabditidae (and *Pelodera*) peak abundances poses questions as to how *Filenchus* responds to the types of soil nutrient enrichment and/or prevailing conditions found in decomposition environments, as well as suggesting its use as a suppression indicator taxon to frame this early decomposition time period. We previously reported low abundances of *Filenchus* in a four-year-old grave [56], suggesting a potential sensitivity to decomposition products. In a controlled heating study of compost, Steel et al. (2013) showed that members of the family Tylenchidae (which includes *Filenchus*) did not survive a simulated heat peak of 60°C, whereas *Aphelenchoides* and Rhabditidae were found to survive this same heating process. While soil temperatures in our study did not approach those found in compost, they do suggest that even slightly elevated temperatures may have had a negative effect upon Tylenchidae. To our knowledge our study constitutes the second observation of an inverse correlation between *Filenchus* and select cp- 1-2 taxa, suggesting either a potential interaction between *Filenchus* and other cp- 1-2 taxa or a sensitivity to physical and/or chemical conditions in the decomposition environment. While it is entirely possible that *Filenchus* suppression could arise as a result of competing ecological niches between cp- 1-2 taxa, studies examining niche partitioning using nematodes are uncommon in natural terrestrial ecosystems, aside from the characterization of nematode assemblages in agricultural, forest, and field settings. Far less is known about the effects of hotspot-type pulse disturbances [74]. Under the conditions associated with this study, fungivores and bacterivores belong to separate trophic

groups and thus are not presumed to be in direct competition for the same resources. Furthermore, the very nature of a hotspot-type pulse of resources provides large quantities of nutrient enrichment, and thus competition is likely to be reduced. In light of this, we are proposing that the response of *Filenchus* is driven more by thermal or chemical changes in the decomposition environment than by competitive interactions. In order to fully ascertain the effect of the decomposition environment upon *Filenchus*, however, interface data must be included from the beginning of the study, since by the time interface sampling was included in the sampling scheme, *Filenchus* abundances had already appeared to have diverged from control levels.

Plectus (B2) has been proposed as a potential indicator taxon responsive to chemical disturbances and stressed environments, shown to be negatively correlated with chemical fertilization, and positively correlated to organic amendments [41, 72]. We previously reported examining nematodes associated with decomposition products in a 4-year old multi-individual grave and found large quantities of *Plectus* within areas of still-decaying human remains [56]. However, in our study with beaver carcasses we observed the opposite: *Plectus* abundances fell below those of controls during the most active stages of decomposition, instead meeting suppression indicator criteria. In light of these new observations, it appears that the decomposition response of *Plectus* is inconsistent and requires further study.

Other taxa exhibited a generalized tendency toward decreased abundances at the onset of active decay and recovery or in some cases reappearance during skeletonization, however few were found with robust abundances or consistent patterns of decrease or increase, and therefore use as indicator taxa would not be compelling. Similarly, Szelecz et al., (2016) noted a general increase over time in the cp-2 class, but explicit partitioning into bacterial and fungal feeders was

not discussed [24, 44].

Seinura (P2) abundances peaked in interfaces on day 110, satisfying non-B1 enrichment indicator criteria during days 110-153 (the transition between early and late skeletonization). While *Seinura* abundances by themselves are not large, the increase of an order of magnitude relative to controls is notable in comparison to response by other taxa. *Seinura* is a predator in the family Aphelenchoididae with an unusually short life span ranging from 3 to 6 days; females can lay a single egg approximately every 2 hours upon achieving maturity [73, 74]. This localized enrichment of *Seinura* in conjunction with increasing density of both bacterial and fungal-feeding taxa around day 153 suggests that it might occupy a very specific environmental niche based upon availability of food supply or momentary competitive advantage, thus making it a potential indicator taxon associated with the community recovery period occurring during mid-skeletonization.

Cp-3 through cp-5 response patterns

In agricultural successional studies, as nutrient enrichment is depleted, community structure shifts toward a greater representation of fungal-feeding taxa and the gradual reappearance of *K*-selected taxa (cp-3 through cp-5); these include predators and omnivores that are shown to be sensitive to environmental perturbation [25, 49, 75]. In our study, cp class 3-5 taxa in carcass interface samples were strongly suppressed or found to be below detection at the onset of active decay in interfaces and during advanced decay in cores, and collectively recovered during skeletonization. Most taxa were of low enough abundance to be considered rare and potentially subject to sampling bias rendering their utility questionable, and thus did not meet suppression indicator taxon criteria; only *Achromadora* (O3), *Clarkus* (P4), and Dorylaimida (O4) were of sufficient abundance in interfaces to merit study, and their collective

reappearance occurred by day 153. Of these, only Dorylaimida met criteria as an enrichment indicator in the final portion of the study.

Of potential additional interest are Tylencholaimidae (F4) and *Prismatolaimus* (B3), which were present in control soils, remained suppressed in interface soils for the duration of the study, but recovered in cores at day 153. Both organisms meet criteria for suppression indicators from active decay through early skeletonization, and by late skeletonization serve as enrichment indicators for core soils. The response in interface soils is similar but less well-defined, particularly in the case of *Prismatolaimus*, thus not making it a robust candidate as an indicator. Given the overall rarity of these *K*-selected organisms, coupled with their environmental sensitivity, it might be preferable to consider functional diversity (cp-class composition or feeding type composition) recovery as a more descriptive diagnostic tool for decomposition progression rather than recovery of individual taxa within the original community membership.

Prior analyses of soil chemistry and microbial ecology in gravesoils have revealed temporal fluctuations in carbon and nitrogen speciation, microbial biomass, and respiration throughout decomposition progress. Keenan et al. (2018), in a recent vertebrate (beaver) decomposition study performed in close physical proximity to our study site, found that during the skeletonization period soil pH, electrical conductivity, respiration (evolved CO_2), and ammonium (NH_4^+-N) returned to near background levels from enrichment during active and advanced decay. Also during skeletonization nitrate (NO_3^--N) increased. That study began in July and occupied a warmer and thus shorter time period than our study which began in March, and therefore cannot be directly compared. However, evidence from our study suggests that several characteristic shifts in nematode populations might correspond to these chemical and microbial fluctuations. In our study B1 enrichment opportunist (Rhabditidae, Diplogastridae)

abundances reduced markedly by the midpoint of skeletonization, commensurate with increases primarily of *Acrobeloides* (B2), *Aphelenchoides*, Tylencholaimidae (F4), and a brief enrichment of *Seinura* (P2). This may correspond to a reduction of microbial activity and/or biomass, particularly bacterial, as shown by a reduction in soil respiration and bacterial production rates [2, 6]. This decrease in respiration and biomass suggests that bacterial abundances in the soil have dropped below levels necessary to sustain B1 reproduction, and thus allowing cp-2 class taxa to proliferate. This subsequent increase in cp-2 taxa during skeletonization also includes the appearance of the first fungal feeders, suggesting that fungal biomass may be increasing during this time. Additionally, high concentrations of ammonium typically found in the soil during the early phases of decomposition may have had a deleterious effect upon the more *K*-selected, and therefore more sensitive, nematode taxa [2, 4-8]. This disruption is supported by Tenuta and Ferris (2004) when they demonstrated that cp 4-5 class nematodes have difficulty tolerating both specific ion as well as osmotic effects of multiple nitrogen compounds [79].

Conclusions

We have confirmed that nematode succession occurs in soils as a result of vertebrate decomposition, and that the pattern is consistent with previous reports from other climates. Surface soils were found to experience the largest impact in abundance, alpha, beta, and functional diversity relative to subsurface (core) soils by up to an order of magnitude. Due to varied abundance responses within nematode colonizer-persister (cp) classes to decomposition-induced soil enrichment we propose a series of eight indicator taxa of mixed family and genus taxonomic rank to describe the progression of decomposition. Enrichment in two families, Rhabditidae and Diplogastridae, were observed during active and advanced decay, concomitant with suppression of the genus *Filenchus*, a fungal feeder normally found in abundance in control

soils. Early suppression of a mixture of bacterial and fungal feeding taxa (*Acrobeloides*, *Aphelenchoides*, and Tylencholaimidae) beginning in active decay and continuing through the early portions of skeletonization, followed by enrichment midway through the skeletonization process characterize the transition to later phases of skeletonization. Brief *Seinura* enrichment during this skeletonization transition may serve to further describe this period. Cp-class 3-5 taxa have previously been shown to display sensitivity to chemical disruption of their environment, and we observed their collective reappearance during the latest portions of skeletonization, when only dry remains were present. We have confirmed the robust presence of Rhabditidae, Diplogastridae, Cephalobidae (*Acrobeloides*), and *Aphelenchoides* as indicators associated with decomposition and enrichment environments common to observations reported from a variety of geographic regions, and have introduced *Filenchus*, Tylencholaimidae, and *Seinura* as new indicators that warrant further study.

Our study has revealed that the inclusion of interface sampling with traditional coring methods shows considerable promise as an analytical tool for nematode community studies, particularly in instances where severe chemical disruption and the potential for soil heating exists.

Having demonstrated in a vertebrate model system that nematode succession follows distinct temporal and vertical partitioning patterns, and that indicator taxa are apparent, we confirmed that patterns of nematode populations can outline portions of the decomposition process and thus support and confirm other chemical and biological studies of vertebrate decomposition in terrestrial ecosystems.

References

1. Kuzyakov Y, Blagodatskaya E. Microbial hotspots and hot moments in soil: Concept & review. Soil Biology & Biochemistry. 2015;83:184-99. doi: 10.1016/j.soilbio.2015.01.025.

2. Keenan SW, Schaeffer SM, Jin VL, DeBruyn JM. Mortality hotspots: Nitrogen cycling in forest soils during vertebrate decomposition. Soil Biology & Biochemistry. 2018;121:165-76. doi: 10.1016/j.soilbio.2018.03.005.

3. Towne EG. Prairie vegetation and soil nutrient responses to ungulate carcasses. Oecologia. 2000;122(2):232-239. doi: 10.1007/pl00008851.

4. Meyer J, Anderson B, Carter DO. Seasonal Variation of Carcass Decomposition and Gravesoil Chemistry in a Cold (Dfa) Climate. Journal of Forensic Sciences. 2013;58(5):1175-1182. doi: 10.1111/1556-4029.12169.

5. Stokes KL, Forbes SL, Tibbett M. Human Versus Animal: Contrasting Decomposition Dynamics of Mammalian Analogues in Experimental Taphonomy. Journal of Forensic Sciences. 2013;58(3):583-591. doi: 10.1111/1556-4029.12115.

6. Cobaugh KL, Schaeffer SM, DeBruyn JM. Functional and Structural Succession of Soil Microbial Communities below Decomposing Human Cadavers. Plos One. 2015;10(6):20. doi: 10.1371/journal.pone.0130201.

7. Metcalf JL, Xu ZZ, Weiss S, Lax S, Van Treuren W, Hyde ER, et al. Microbial community assembly and metabolic function during mammalian corpse decomposition. Science. 2016;351(6269):158-162. doi: 10.1126/science.aad2646.

8. Macdonald BCT, Farrell M, Tuomi S, Barton PS, Cunningham SA, Manning AD. Carrion decomposition causes large and lasting effects on soil amino acid and peptide flux. Soil Biology & Biochemistry. 2014;69:132-140. doi: 10.1016/j.soilbio.2013.10.042.

9. Benninger LA, Carter DO, Forbes SL. The biochemical alteration of soil beneath a decomposing carcass. Forensic Science International. 2008;180(2-3):70-75. doi: 10.1016/j.forsciint.2008.07.001.

10. Aitkenhead-Peterson JA, Owings CG, Alexander MB, Larison N, Bytheway JA. Mapping the lateral extent of human cadaver decomposition with soil chemistry. Forensic Science International. 2012;216(1-3):127-134. doi: 10.1016/j.forsciint.2011.09.007.

11. Fancher JP, Aitkenhead-Peterson JA, Farris T, Mix K, Schwab AP, Wescott DJ, et al. An evaluation of soil chemistry in human cadaver decomposition islands: Potential for estimating postmortem interval (PMI). Forensic Science International. 2017;279:130-139. doi: 10.1016/j.forsciint.2017.08.002.

12. Lühe B, Fiedler S, Mayes RW, Dawson L. Temporal fatty acid profiles of human decomposition fluid in soil. Organic Geochemistry. 2017;111:26-33. doi: 10.1016/j.orggeochem.2017.06.004.

13. Lühe B, Birk JJ, Dawson L, Mayes RW, Fiedler S. Steroid fingerprints: Efficient biomarkers of human decomposition fluids in soil. Organic Geochemistry. 2018;124:228-237. doi: 10.1016/j.orggeochem.2018.07.016.

14. Carter DO, Metcalf JL, Bibat A, Knight R. Seasonal variation of postmortem microbial communities. Forensic Science Medicine and Pathology. 2015;11(2):202-207. doi: 10.1007/s12024-015-9667-7.

15. Weiss S, Carter DO, Metcalf JL, Knight R. Carcass mass has little influence on the structure of gravesoil microbial communities. International Journal of Legal Medicine. 2016;130(1):253-263. doi: 10.1007/s00414-015-1206-2.

16. Hauther KA, Cobaugh KL, Jantz LM, Sparer TE, DeBruyn JM. Estimating Time Since Death

from Postmortem Human Gut Microbial Communities. Journal of Forensic Sciences. 2015;60(5):1234-1240. doi: 10.1111/1556-4029.12828.

17. DeBruyn JM, Hauther KA. Postmortem succession of gut microbial communities in deceased human subjects. Peerj. 2017;5:14. doi: 10.7717/peerj.3437.

18. Metcalf JL, Parfrey LW, Gonzalez A, Lauber CL, Knights D, Ackermann G, et al. A microbial clock provides an accurate estimate of the postmortem interval in a mouse model system. Elife. 2013;2:19. doi: 10.7554/eLife.01104.

19. Pechal JL, Crippen TL, Benbow ME, Tarone AM, Dowd S, Tomberlin JK. The potential use of bacterial community succession in forensics as described by high throughput metagenomic sequencing. International Journal of Legal Medicine. 2014;128(1):193-205. doi: 10.1007/s00414-013-0872-1.

20. Perotti MA, Braig HR. Phoretic mites associated with animal and human decomposition. Experimental and Applied Acarology. 2009;49(1-2):85-124. doi: 10.1007/s10493-009-9280-0.

21. Braig HR, Perotti MA. Carcases and mites. Experimental and Applied Acarology. 2009;49(1-2):45-84. doi: 10.1007/s10493-009-9287-6.

22. Seppey CVW, Fournier B, Szelecz I, Singer D, Mitchell EAD, Lara E. Response of forest soil euglyphid testate amoebae (Rhizaria: Cercozoa) to pig cadavers assessed by high-throughput sequencing. International Journal of Legal Medicine. 2016;130(2):551-562. doi: 10.1007/s00414-015-1149-7.

23. Szelecz I, Fournier B, Seppey C, Amendt J, Mitchell E. Can soil testate amoebae be used for estimating the time since death? A field experiment in a deciduous forest. Forensic Science International. 2014;236:90-98. doi: 10.1016/j.forsciint.2013.12.030.

24. Szelecz I, Sorge F, Seppey CVW, Mulot M, Steel H, Neilson R, et al. Effects of decomposing cadavers on soil nematode communities over a one-year period. Soil Biology & Biochemistry. 2016;103:405-416. doi: 10.1016/j.soilbio.2016.09.011.

25. Bongers T, Ferris H. Nematode community structure as a bioindicator in environmental monitoring. Trends Ecol Evol. 1999;14(6):224-228. doi: 10.1016/s0169-5347(98)01583-3.

26. Sechi V, De Goede RGM, Rutgers M, Brussaard L, Mulder C. Functional diversity in nematode communities across terrestrial ecosystems. Basic and Applied Ecology. 2018;30:76-86. doi: 10.1016/j.baae.2018.05.004.

27. Porazinska DL, Giblin-Davis RM, Powers TO, Thomas WK. Nematode Spatial and Ecological Patterns from Tropical and Temperate Rainforests. Plos One. 2012;7(9). doi: 10.1371/journal.pone.0044641.

28. Hoogen J, Geisen S, Routh D, Ferris H, Traunspurger W, Wardle DA, et al. Soil nematode abundance and functional group composition at a global scale. Nature. 2019;572(7768):194-198. doi: 10.1038/s41586-019-1418-6.

29. Yeates GW, Bongers T, Degoede RGM, Freckman DW, Georgieva SS. Feeding habits in soil nematode families and genera – An outline for soil ecologists. Journal of Nematology. 1993;25(3):315-331.

30. Bongers T, Bongers M. Functional diversity of nematodes. Appl Soil Ecol. 1998;10(3):239-251. doi: 10.1016/s0929-1393(98)00123-1.

31. Briar S, Tenuta M, Barker C, Entz M. Soil nematode community response to long-term crop rotation, organic management and prairie restoration in the Red River Valley of central North America. Journal of Nematology. 2009;41(4):313.

32. Ferris H, Bongers T. Nematode indicators of organic enrichment. Journal of Nematology.

2006;38(1):3-12.

33. Bongers T. The maturity index: an ecological measure of environmental disturbance based on nematode species composition. Oecologia. 1990;83(1):14-19. doi: 10.1007/BF00324627.

34. Neher DA. Role of Nematodes in Soil Health and Their Use as Indicators. Journal of Nematology. 2001;33(4):161-168.

35. Briar SS, Barker C, Tenuta M, Entz MH. Soil Nematode Responses to Crop Management and Conversion to Native Grasses. Journal of Nematology. 2012;44(3):245-254.

36. Crotty FV, Fychan R, Sanderson R, Rhymes JR, Bourdin F, Scullion J, et al. Understanding the legacy effect of previous forage crop and tillage management on soil biology, after conversion to an arable crop rotation. Soil Biol Biochem. 2016;103:241-252. doi: 10.1016/j.soilbio.2016.08.018.

37. Hoss S, Nguyen HT, Menzel R, Pagel-Wieder S, Miethling-Graf R, Tebbe CC, et al. Assessing the risk posed to free-living soil nematodes by a genetically modified maize expressing the insecticidal Cry3Bb1 protein. Science of the Total Environment. 2011;409(13):2674-2684. doi: 10.1016/j.scitotenv.2011.03.041.

38. Ortiz V, Phelan S, Mullins E. A temporal assessment of nematode community structure and diversity in the rhizosphere of cisgenic Phytophthora infestans-resistant potatoes. Bmc Ecology. 2016;16. doi: 10.1186/s12898-016-0109-5.

39. Porazinska DL, McSorley R, Duncan LW, Graham JH, Wheaton TA, Parsons LR. Nematode community composition under various irrigation schemes in a citrus soil ecosystem. Journal of Nematology. 1998;30(2):170-178.

40. Porazinska DL, Duncan LW, McSorley R, Graham JH. Nematode communities as indicators of status and processes of a soil ecosystem influenced by agricultural management practices.

Appl Soil Ecol. 1999;13(1):69-86. doi: 10.1016/s0929-1393(99)00018-9.

41. Zhao J, Neher DA. Soil nematode genera that predict specific types of disturbance. Applied Soil Ecology. 2013;64:135-141. doi: 10.1016/j.apsoil.2012.11.008.

42. Althoff PS, Todd TC, Thien SJ, Callaham MA. Response of soil microbial and invertebrate communities to tracked vehicle disturbance in tallgrass prairie. Appl Soil Ecol. 2009;43(1):122-130. doi: 10.1016/j.apsoil.2009.06.011.

43. Blakely JK, Neher DA, Spongberg AL. Soil invertebrate and microbial communities, and decomposition as indicators of polycyclic aromatic hydrocarbon contamination. Applied Soil Ecology. 2002;21(1):71-88. doi: 10.1016/s0929-1393(02)00023-9.

44. Steel H, de la Pena E, Fonderie P, Willekens K, Borgonie G, Bert W. Nematode succession during composting and the potential of the nematode community as an indicator of compost maturity. Pedobiologia. 2010;53(3):181-190. doi: 10.1016/j.pedobi.2009.09.003.

45. Steel H, Buchan D, De Neve S, Couvreur M, Moens T, Bert W. Nematode and microbial communities in a rapidly changing compost environment: How nematode assemblages reflect composting phases. European Journal of Soil Biology. 2013;56:1-10. doi: 10.1016/j.ejsobi.2013.01.003.

46. Ruess L. Nematode soil faunal analysis of decomposition pathways in different ecosystems. Nematology. 2003;5:179-181. doi: 10.1163/156854103767139662.

47. Meng FX, Ou W, Li Q, Jiang Y, Wen DZ. Vertical distribution and seasonal fluctuation of nematode trophic groups as affected by land use. Pedosphere. 2006;16(2):169-176. doi: 10.1016/s1002-0160(06)60040-4.

48. Arieira GdO, Santiago DC, Franchini JC, Guimaraes MdF. Depth-stratified soil sampling for assessing nematode communities. Semina-Ciencias Agrarias. 2016;37(2):715-727. doi:

10.5433/1679-0359.2016v37n2p715.

49. Ferris H, Matute MM. Structural and functional succession in the nematode fauna of a.soil food web. Applied Soil Ecology. 2003;23(2):93-110. doi: 10.1016/s0929-1393(03)00044-1.

50. Dautartas A, Kenyhercz MW, Vidoli GM, Jantz LM, Mundorff A, Steadman DW. Differential Decomposition Among Pig, Rabbit, and Human Remains. Journal of Forensic Sciences. 2018;63(6):1673-83. doi: 10.1111/1556-4029.13784.

51. Steadman DW, Dautartas A, Kenyhercz MW, Jantz LM, Mundorff A, Vidoli GM. Differential Scavenging Among Pig, Rabbit, and Human Subjects. Journal of forensic sciences. 2018. doi: 10.1111/1556-4029.13786.

52. Climate Data Online (CDO). National Climatic Data Center (NCDC): National Centers for Environmental Information, National Oceanic and Atmospheric Administration; 2018 [cited 16 April 2018]. Available from: https://www.ncdc.noaa.gov/cdo-web/datasets#LCD.

53. Soil Survey Staff. Soil Map: Natural Resources Conservation Service, United States Department of Agriculture; 2018 [cited 2018 16 April]. Available from: https://websoilsurvey.nrcs.usda.gov/app/WebSoilSurvey.aspx.

54. Payne JA. A summer carrion study of the baby pig *Sus scrofa* Linnaeus. Ecology. 1965;46(5):592-602. doi: 10.2307/1934999.

55. Jenkins WR. A rapid centrifugal-flotation technique for separating nematodes from soil. Plant Dis Rep. 1964;48((9)):692-692.

56. Keenan SW, Emmons AL, Taylor LS, Phillips G, Mason AR, Mundorff AZ, et al. Spatial impacts of a multi-individual grave on microbial and microfaunal communities and soil biogeochemistry. PloS one. 2018;13(12):e0208845-e. doi: 10.1371/journal.pone.0208845.

57. Okada H, Harada H, Kadota I. Fungal-feeding habits of six nematode isolates in the genus

Filenchus. Soil Biology & Biochemistry. 2005;37(6):1113-1120. doi: 10.1016/j.soilbio.2004.11.010.

58. Qing X, Bert W. Redefinition of Genus Malenchus Andrassy, 1968 (Tylenchomorpha: Tylenchidae) with Additional Data on Ecology. Journal of Nematology. 2017;49(2):189-206.

59. Siddiqi MR. Suborder Tylenchina. Tylenchida: parasites of plants and insects. 2000;(Ed.2):122-224. doi: 10.1079/9780851992020.0122.

60. Ferris H, Bongers T, de Goede RGM. A framework for soil food web diagnostics: extension of the nematode faunal analysis concept. Applied Soil Ecology. 2001;18(1):13-29. doi: 10.1016/s0929-1393(01)00152-4.

61. Kolde R. pheatmap: Pretty Heatmaps. 2019. Available from: https://CRAN.R-project.org/package=pheatmap.

62. Neuwirth E. RColorBrewer: ColorBrewer Palettes. 2014. Available from: https://CRAN.R-project.org/package=RColorBrewer.

63. R Development Core Team. R: A language and environment for statistical computing. Vienna, Austria. 2018. Available from: https://CRAN.R-project.org.

64. Wickham H. ggplot2: Elegant Graphics for Data Analysis. New York. Springer-Verlag; 2016.

65. Oksanen J, Blanchet FG, Friendly M, Kindt R, Legendre P, McGlinn D, et al. vegan: Community Ecology Package. R package version 2.4-2. 2017. Available from: https://CRAN.R-project.org, https://github.com/vegandevs/vegan.

66. Fox J. Companion to Applied Regression. Comprehensive R Archive Network. 2016. Available from: https://CRAN.R-project.org/package=car.

67. Wickham H. Easily Install and Load 'Tidyverse' Packages. Comprehensive R Archive

Network. 2017. Available from: https://CRAN.R-project.org/package=tidyverse.

68. Bongers T. The Maturity Index, the evolution of nematode life history traits, adaptive radiation and cp-scaling. Plant and Soil. 1999;212(1):13-22. doi: 10.1023/a:1004571900425.

69. Carter DO, Yellowlees D, Tibbett M. Cadaver decomposition in terrestrial ecosystems. Naturwissenschaften. 2007; 94:12-24. doi: 10.1007/s00114-006-0159-1.

70. Heaton V, Moffatt C, Simmons T. Quantifying the Temperature of Maggot Masses and its Relationship to Decomposition. Journal of Forensic Sciences. 2014;59(3):676-682. doi: 10.1111/1556-4029.12396.

71. Steel H, Verdoodt F, Cerevkova A, Couvreur M, Fonderie P, Moens T, et al. Survival and colonization of nematodes in a composting process. Invertebrate Biology. 2013;132(2):108-119. doi: 10.1111/ivb.12020.

72. Venette RC, Ferris H. Thermal constraints to population growth of bacterial-feeding nematodes. Soil Biology & Biochemistry. 1997;29(1):63-74. doi: 10.1016/s0038-0717(96)00259-3.

73. Felix M-A, Ailion M, Hsu J-C, Richaud A, Wang J. *Pristionchus* nematodes occur frequently in diverse rotting vegetal substrates and are not exclusively necromenic, while *Panagrellus redivivoides* is found specifically in rotting fruits. PloS one. 2018;13(8):e0200851. doi: 10.1371/journal.pone.0200851.

74. Neher DA. Ecology of Plant and Free-Living Nematodes in Natural and Agricultural Soil. Annual Review of Phytopathology. 2010; 48:371-94.

75. Fiscus DA, Neher DA. Distinguishing sensitivity of free-living soil nematode genera to physical and chemical disturbances. Ecological Applications. 2002;12(2):565-575. doi: 10.2307/3060963.

76. Wood FH. Biology of *Seinura Demani* (Nematoda-Aphelenchoididae). Nematologica. 1974;20(3):347-353. doi: 10.1163/187529274x00384.

77. Hechler HC, Taylor DP. The life histories of *Seinura celeris, S. oliveirae, S. oxura*, and *S. steineri* (Nematoda: Aphelenchoididae). Proceedings of the Helminthological Society of Washington. 1966;33(1):71-83.

78. Ettema CH, Bongers T. Characterization of nematode colonization and succession in disturbed soil using the maturity index. Biology and Fertility of Soils. 1993;16(2):79-85. doi: 10.1007/bf00369407.

79. Tenuta M, Ferris H. Sensitivity of nematode life-history groups to ions and osmotic tensions of nitrogenous solutions. Journal of Nematology. 2004;36(1):85-94.

Appendix 2

Table 2.1: Study day, sampling date, and morphological decomposition stage.

Study day	Sampling date	Decomposition stage
0	29-Mar-17	Placement
2	31-Mar-17	Fresh
6	4-Apr-17	Bloat
15	13-Apr-17	Active decay
21	19-Apr-17	Advanced decay 1
40	8-May-17	Advanced decay 2
78	15-Jun-17	Early skeletonization 1
110	17-Jul-17	Early skeletonization 2
153	29-Aug-17	Late skeletonization 1
188	3-Oct-17	Late skeletonization 2
250	4-Dec-17	Late skeletonization 3
317	9-Feb-18	Late skeletonization 4

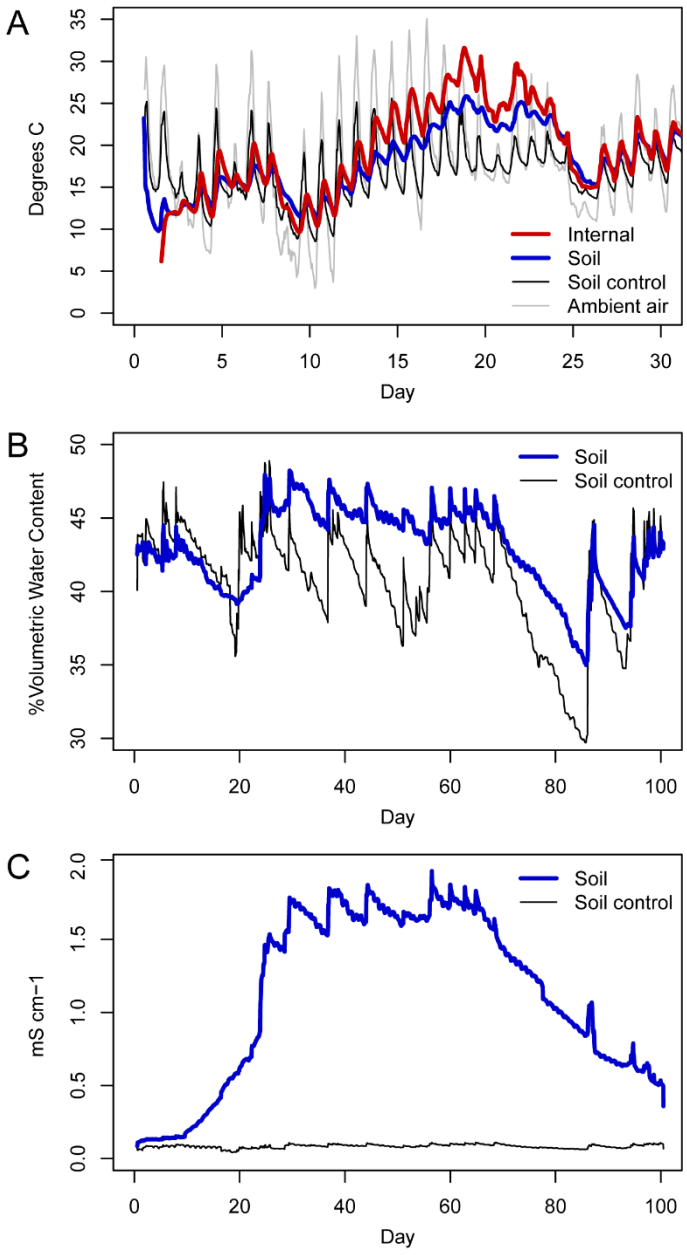

Figure 2.1: Soil and ambient environmental sensor data. (A) Mean internal, ambient, and soil temperatures, (B), mean soil moisture, and (C) mean soil electrical conductivity. Internal carcass temperature increased beginning on day 13 and remained elevated until day 25. Soil moisture and electrical conductivity rapidly increased following day 21 and remained elevated until day 95. Decomposition-impacted soils are shown in blue (A-C), soil controls are shown in black (A-C), internal temperatures are shown in red (A), and ambient air temperatures are shown in gray (A).

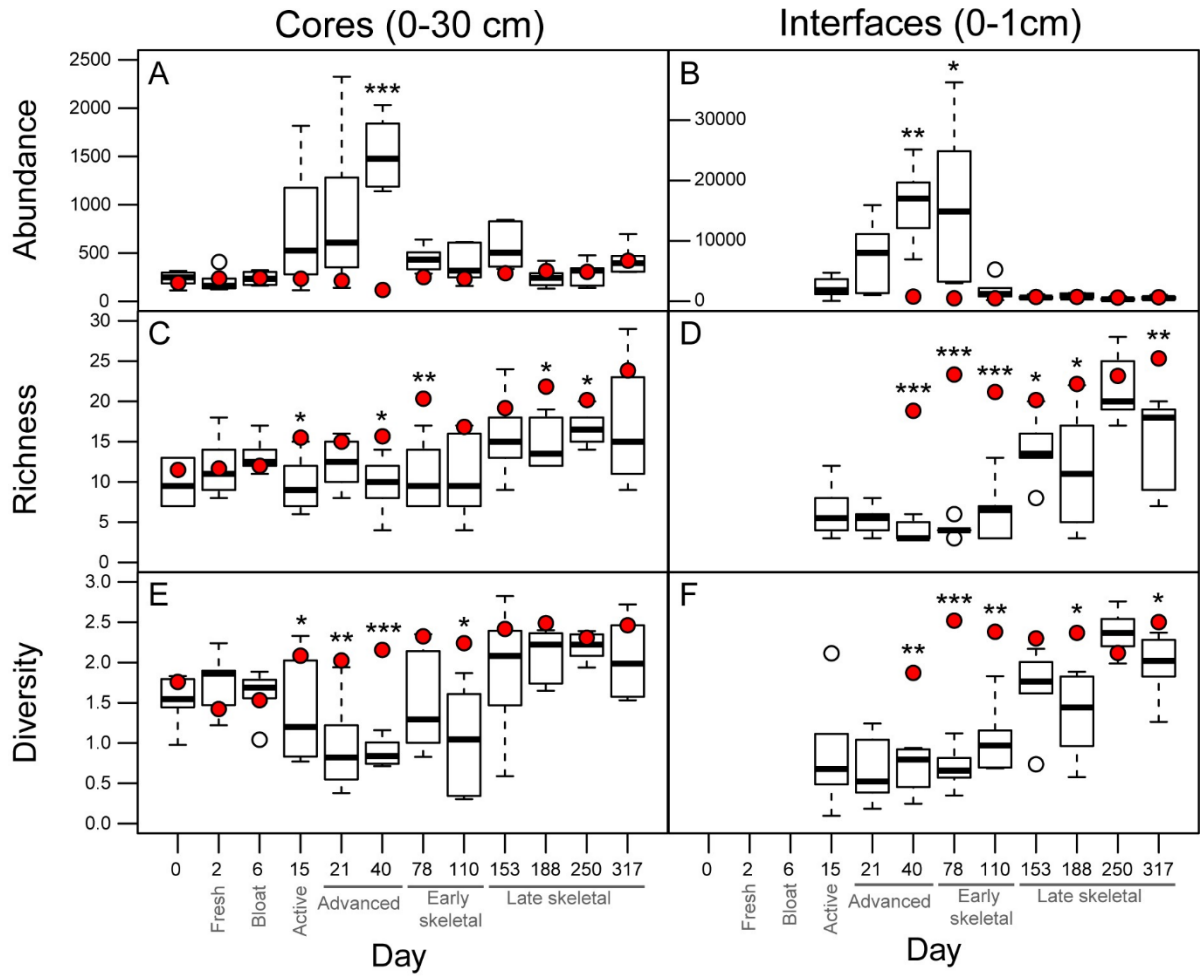

Figure 2.2: Nematode abundance, richness, and diversity. (A-B) Nematode abundances, (C-D) richness, and (E-F) Shannon diversity found in core (0-30 cm) and interface (0-1 cm) soils. Control means are represented by red dots. Interface data collection began on day 15, and interface control data collection began on day 40. Boxes display 25th and 75th quartiles and medians; whiskers display ± 1.5 quartiles.

This resource was prepared by the author(s) using Federal funds provided by the U.S. Department of Justice. Opinions or points of view expressed are those of the author(s) and do not necessarily reflect the official position or policies of the U.S. Department of Justice.

Table 2.2: Mean nematode abundance and alpha diversity by sampling depth.

		Core (0-30 cm)			Interface (0-1 cm)		
Day	**Location**	**Abundance**	**Richness**	**Diversity**	**Abundance**	**Richness**	**Diversity**
0	**Carcass**	**235 ± 75**	**9.8 ± 2.7**	**1.5 ± 0.3**	**-**	**-**	**-**
0	Control	193 ± 66	11.5 ± 2.2	1.8 ± 0.2	-	-	-
2	**Carcass**	**204 ± 107**	**11.8 ± 3.7**	**1.8 ± 0.4**	**-**	**-**	**-**
2	Control	237 ± 112	11.7 ± 2.9	1.4 ± 0.3	-	-	-
6	**Carcass**	**238 ± 66**	**13.2 ± 2.1**	**1.6 ± 0.3**	**-**	**-**	**-**
6	Control	242 ± 110	12.2 ± 3.7	1.5 ± 0.2	-	-	-
15	**Carcass**	**740 ± 651**	**9.7 ± 3.4***	**1.4 ± 0.7***	**2228 ± 1730**	**6.3 ± 3.4**	**0.9 ± 0.7**
15	Control	235 ± 80	15.5 ± 2.9	2.1 ± 0.1	-	-	-
21	**Carcass**	**886 ± 809**	**12.3 ± 3.1**	**1.0 ± 0.6****	**7581 ± 5738**	**5.3 ± 1.8**	**0.6 ± 0.4**
21	Control	214 ± 68	15.0 ± 1.7	2.0 ± 0.2	-	-	-
40	**Carcass**	**1525 ± 364*****	**9.7 ± 3.5***	**0.9 ± 0.2*****	**16323 ± 6251****	**3.8 ± 1.3*****	**0.7 ± 0.3****
40	Control	118 ± 31	15.7 ± 3.1	2.2 ± 0.3	783 ± 381	18.8 ± 4.0	1.9 ± 0.3
78	**Carcass**	**439 ± 127**	**10.7 ± 4.1****	**1.5 ± 0.6**	**16188 ± 13026***	**4.2 ± 1.0*****	**0.7 ± 0.3*****
78	Control	251 ± 154	20.3 ± 2.9	2.3 ± 0.4	503 ± 333	23.3 ± 5.4	2.5 ± 0.3
110	**Carcass**	**378 ± 192**	**10.5 ± 5.1**	**1.0 ± 0.7***	**1816 ± 1809**	**6.5 ± 3.7*****	**1.1 ± 0.4****
110	Control	235 ± 210	16.8 ± 4.4	2.2 ± 0.2	501 ± 235	21.2 ± 2.6	2.4 ± 0.3
153	**Carcass**	**562 ± 234**	**15.7 ± 5.1**	**1.9 ± 0.8**	**669 ± 289**	**14.0 ± 3.9***	**1.7 ± 0.5**
153	Control	292 ± 100	19.2 ± 1.9	2.4 ± 0.2	715 ± 340	20.2 ± 3.1	2.3 ± 0.2
188	**Carcass**	**250 ± 105**	**14.7 ± 3.1***	**2.1 ± 0.3**	**840 ± 400**	**11.5 ± 7.8***	**1.4 ± 0.6***
188	Control	315 ± 120	21.8 ± 2.9	2.5 ± 0.1	724 ± 195	22.2 ± 1.7	2.4 ± 0.2
250	**Carcass**	**293 ± 124**	**16.7 ± 2.2***	**2.2 ± 0.2**	**387 ± 255**	**21.5 ± 4.1**	**2.4 ± 0.3**
250	Control	306 ± 104	20.1 ± 3.1	2.3 ± 0.2	619 ± 139	23.2 ± 4.9	2.1 ± 0.4
317	**Carcass**	**428 ± 146**	**17.0 ± 7.7**	**2.0 ± 0.5**	**583 ± 313**	**15.2 ± 5.7****	**2.0 ± 0.4***
317	Control	421 ± 143	23.8 ± 1.9	2.5 ± 0.2	670 ± 183	25.3 ± 1.2	2.5 ± 0.2

Means are shown for soils underneath decomposing carcasses and for control soils (± one standard deviation). Paired-sample T-tests were conducted at each sampling time point and significant differences based upon $p < 0.05$ are denoted by asterisks. Levels of significance are indicated as follows: (*) $p < 0.05$, (**) $p < 0.01$, (***) $p < 0.001$.

Table 2.3: Effects of decomposition-impacted soils and time on nematode abundances and alpha diversity. Results of two-way ANOVAs comparing impacted soils (Treatment) and study date (Day), as well as interaction effects.

		Treatment		Day		Treatment*Day	
		F	**p**	**F**	**p**	**F**	**p**
Cores	**Abundance**	37.649	**<0.001*** **	5.641	**<0.001*** **	8.488	**<0.001*** **
	Richness	53.290	**<0.001*** **	9.278	**<0.001*** **	2.456	**0.008** **
	Shannon diversity	66.665	**<0.001*** **	8.041	**<0.001*** **	5.153	**<0.001*** **
Interfaces	**Abundance**	29.378	**<0.001*** **	11.164	**<0.001*** **	11.189	**<0.001*** **
	Richness	155.625	**<0.001*** **	10.871	**<0.001*** **	6.269	**<0.001*** **
	Shannon diversity	135.219	**<0.001*** **	11.632	**<0.001*** **	10.736	**<0.001*** **

Significant differences based upon $p < 0.05$ are presented in bold type. Asterisks indicate levels of significance: * $p < 0.05$, ** $p < 0.01$, *** $p < 0.001$

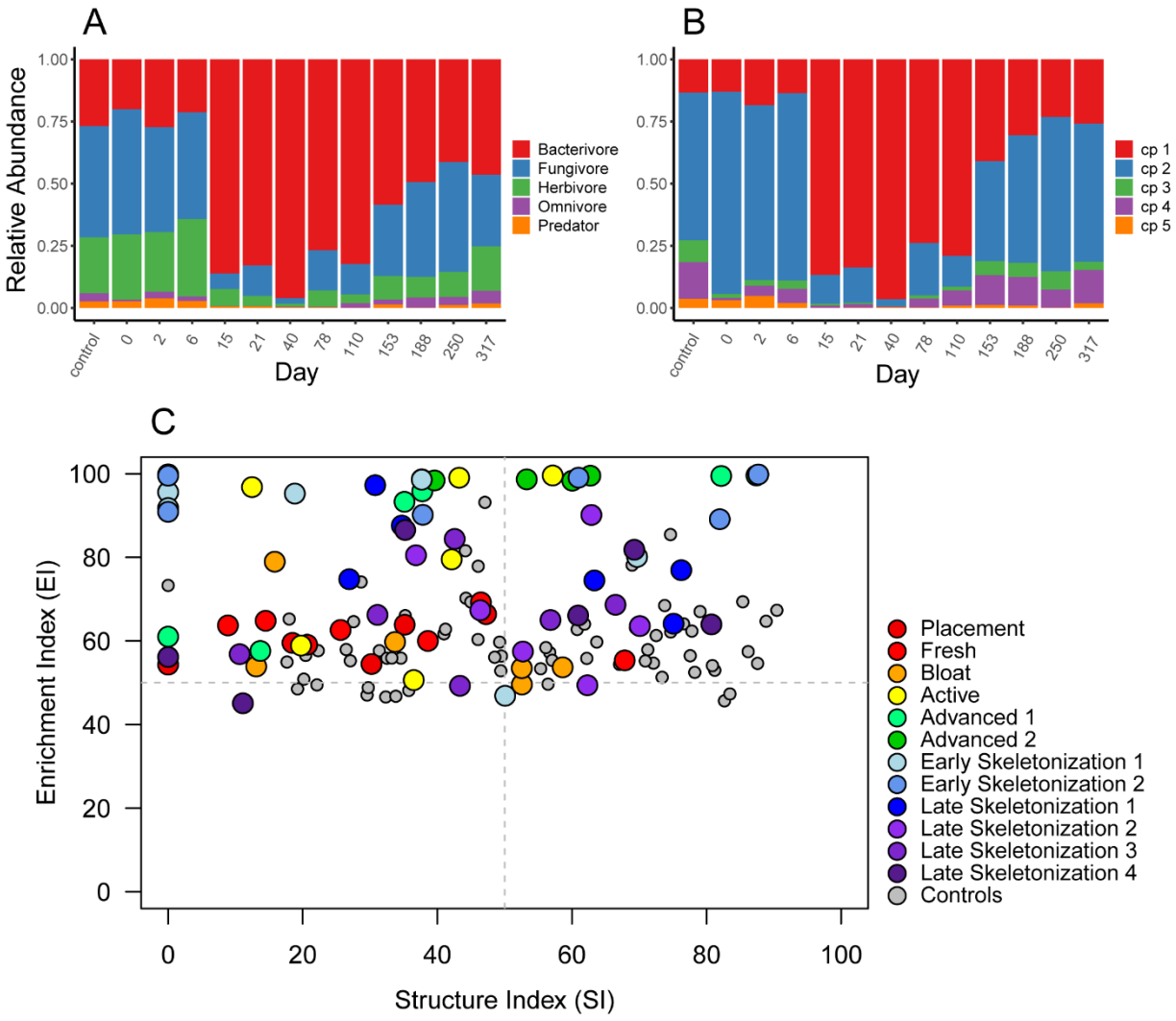

Figure 2.3: Temporal changes in nematode community composition and functional diversity in core (0-30 cm) soils. Relative abundances of (A) trophic groups, (B) cp-classes, and (C) functional diversity analysis for core (0-30 cm) soils.

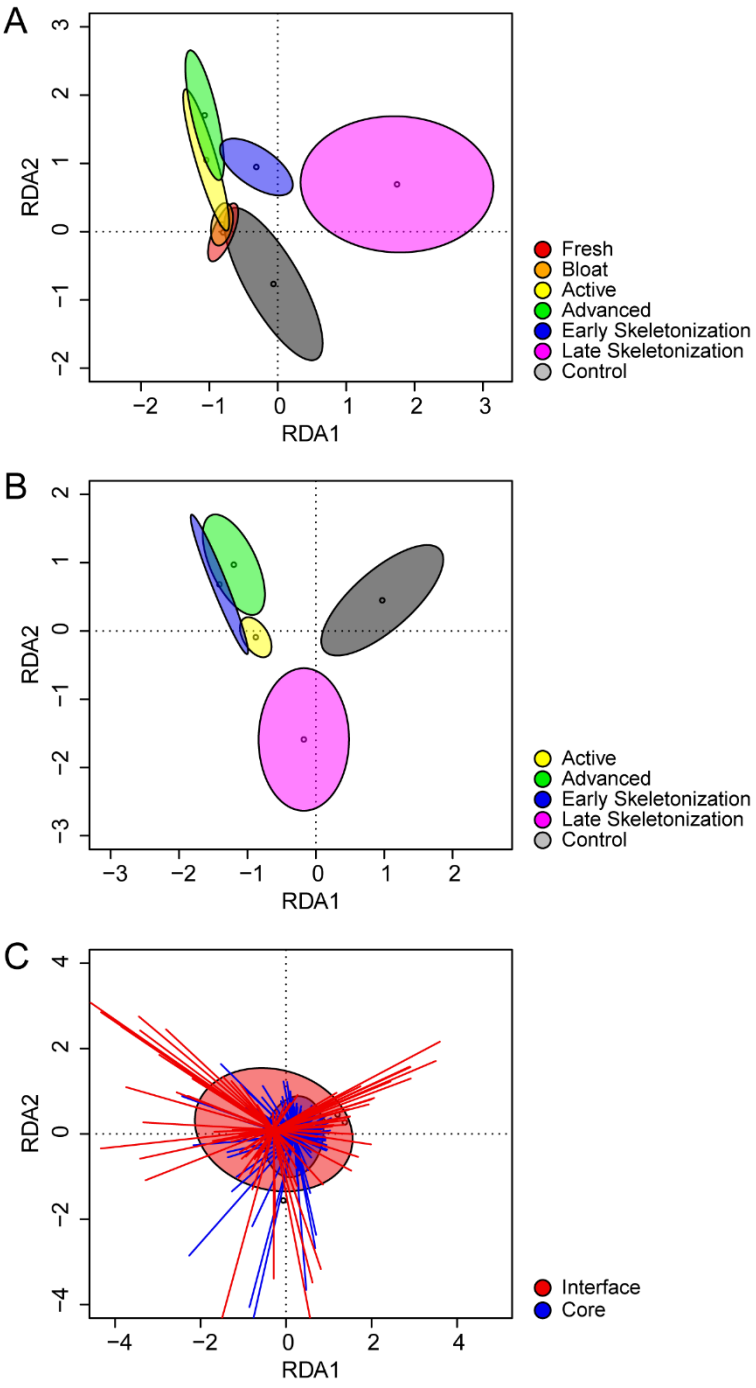

Figure 2.4: Nematode beta diversity. RDA biplots of nematode community trajectory during decomposition progress in (A) core (0-30 cm) and (B) interface (0-1 cm) soils. Ellipses represent standard deviations from decay stage centroids. Samples are grouped by morphological decomposition stage. Comparative changes at both soil depths (C) are shown for the entire study. Ellipses represent standard deviations from depth centroids, and spiders show distances from centroids.

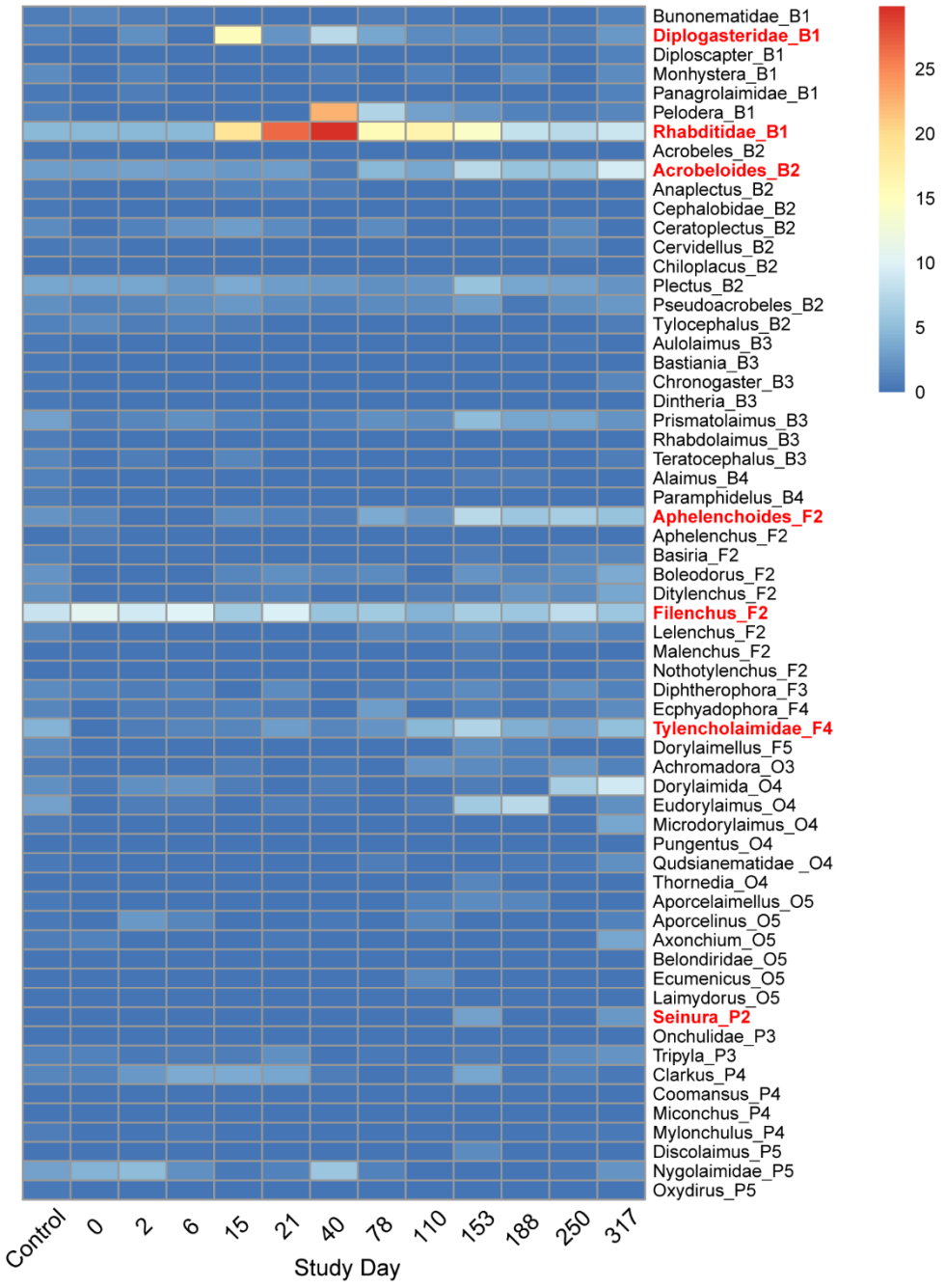

Figure 2.5: Temporal changes in nematode community composition for core (0-30 cm) soils. Heatmap showing mean abundances of taxa present in the following trophic groups: bacterivores, fungivores, omnivores, and predators. Samples are grouped by increasing cp-class, and cp designations are shown. All bacterial and fungal mean abundances are square-root transformed for scaling.

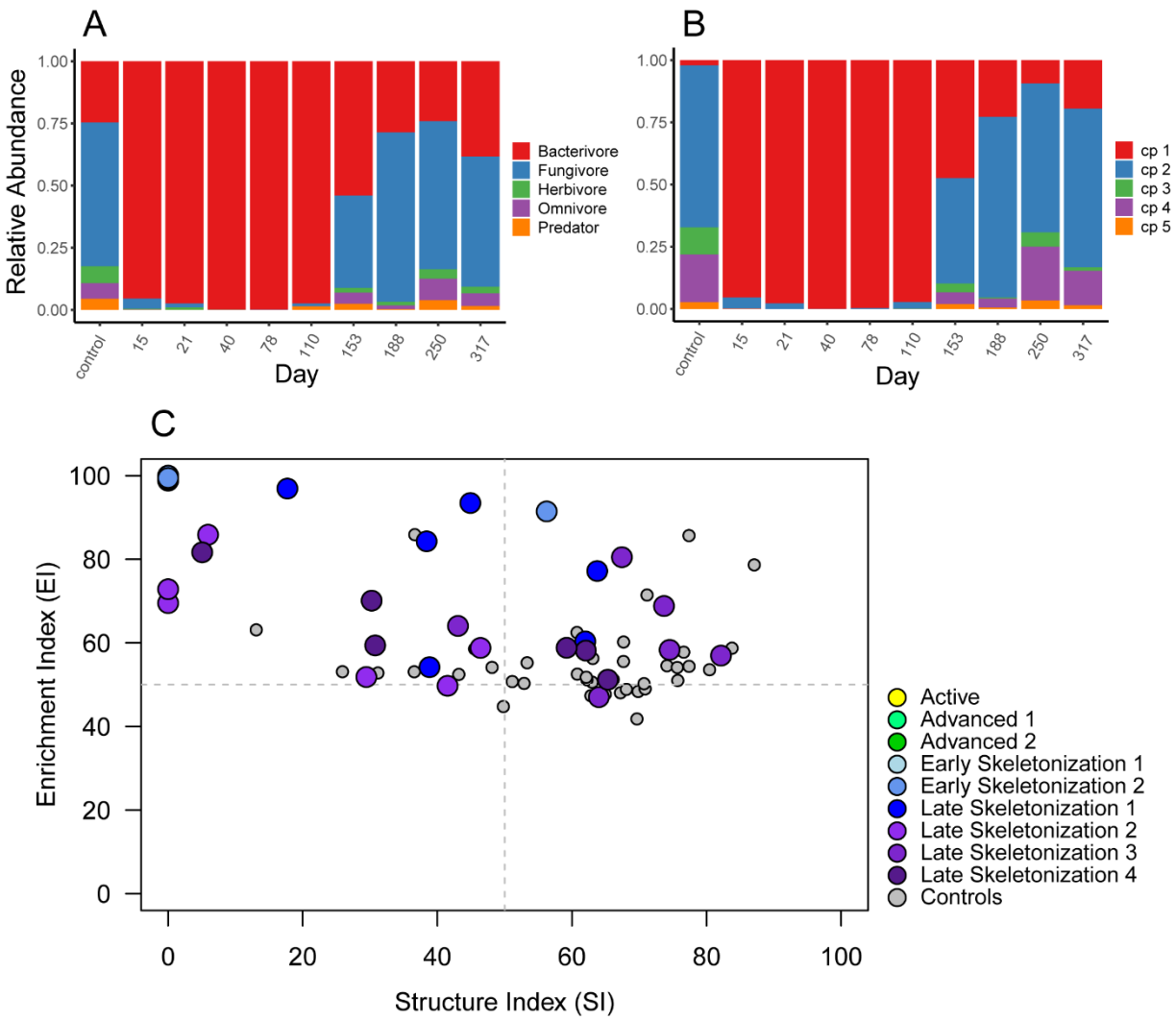

Figure 2.6: Temporal changes in nematode community composition and functional diversity in interface (0-1 cm) soils. Relative abundances of (A) trophic groups, (B) cp-classes, and (C) functional diversity analysis for core (0-1 cm) soils.

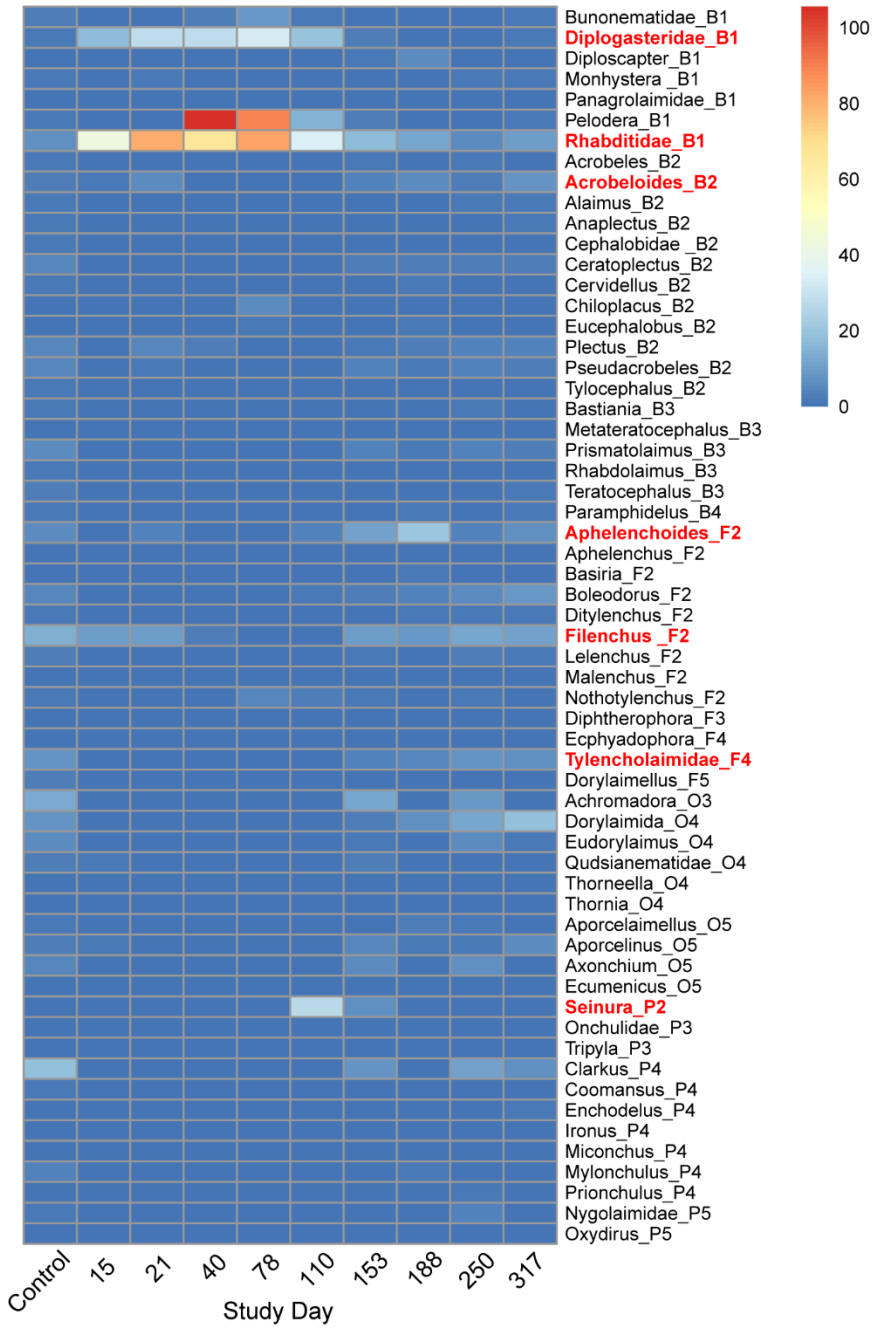

Figure 2.7: Temporal changes in nematode community composition for interface (0-1 cm) soils. Heatmap showing mean abundances of taxa present in the following trophic groups: bacterivores, fungivores, omnivores, and predators. Samples are grouped by increasing cp-class, and cp designations are shown. All bacterial and fungal mean abundances are square-root transformed for scaling.

This resource was prepared by the author(s) using Federal funds provided by the U.S. Department of Justice. Opinions or points of view expressed are those of the author(s) and do not necessarily reflect the official position or policies of the U.S. Department of Justice.

Chapter 3: Soil fungal and nematode community changes as a methodology for determining long-term postmortem interval after cadaver mass loss

Abstract

Human decomposition on the soil surface is a dynamic process, and the study of its progression through time under varied environmental conditions is crucial to our understanding of the processes involved, and, ultimately, refining estimates of postmortem interval (PMI). In the area of environmental and ecosystem vertebrate decomposition studies, soil physicochemistry has the largest and most extensive body of literature attributed to it. The study of microbial ecology, via the use of molecular investigation methods, is relatively new, and employs the use of high-throughput sequencing technology to examine entire microbial communities and their successional patterns in order to create PMI estimates. The use of sequencing technology to track changes in microbial community patterns is predicated on the concept that microbial decomposers in soil have important but differentiated functional roles in decomposition, and thus the continually changing conditions in the local environment (food accessibility, pH, salinity, etc.) will exert selective pressures on these communities driving their respective successional patterns. Microbial studies, however, seldom report soil chemistry data, and without this or supplementary environmental data it is only possible to infer how these organisms might be responding to these myriad environmental pressures. A third area of decomposition soil study has been largely neglected: that of microfaunal decomposers that utilize bacteria and fungi as food sources. Nematodes are uniquely situated in the foodweb as organisms most likely to be directly affected by fluctuating bacterial and fungal communities during decomposition processes, however their successional patterns under these circumstances have only been explored in animal model systems. Therefore, it is imperative that if nematode community dynamics are to be considered as a potential forensic tool, or even as supporting data, there needs to be a comprehensive understanding of their strengths and limitations in these environments. To

address these knowledge gaps between disciplines, we designed a pair of human decomposition studies with the following objectives: (1) characterize long-term decomposition progression in high temporal resolution, integrating soil physicochemistry, fungal ecology, and nematode ecology, and (2) characterize seasonal differences. In this high-resolution study we have demonstrated that environmental and soil chemistry parameters, soil fungal community succession, and free-living soil nematode succession are inextricably interlinked, and that these synergistic processes vary by season. Temporal patterns in fungal community composition revealed two prominent changes of successional trajectory, paralleling major changes across all soil chemical parameters, and specifically corresponded to transitions into and out of reduced-oxygen soil conditions. This evidence of direct linkage between soil chemistry and fungal succession further supports existing biogeochemical models, suggesting that fluctuations within soil chemical parameters may function as predictors for fungal successional patterns. Seasonal changes in nematode abundances are likely attributable to effects arising from larval thermogenesis. Based upon these collective results, we have shown that a comprehensive multidisciplinary approach is crucial for the effective study of human decomposition processes in soil.

Introduction

Human decomposition on the soil surface is a dynamic process, and the study of its progression through time under varied environmental conditions is crucial to our understanding of the processes involved, and, ultimately, refining estimates of postmortem interval (PMI). In the area of environmental and ecosystem vertebrate decomposition studies, soil physicochemistry has the largest and most extensive body of literature attributed to it, composed of a mixture of carrion and human studies, which can be further subdivided by surface-decomposed or buried remains, however for the purposes of this introduction we will focus on surface-decomposed remains. Edaphic parameters and soil chemistry data are reported unevenly throughout the literature. Standard physical soil characteristics are typically included, such as: soil series, parent material, soil horizons, and occasionally textural class. Climatological information ranges from the reporting of annual temperature and moisture means, to detailed temperature and moisture profiles throughout the study. Soil chemical characteristics generally focus on a core set of parameters, pH [1-13], and soil conductivity [1-6], followed by N and C speciation pools [1-5, 7-12, 14] which vary widely between studies and include total carbon and nitrogen (TC and TN), organic carbon and nitrogen (TOC, TON, ninhydrin-reactive nitrogen), and inorganic nitrogen (NH_4^+ and NO_3^-). Elemental analysis [4, 5, 7, 13, 15], as well as extracellular enzymes [2], protein, fatty acid, amino acid and peptide levels [1, 2, 9] are periodically analyzed. Measures of microbial activity, which include soil respiration, are infrequently reported in decomposition soil chemistry literature except as supporting data for microbial studies, or as means of focusing on carbon cycling via the release of CO_2 [2, 14, 16]. Given that microbial decomposers are an integral part of the soil environment, decomposition-induced changes in the soil will have profound effects upon their community structure and

functionality [17-19]. Therefore, it is critical that soil chemistry studies include parameters that are known influences upon microbial community structure in order for these studies to be relevant across disciplines.

The study of microbial ecology, via the use of molecular investigation methods, is a relatively new addition to forensic study and employs the use of high-throughput sequencing technology to examine entire microbial communities and their successional patterns in order to create PMI estimates. The use of sequencing technology to track changes in microbial community patterns is predicated on the concept that microbial decomposers in soil, at the domain level as well as all constituent taxonomic ranks, have important but differentiated functional roles in decomposition, and thus the continually changing conditions in the local environment (food accessibility, pH, salinity, etc.) will exert selective pressures on these communities driving their respective successional patterns. As applied to vertebrate decomposition, the majority of this work has been focused on exploring bacterial successional patterns [14, 16, 20-33] often associated with the early period of decomposition during which there is the greatest soft tissue mass loss [14, 22-24, 26]. Terrestrial studies have demonstrated that pH and electrical conductivity (often expressed in terms of salinity or ionic strength) are strong drivers of bacterial community structure [18, 19]. Likewise, organisms responsible for nitrogen cycling in the soil have been shown to be particularly sensitive to both pH and soil oxygen levels [17], and thus changes in redox status within soil aggregates, or soil as a whole, coupled with significant shifts in pH may exert strongly selective pressure not only on community composition but on nitrogen cycling pathways [9, 34]. Bacterial communities also generally have narrow optimal growth tolerances, and variances of + 1.5 pH units have been shown to affect activity by approximately 50% [19]. In comparison with evaluations of bacterial

communities, a small but growing body of study is dedicated specifically to exploring fungal community changes in decomposition environments [30, 32, 35-37]. Terrestrial studies examining pH gradients in soil have demonstrated that soil fungal communities tolerate much wider pH ranges than do bacteria, and that their degradative ability increases under acidic conditions [19, 38]. Saprophytic soil fungi produce enzymes that degrade cellulose, hemicellulose, and lignin [38], however plant residues have much higher C:N ratios than vertebrate resources [39]. Fungal fruiting structures have been observed associated with grave soil, and based upon the respective affinity of these organisms for ammonia or nitrate, it has been proposed that a functional grouping of nitrogen-associated fungi might be potentially useful for constructing time markers of late-stage decomposition progression [40-42], and yet the visual appearance of these taxa has not been confirmed. Additionally, human fungal commensals, symbionts, and pathogens have been characterized in living humans, however the presence of these organisms is inconsistent with currently reported data from 18S and ITS decomposition sequencing surveys (but see [43-45]). Data originating from soil chemistry studies have reported large fluctuations in all of these drivers of microbial community structure, as well as many others. Microbial studies, however, seldom report soil chemistry data, and without this or supplementary environmental data it is only possible to infer how these organisms might be responding to these myriad environmental pressures. Furthermore, microbial models proposed to date have been based upon a small number of study results garnered from a mixture of laboratory and field experiments, and thus are not robust over multiple climates, soil conditions, and seasons, nor do they take in to account intrinsic human variability [46, 47]. As a result, there is a critical need to equally examine bacterial and fungal patterns in soil in detail over the entire

temporal decomposition spectrum from early to late, and to fully support these results with comprehensive environmental and chemical data.

Another area of decomposition soil study has been largely neglected: that of microfaunal decomposers that utilize bacteria and fungi as food sources. There is a small body of literature that has studied these organisms in decomposition environments, which include mites, testate amoeba, and nematodes [48-55]. Of these organisms, nematodes have an extensive body of literature dedicated to their ecosystem functions. They can be partitioned into five principal trophic groups (bacterial feeders, fungal feeders, predators, omnivores, and plant feeders), they have well-described r-K selection attributes within each of those trophic classes, and there are a variety of nematode-specific ecological indices designed to describe their collective response to physical and chemical disturbances [56-67]. As a result, nematodes are uniquely situated in the foodweb as organisms most likely to be directly affected by fluctuating bacterial and fungal communities during decomposition processes. We previously proposed that nematodes might function as indicators for decomposition progression, as well as providing foodweb feedback information to supplement observations derived from changes in soil chemistry and microbial ecology [55]. They have also been regularly reported in 18S rRNA amplicon sequencing surveys as well-represented organisms present during early decomposition [21, 31-33], however the reported results of those surveys only present a very specific subset of taxa that are associated with enrichment events, but are not representative of nematode successional patterns as a whole [31, 32]. Therefore, it is imperative that if nematode community dynamics are to be considered as a potential forensic tool, or even as supporting data, there needs to be a comprehensive understanding as to their successional characteristics, as well as their strengths and limitations.

To address these knowledge gaps between disciplines, we designed a pair of human decomposition studies with the following objectives. The first of these objectives was to characterize long-term decomposition progression in high temporal resolution, integrating soil physicochemistry, fungal ecology, and nematode ecology. The second objective was to characterize seasonal differences in decomposition between a spring and winter trial.

In order to control as many variables as possible, we included three secondary criteria for human donor choice and for data presentation: replicate human donors used were within a very narrow weight range, donors were placed simultaneously so that environmental conditions within each season trial would be the same, and local temperatures were monitored so that data could be presented in terms of accumulated degree hours (ADH), allowing for comparison between seasonal trials since temperature is a known driver of decomposition progression. Of these criteria, the second is the most commonly satisfied in the human decomposition literature, however for reasons of study design it can be difficult or impossible to impose in all cases. To our knowledge, this study is one of the few that has successfully employed all three criteria for human donors.

Two other parameters were highlighted for investigation that are not typically assessed or that have been overlooked in decomposition study. We elected to focus on characterizing the fungal microbial succession, both to support findings of fungal-feeding nematode proliferation and to re-evaluate literature proposing fungi that are specifically associated with nitrogen deposition [32, 39, 40, 42, 68]. We also investigated the comparative results obtained by temperature sensors recording soil temperature data against those recording ambient temperatures; effects of larval thermogenesis can be directly recorded by the former, however ambient temperature recordings are assumed to mimic nearest-weather-station data typically

obtained and used for calculations of PMI. Soil sensors also recorded temperatures that are directly associated with chemical, microbial, and microfaunal activity [69-71].

Our study was designed to fill gaps in our understanding of decomposition progression by providing high-resolution, long-term, seasonal datasets, and simultaneously integrating three fields of study: microbial ecology (specifically fungal ecology), nematode ecology, and soil chemistry. We hypothesized that we would observe a detailed and nuanced view of long-term decomposition progression resulting from this high-resolution sampling scheme, and that we would also observe fungal and nematode successional changes that would be of forensic utility. As a result of the integration of soil chemistry, microbial ecology, and nematology, we expected to observe systematic changes in decomposition progression that could be newly linked across these disciplines, thus increasing robustness of conclusions drawn, as well as generating targeted avenues for further study. Finally, we expected to observe seasonal differences in patterns associated with all three disciplines, driven in part by the presence or absence of insect activity, and we expected to detect a relationship between these seasonal changes in terms of accumulated temperatures (ADH). Collectively, this body of work has the potential to define a new standard of expectation in multidisciplinary soil study that is necessary for refining estimates of the PMI across disparate seasons, soils, and geographical locations.

Materials and methods

Experimental site

This study took place at the University of Tennessee Anthropology Research Facility (ARF), Knoxville, TN, United States. The ARF is part of the University of Tennessee Forensic Anthropology Center (FAC), and is the longest running outdoor human decomposition facility in

the United States, in service since the 1980s [72]. The site is a temperate mixed deciduous forest, with understory of varying density throughout the facility. The Köppen climate classification is *Cfa* (humid subtropical). This facility sits on a ridgeline above the Tennessee River and is composed of a mixture of soils belonging to the Loyston-Talbott-Rock outcrop (LtD) and Coghill-Corryton (CcD) complexes. LtD soils are composed of clayey residuum weathered from limestone and have typical soil profiles consisting of silty clay loam and channery clay (0-25 cm) extending to lithic bedrock. Loyston soils are classified as clayey, mixed, active, Lithic Hapludalfs, and Talbott soils are classified as fine, mixed, semiactive, thermic Typic Hapludalfs. CcD soils are composed of clayey residuum weathered from quartzose limestone interbedded with calcareous sandstone, and shale. Coghill and Corryton series soils are both classified as fine, mixed, semiactive, thermic Typic Hapludults. Both Coghill and Corryton soils are common to Southern Appalachian ridges and slopes [73, 74]. Soils for the spring donor site were composed of 6.34% sand, 85.02% silt, and 8.64% clay. Soils from the winter site were composed of 10.96% sand, 81.44% silt, and 7.6% clay.

Site layout and donor placement

A total of six deceased human subjects (donors) were used in this study, which were donations to the FAC (https://fac.utk.edu/body-donation/) specifically for the purposes of decomposition research. No living human subjects were involved, and therefore this study was exempt from review by the University of Tennessee Institutional Review Board. No preferences were made for sex, ancestry, age, or height. Donors had not been autopsied nor were observed to have sustained physical trauma that might create artificial points of ingress for insects, microbes, or scavengers. Donors were selected within a weight range of 68-91 kg (150-200 lbs). Specific placement sites were chosen within new sectors of the ARF that had no records of previous use

for surface or burial decomposition experiments.

Donor placement in Spring 2018

Three male donors within a weight range of 90.7-91.6 kg (200-202 lbs) were accepted for this study. Heights varied by 5 cm, and ages by 14 years. Prior to placement in the field, internal temperature probes (Decagon Devices, RT-1) were inserted rectally into each donor, and donors were immediately frozen to ensure that conditions during field placement were consistent. Donors were placed at the study site unclothed, facing up, and in direct contact with soil to allow access to insect and scavengers, and were spaced 2 m apart to ensure isolation of replicates. Sensors were placed in the soil underneath each donor to measure soil temperature, moisture, and electrical conductivity (Decagon Devices, GS3). Sensors were placed approximately 50 cm above the soil surface to capture local ambient air temperature, but to avoid influence of elevated cadaver temperatures during decomposition. Data was collected from May 2, 2018 through May 13, 2019 (376 days), and consisted of daily photographs, visual assessment of decomposition stages according to Payne (1965) and Megyesi et al. (2005) [71, 75], local environmental data, and soil samples for soil chemistry, DNA extraction, and nematode community analysis.

Donor placement in Winter 2019

Three male donors within a weight range of 68.5-87.1 kg (151-192 lbs) were accepted for this study. These donors were placed 9 months after the start of the spring 2018 study in order to capture seasonal differences in decomposition patterns. Heights varied by 20 cm, and ages by 21 years. Pre-placement, placement, and data collection protocols were the same as those used in the spring study. Data collection began on February 8, 2019 and continued through February 27, 2020 (384 days).

Sample collection

Soil samples were taken at twenty time points throughout the year-long decomposition process in the spring study, and at nineteen points during the winter study. The first four samples in each series corresponded to visual assessments of decomposition stages after Payne (1965) and Megyesi et al. (2005) [71, 75]: Placement, day 0; bloat, day 8 (spring) or day 21 (winter); active decay, day 12 (spring) or day 38 (winter); onset of advanced decay, day 16 (spring) or days 55-75 (winter). Once advanced decay had begun, sampling continued at approximately evenly spaced intervals based upon equivalent thermal units: 8400 accumulated degree hours (ADD) or 350 accumulated degree days (ADD), as calculated by ambient air temperature measurements with a baseline threshold of 0 ^{o}C. For the spring study, the remainder of the sampling dates corresponded to days 27, 43, 58, 72, 86, 103, 117, 132, 150, 168, 201, 254, 303, 340, 357, and 376, with skeletonization occurring by day 303. For the winter study, the remainder of the sampling dates corresponded to days 94, 110, 126, 140, 158, 172, 186, 201, 216, 234, 252, 290, 335, and 384, with skeletonization occurring by day 158 (Tables 3.1-3.2).

Soil sampling was performed using a 1.9-cm (¾-inch) diameter soil auger to remove five 16-cm cores (or sufficient soil to equal 200 g) from underneath each donor as well as from paired control plots located 2 m away. Cores were divided into two depth segments: 0-1 cm, and 1-16 cm, and soils from each depth were composited to create single samples from underneath each donor and from control plots. Additional soil to the depth of 1 cm was removed from underneath donors and from control areas to bring the 1 cm-depth soil sample to 125 g. This 1 cm-depth sample was referred to as an interface sample and was designed to capture hot-spot effects in the immediate proximity to decomposing remains. Dissolved oxygen (DO) was measured underneath donors and in controls using an Orion Star A329 multiparameter meter

(ThermoScientific). A total of twelve samples were collected per sampling time point (six cores and six interfaces). Samples were transported back to the laboratory where soil aliquots for DNA extraction were flash-frozen and stored at -80C. All other soils were stored at 4^{o}C and were processed within 48 hours.

Soil chemical analyses

Soil chemical analyses followed methods detailed in Chapter 1 and Keenan et al. (2018) [2, 53]. Soils were hand-homogenized; rocks, insects, and large debris (> 2 mm) were removed, allowing small filamentous roots to remain in the samples to avoid artificially biasing samples against free-living plant-associated nematodes. Gravimetric moisture was calculated from mass loss following heating for 72 h at 105 ^{o}C. Soil pH and electrical conductivity (EC) were measured on soil slurries of 1:2 soil: deionized water using an Orion Star A329 multiparameter meter (ThermoScientific). Respiration rates were assessed according to protocols outlined in Keenan et al. (2018) [2]. Briefly, soils were sealed in 60 ml serum vials, and 0.5 ml headspace aliquots were removed immediately after sealing (T0), and again following a 24-hour incubation (T24). Measurements were conducted in duplicate using a LI-820 CO_2 gas analyzer (LICOR), and consisted of injection of 0.5 ml of the serum vial headspace. Soils were extracted in 0.5 M K_2SO_4, 1:4 parts soil and salt solution. Slurries were shaken at room temperature for four hours at 160 rpm, after which they were allowed to settle and then were vacuum-filtered using 1µm glass microfiber filters (Ahlstrom). Filtrates were stored at -20 ^{o}C until downstream processing. Ammonium and nitrate in filtrates were quantified colorimetrically in triplicate according to protocols outlined in Keenan et al. (2018a) and (2018b), and based off methods detailed by Rhine et al. (1998) [76], and Doane and Horwath (2003) [77], respectively. The following modifications were used for the ammonium protocol: ammonium standards [$(NH_4)_2SO_4$] were

dissolved in 0.5 M K_2SO_4 rather than in deionized water, 70 µl of sample filtrates were used in each microplate well rather than 50 µl, and 50 µl of deionized water was used in each microplate well rather than 100 µl.

Soil physical analyses

Particle size analysis (PSA) was performed on homogenized control soils. Soils were air-dried and sieved using 2 mm sieves. Following the removal of organic matter, particle size analysis was performed using a Malvern Mastersizer 3000 laser particle size diffractor. Analysis of clay minerals was performed according to methods outline in Soukup et al. (2008) [78]. Briefly, carbonates, organic matter, and free iron oxides were removed from soils prior to particle size fractionation and mounting of the clay-sized fraction for X-ray diffraction analysis (XRD). Carbonates and exchangeable divalent cations were removed by repeated centrifuge washings of soil with a 1M pH 5 Na acetate buffer. Organic matter and Mn oxides were removed by repeated additions of 30% H_2O_2 at 80^{o}C, followed by a four-hour digestion also at 80^{o}C. Fe oxides were removed by the additions of 0.3M Na citrate and 1M Na bicarbonate, followed by the addition of Na dithionite at 75^{o}C. Soils were then Na-saturated, and particles < 2µm (clay fraction) were isolated using Stoke's Law sedimentation. The clay fraction was saturated with K, Mg, and Mg-glycol and three slides were prepared for XRD: K-saturated at room temperature, Mg-saturated, and Mg-glycol-saturated. The K-saturated slide was subsequently heated to 300 ^{o}C, and 550 ^{o}C. Diffractograms were created using a Brüker D8 goniometer with Ni-filtered, Cu Kα radiation, operating at 20kV and 5 mA. Scan ranges were 2-30 $^o2\theta$, with a step size of 0.05 $^o2\theta$, and step rate of 3 sec.

DNA extraction, library preparation, and sequence processing

DNA was extracted from 250 mg samples using the QIAGEN DNeasy® PowerLyzer® PowerSoil® kit (Hilden, Germany) according to manufacturer's protocols, and including a prolonged bead beating step (4000 rpm for 45 s) recommended for soils with high clay content. DNA concentrations were quantified using a Nano Drop One spectrophotometer (ThermoScientific). Library preparation and sequencing was performed on the Illumina MiSeq platform at the Genomics Core Facility at the University of Tennessee, Knoxville. Sample preparation for amplicon sequencing consisted of PCR amplification of the fungal ITS2 rRNA region using a mixture of primers (6 forward and 2 reverse: ITS3NGS1, ITS3NGS2, ITS3NGS3, ITS3NGS4, ITS3NGS5, ITS3NGS10, ITS4NGR, and ARCH-ITS4) as previously described [79], to amplify regions of approximately 300-400 nucleotides in length. DNA samples were diluted 1:10 and PCR amplification was performed using 12.5 µl 2x KAPA HiFi HotStart ReadyMix Taq (Roche, Indianapolis, Indiana), 5 µL each of 1.5 µM forward and reverse primers, and 2.5 µl sample, for a total volume of 25µl per sample. PCR amplification consisted of denaturation at 95 ^{o}C for 3 minutes followed by 30 cycles of denaturation (95 ^{o}C for 30 s), annealing (55 ^{o}C for 30 s), and extension at (72 ^{o}C for 30 s), and a final elongation for 5 minutes at 72 ^{o}C. Results were visualized by gel electrophoresis. PCR cleanup was performed using AMPure beads (Agencourt, Beverly, Massachusetts). A second indexing PCR reaction was performed using Nextera XT indexes. PCR cycling was performed as described above except with 8 cycles of elongation. Index PCR cleanup was performed using AMPure beads, and concentrations were quantified using a Nano Drop spectrofluorometer. concentrations were determined on a Bioanalyzer (Agilent, Santa Clara, California). Loading concentrations were

4pM, 15% PhiX, and run paired-end on a V3 flow cell, on the Illumina MiSeq sequencing platform.

Quality control of reads was performed using a customized MOTHUR (v. 1.44.0) pipeline [80]. Briefly, paired end reads were merged and primers were trimmed, allowing a maximum of two differences on both forward and reverse primers. Sequences were screened to remove ambiguous bases, read lengths shorter than 200 bp, and duplicate sequences. Initial clustering was performed, allowing up to three differences between sequences. Chimeras were removed using VSEARCH, and sequences were mapped to the UNITE 8.2 reference database using the standard cutoff of 80% [81]. Unwanted lineages were removed. Since ITS sequences are of differing length, sequences were clustered into OTUs using greedy clustering with a cutoff of 0.05 in VSEARCH, and classified into OTUs. The final dataset contained 9,195,560 sequences with 25,666 unique OTUs for the spring dataset 5,869,460 sequences with 21,597 unique OTUs for the winter dataset.

Nematode extraction and calculation of alpha, beta, and functional diversity

Nematodes were extracted from soil using sugar-flotation centrifugation according to Jenkins (1964) [82]. Total abundances (N) were expressed as nematodes per 100 g dry weight of soil. Nematodes were counted and microscopically identified to primarily genus level with live samples under differential interference contrast (DIC) microscopy. Community richness was defined as the quantity of unique OTUs.

All calculations have been performed as described in Keenan et al. (2018) and Taylor et al. (2020) [53, 55]. Visualizations were created in R (version 3.6.1) and using the pheatmap (version 1.0.12) package [83, 84].

Statistical Analyses

Donors (n = 6) were treated as experimental replicates, each with a paired control site, and pooled by season: n = 3 in the spring, and n = 3 in the winter. One-way ANOVA ($p < 0.05$) was conducted to test for significant differences between impacted soils and control soils at each sampling time point for both soil chemistry and nematode data. Paired T-tests for each sampling time point were conducted to determine if impacted soils significantly differed from controls. PCoA on Bray-Curtis distances was performed on fungal communities, followed by PERMANOVA ($p < 0.05$) in order to test for significant differences by study day and decomposition morphological stage. Analyses and visualizations were conducted in R (version 3.6.1) using the tidyverse (1.2.1), car, (version 3.0-7), vegan, ggplot2 (version 3.2.1), RColorBrewer (version 1.1-2), and Phyloseq (Bioconductor BiocManager 1.30.10) packages [83, 85-90].

Results

Decomposition stages

Spring 2018

Three frozen deceased human subjects (hereafter, “donors”) were placed at the study site unclothed, facing up, and in direct contact with soil at the experimental site on day 0. By study day 1, fly egg masses were visible in the nasal cavities of all donors, and oral cavities of two donors. Some skin slippage was visible on arms, and skin color was tinged gray.

By day 2, extensive fly egg oviposition was evident throughout facial areas, and fly larval masses were present in the orbital areas. By study day 4, internal temperatures of the donors had equilibrated with ambient air temperatures. The faces of all donors were completely covered with

larval masses, and larval activity was extending toward the neck area. Small larval masses were developing in the genital areas, and the first evidence of bloating was visible on the sides of the donors' abdomens. Differential decomposition between donors became apparent by day 7: while all three donors increasingly showed signs of bloat, donor 2 exhibited partial skeletonization of the cranium along with the first evidence of purge fluids in the soil. Donors were sampled on study day 8 when all three donors exhibited extensive bloated conditions, such that the torso area was distended, and skin was taut (Table 3.1). Day 9 marked the beginning of fluid seepage from the genital area of donor 3, the formation of the "cadaver decomposition island" (CDI, *sensu* Carter (2007) [39]) for donor 2, while donor 1 remained bloated with larval activity restricted to the head and shoulder areas. By study day 12, the torso areas of all donors had begun to cave in. Throughout days 13-15, larval mass sizes peaked, and cervical spine exposure was evident in most donors. Donors were sampled again on day 16 at the onset of advanced decay. At this point, donor 1 still had larval masses in the groin area. Generally, visible changes in decomposition progression had slowed, and all donors exhibited noticeable mass loss, however donor 1 decomposed the most slowly of the three. By study day 20, only a few larvae were visible on any of the donors, and soils were noticeably greasy. Donor 1 was showing signs of mummification, as well as the first visible evidence of fungal growth on the limbs. From this point forward, sampling occurred at approximately 350 ADD (8400 ADH) intervals, in order to track decomposition in terms of equivalent thermal units. The remainder of advanced decay sampling occurred on study days 27, 43, 58, 72, 86, 103, 117, 132, 150, 168, 201, and 254. During this time all three donors and the soils beneath them exhibited intermittent white fungal growth. Beginning in day 35, the CDIs surrounding donors were less visible than previously, and skin on donors in the abdomen area began to show holes as it became thinner. A large pocket of

adipocere had developed underneath donor 1 by day 43, and *Piophila casei* ("cheese skipper") fly larvae were also present in the samples from this donor; adipocere remained until study day 72 at which point soils exhibited the crusty hard character than had been observed underneath donors 2 and 3 earlier. As the CDIs became less apparent, soils underneath donors 2 and 3 developed a crust. White fungal growth was still visible on the soil surface during this time. During the latter period of advanced decay (days 72-303) white and black fungal growth was visible on donor surfaces and on soil beneath them. Sampling continued through skeletonization on days 303, 340, 357, and 376. By the end of the study (day 376) donor 1 was fully skeletonized and disarticulated, donor 2 was mostly disarticulated with some tissue still present around the vertebral column, and donor 3 was still partially mummified but progressing toward skeletonization.

Winter 2019

A second set of three frozen donors was placed at the ARF nearby the first trio of donors such that local environmental and edaphic conditions as well as forest canopy and understory conditions were similar. By study day 3 some marbling of the torsos was present, and minor scavenging (primarily restricted to limbs) was observed. There were no signs of insect activity. By study day 5, internal temperatures had equilibrated with ambient temperatures. Between days 5 and 20 intermittent scavenging occurred, which largely subsided after day 20. Also, during this time limbs that were scavenged began to exhibit seepage of fluids. Donors were sampled on study day 21, which appeared to mark to onset of the bloat stage (Table 3.2). In the winter study the bloat stage was less-well defined than in the spring study. During the spring, considerable torso distention was observed that transitioned very suddenly to a purge of decomposition fluid. In contrast, during the winter the degree of bloating was very slight and transitioned to a

continual seepage of fluid. Donors were sampled on day 38 during active decay. Flies were observed in the vicinity, however there was no evidence of egg masses or fly larvae. Adipocere was present in soils under the torso region for all donors, and all donors had well-developed CDIs. As with the transition from bloat to active decay, it was difficult to judge the transition from active decay to advanced decay, therefore two samplings were performed on days 55 and 75, covering "active-advanced" and "advanced decay 1" respectively. On day 55, adipocere was still present, soils were visibly "greasy", and small amounts of larvae were found underneath donor 1. By day 75, few to no larvae were present, and adipocere was disappearing. The remainder of advanced decay samples were taken on days 94, 110, 126, and 140. During this time fungal colonies were observed on soils underneath donors. Very little differential decomposition was observed and mass loss was very gradual. On day 110, cheese skippers were observed underneath donor 3. On day 140, significant progress toward skeletonization was observed in donors 1 and 2; tissue loss increased and ribs were disarticulated. Soils underneath donor 2 contained large quantities of white filamentous fungi, while donor 3 had a crusty orange fungus on the remaining tissue covering the cranium. With the exception of donor 3, which mummified, donors were mostly skeletonized by sampling day 158, and the remaining sampling dates occurred during the dry remains stage for all donors: days 172, 186, 201, 216, 234, 252, 290, and 335. During this time period *Hermetia illucens* ("black soldier fly") larvae appeared under donor 3 on day 158, and white fungus was present on remaining tissue and in soils intermittently through day 216.

Environmental sensor data

Spring 2018

Sensors were placed inside donors (posterior insertion) to measure internal temperatures,

as well as beneath donors to capture changes in soil temperature, moisture, and electrical conductivity during the decomposition process. Additionally, ambient air temperature was measured approximately 50 cm above the ground surface (Figure 3.1A).

Donor internal temperatures and decomposition-impacted soil temperatures equilibrated with ambient air temperatures by day 4, and began to increase with respect to ambient air temperatures on day 8, the point at which donors were fully bloated. This period of elevated temperatures continued through day 80, halfway through advanced decay. The mean maximum internal donor temperature was 39.2 ^{o}C, and individual donor maxima ranged from 41.3-45.6 ^{o}C, corresponding to days 9-18, the period of time encompassing bloat through the transition to active decay, and commensurate with peak visible larval activity. The mean maximum soil temperature underneath donors was 41.7 ^{o}C and individual maxima ranged from 40.2-42.8 ^{o}C, corresponding to days 23-24, during early advanced decay. Ambient air and soil control temperatures did not differ from one another; overall temperature means for the study were 15.8 ^{o}C in both instances. Mean internal and soil temperatures were 18.8 ^{o}C and 17.7 ^{o}C, respectively. Increases in all temperatures, when tracked in ADH, reflect similarities between ambient air and soil control temperatures, as well as similarities between donor and impacted soil temperatures (Figure 3.2)

Soil moisture increased immediately upon donor placement and remained elevated for the majority of the study (Figure 3.1B). The largest increase above control values occurred between days 91-122, in the latter half of the advanced decay period, during which time soils were still covered by donor remains as well as what appeared to be a hard crust partially composed of decomposition materials. Soil moisture maxima in impacted soils ranged from 52.1-54.7 percent volumetric water content (%VWC) with a mean maximum of 52.9 %VWC, in contrast with

control soils in which the mean maximum reached 48.9 %VWC and control maxima that ranged between 36.5-55.3 %VWC. Over the course of the study, mean soil moisture was 36.9 %VWC in impacted soils and 29.4 %VWC in controls.

Electrical conductivity (EC) also increased immediately upon donor placement and remained elevated throughout the study (Figure 3.1C). A peak was observed on day 101 in advanced decay, followed by a general increase in conductivity throughout the remainder of advanced decay and skeletonization. Conductivity maxima ranged from 1.2-2.0 mS cm^{-1}, with an overall mean maximum of 1.2 mS cm^{-1} in impacted soils; the mean control soil maximum was 0.3 mS cm^{-1} and exhibited a range of 0.1-0.3 mS cm^{-1}. Conductivity study means in impacted soils were 0.4 mS cm^{-1} and in control soil were 0.1 mS cm^{-1}.

Winter 2019

In contrast to patterns observed in the spring, no distinct difference was apparent between internal, ambient, and soil temperature data; mean temperatures for the different series ranged from 15.1-16.4 ^{o}C (Figure 3.2, 3.3A).

Patterns in soil moisture mirrored those observed in temperature data. Soil moisture in impacted soils did not appreciably deviate from those of controls throughout the study; mean moisture for impacted soils and controls were 31.4 %VWC and 31.6 %VWC, respectively (Figure 3.3B). A general trend toward lower soil moisture was observed between days 75-275, corresponding to the onset of advanced decay through the latter portions of skeletonization, which occurred in late spring through early fall.

As observed with the spring study, conductivity increased immediately after donor placement, remaining enriched through day 210, and intermittently enriched through the remainder of the study (Figure 3.3C). The mean maximum conductivity in impacted soils was

0.8 mS cm^{-1} with individual donor maxima ranging from 0.7-1.2 mS cm^{-1}, in comparison with a control mean maximum of 0.2 mS cm^{-1} and individual range of 0.2-0.3 mS cm^{-1}. Over the course of the study, mean conductivity was 0.3 mS cm^{-1} in impacted soils and 0.1 mS cm^{-1} in controls.

Soil physicochemistry

Spring 2018 core (1-16 cm) samples

All soil chemical parameters in impacted soils differed significantly from control soils (ANOVA, $p < 0.001$) (Tables 3.3-3.4). The first changes to soil chemistry were detected during the bloat phase (day 8; 2,703 ADH based on donor soil); bloat was well-developed in these donors, and the first evidence of fluid seepage into the soil was visible at this time (Figure 3.4 A, C, E, G, I, K, Figure 3.5 A-F, Tables 3.4-3.5). During this bloat period, decreases in pH and increases in electrical conductivity (EC) were significant. Soil oxygen (DO) decreased, and respiration increased significantly by active decay (day 12; 5,362 ADH). Depending upon whether soil chemistry parameters responded to decomposition by increasing (EC, respiration, ammonium, and nitrate) or decreasing (pH and soil oxygen), the widest response margin between any parameter and its respective control occurred between active and early advanced decay (days 12-58; 5,362-41,581 ADH). The pH of all donors decreased until early advanced decay (day 43; 30,771 ADH) and remained variable thereafter. Mean conductivity increased during bloat (day 8; 2,703 ADH), peaking during the onset of advanced decay (day 16; 8,360 ADH) at 568.7 ± 232.3 µS cm^{-1}. Respiration rates increased between active and early advanced decay (days 12-58; 5,362-41,581 ADH), peaking at 60 ± 10 µmol CO_2 gdw^{-1} day^{-1} on day 58 (41,581 ADH). Ammonium concentrations were enriched during the early portion of the study, peaking during early advanced decay (day 16; 8,360 ADH) at 665.17 ± 375.55 µg gdw^{-1}. Mean dissolved oxygen decreased to 59.7% during bloat (day 8; 2,703 ADH), ultimately reaching a minimum

value of 38.9% at the subsequent sampling during active decay (day 12; 5,362 ADH), after which it gradually recovered by day 168 (107,850 ADH). Nitrate levels remained low through the early phase of the study while soil oxygen was depleted and ammonium was enriched; as soil oxygen and ammonium recovered, nitrate increased to a maximum during late advanced decay (day 117; 79,553 ADH) at 72.62 ± 56.16 µg gdw^{-1}.

Spring 2018 interface (0-1 cm) samples

As observed in core samples, all parameters in decomposition-impacted interface soils differed significantly from controls (ANOVA, $p < 0.001$) (Tables 3.3, 3.6). Initial changes to soil chemistry were detectable during the bloat stage (day 8; 2,703 ADH), and overall response patterns were consistent with those observed in core soils, however the data range was wider in both impacted soils as well as controls (Figure 3.4 B, D, F, H, J, Figure 3.6 (A-E), Tables 3.5-3.6). All soil chemistry parameters reached their maxima between bloat and early advanced decay (days 8-27; 2,703-18,289 ADH) with the exception of pH and nitrate; pH decreased intermittently throughout the study and nitrate reached a maximum during late advanced decay (day 168; 107,850 ADH) 220.5 ± 116.54 µg gdw^{-1}. Mean conductivity reached a maximum enrichment of 969.1 ± 1336.7 µS cm^{-1} during bloat (day 8; 2,703 ADH), with a subsequent drop to 4 ± 0.9 µS cm^{-1} in active decay (day 12; 5,362 ADH); this latter was commensurate with high quantities of "greasy" decomposition products in soil samples and extracts, and was observed in soils beneath all three donors. Respiration peaked in early advanced decay (day 27; 18,289 ADH) at 94.2 ± 19.3 µmol CO_2 gdw^{-1} day^{-1}. The maximum for ammonium occurred during active decay (day 12; 5,362 ADH), at 6905.52 ± 1325.29 µg gdw^{-1}.

Winter 2019 core (1-16 cm) samples

Progression through the early morphological stages of decomposition was slower during

the winter trial than in the spring trial, and exhibited a more gradual mass loss. As noted earlier, the release of internal fluids was gradual during the winter trial in comparison with the spring trial, and occurred over a longer period of time. Soil chemical parameters in decomposition-impacted soils all significantly differed from control soils throughout the study as a whole (ANOVA, $p < 0.001$) (Figure 3.7, Table 3.7-3.8). However, in comparison with immediate soil response apparent during bloat in the spring study, parameters in the winter study underwent a gradual enrichment (or decrease), until active and early advanced decay (days 38-75; 7,594-22,782 ADH), and maxima (or minima) occurred throughout advanced decay into skeletonization (days 75-158; 22,782-71,952 ADH) (Figure 3.5 (A-F), Figure 3.7 A, C, E, G, I, K, Tables 3.8-3.9). Mean soil pH gradually declined to a minimum of 6.3 ± 0.3 in early skeletonization (day 158; 71,952 ADH). Conductivity and respiration rates both reached maximum values on day 110 (43,005 ADH) at 356.4 ± 184.9 µS cm^{-1} and 36.3 + 21.9 µmol CO_2 gdw^{-1} day^{-1}. Soil oxygen levels declined gradually over 75 days, dropping to only 71.3% of initial values and recovered by day 201 (95,552 ADH). Ammonium exhibited broad enrichment throughout active decay and early skeletonization (days 38-172; 7,594-79,891 ADH), however both ammonium and nitrate exhibited enrichment maxima on day 140 (60,714 ADH) at 329.38 ± 210.54 and 75.67 ± 48.93 µg gdw^{-1}, respectively. The log ratio of ammonium to nitrate, 0 (1:1) in initial soils, crossed the zero threshold (1:1) again at approximately 100,000 ADH, concurrent with soil reoxygenation to 100%; this is consistent with patterns in the log ratio for spring soils (Figure 3.8A).

Winter 2019 interface (0-1 cm) samples

As observed in winter trial core samples, all interface soil chemical parameters differed significantly from control soils (ANOVA, $p < 0.001$) (Figure 3.7, Tables 3.9-3.10). With the

exception of pH and nitrate, soil chemical parameter maxima (or minima) occurred during active and early advanced decay (days 55-94) (Figure 3.6 (A-E), Figure 3.7 B, D, F, H, J, Tables 3.8-3.10). In a manner similar to that observed in winter trial cores, pH declined intermittently throughout the study, falling to a minimum of 6.2 ± 0.2 mid-way through skeletonization (day 216; 104,845 ADH). Mean conductivity and ammonium concentrations both reached their maxima during active decay (day 55; 12,127 ADH) at 926.8 ± 576.7 µS cm^{-1} and 2,811.16 ± 2,241.18 µg gdw^{-1}. Respiration was enriched beginning in bloat (day 21), reaching a maximum in early advanced decay (day 94; 33,575 ADH) of 105.6 ± 8.3 µmol CO_2 gdw^{-1} day^{-1}. Nitrate enrichment peaked during skeletonization (day 216; 104,845 ADH) at 241.32 ± 139.96 µg gdw^{-1}. The log ratio of ammonium to nitrate reflected patterns observed in both cores and in spring samples (Figure 3.8B).

Soil Mineralogy

Spring and winter trial soils were located approximately 20 m apart, and similarity in x-ray diffractograms reflect a similarity in clay mineral composition of the soil (Figures 3.9 A-B). A characteristic shift in d-spacing from 1 nm under K^+ saturation to 1.4 nm under both Mg^{2+} and glycol saturation, was indicative of the presence of vermiculite [91, 92]. Since under Mg^{2+} and glycol saturation these peaks are not differentiated individually, this indicated the presence of interstratification with mica. Kaolinite (d=0.7 nm) was also present.

Fungal communities

Following initial pre-processing and library assembly, 9,195,560 sequences with 25,666 unique OTUs were generated for spring trial samples, and 5,869,460 sequences with 21,597 unique OTUs were generated for winter data. Singleton and doubleton OTUs were removed from datasets, leaving 6,021 and 5,808 remaining OTUs for spring and winter, respectively.

Principal coordinates analyses (PCoA) of Bray-Curtis distances were used to assess beta diversity by study day within both seasonal datasets. One-way PERMANOVA tests were run to assess significance by day and morphological stage. Composition differed between groups in all cases ($p < 0.001$) (Figures 3.10-3.13). In both spring and winter trials, PCoA results demonstrated that community changes occurred throughout the entire decomposition process, and that recovery to initial conditions did not occur by the end of one year for either seasonal study (Figures 3.10-3.13).

Of phyla representing greater than 2 percent contribution to relative abundance in spring trial soils, the dominant phylum found in both soil depths of controls was Ascomycota, followed by Basidiomycota, Mortierellomycota, Mucoromycota, and Rozellomycota (Figure 3.14). From bloat through early advanced decay (days 8-58) in interfaces, there was a shift to community composition almost exclusively composed of Ascomycota, concomitant with a reduction in relative abundances of Basidiomycota, Mucoromycota and Rozellomycota. This pattern was also observed in cores, however occurred over a shorter period of time (days 12-43). Shifts toward communities dominated by Ascomycota occurred simultaneously with decreases in pH and soil oxygen levels, and peak elevations of electrical conductivity (day 8 in interfaces and day 16 in cores), respiration rates (day 27 in interfaces and day 58 in cores), and ammonium concentrations (day 12 in interfaces and day 16 in cores). During this same period of time, soil temperatures remained consistently elevated above 30 ^{o}C, fly larval activity was present, and nematode abundances were reduced.

Community composition and relative abundances of phyla during the winter trial were similar to those found in the spring trial. However, during initial decomposition, a shift to Ascomycota dominance was less pronounced than in the spring (Figure 3.15). Rozellomycota

abundances were reduced from active decay through skeletonization (day 55-335). On day 38 of all samples (controls and impacted soils) Mortierellomycota, Mucoromycota were both enriched; this degree of enrichment happened at no other time point.

At class-level, dominant (> 5 % sample relative abundance) taxa in spring trial impacted soils were those of Saccharomycetes (Ascomycota) and Sordariomycetes (Ascomycota) (Figure 3.16A). Relative abundances of Saccharomycetes increased between bloat and advanced decay days 8-72) and constituted the bulk of impacted interface samples (approximately 75%); the temporal pattern of Saccharomycetes enrichment was the same in cores, however relative abundances were reduced in comparison with interfaces (approximately 50%). In controls, Sordariomycetes generally constituted 20-40% of sample relative abundances (Figure 3.16B). However, during Saccharomycetes enrichment, Sordariomycetes percentages dropped to below 20% relative abundance in interfaces, and following the reduction of Saccharomycetes, Sordariomycetes became dominant in terms of relative abundances in interfaces throughout the remainder of the study (>25%) (Figure 3.16A). In impacted cores, Sordariomycetes still constituted the single dominant taxon, but with relative abundances of approximately 20-40%. In impacted soils, Tremellomycetes (Basidiomycota) increased beginning in early advanced decay (day 27), peaking in days 86-117; this taxon was not present in control soils above 5% relative abundance. Eurotiomycetes (Ascomycota) relative abundances decreased between bloat through early advanced decay (days 8-27), and recovered on day 43. Agaricomycetes relative abundances dropped below the 5% relative abundance on day 8, and only appeared intermittently following that point in interfaces; relative abundances declined in cores through days 12-27, and remained low for the remainder of the study. Archaeorhizomycetes (Ascomycota) fell below 5% in cores by day 12 and remained below detection for the remainder of the study; this class was not

observed in interface soils. Spring control soils were composed primarily of Sordariomycetes, Agaricomycetes, Eurotiomycetes, Dothideomycetes (Ascomycota). In contrast with the high relative abundances observed in impacted soil, the presence of Saccharomycetes in controls was intermittent in interfaces (fewer than 50% of samples) and uncommon in cores (fewer than 20% of samples); when present, relative abundances did not exceed 20% of sample contribution. As observed in impacted soils, Archaeorhizomycetes was present in cores but not in interfaces.

Winter trial successional patterns at the class level were similar to those observed in the spring trial, with respect to community composition, however relative abundances within these community shifts followed timings observed in soil chemistry (Figure 3.17A). Here again, the dominant contributors in impacted soils (> 5 % sample relative abundance) were Saccharomycetes and Sordariomycetes in both soil depths. Saccharomycetes relative abundances increased in advanced decay (days 75-110), and constituted > 25% of sample contribution in cores. Following this Saccharomycetes enrichment, Sordariomycetes became dominant with 10-50% relative abundances, and abundances continually increased throughout the remainder of the study. In a manner similar to the spring trial, Tremellomycetes increased beginning in bloat (day 21) with enrichment throughout advanced decay and into the beginning of skeletonization (days 55-158) in interfaces; similar patterns occurred in cores beginning in active decay (day 38). Unlike in the spring trial, while Tremellomycetes relative abundances exceeded 5% in winter control soils, relative abundances were low (< 25%). Eurotiomycetes, Agaricomycetes, Mortierellomycetes (Mortierellomycota), and Pezizomycetes (Ascomycota) relative abundances varied throughout the study, exhibiting no discernable patterns except that their relative abundances were more variable than in controls (Figure 3.17B). Archaeorhizomycetes was once again only detected in core samples. As observed in the spring trial, winter trial control soils

contained primarily Sordariomycetes, Agaricomycetes and Eurotiomycetes. Dothideomycetes was found primarily in cores. Archaeorhizomycetes was present in cores but not in interfaces. Saccharomycetes was not observed at >5% relative abundance.

At order-level, the dominant (> 8% relative abundance) taxa in spring impacted soils belonged to Saccharomycetales (Ascomycota, Saccharomycetes). Saccharomycetales is the single order within the class Saccharomycetes, and thus patterns at order level reflected those at class level (Figure 3.18A). Hypocreales (Ascomycota, Sordariomycetes) became enriched in cores by active decay (day 12), and during early advanced decay (day 43) in interfaces, remaining enriched thereafter. Eurotiales (Ascomycota, Eurotiomycetes) became enriched at the onset of advanced decay in interfaces (day 16), and at the following sampling time point in cores (day 27), gradually increasing through day 72, with relative abundances remaining comparatively static for the remainder of the study. Microascales (Ascomycota, Sordariomycetes) became enriched in both soil depths by day 43 in early advanced decay, and by day 117 in mid-advanced decay. Both Microascales and Hypocreales dominated communities for the remainder of the study. Trichosporonales (Basidiomycota, Tremellomycetes) appeared by day 43 in interfaces, peaking on day 86, and remained throughout the study; relative abundances in cores were reduced but temporal patterns were similar to those of interfaces. Control soil composition exhibited considerable variation, however Hypocreales was the most common taxon with consistent and well-represented relative abundances throughout the study (Figure 3.18B).

In contrast with the spring trial, no one order dominated samples in the winter trial, however there were several major contributing taxa at different timepoints (Figure 3.19A). Saccharomycetales patterns and relative abundances reflected patterns observed at the class level. Trichosporonales appeared at the onset of advanced decay (day 55) and remained at

moderate relative abundances throughout the remainder of the study. Following day 110, Microascales and Hypocreales collectively dominated sample composition for the remainder of the study. Eurotiales was not a notable contributor. Winter trial control soils exhibited considerable variation in taxon contribution, however Hypocreales was the most common taxon, found in all interface samples and all but one core sample throughout the study, similar to patterns observed in spring trial soils (Figure 3.19B).

Nematode abundances and alpha diversity

Spring 2018

Nematode abundances and alpha diversity (which includes richness as determined by unique genera and family-level identification, and diversity as estimated by calculating Shannon diversity indices) in decomposition-impacted soils all differed significantly from control soils throughout the study (ANOVA, $p < 0.001$) (Table 3.11).

In core soils, during the onset of advanced decay (day 16), mean abundances decreased to 81 $\pm$ 23 taxa per 100 gdw soil, a reduction of 71%. This was followed by an abrupt ten-fold increase above initial values on day 58 (2897 ± 3555 taxa per 100 gdw soil) (Figure 3.20, Tables 3.12-3.14). In interface soils, during early advanced decay (days 16-27), mean abundances dropped to 5-12% of initial values (29 ± 51, and 67 ± 115 taxa per 100 gdw soil, respectively). Some individual sample extracts showed no evidence of nematodes at this time, and others contained only a few dead specimens. It is interesting to note that these sample extracts contained large quantities of organic globules (including grease), and not only were nematodes in low abundance or absent entirely, other taxa commonly seen in these soils were absent as well, namely tardigrades, mites, rotifers, and collembola. Dead nematodes were counted and included in abundance estimates; however, since these nematodes could not be identified they were not

included in either alpha diversity (this section) or beta diversity (subsequent sections). Overall, abundances in both soil depths were lower than initial values during bloat to early advanced decay (days 8-58), corresponding to the period of time in which soil temperatures were elevated above 30 ^{o}C (Figures 3.1, 3.20). On and following day 58, abundances increased in both soil depths, exceeding initial values, and remained elevated throughout the remainder of the study. Core and interface soils both reached mean maximum abundances on day 86 at 3094 ± 777 and 29,708 ± 23,622 taxa per 100 gdw soil, respectively.

Nematode diversity (richness and Shannon diversity) decreased significantly during bloat and the beginning of advanced decay (days 8-16) and did not recover by the end of the study. Minimum richness in soil cores occurred during active decay on day 16 at 5 ± 4.6 unique taxa per 100 gdw soil, and the Shannon diversity minimum occurred during the latter portion of advanced decay on day 168 at 1.1 ± 0.3. Richness and diversity in interface soils reached minima during days 16-43 when few to no nematodes were present in sample extracts. By the end of the study, richness and Shannon diversity were still significantly impacted (Student's t-test, $p < 0.05$).

Winter 2019

Nematode indices in impacted soils all significantly differed from control soils throughout the study (ANOVA, $p < 0.001$) (Table 3.15). As mentioned previously, decomposition progression was more gradual during the winter trial than in the spring trial, and not accompanied by changes in soil temperature. In contrast with the decrease of nematode abundances found during elevated soil temperatures in the spring trial, nematode abundances in the winter trial became enriched during bloat on day 21 (994 ± 802 and 4926 ± 1808 taxa per 100 gdw soil in cores and interfaces respectively), and continued to increase, reaching mean

maxima during the beginning of advanced decay in interfaces on day 75 (116,248 ± 76,810 taxa per 100 gdw soil), and the latter portion of advanced decay on day 140 in cores (16,155 ± 11,950 taxa per 100 gdw soil) (Figure 3.21, Tables 3.16-3.18).

Richness and diversity decreased during bloat (day 21), reaching minimum values in cores during advanced decay on day 75 (6.7 ± 1.2 unique taxa per 100 gdw soil and 0.5 ± 0.2, respectively). Richness and diversity in interface soils reached minima by active decay (day 38) at 3.7 ± 3.1 unique taxa per 100 gdw and 0.3 ± 0.3, respectively. All indices differed significantly from controls at the end of the study (Student's t-test, $p < 0.05$).

Nematode beta diversity

Spring 2018

Bacterivores and fungivores, followed by plant feeders, were the primary trophic groups found in control and initial soils prior to any impact of decomposition products (Figure 3.22A-B, Figure 3.23A-B). As previously discussed, overall abundances began to decrease in days 8-16, and nematode extracts contained large quantities of suspended organic matter during this period of the decomposition process. Organisms identified as dead and/or degraded nematodes were included in abundance data, but due to the inability to assign specific identification to these nematodes they were not counted as part of beta diversity. During this period no large community composition shifts were apparent. As advanced decay progressed through days 43-58 a strong shift was observed in trophic composition toward dominance by bacterial feeding taxa, with marked reductions in all other trophic groups. Also during this time, abundances of taxa within cp-class 1 markedly increased and cp classes 2-5 decreased; cp classes 3-5 remained low contributors to community composition for the remainder of the study (Figures 3.22A-B, 3.23A-B). By day 58, and commensurate with soil temperatures falling below 30 ^{o}C, abundances began

increasing, composed primarily of cp-1/B1 taxa. With the exception of brief increases of cp-2/F2 fungivores and cp-2/B2 bacterivores days 150-168, cp-1/B1 enrichment dominated community composition throughout the remainder of the study. Cp-1 class taxa are opportunistic, r-selected organisms, and are stimulated to reproduce in large quantities during high enrichment conditions. This succession of changes in community composition and structure is clearly visible in functional diversity indices (Figure 3.22C, 3.23C). Controls and soils with only minor impacts occupy the center of the ordination, indicating a relatively even distribution of mixed cp-1 and cp-2 bacterial and fungal feeders, as well as moderate enrichment by cp 3-5 classes of all other trophic groups. As decomposition progresses, points representing advanced decay (green) begin to accumulate in the upper left-hand portion of the diagram (Figure 3.22C, 3.23C), indicating a functional shift from taxa that are associated with stable conditions (cp-classes 2-5 organisms with moderate to high K-selection), to those associated with responses to high enrichment (cp-1/B1 organisms that are exclusively r-selected). By the end of the study (skeletonization, denoted in blue) communities largely remain in this enriched sector of the ordination (Figures 3.22C, 3.23C). Aside from this gradual and brief increase of cp-2 class fungivores and bacterivores just prior to skeletonization, communities at the end of the study remained highly impacted compared to original community constituency.

Several bacterial-feeding taxa, primarily from cp-classes 1 and 2, changed in decomposition-impacted soils. In general, bacterial-feeding populations in initial soils and controls spanned cp-classes 1-4, but were largely composed of cp-class 2 taxa. These cp-2 taxa are considered “basal” taxa and tend to be the primary constituents of most soils that have not undergone major chemical or physical disturbances, and of these the three most common in un-impacted soils were: *Acrobeloides* (cp-2/B2), *Pseudoacrobeles* (cp-2/B2), and *Plectus* (cp-2/B2).

As impacted soils began to experience community shifts toward that of cp-1/B1 dominance, enrichment only occurred in three taxa over the course of the study: *Diploscapter* and Rhabditidae both experienced increased abundances on study day 58, and Diplogastridae by the following time point on day 72 (Figures 3.24-3.25). Diplogastridae abundances peaked twice in both soil depths: the first enrichment, an increase of 3 orders of magnitude, occurred between days 72-103 in advanced decay, and the second began on day 254 and continued throughout the end of the study during skeletonization. Abundances of the family Rhabditidae, as well as *Diploscapter,* which is a genus within Rhabditidae, remained generally enriched after day 58 by up to two orders of magnitude higher than initial values. As communities shifted toward this cp-1/B1 dominance, out of the three cp-2/B2 taxa commonly found in initial soil communities, only *Acrobeloides* (cp-2/B2) maintained a robust presence, particularly in core soils. In cores, *Acrobeloides* abundances initially dropped to 6% of original abundances but then increased by an order of magnitude by day 58. These values gradually declined, however they had not recovered to by the end of the study. With the exception of *Acrobeloides*, *Pseudoacrobeles*, and *Plectus,* all other bacterial (cp 2-4) abundances declined between the beginning of the study and day 16, only appearing sporadically after that time. *Pseudoacrobeles* abundances recovered by day 117. *Plectus* abundances remained below detection until skeletonization (day 303), increasing up to an order of magnitude higher than initial abundances by the final sampling date of the study.

Fungal feeding populations in initials soils consisted primarily of *Filenchus* (cp-2/F2) and *Aphelenchoides* (cp-2/F2). By the onset of advanced decay (day 16) *Filenchus* abundances dropped to 34% of original levels in core soils, were undetectable in interfaces, and remained suppressed throughout the remainder of the study. Conversely, *Aphelenchoides,* after initial

suppression became strongly enriched on day 58 and remained enriched for the remainder of the study. Abundances peaked on day 150 by two orders of magnitude in interfaces , and in cores on day 168 by a single order of magnitude.

Omnivorous and predatory taxa were generally found in low abundance throughout the study, however populations as a whole declined following active decay (day 12). One notable exception was the predator *Seinura* (cp-2/P2). *Seinura* was found in low abundances in controls, and completely absent from impacted soils, except between days 58-168 where it became enriched by almost three orders of magnitude with respect to controls at both soil depths. Dorylaimids (cp-4/O4) and *Clarkus* (cp-3/P3), both with notable abundances in controls, exhibited suppression in cores until day 254 after which their numbers increased above initial levels.

Winter 2019

Community composition and temporal patterns in winter samples reflected overall trends observed in the spring, however with two key differences: magnitude and timing of effect. In direct contrast to early-decomposition suppression of nematode abundances observed in the spring, abundances in the winter were enriched immediately with deposition of decomposition products into the soil (bloat and active decay, days 21-38) (Figures 3.26A-B, 3.27A-B). Compared with spring community profiles, fungivores constituted a smaller proportion of the control and initial community in the winter study; obligate plant feeders, particularly at the beginning of the study, comprised a larger proportion. Community compositional changes in trophic groups and cp-classes shifted toward populations composed of cp-1/B1 enrichment opportunists during bloat in interfaces, and in conjunction with a nearly 7-fold increase in abundances by the onset of active decay (day 38) in cores. It is noteworthy that the suppressed

and delayed abundance response in the spring study co-occurred with the presence of fly larvae and changes in soil temperature; conversely, the immediate and enhanced abundance response in the winter is associated with the absence of both larvae and soil heating. Also as observed in spring, as decomposition progressed after the initial community shift to cp-1/B1 dominance, both fungivores (cp-2/F2) and bacterivores (cp-2/B2) reappeared during advanced decay (day 94), increased substantially during days 110-140, and remained at moderate levels throughout the remainder of the study. These community shifts are readily apparent on the functional diversity ordinations (Figure 3.26C, 3.27C).

Three cp-1/B1 taxa were responsible for increased abundances in the winter: Diplogastridae, *Diploscapter*, and Rhabditidae. During active decay (day 38), Rhabditidae and Diplogastridae abundances increased 48- and 26-fold, respectively, in cores (Figures 3.28-3.29). Diplogastridae remained enriched throughout a reduced time frame (active decay through early skeletonization (days 38-158), whereas Rhabditidae enrichment persisted throughout the study following peak activity on day 75. Interfaces followed similar patterns, however Diplogastridae enrichment occurred during the bloat stage and throughout advanced decay (days 21-140), with peak abundances four orders of magnitude higher than found in controls by active decay (day 38). Likewise, Rhabditidae was enriched continuously beginning in bloat (day 21), and by two orders of magnitude with respect to initial abundances on day 75. *Diploscapter*, exhibited enrichment beginning on day 94, and continuing through day 335, corresponding the advanced decay and skeletonization. In interfaces *Diploscapter* peak enrichment exceeded initial values by four orders of magnitude on day 172. Excepting *Acrobeloides*, *Pseudoacrobeles*, and *Plectu*s, all other bacterial-feeding taxa exhibited general suppression following bloat. *Acrobeloides* displayed notable enrichment in cores beginning on day 75, and continuing throughout the study,

with a maximum on day 140, an order of magnitude higher than initial values. In interfaces, *Pseudoacrobeles* abundances recovered during skeletonization (day 186) becoming enriched thereafter, and *Plectus* became enriched by a factor of four during the final two sampling dates.

Several F2 fungivores exhibited enrichment in the winter: *Aphelenchoides*, *Aphelenchus*, *Boleodorus*, *Ditylenchus*, and *Filenchus*. *Aphelenchoides* exhibited early suppression in cores with abrupt 36-fold enrichment during advanced decay (day 94), and abundances remained strongly elevated thereafter. In interfaces this pattern occurred earlier; here, suppression continued through day 55, and enrichment was present thereafter, peaking on day 140, two orders of magnitude higher than initial values. *Aphelenchus*, closely related to *Aphelenchoides*, exhibited a brief enrichment in cores during the latter portion of advanced decay and early skeletonization (days 126-158); at its peak on day 140 this enrichment reached three orders of magnitude higher than initial values. In interfaces *Aphelenchus* enrichment was sporadic, with enrichment of up to three orders of magnitude adjacent to sampling time points in which abundances were undetectable. *Boleodorus*, relatively common in control soils, did not seem to be particularly affected throughout the study with the exception of a brief enrichment on day 172. *Ditylenchus*, another nematode relatively common in control soils exhibited mild suppression at the beginning of the study and displayed enrichment between days 110-126. A 120-fold and 400-fold enrichment was observed on day 140 in cores and interfaces respectively, and general enrichment continued until day 290. Interestingly, *Filenchus* abundances were variable throughout the study but did not exhibit noticeable suppression as observed in the spring study.

With the exception of Dorylaimids and *Seinura*, all other omnivorous and predatory taxa largely disappeared by early advanced decay (day 94), with occasional enrichment limited to

individual sampling time points. *Seinura*, absent in core control and initial soils, appeared during advanced decay and early skeletonization (day 110-216), and peaked on day 158 with abundances exceeding 140. *Seinura* in interfaces became enriched between 140-216, peaked with abundances exceeding 2000 on day 172. The Dorylaimids were suppressed at the onset of active decay and partially through advanced decay (days 38-94) after which point abundances were variable.

Discussion

Temporal studies assessing effects on soil chemistry during vertebrate decomposition fall into two large divisions: surface-decomposition or burial environments, and animal or human (rarely both) as choice of decomposing organism. Decomposing organisms can be further subdivided into the use of whole remains, tissue remains, or bones, and used in experimental design frameworks that range from *in situ* environmental placement to variable-controlled laboratory mesocosms. Accordingly, data collection and statistical replicability varies considerably based upon decomposing organism and experimental design. Whole-organism human studies are inherently complex to perform, and there are few facilities designed specifically for this purpose. As a result, in order to obtain data associated with human decomposition, researchers often avail themselves of experimental options that vary from traditional experimental design frameworks. These deviations may take the form of single-sample case studies that either originate from criminal investigations, or from unusual opportunities, such as the characterization of an exhumation. Other options frequently pursued include replication optimization predicated on the fact that both human donors and space within human decomposition facilities are limited, thus resulting in numerical and spatial replication constraints. In order to work around these constraints, human donors may be placed

simultaneously, however this may require pre-placement refrigeration or freezing as well as potentially significant facility space if replicates are to be placed together. Another experimental design framework appears unique within human decomposition facilities; placement of fresh remains in a field setting as they become available. This type of placement artificially deletes seasonal variation as part of the study design and risks obscuring trend analysis. However, it does allow for greater freedom of donor placement within the facility, and thus the potential for larger numbers of donors. Replication in this instance is occasionally binned by morphological decomposition stage or by accumulated heat units for statistical analysis.

Our study was designed as a surface-decomposition of whole human remains, incorporating simultaneously-placed donors within narrow size constraints, which were sampled at high resolution throughout a year of decomposition. Therefore, for the purposes of this discussion we are restricting our comparisons to results documented in the literature for above-ground decomposition experiments involving whole remains, and that were sampled for more than two time-points, unless stated otherwise. We are including results from both animal and human studies, since there are very few human studies that satisfy these criteria simultaneously. We are also including studies that have placed replicates at variable time points.

Environmental data

Temperature

Environmental data retrieved from soil sensors followed distinctly different patterns in the spring and winter trials. In the spring trial, internal donor temperatures and temperatures in soils located directly beneath donors increased over those of ambient air and soil controls beginning during the bloat phase, and continued into advanced decay (days 8-80), during which time both donor and impacted soil mean temperatures approached 40 ^{o}C. Within this 72-day time

frame, was a 50-day period (days 8-58) during which donor and impacted soil temperatures consistently exceeded 30 ^{o}C (Figure 3.1A). This 50-day period additionally corresponded to several soil chemistry parameter changes: a decrease in pH, and increases in conductivity, respiration rates (evolved CO_2), and ammonium concentrations (NH_4^+), as well as both the decrease and partial recovery of soil oxygen levels (Figure 3.4-3.6, Tables 4,6). This 50-day period also corresponded to a suppression in nematode abundance, concurrent with the presence of fly larval masses (Figure 3.20, Tables 3.12, 3.14). In contrast with these collective observations, there was no notable temperature increase observed between soil, ambient, and internal sensor data in the winter trial (Figure 3.3A). Nematode abundances exhibited immediate and considerable enrichment, both with respect to controls and spring abundances, in contrast with the suppression observed in the spring trial, and fly larval masses were not present. (Figure 3.21, Tables 16-17).

Temperatures of decomposing remains are often reported to increase above ambient temperatures in warm weather, however information assessing cold-weather trends is sparse. Payne (1965) measured internal, soil, and ambient temperatures associated with a pig decomposition (baby pig mass 1-1.4 kg) over a period of seven days in the summer. This study revealed that carcass temperatures exceeded soil temperatures, and that both carcass and impacted soil temperatures exceeded ambient air temperatures during the period of bloat through advanced decay (days 2-4). Temperature ranges between ambient air and carcasses varied by up to 15.7 ^{o}C (22-37.7 ^{o}C), and it was noted that higher temperatures were associated with increased overall insect activity. A second insect-exclusion experiment was performed by Payne (1965), which demonstrated that mass loss occurred more quickly in the presence of insects [71]. Quaggiotto et al. (2019) recorded temperatures underneath decomposing rabbits of

approximately the same size as used in Payne (1965), and reported temperature increases of up to 15 ^{o}C, corresponding to the presence of larval masses during active decay [3, 71]. Keenan et al. (2018) performed a decomposition experiment using beavers (13.5-23 kg) as subjects. Probes were used to measure temperatures inside carcasses, in soil directly underneath carcasses, soil controls, and ambient air, and found that both carcass and soil temperatures were elevated for approximately seven days, corresponding to larval masses on the carcass, and that temperatures approached 50 ^{o}C during active decay [2]. In a related study using beaver carcasses, Taylor et al. (2020) found similar patterns: elevated carcass and soil temperatures during active through advanced decay (days 15-24), concurrent with the presence of extensive larval masses [55]. Heat associated with larval masses, also known as thermogenesis, is a well-documented phenomenon during decomposition [69, 93], and degree of heat can be partially attributed to the size of the larval mass [94]. The soil and internal donor heating results documented in our spring human decomposition study are consistent with previous reports for warm-weather decomposition soil heating [2, 3, 55, 71]. However, our winter trial results did not show soil or donor temperature increases above those of ambient temperature, nor were insects present during active decay; additionally, overall decomposition patterns were gradual in the early phases of decomposition during cold weather. While it has been noted that insects are generally not present during decomposition in cold weather [95], ours is the first known study that has directly measured internal, soil, and immediately local ambient air temperatures associated with decomposing human remains for the express purpose of investigating and comparing seasonal patterns.

There are numerous implications of these differences in seasonal temperature patterns. By the end of the spring study, cumulative ambient air temperatures had reached 143,017 accumulated degree hours (ADH), while cumulative internal and soil temperatures reached

156,039 and 159,517 ADH respectively (Table 1). It is general practice in forensic study to use ambient air temperatures, generally accessed from nearest-weather station data to calculate the number of degree-days (or degree-hours in this case) associated with developmental stages of fly larvae, and from this information formulate estimates the postmortem interval (PMI). However, in the interests of obtaining precise calculations of these cumulative temperatures, there is concern that nearest-weather station data may introduce inaccuracies in comparison with temperatures measured locally [96, 97]. Here, we have shown that in the presence of larval activity, there is a continually increasing gap between even locally-measured ambient air ADH and internal or soil ADH, and the cumulative difference between soil and ambient air ADH by the end of the spring study reached 16,500 ADH (Figure 3.2). Summer days in East Tennessee can average 25 ^{o}C, which would be roughly equivalent to 600 ADH over the course of 24 hours. Assuming these summer temperatures, a 16,500 ADH difference would correspond to a 27.5 day discrepancy between temperature values obtained from direct temperature measurement beneath decomposing remains and from ambient air temperatures obtained nearby. Likewise, assuming a winter daily cumulative temperature of 120 ADH based on a mean of 5 ^{o}C, this uncertainty increases to 137.5 days. During the winter study, the absence of a noticeable thermogenesis effect makes this gap narrower, but there is still a difference of some 7,495 ADH by the end of the study (Table 2). This would give rise to potential discrepancies of 12.5-62.5 days, using daily values of 600 and 120 ADH respectively. Given that a number of climatological and locational factors may influence accuracy with which nearest weather station data reflect temperatures on the ground in the immediate vicinity to decomposing remains, the use of these data should be considered carefully when constructing PMI estimates and error margins. Furthermore, while presumably size or duration of larval masses would depend on carcass size, and thus influence

magnitude or extent of soil heating, to our knowledge it is not known whether this is the case. Soil heating magnitudes reported in the literature and in Taylor et al. (2020), do not appear to indicate a dependence on carcass mass [2, 3, 55, 71]; however, duration of soil heating may be influenced by mass. Therefore, examination of magnitude and extent of soil heating, particularly in conjunction with seasonality and carcass mass, is a knowledge gap that warrants further exploration. Values for Q_{10} for peptidase activity in calcareous and silicate soils have been shown to range from 1.3-1.7 [98]. Chemical and enzymatic reactions, microbial growth and respiration, and soil microfauna are all directly affected by the temperatures of their immediate surroundings. Our observations provide detailed data of temperature trends and decomposition progression outside the boundaries of what is normally used for insect-based estimates, and support assertions that more work needs to be done in creating appropriate temperature models and correction factors in order to improve accuracy in temperature reporting.

Soil moisture

In the spring trial soil moisture increased, remaining elevated throughout the study, with greatest increases during advanced decay (days 91-122), however in the winter trial no discernable increase was observed (Figures 3.1B, 3.3B). The spring trial pattern is consistent with results reported by both Keenan et al. (2018) and Quaggiotto et al. (2019) where soil volumetric water content increased upon movement of decomposition products into the soil during active decay [2, 3]. Keenan et al. (2018) observed recovery later in the study, however Quaggiotto et al. (2019) did not, possibly due to study length, 135 days and 20 days, respectively. In Taylor et al. (2020), soil moisture increased during advanced decay and remained elevated through early skeletonization [55]. All cases where moisture was observed to change occurred during warm-weather decomposition and were associated with bloating and

larval masses on carcasses. This moisture change is suggestive that greater quantities of fluids are present in situations where bloating occurs, and that these fluids pass into the soil quickly as a nutrient pulse when the skin barrier of the cadaver or carcass is breached during active decay due to the combined effects of fly larval activity, scavenging, and general decomposition progression. During our winter trial, minor scavenging occurred during the early portions of decomposition, and minimal to no bloating occurred, with no insect activity. The resulting slow seep of decomposition fluids into the soil and the relative lack of change in soil moisture that accompanied it further suggests that seasonal variation in decomposition exhibits entirely different patterns. This may be partially attributed to differences in maximum temperatures observed between the studies. As discussed earlier, temperature flux in warm weather is driven not only by ambient air, but also by larval (and microbial) metabolic heating (thermogenesis), and the substantially elevated temperatures found inside warm-weather decomposing organisms will have higher enzymatic and microbial metabolic rates associated with them than their cool-weather counterparts. As a result, it is likely that these enhanced enzymatic and metabolic rates allow for the production of larger and perhaps different (by comparison) quantities of fluids and gasses over a very short period of time thus creating a dramatic pulse of soil moisture when these fluids are released, as well as the characteristically different visual stages of decay between the two seasons.

Soil chemistry

Patterns associated with pH

In general, soil chemistry data followed patterns documented in the literature for above-ground decomposition, however, the sampling resolution and duration of our study was able to add a more nuanced interpretation to previous material. The exception to this is pH; of all soil

chemical parameters measured during decomposition, wide variability has been observed in response patterns of soil pH between studies. Vertebrate (non-human) surface-decomposition studies have generally shown pH to increase [1-3, 9, 10, 12, 31, 32], however a few have reported decreases in pH [8, 13]. In a pig decomposition study performed on soils classified as Darlington series Podzols (Spodosols, USDA soil classification equivalent [99]) of initial pH 7.3 in Southern Ontario, Canada, Benninger et al. (2008) found that pH increased during putrefaction and remained elevated into skeletonization [9]. Meyer et al. (2013) performed a pair of pig decomposition seasonal trials during the summer and winter in Nebraska on soil classified as a Mollic Hapludalf (Yutan series) with pH of 6.4, and found that pH increased in both cases [12]. Metcalf et al. (2013) performed a 48-day temperature-controlled laboratory mouse model study, allowing mice to decompose on beds of Colorado soils (unclassified), and reported that pH increased during the rupture phase of decomposition. A second mouse model experiment using soil beds created from three different Colorado soils (unclassified) resulted in increased pH throughout the study (70 days) [31, 32]. In a 24-week kangaroo decomposition in Australia, Macdonald et al. (2014) found that soil pH became elevated by week 12 ("dry decay") and remained elevated throughout the end of the study (week 24); Barton et al. (2016) resampled after five years and found no differences in pH or any other previously affected chemical parameters (conductivity, ammonium, or nitrate) from control soils [6]. Soils in the research area were listed as a varied mixture of Rudisols (USDA: Entisols), Tenosols (Entisols), Chromosols (Alfisols), Sodosols (natric great group belonging several USDA orders), Regosols (Inceptisols), Leptosols (Entisols), Luvisols (Alfisols), and Solonetz (natric great groups belonging to several USDA orders) [99], with an estimated control pH of 4 (based upon graphical results) [1]. In a year-long pig decomposition study in Switzerland, on an Endogleyic Umbrisol (USDA: Entisols

and Inceptisols)[99] of pH 6.01, Szelecz et al. (2018) reported that soil pH increased significantly during active decay (day 15), followed by a significant decrease during the later phases of dry decomposition and remains (day 263) [10]. Keenan et al. (2018), in a long-term beaver decomposition study in Tennessee with soils classified as Typic Paleudults, having initial pH values of 6.68-6.85, reported a similar pattern: pH significantly increased during active decay, returning to initial conditions during skeletonization [2]. During a 20-day rabbit decomposition in Australia, Quaggiotto et al. (2019), reported that pH increased under carcasses by active decay (day 4) and remained elevated through the duration of the experiment (day 20). Soils in the research area were characterized as chromosols, sodosols, kurosols (USDA: Ultisols)[99], luvisols, and solonetz, with control pH values of 6.3 (estimated from graphical results) [3]. Only two animal studies reported that pH decreased over the course of decomposition. Towne (2000) examined effects due to the decomposition of large ungulate carcasses at the Konza Prairie Research Natural Area on soils classified as Udic Argiustolls, Lithic Haplustolls, and Pachic Argiustolls with mean pH values 7.34. It was found that pH decreased and remained lower than nearby soils for three years [8]. Perrault et al. (2016) performed a pair of pig decomposition studies in Southern Ontario, and in contrast to results reported by Benninger et al. (2008) at a similar location, found that soil pH decreased during decomposition from initial values of pH 8-9. The two Perrault et al. (2016) decomposition trials were offset by three months, and while the authors did not formally frame the description of their study in terms of seasonal differences, this time offset did serve to capture warmer and cooler conditions, leading to reports of significant changes in pH by early to active decay in warmer temperatures, and to dry remains during cooler temperatures, shifting from approximately 1000 to 200 ADD (based on graphical results) [9, 13].

Detailed longitudinal human decomposition studies reporting soil chemistry trends are sparse in the literature. Three such studies have been performed at the University of Tennessee Anthropology Research Facility (UT ARF) in Knoxville, TN. The UT ARF is situated on a ridgeline overlooking the Tennessee river and soil series are variously described as Typic Paleudalf [7], well-drained clayey soil [14, 72], or as composed of a mixture of soils classified as Lithic and Typic Hapludalfs belonging to the Loyston-Talbott-Rock outcrop (LtD) and Coghill-Corryton (CcD) complexes [73, 74]. In a study involving the placement of seven deceased human subjects (donors) at the UT ARF, Vass et al. (1992) reported a rise in pH beginning almost immediately after donor placement, peaking at 750 accumulated degree days (ADD), noting soil acidification later in the study [7]. Cobaugh et al. (2015) reported that individual variability associated with four human donors led to findings of no statistical significance in pH [14]. The experimental designs used in both Vass et al. (1992) and Cobaugh et al. (2015) called for donors to be placed at the UT ARF as they were acquired, and thus decomposition timelines were not concurrent in either study, nor were they representative of any particular season. In our study at the same facility, donors enrolled in each seasonal trial were placed simultaneously, and weight constraints were placed on donors in an attempt to control for effects due to size variation as much as possible. During the bloat stage, pH was observed to decrease in both soil depths and across all donors during both seasonal trials, and remained generally impacted throughout the end of the study (Figures 3.4 A-B, 3.5 A-B, 3.6-3.7). Control soil pH values reported by Vass et al. (1992) and Cobaugh et al. (2015) ranged from 5.7-6.5 and 6.34-6.58, respectively, and our study reported a mean pH of 7.3. All three of these studies utilized soil that had not (knowingly) previously been exposed to decomposition. Donors in Cobaugh et al. (2015) ranged in weight from 56-77 kg. Donors in Vass et al. (1992) ranged from 44-88 kg, and donors in this study

ranged from 68-92 kg. Given soil variability throughout the UT ARF, overlap in donor sizes, and reported variations in pH between these studies, it is unknown whether variations in edaphic features, body composition, pharmaceutical loading, and/or medical conditions may influence the pH trends.

In an analogous example to the reporting of varied pH responses associated with human decomposition at the UT ARF, two separate pig decomposition studies performed in Ontario also varied in direction of pH trajectory from initial controls. Both studies appear to have been carried out at the same or similar location. The pigs used in these studies were of similar size, 25-30 kg, and the only major difference between the studies, discounting seasonality in Perrault et al. (2016), was the method of euthanasia: captive bolt [13] or an overdose of anesthetic administered by a veterinarian [9]. Nominally, this gives some support to the idea that intrinsic properties of the pigs themselves (i.e. veterinary pharmaceuticals, age, diet, medical conditions, or point of origin) may drive the trajectory of decomposition pH. Briefly expanding our literature comparison parameters, in a novel experimental design carried out by Fancher et al. (2017), a series of 63 human decomposition sites were surveyed in San Marcos, Texas at their Forensic Anthropology Research Facility (FARF) [5]. Human donors had been placed in the facility at various times ranging from 6 to 1752 days (4.8 years) prior to sampling for this particular study. Soil samples were taken from CDIs at a single sampling time, and PMI was calculated for each donor/CDI based upon placement dates in the facility. From these varied PMIs a chronosequence of decomposition was created, and results were sorted according to the two known soil series present at the facility; a Comfort-Rock outcrop (CrD) composed of Lithic Aguistoll, and a Rumple-Comfort association (RUD) composed of Typic Arguistoll. It was found that in both soil series, pH was observed to vary both higher and lower than found in controls. Interpretation of

this data, particularly as a chronosequence, should be viewed carefully; individual time points correspond to single donors, each of which has its own unique medical history, size, and body composition. This study format does not constitute a detailed longitudinal observation series associated with a particular donor or set of donors, and will therefore homogenize size, season, medical history, and environmental parameters. It does, however, suggest that several gross trends are apparent. With respect to pH in particular, it serves to underscore the conclusion that not enough information exists about the effect of intrinsic donor variability on decomposition, and how this variability translates into interactions with the microbial decomposing community and edaphic factors.

Patterns associated with soil oxygenation and respiration

Changes in soil oxygenation and respiration have historically been discussed within the context of buried remains, whole or tissue [17, 39, 100-103]. In surface decomposition experiments, soil oxygenation has largely been inferred relative to the context of this body of burial literature, or by oxygen requirements of bacterial communities in the soil, or infrequently, by measurement of soil respiration rates [4, 5, 39]. High microbial metabolic activity and elevated soil respiration during active and advanced decay are assumed to cause localized anoxia in soil; further, evidence of anaerobic bacteria in soils during time periods of elevated respiration have supported these conclusions [14]. Soil oxygen levels have only recently been empirically measured during the process of decomposition, and found to decrease, supporting these assumptions [2].

Soil respiration is typically used as an indirect means of assessing microbial catabolic rates, however few surface decomposition studies include this parameter as part of their datasets [2, 14, 16]. Cobaugh et al. (2015) observed increased soil respiration beginning in the transition

from bloat to active decay, and appearing to peak in early advanced decay; however, since the study did not extend into later phases of decomposition it is not known at what point soil respiration might have recovered to background levels [14]. Keenan et al. (2018) observed strongly elevated respiration rates concurrent with a measured decrease in soil oxygen during active decay [2]. Based upon this direct observation of changes in soil oxygen in combination with other temporal changes in nitrogen and carbon speciation pools, a biogeochemical model was proposed demonstrating that soil oxygen availability could divide the progression of vertebrate decomposition into three distinct phases, with unique carbon and nitrogen speciation attributed to each. This experiment carried out by Keenan et al. (2018) encompassed the entirety of decomposition progression through skeletonization, and most measured study parameters had partially or completely recovered to control levels by the termination of the study.

We elected to measure respiration both as a means to evaluate soil microbial activity, and to explore its relationship with soil oxygen during seasonal human decomposition trials, and thus validate and/or amend the biogeochemical model proposed by Keenan et al. (2018). We found an abrupt increase in respiration rates during the spring trial beginning in the bloat and active decay stages (days 8-12) and continuing through the latter portions of advanced decay (day 150), concurrent with the reduction and recovery of soil oxygen levels (Figure 3.4 E-F, K; Figure 3.5C, F; Figure 3.6C, F; Table 3.4). Respiration rates in interface soils were almost twice those observed in core soils, which is not unexpected as interfaces were in direct contact with decomposition products. While soil oxygen levels fully recovered by day 168 in very late advanced decay, respiration rates remained slightly elevated throughout the study. In the winter trial, a similar trend was observed; respiration began to increase during active decay and remained elevated through early skeletonization, exactly commensurate with the reduction and

recovery of oxygen levels in the soil (Figure 3.5C, F; Figure 3.6C, F; Figure 3.7 E-F, K; Table 3.8). Seasonal differences were evident, notably that the magnitude of respiration rates in core soils was lower in the winter trial than in the spring trial, and that initial changes in respiration rates and soil oxygenation were more gradual in the winter trial as opposed to the abrupt increases observed in the spring trial. This reflects observations that decomposition is a slower process in the winter without the dramatic flush of fluids into the soil that is characteristic of warm weather decomposition (Figures 3.5-3.6). Comparing the magnitude of respiration rates in core soils to those of interfaces suggests that soil microbes in the interfaces are more readily able to assimilate the gradual deposition of decomposition products during the winter, and thus less material is available to infiltrate into deeper soil layers.

Of potential interest is one respiration pattern that occurred only in core soils from the spring trial. Here, respiration rates increased through day 58, followed by an abrupt decrease of approximately 30% that remained consistent from days 72-150. The decrease in soil respiration rate is commensurate with the equally sudden emergence of high abundances of bacterial-feeding nematodes, and co-occurs with decrease of previously elevated soil temperatures dropping to below 30 ^{o}C (Figures 3.1A, 3.4E, 3.20A, Tables 3.12, 3.14). This suggests that bacterial populations may have been under top-down control by nematodes which are bacterial enrichment opportunists. If this is indeed the case, it might support the observations by Cobaugh et al. (2015) that during active and early advanced decay high respiration rates were accompanied by a lower biomass production. Cobaugh et al. (2015) attributed this to a reduction in microbial growth efficiency, and while this is quite probable, it is also possible that another organism reproducing in high abundances that is consuming large quantities of bacteria might exacerbate the observed effect. This respiration pattern is not readily observed in interfaces; magnitudes of both

respiration rates and nematode abundances are higher in interfaces than they are in cores, as well as having more variability, and both of these factors might obscure any top-down effects.

Patterns associated with inorganic nitrogen speciation

Vertebrate carcasses have a low C:N ratio and are a rich source of N as they decompose [39]. As tissue breakdown progresses during protease secretion from fly larvae, and from microbial and extracellular enzyme activity within the soil, ammonium enrichment occurs very early in the decomposition process, a pattern which has been shown as fairly consistent over a variety of soil and climate types [1-3, 5, 7, 10, 12, 14, 32]. In the presence of oxygen, ammonium accumulation is transformed via nitrification to nitrite and nitrate, and thus nitrogen pools resulting from transformations of carcass-derived organics peak at different times as decomposition progresses [17]. The inorganic nitrogen species ammonium and nitrate are the most commonly reported nitrogen parameters in decomposition-impacted soils, however due to generally low study resolution, the temporal differentiation of these species is not well-described. Vertebrate low-resolution temporal studies (3-4 sampling time points) have shown that ammonium peaks early, and as it declines an increase in nitrate is observed [1, 12].

Vertebrate short-term studies have reported the presence of ammonium, but not nitrate. For example, Quaggiotto et al. (2019) reported in a 20-day rabbit decomposition that while ammonium became enriched by active decay, no enrichment in nitrate was observed, and graphical results show nitrate levels in impacted soils as lower than found in controls [3]. From the perspective of a complete organismal decomposition cycle, this response of nitrate is inconsistent with other reports in the literature. However, reports that run for longer periods of time report nitrate increases far later in the decomposition process, therefore it is likely that nitrogen transformations are not appreciable within a 20-day time frame.

High resolution vertebrate studies have reported distinct temporal separations of ammonium and nitrate enrichment in soil. In a temperature-controlled mouse model system, Metcalf et al. (2016) reported peak ammonium enrichment by day 30, however, despite decreasing, ammonium concentrations remained elevated at the end of the experiment on day 70. Nitrate began to increase by approximately day 20, and continued to increase thereafter [32]. In a pig decomposition study sampled for a year, Szelecz et al. (2018) reported that ammonium increased during active decay (day 15), peaking during later portions of advanced decay and early dry remains (day 59), and returned to basal levels by day 263. Nitrate elevations occurred later in the study, consistently increasing by day 263 [10]. The authors proposed a series of early and late time markers of decomposition progression based upon physiochemical response patterns; the shift between early and late markers occurred on day 59, corresponding to the period of time of greatest mass loss after advanced decay, and ammonium was considered as both an early and late marker, while nitrate was judged to be a late marker. This late peak of nitrate was attributed to a proposed return to aerobic conditions in soil allowing for nitrification. Keenan et al. (2018), in the first known study to directly measure soil oxygen during decomposition, found ammonium significantly elevated during active and advanced decay, corresponding to soil conditions with measured oxygen depletion. Ammonium returned to non-significant levels during skeletonization [2]. Similar to the timing observed in Szelecz et al. (2018), nitrate significantly increased briefly during skeletonization. As discussed above, this timing of nitrogen transformation from ammonium to nitrate marks the beginning of the third phase in the biogeochemical model whereby the reoxygenation of soil is accompanied by increases in nitrate via nitrification, an oxygen-dependent process.

Collectively, these vertebrate studies utilized different organisms with different masses, and little is known about nitrogen dynamics stemming from variations in carcass size. In field studies, ammonium deposition into soil in warm weather consistently occurs during active decay, coincides with peak larval activity, and is commensurate with the sudden pulse of nutrient addition to the soil following bloat. In larger animals (27.8 kg mean pig weight [10], 13.5-23 kg beaver weight range [2], and 17-80 kg kangaroo weight range [1]), this ammonium flush lasted through advanced decay and into early skeletonization, with length of time broadly appearing to coincide with the mass of the animals involved. Specific timing is difficult to quantify and should be cautiously compared; each of these studies has reported data from different climate zones and dates, and thus a given day between studies cannot be considered equivalent in terms of thermal units. Comparison at this stage can only be inferred or catalogued in terms of morphological staging descriptions which have repeatedly shown to be variable in humans and only partially applicable to animals [104-107]. Nitrate has consistently appeared during skeletonization in field studies surpassing 100 days [1, 2, 10]. Thus it is possible that the lack of observed nitrate accumulation under skeletonized rabbits by day 20 in Quaggiotto et al. (2019) may be attributed to impacted soil oxygen, and thus for small animals these nitrogen speciation shifts may appear to be quite different with respect to later morphological staging than for larger animals or humans [3].

Our study found that nitrogen dynamics under humans is consistent with other reports from the human-based literature, however our sampling resolution allowed us to observe considerable nuance in the speciation patterns. Cobaugh et al. (2015) found that ammonium concentrations increased during the bloat-active decay stage and remained elevated through advanced decay [14]. Later timepoints in the study showed that while ammonium concentrations

were still elevated, the beginnings of a decrease became apparent, however the study did not continue long enough to determine whether ammonium would recover to background concentrations. Nitrate did not exhibit a significant change, however since the study terminated in early advanced decay, reports from vertebrate studies would suggest that an increase in nitrate may not have begun to occur. Vass et al. (1992) found that of from an initial panel of sixteen cations and anions, seven (Na^+, Cl^-, NH_4^+, K^+, Ca^{2+}, Mg^{2+}, and SO_4^{2-}) peaked early, and of these, ammonium peaked at concentrations almost twice that of any other cations or anions (nitrate, while measured, was not listed as a notable anion) [7]. Our study results found that ammonium enrichment in the spring trial followed patterns reported in the literature: enhanced enrichment during active decay, and a gradual reduction over time throughout advanced decay and into skeletonization (Figure 3.4 G-H, Figure 3.5D; Figure 3.6D, Tables 4, 6). In the winter trial this pattern occurred less dramatically as fluids were gradually incorporated into the soil, and reflected the likelihood that the soil microbial community was more easily able to assimilate the slow seep of fluids compared to the large flush that typifies warm weather decomposition (Figure 3.5D; Figure 3.6D, Figure 3.7 G-H, Tables 8,10). In the spring, nitrate concentrations fell below those of controls during the early phases of decay when ammonium levels were high and soil oxygen was low (days 12-58), only increasing in cores once oxygen levels had recovered to approximately 70% of original values. In the winter trial, nitrate concentrations only dropped below those of controls on days 33, 55, and 94 in interfaces, however did not fall below those of controls in core soils (Figures 3.4-3.7). These ammonium and nitrate peaks do not occur independently of each other, and in most studies reported previously, decreasing ammonium concentrations overlap initial nitrate increases. We found this overlap to be greatest in cores during the winter trial. Our study found that in controls, ammonium and nitrate concentrations

were roughly equal (Tables 4, 6, 8, 10). These relationships can be visualized by taking the natural log of the ratio of ammonium and nitrate concentrations, which at a 1:1 ratio is equal to zero, as is demonstrated for control soils (Figure 3.8). During ammonium enrichment the log ratio is positive, however as ammonium concentrations decrease and nitrate increases, a 1:1 ratio between the two species is reestablished, bringing the log ratio back to the zero line, which occurs concurrently with complete reoxygenation of the soil in both seasons (Figures 3.6-3.8). It should be noted that this 1:1 relationship now occurs as nitrate concentrations are high, and thus both nitrate and ammonium are elevated with respect to controls, even though their concentrations are equivalent. Over time, this ratio remains approximately 1:1, however both nitrogen species gradually diminish. This pattern is suggestive of several things. First, while nitrogen species' seasonal difference patterns vary in magnitude and peak timing, particularly in cores, the return to a 1:1 ratio relationship between the inorganic nitrogen species coincided with the reoxygenation of soil when presented in terms of soil ADH. This implies that while the augmentation of a particular nitrogen species may be notable by itself, the ratio of multiple species may be a better indicator of decomposition progression and soil recovery status. Secondly, it suggests that the anaerobic secondary phase of the biogeochemical model proposed in Keenan et al. (2018) might require amendment to include decomposition processes that occur in the winter. Our winter decomposition patterns saw less of an oxygen depletion, and a greater overlap between ammonium and nitrate concentrations, suggesting that while anaerobic nitrogen transformations were likely occurring (denitrification, dissimilatory nitrate reduction (DNRA), and annamox), nitrification was still able to proceed to a potentially greater degree than in the spring trial. This suggests that there might be considerable change in the contributions of these three processes depending upon when decomposition is initiated.

Denitrification is considered a major process in soil, and requires the presence of nitrate as well as anaerobic conditions. However, the conditions present in spring trial decomposition soils in particular might be conducive to a greater percentage of anammox. The presence of enhanced anammox, or anaerobic ammonia oxidation, has been hypothesized before based on the observations of negligible changes to nitrification potential during the reduced-oxygen phase of decomposition [2]. The anammox process has largely been studied in bioreactors where it was first discovered, and generally is associated with temperature optima of 30-40 ^{o}C based on organism. Below these temperatures, anammox becomes less efficient. Growth rates for annamox bacteria are slow, and doubling time can range between 9-29 days under optimal temperature conditions; thus it follows that doubling times are longer at low temperatures and shorter at high temperatures. Anammox also is sensitive to pH, however the sensitivity appears most acute at high pH as ammonium is converted to ammonia, rather than at low pH [34] . The pH of our soils falls well below the pKa at which ammonium is in equilibrium with ammonia (pKa = 9.2), thus we do not have the alkaline soil conditions such that ammonium is likely to convert to ammonia gas and volatilize, as is frequently found in animal decomposition soils in which pH rises. Therefore, without this known inhibitor (ammonia), it is possible that anammox is a significant contributor to the nitrogen cycling during warm weather decomposition. In our spring study, during the period of elevated temperatures (days 8-58), low soil oxygen, and low pH, ammonium concentrations were high and nitrate concentrations fell below those found in controls. Given that both denitrification and anammox rely upon anaerobic conditions, it is possible that both processes were occurring during this time. In the winter study, overall soil conditions were very different. Soil oxygenation and nitrate concentrations were both higher during early decomposition, suggesting that the second biogeochemical phase as outlined in

Keenan et al (2018) might be condensed, as well as the possibility of a different balance between denitrification and anammox, particularly since low temperatures found in winter conditions could lead to lowered efficiency of the anammox process.

Patterns associated with electrical conductivity

Electrical conductivity is reported less frequently in decomposition studies than are nitrogen and carbon results, however it is directly related to the ionic strength of the soil and reflects collective changes in concentrations of K^+, Na^+, Ca^{2+}, Mg^{2+}, NH_4^+, NO_3^-, and SO_4^{2-}, reported as the most commonly occurring anions and cations present in the soil solution during the decomposition process [4, 5, 7, 10, 13, 15]. Macdonald et al. (2014) and Barton et al. (2016) reported generally elevated conductivity in a kangaroo study, with a return to background conditions after five years [1, 6]. In a more finely detailed temporal study, Keenan et al. (2018), found that conductivity significantly increased during active decay, returning to initial conditions during skeletonization [2]. Quaggiotto et al. (2019) reported that conductivity increased under decomposing rabbit carcasses on day 4 (active decay) and remained high for the duration of the experiment (day 20), past skeletonization [3]. Fancher et al. (2017) measured K^+, Na^+, Ca^{2+}, Mg^{2+}, NH_4^+, and NO_3^-, as well as conductivity. Given the study design, patterns in each of the cations and anions throughout the constructed chronosequence were not discernable, and conductivity, as a collective measure of all of these parameters, thus only exhibited generalized increases [5].

Our results showed that conductivity significantly increased during active decay in the spring, and during advanced decay in the winter, and that enrichment occurred with no distinctive patterns throughout, much in the same manner as other studies have demonstrated (Figures 3.4-3.7, Tables 4, 6, 8, 10) [1-3, 5]. Results from soil sensors indicated an enrichment

pattern with two peaks in the spring trial (Figure 3.1C), and a pattern with three peaks in the winter trial (Figure 3.3C). When conductivity sensor data is compared to ammonium and nitrate concentrations, it is interesting to note that conductivity peaks roughly align with peaks of both nitrogen species, however, this is somewhat deceptive; other monovalent and divalent cations present in the soil solution will also be represented in conductivity values, and currently their contributions are unknown. Two points are notable, however: conductivity in interface soils is enhanced in comparison to cores in both seasons. This is expected, simply because this soil originates from areas directly in contact with decomposing donors. The second notable observation is that conductivity in spring interfaces during days 8-16 (bloat through the onset of advanced decay) was associated with soils that were described as very greasy, and through this period extremely high values of conductivity alternated with extremely low values as shown by ranges between 969.1 ± 1336.7 μS cm^{-1} and 4 ± 0.9 μS cm^{-1} on adjacent study days. In contrast, during the winter the soils did not become as wet and greasy, presumably due to a slower release of decomposition products. Overall, conductivity patterns suggest that ammonium in particular is the dominant cation present in early decomposition soils, however since conductivity is a collective reflection of all cations and anions in the soil solution, further study of individual cation and anion contribution would be instructive.

Fungal succession patterns

To date there is a small but growing body of literature discussing longitudinal changes of fungal communities in decomposition-impacted soil. These studies have largely focused on reporting surveys of taxon changes or results deriving from the construction of arguably robust PMI models. Collectively, these fungal studies have relied principally (but not exclusively) upon animal model systems, often with low sample coverage and short study duration, and without the

inclusion of supporting soil chemistry data. Of these few fungal studies, a progression of study is visible, notably an evolution from the use of 18S rRNA to the ITS region as choice of sequencing element. However, the progression of conclusions from this body of material remains relatively static, limited to proposals that successional patterns are broadly evident, and assertions that these patterns are reproducible. One of the first culture-independent studies of soil fungi in decomposition was performed by Parkinson et al. (2009), at the University of Tennessee, using human donors [30]. This study used terminal restriction fragment length polymorphism (T-RFLP) analysis of internal transcribed spacer (ITS) genes as a means of profiling fungal communities in soil during decomposition. Bacterial results (16S rRNA genes) that accompanied this fungal study clearly showed successional patterns, roughly progressing by morphological decomposition stages, however the fungal results did not show a clear trend other than to differentiate control soils from decomposition soils as a whole. Metcalf et al. (2013) performed one of the early high-throughput sequencing characterizations of eukaryotic (18S rRNA genes) community changes in a mouse-model system examining body sites and soil underneath decomposing mice for a period of 48 days, with a resolution of eight sampling points [31]. The authors reported that major eukaryotic groups changed in a predictable manner, and therefore had potential for use as a diagnostic forensic tool. The authors also concluded that the fungus Boletales (Basidiomycota, Agaricomycetes) was a notable contributor to estimations of PMI, and that the fungal class Zygomycetes constituted one of five notable eukaryotes that changed in soil, increasing in abundance. Carter et al. (2015) performed a seasonal study evaluating eukaryotic (18S rRNA) community changes under decomposing pigs for a period of 60 days, with a resolution of four sampling time points [21]. The authors concluded that post-rupture communities were different in summer and winter, and that taxa belonging the fungal

classes Eurotiomycetes and Tremellomycetes exhibited greater relative abundances in summer in comparison with winter. Weiss et al. (2016) examined mass effects in a pig decomposition study, evaluating eukaryotic (18S rRNA) community changes for 15 days over 8 sampling time points, concluding that a dominance in eukaryotic taxa stemmed largely from fungi and nematodes [33]. Metcalf et al. (2016) performed two experiments, one a mouse model using three separate soils (as discussed previously in the soil chemistry portion of this manuscript), and the other using four human donors in a pair of seasonal trials (143 days in the winter; 82 days in the spring), in order to investigate eukaryotic (18S rRNA) and fungal (ITS) community assemblages during decomposition progression [32]. Both skin and gravesoils of donors were sampled frequently during the early portion of the study, and less frequently as decomposition progressed. Network analysis of the mouse model indicated that Eurotiales (an Ascomycete) was a strong driver of community structure. Fu et al. (2019) examined fungal communities specific to the ITS1 region in a 58-day indoor/outdoor juvenile pig decomposition study [37]. Skin sites were sampled at 12 time points, and soil was sampled 5 times over a period of 14 days, primarily by morphological decomposition stage. The authors reported that soil fungal communities differed from control soil, but that they were similar to body site communities on the pigs between days 4-14 of the decomposition process. They also demonstrated a gradual increase and ultimate dominance of two ascomycete yeasts (Saccharomycetes, Saccharomycetales), *Yarrowia lipolytica* and *Candida catenulata* during this period of time, and that these increases in relative abundance were related to increases of accumulated degree hours (ADH). Risch et al. (2020) examined fungal communities (ITS2 region) for soils underneath elk and bison carcasses that had decomposed in Yellowstone national park [35], however this study emphasized comparing elk and bison carcass signatures in soil rather than constructing a longitudinal decomposition sequence. Procopio et al.

2020 compared the results of ITS1 and ITS2 primer sets in a 6-month pig burial decomposition study, not only to discern fungal successional patterns, but to assess primer performance [36]. This study contained 4 sampling time points, and the authors reported that the phylum Ascomycota increased during month 2 associated with putrefaction and liquidation of the carcasses, and that the phylum Mortierellomycota increased thereafter. Several taxa were suggested as possible indicators for various points of decomposition progression. It is generally agreed throughout all studies that decomposition-induced fungal successional patterns are present in soil and that there is potential forensic merit in these patterns in a similar manner as those found in bacterial studies.

In this study, successional progressions in beta diversity, as shown by PCoA, display distinct triangular patterns in both seasons that mirror changes in soil chemistry; this infers at least two phases within decomposition progression, and thus perhaps separate environmentally-derived pressures on community changes (Figures 3.10-3.13). In the spring trial, control samples and initial community samples are tightly clustered in the upper left-hand corner of the ordination diagrams (Figures 3.10-3.11). There were distinct community shifts beginning as early as bloat (day 8) as points begin to move primarily along the vertical axis of the PCoA until an inflection point occurring at the onset of advanced decay (day 16). This period corresponded exactly to the initial pH decrease, conductivity and ammonium maxima, soil oxygen minimum, respiration increases, nitrate minimum, increased soil temperatures, and the initial decline of nematode communities. In the biogeochemical model proposed by Keenan et al. (2018) [2], this inflection point on the PCoA corresponds to the transition between initially oxic soil, and the onset of anoxia and anaerobic conditions (first to second biogeochemical phases). Following the day 16 inflection point, communities shifted towards the upper right-hand portion of the PCoA

plot through day 86, approximately half-way through advanced decay. This corresponded to soil reoxygenation to approximately 85% of initial levels, continued elevated respiration rates, decreased ammonium, increases in nitrate, and a reduction of elevated soil temperatures; these changes correspond to the transition from second to third biogeochemical phase in the Keenan et al. (2018) model. Communities thereafter remained tightly clustered in the upper right-hand corner of the ordination diagram and did not return to initial community structures by the end of the study.

Winter trial patterns also display a triangular pattern in the PCoA ordination. Here, the controls and initial communities were again tightly clustered at the left-hand side of the ordination, and moved to the first inflection point in the upper-right-hand side of the diagram during active decay (day 38) and throughout early advanced decay (days 75-94). The second community shift, noted by the migration of points to the inflection point in the lower right-hand portion of the ordination diagram occurred between the transition from advanced decay to skeletonization (days 140-158). Both inflection points corresponded to similar soil chemical changes as observed in the spring trial. However, here the similarities between the winter and spring trials showed the effects of seasonal differences. In the winter study, a third community shift can be observed by a gradual transition toward the center of the ordination throughout the remainder of the study, and rather than the distinctive clustering of early and late decomposition communities evident in the spring trial, there is more dispersion throughout the movement on the ordination diagram. The dispersion appears to reflect the gradual deposition of decomposition products and accompanying lower magnitudes of effects observed in soil chemistry patterns as previously discussed. These first two shifts across the ordination diagrams of both seasons correspond to changes in all soil chemistry parameters, but notably those of oxygen, ammonium,

and nitrate. The patterns in beta diversity shift underscore two observations: that while distinctive seasonal differences are evident in fungal successional patterns, both sets of patterns are inextricably tied to soil chemical transformations and their respective rates and magnitudes of change. This further suggests that constructing models that incorporate microbial and soil chemical data must at minimum be able to accommodate the effects of non-linear relationships (as demonstrated by offset peaks evident in ammonium and nitrate patterns).

With our intent to integrate microbial ecology data with that of soil chemistry, our focus was to determine fungal successional patterns in fine scale, over two different seasons, and to discuss how changes in soil chemistry might be impacting these community changes. Therefore, our study integrating fungal microbial ecology with soil chemistry and environmental effects is a necessary first step for the construction of datasets suitable for PMI models that will have the capacity to be robust across time and location. Our study found similar results across three taxonomic ranks: phylum, class, and order level. It is generally agreed across all studies that the phylum Ascomycota dominates decomposition soils, although the degree of dominance and timing is unclear. Our spring trial found that during the period encompassing bloat through early advanced decay (days 8-58) soil communities shifted from a general to almost complete dominance by Ascomycota, while the phylum Basidiomycota decreased to almost undetectable levels. This community shift was concurrent with numerous biotic and abiotic changes: elevated soil temperatures exceeding mean values of 30 ^{o}C, large fly larval masses, reduced nematode abundances (particularly fungal-feeding taxa), lowered pH, an initial drop and partial recovery of soil oxygen levels, maximum values for electrical conductivity and ammonium concentrations, and initial elevations of soil respiration. In contrast, winter trial community shifts during the same morphological stages (days 21-126) show a slight increase in prevalence of Ascomycota,

but not the magnitude observed in the spring, nor is there the same degree of negative impact to Basidiomycota. This attenuated response is consistent with patterns observed in soil chemistry both with respect to timing and magnitude of effects. It is also notable that soil temperatures during this time did not exceed those of ambient temperatures, which lay well below 30 ºC. General variation observed between seasonal patterns is consistent with reports from eukaryotic studies (18S) performed by Carter et al. (2015)[21] and Metcalf et al. (2016)[32], however it is difficult to draw substantive conclusions regarding successional progression between fungal-specific studies (ITS), and those designed to explore eukaryotes more generally (18S). In contrast, Fu et al. (2019) provides a detailed look at fungal successional patterns in soil in a July pig decomposition study, noting a strong shift to dominance by two taxa, *Yarrowia lipolytica* and *Candida catenulata*, both of which are Ascomycete yeasts [37]. The authors also show the relationship between ADH and the increase in both of the ascomycetes, and demonstrate that by day 14 of their study, which corresponds to 10,000 ADH, that these taxa constitute almost the entire community. Our spring study reaches 10,000 ADH shortly following study day 16, and we also observed a Ascomycota-dominated community. While it is not known to what degree pigs can represent humans as decomposition analogs [104-107], the results from Fu et al. (2019) and those of our spring trial are consistent [37]. A burial study reported by Procopio et al. (2020) showed that Ascomycota increased during carcass putrefaction [36]. Care must be taken in comparing results observed from surface-decomposed remains to those from burials; it has been shown that the decomposition patterns differ, and it is difficult to infer similarities between microbial data without robust data in both areas [17]. Taken together, our results suggest that the bloat through early advanced decay period tend to select most strongly for the presence for Ascomycota and against the presence of Basidiomycota during the period of soil acidification,

elevated ammonium and conductivity, increased respiration rates, reduced oxygen, and the soil heating that is characteristic of warm-weather decomposition, and our spring trial specifically.

Distinct successional patterns within Ascomycota and Basidiomycota began to emerge at the class taxonomic level. In both seasonal studies the primary contributors with the most conspicuous successional patterns were two Ascomycetes: Saccharomycetes and Sordariomycetes. The order Saccharomycetales is the single order within the class Saccharomycetes, and thus no pattern differentiation is detected. Saccharomycetales are monophyletic yeasts, most of which live as saprobes associated with a variety of ecological niches including soil, or in association with plants and animals [108]. Saccharomycetes enrichment occurred during bloat through advanced decay (days 8-72) in the spring, however only during advanced decay 75-158 in the winter study. Saccharomycetes enrichment is consistent with reports from eukaryotic studies [21, 32, 33], and closely aligns with patterns for increases in *Yarrowia lipolytica*, (a Saccharomycete yeast) described by Fu et al. (2019) [37]. The same study also showed that fungal communities obtained directly from cadavers (and not soil) gradually shifted to communities almost excusive to *Y. lipolytica*, so it is entirely possible that if this also holds true for humans, that cadaver inputs may be the driver of Saccharomycetes blooms. Collectively, these observations suggest that of the classes belonging to Ascomycota, that Saccharomycetes is the class most strongly selected for by decomposition chemistry, thus driving relative abundance, or that large absolute abundances derive directly from cadaveric inputs. Sordariomycetes is one of the larger classes within the phylum of Ascomycota, and many members are common saprobes in soil [109]. Sordariomycetes constituted the bulk of both seasonal samples following Saccharomycetes enrichment, and remained highly enriched in comparison with unimpacted soils for the remainder of the study. Given that this taxon became

continuously enriched throughout both studies, and notably in winter, suggests that they thrive in nitrogen-rich environments. It is also possible that Sordariomycetes might constitute members of a grouping of fungi termed early ammonia fungi; fruiting bodies of these fungi have been observed approximately 8 months following decomposition [42, 110, 111]. Their presence in the soil could easily be registered by amplicon sequencing prior to observed fruiting. At the class level, taxa within Sordariomycetes appear to be evenly split between the orders Hypocreales and Microascales, both of which exhibited the same successional patterns. Both of these taxa are present in control samples and initially-unimpacted soils, however following Saccharomycetes enrichment they form a larger proportion of impacted soils, commensurate with overall Sordariomycetes enrichment. Aside from the division of the class Sordariomycetes into approximately equal components of Hypocreales and Microascales at the order level later in the decomposition timeline, successional pattern resolution at the order level does not appear particularly instructive.

Relative abundances of the phylum Basidiomycota appear to be reduced, and thus negatively affected, during active decomposition, however these fungi do appear with moderate relative abundances later in decomposition progression. In the spring trial, Tremellomycetes (Basidiomycota) relative abundances were enriched during mid-advanced decay (following day 72), concurrent with increases in soil nitrate; likewise, increases of both Tremellomycetes and nitrate occurred earlier in the winter trial. In both trials, the presence of Tremellomycetes in control soils was varied. Overall, this reflects patterns reported for Basidiomycota in impacted soils, however it is not consistent with the presence of Basidiomycota in controls, suggesting that there might be a shift within Basidiomycota towards classes with an affinity for nitrate. These types of fungi have been identified as late ammonia fungi, and are generally attributed to the

appearance of fruiting structures after 1-4 years. However, it is entirely possible that sequencing studies would register the appearance (and presumed proliferation) of these taxa concurrent with elevated nitrate prior to the development of fruiting bodies, and thus earlier than previously reported in the literature [42, 110, 111]. At the order level, Trichosporonales (Basidiomycota, Tremellomycetes) strongly reflected patterns of Tremellomycetes observed at the class level in both seasonal studies. Agaricomycetes (Basidiomycota), decreased in relative abundance in the presence of decomposition products in the spring trial. Relative abundances of Agaricomycetes varied between time points in the winter trial, however in both seasonal studies the taxa had consistent relative abundances in controls. This suggests the possibility that decomposition products as a whole may negatively affect these taxa, and they may not fare well in higher nitrogen environments or situations in which elevated ionic strength could cause osmotic stress. Eukaryotic (18S rRNA) studies have shown mixed results; Metcalf et al. (2013) concluded that Boteales, an Agaricomycete, was a strong contributor to PMI regressions, although directional trends (increases or decreases of the taxon) were not discussed. Carter et al. (2015) showed the presence of Agaricomycetes in soil associated with decomposing pigs in two seasonal trials, but no patterns of change in relative abundances of Agaricomycetes in impacted or control soils were readily observable, except in the spring when nematodes dominated the community to the exclusion of most other taxa [21, 31]. We had hypothesized that *Malassezia* (Basidiomycota, Exobasidiomycetes, Malasseziales), a human (and mammalian) cutaneous lipophilic yeast, might be present in impacted soils, and we found no evidence of this. Given the feeding requirements, it is entirely possible that Malassezia does not survive in the soil, or there is not sufficient abundance of this yeast in comparison with other taxa to render it significant.

Our study does support previous work demonstrating that microbial (and in this case, fungal) successional patterns are present in soil impacted by decomposition products [30, 32, 35-37] , and we are able to demonstrate in detail that seasonal differences impact the magnitude and timing of those successional changes. We find that Saccharomycetes/Saccharomycetales spp. have a distinctly strong signature in soil associated with a short lifespan of effect from bloat through late advanced decay and early skeletonization, peaking at the onset of advanced decay and lasting throughout early advanced decay, and spanning approximately 8,000-22,000 ADH as measured by soil temperatures. We have found that in terms of observed successional patterns, the class taxonomic rank appeared to exhibit the cleanest and most instructive patterns of apparent successional changes under high-resolution inquiry. In addition to this we have discovered compelling evidence that changes in beta diversity are directly linked to changes in all soil chemistry parameters measured, and that these relationships are consistent across seasons. However, we are hesitant to go so far as to assert that these observed changes can be considered repeatable, let alone robust, without considerable further supporting study of similar nature, i.e. repeated over multiple climates at similar resolution and including soil chemistry data. It is reasonable to assume that decomposition in different environments and soil chemistries might yield entirely different microbial signatures and patterns in soil at all taxonomic ranks. Furthermore, taxon-based amplicon sequencing studies have two principal weaknesses: the lack of ability to distinguish between live and dead taxa, and that taxon abundances cannot be directly quantified without supplementary assays specifically designed to do so; these are not elements that are typically addressed in the discussion of taxon-based modelling systems currently under development [31, 32, 46]. The observation of generalized fungal succession is robust; however, the question arises as to whether it is preferable to continue to probe these successional patterns

from an organismal standpoint, given the overwhelming evidence of ecological variation. Perhaps it is time to build upon our knowledge of succession and its relationship to soil chemistry by switching tools to transcriptomics and metabolomics approaches whereby it is possible to assess the response of living organisms to their environment from a functional rather than taxon-based standpoint. Initial modelling studies using metatranscriptomics have been conducted, and their results are promising in this regard [112].

Nematode diversity and successional patterns

Changes in nematode abundances and diversity most strongly reflected environmental trends early in the seasonal trials, and continued soil impaction, as seen by consistent augmentation of bacterial-feeding enrichment opportunists at the end of both studies. No trophic group or class of nematodes exhibited any discernable relationship to changes in soil fungal populations. In both seasonal trials, alpha diversity indices (richness and Shannon diversity) decreased during bloat and active decay, and remained significantly reduced after one year. Abundances increased, although with very different timings and magnitudes between the two seasons, and recovered by the end of both trials, although the ending abundances exhibited considerable variance not found in controls or initial soils. In the spring trial, initial communities were dominated by a mixture of cp-2 bacterial and fungal feeders until days 43-58 in early advanced decay. By day 58 community composition, shifted substantially towards cp-1 bacterial-feeding communities. This change was attenuated in cores, but still present. By the end of each of the seasonal trials, communities in both depths were still dominated by B1 bacterial feeders, with low to moderate representation of cp-2 class bacterial and fungal feeders (Figures 3.22-3.23, 3.26-3.27). It is apparent that seasonal differences drove the disparities in timing and magnitude of nematode abundance increases during the earliest phases of decomposition. However, within

both seasonal trials, once abundances had increased and the community shift to bacterial enrichment opportunists had taken place, the subsequent successional trajectory was similar between the two studies; bacterial and fungal community compositions largely maintained a continuous level of impaction for the remainder of both studies. Ultimately, this indicates that after a year, nematode communities were still very highly impacted by the decomposition process, and that enough bacterial biomass is readily available that cp-1/B1 bacterial feeders are stimulated to produce in moderate quantity. Cp-2/F2/B2 taxa are not considered enrichment opportunists and while abundant food supplies may be available, they will not reproduce in the same quantities as cp-1/B2 taxa. This suggests that for both seasonal trials, expected successional patterns have only begun to emerge, and that a study length of one year is not sufficient to observe return to initial community composition for human decomposition under the conditions imposed both by this environment and study design.

In the literature there are few studies reporting nematode responses in human or carcass decomposition hotspots. Nematode field ecology studies have been primarily concerned with agricultural and field soils [56, 113-120]. While successional patterns have been explored in those agricultural contexts, the nature of the disturbances investigated were often minor pulse or pressure events in comparison with hotspot pulse events associated with the decomposition of vertebrate resources. In the existing literature, the closest comparisons that can be made are successional patterns in the rather extreme environments found within compost systems [121-123] and the enriched decomposition environments found in decaying vegetal matter, particularly that of fruit [124], which provide a greater degree of community disturbance. Vertebrate resources consist of protein-rich tissues with much lower C:N ratios than vegetal matter, decompose in a much shorter time period, and result in high nitrogen inputs into the soil,

thus removing any potential nitrogen limitations that may previously have existed [39]. This in turn incurs a sizeable microbial bloom as demonstrated earlier in this study and in Cobaugh et al. (2016), which can produce ample resources for nematodes [14]. Szelecz et al. (2016) examined nematode community impacts resulting from pigs decomposing on the soil surface, and found increased nematode abundance during active decay (day 15), followed by a sharp decline in abundance to almost zero through the continuation of active decay (days 22-36) [50]. Following active decay, abundances exhibited general recovery and slight but primarily non-significant enrichment thereafter. The authors also noted that a trophic shift toward bacterial feeding taxa occurred during active decay, and that other trophic groups gradually returned at much later time periods in the study, and thus concluded that community recovery was occurring. In Taylor et al. (2020), nematode abundances in soils associated with decomposing beavers increased during active decay (day 15) and remained elevated through skeletonization (day 153), after which overall abundances, alpha, beta, and functional diversity began to recover [55]. There were no observed decreases in abundance in the early portion of the study as reported by Szelecz et al. (2016). In our seasonal human decomposition studies, overall trends in abundance increases, alpha diversity decreases, and changes in beta and functional diversity are relatively consistent with results reported from both of these vertebrate studies, however there are key differences in the timing and magnitude of these changes. In the spring study, nematode abundances were shown to decrease well below control values between active and early advanced decay (days 12-58), only after which abundances became strongly enriched. This abundance suppression occurred during the period of time when soil temperatures were continually elevated above 30 ^{o}C and fly larval masses were present, and is consistent with patterns reported by Szelecz et al. (2016) for approximately the same morphological decomposition phases, and including the

presence of larval masses. Szelecz et al. (2016) had proposed that reductions in nematode density might be attributed to a combination of insalubrious environmental conditions resulting from decomposition products, and/or elevated temperatures present during the decomposition process [50]. However, neither carcass nor ground temperatures were measured during that study. Our human study found that consistently elevated temperatures above 30 ^{o}C in both donors and soil occurred exactly at the times that nematode abundances were reduced in the spring study.

The absence of soil (and donor) heating appears to drive abundance timing and magnitude in the winter study, and the resulting patterns in the early portion of the study are entirely different from those observed in the spring study when temperatures were higher and larval activity was present. In the winter, at the onset of active decay (day 38), nematode abundances did not decline but instead exhibited immediate and strong enrichment, with magnitudes up to five times higher than observed in the spring. This winter decomposition pattern somewhat resembles observations from Taylor et al. (2020), in which nematode abundances increased during deposition of decomposition products [55]. However, the study referenced in Taylor et al. (2020) was performed during the summer, and accompanied by both active larval masses and soil heating for approximately 12 days. In contrast, the human spring study soil heating occupied a period of approximately 50 days [55]. Given the relative differences between the masses involved, it is likely that soil heating during the beaver study was insufficient in magnitude or duration to incur notable changes to the nematode communities beyond what was already observed in the cp-class shifts.

Nematode thermal responses have been investigated in laboratory experiments [125, 126] and under field conditions [127], however the closest comparison to the enhanced heating observed during decomposition would most likely be found in compost systems. Compost

systems are characterized by changes in temperature, pH, moisture, and CO_2 output, in patterns that somewhat mimic those found in vertebrate decomposition under conditions of thermogenesis. Early in the composting process there is a period of high temperature (thermophilic phase) that often exceeds 60 ^{o}C, after which general cooling and maturation of the compost follows [121-123]. Steel et al. (2010) examined nematode abundance and successional patterns in compost and found that abundances declined to undetectable levels during the thermophilic phase of compost development, however as temperatures began to decrease, the compost was colonized first by cp-1 bacterivores followed by cp-2 taxa [121]. Szelecz et al. (2016) suggested that compost might be considered as a possible analogue for decomposition progression, noting similarities between the two processes during their early phases with respect to both cp-class shifts and associated taxa [50]. However, dissimilarities were noted in the later portions of both processes, in particular, the lack of increase of fungal feeders in decomposition in comparison with compost. Vertebrate decomposition entails the breakdown of tissues with C:N ratios of about 8, and reported C:N ratios of the plant material used to create this compost mixture ranged from 15-90 [39, 121-123]. Thus this lack of increase in fungal-feeding nematodes in the later time periods of vertebrate decomposition reported by Szelecz et al. (2016) might stem from the differences in chemical environment due to a higher quality enrichment source (low C:N), or incomplete successional patterns, since it was also pointed out in the same study that cp-2 class taxa (bacterivores) only reappeared by day 263-367 at the very end of the study. It is also quite possible that the only similarity between the two processes (vertebrate decomposition and composting) involves the initial effect of high temperature flux and its impact upon the upper thermal limits of nematodes. The exertion of selective pressure favoring taxa that can survive the heating process would presumably determine the ensuing successional

characteristics. Taken together, the results from our spring human decomposition study suggested that elevated temperature flux during larval thermogenesis suppress nematode abundances during the early phases of early decomposition, in much the same manner that heat peaks in compost inhibit nematode abundances and drive successional characteristics. In stark contrast, the human winter study data shows no evidence of heat flux impacts to nematode communities that delay or attenuate initial nematode abundance increases. Likewise, overall nematode abundances in the winter study remained higher than post-heating abundance enrichment in the spring study, and this disparity in magnitude between the two seasonal studies remained until 100,000 ADH, suggesting that nematode abundances are primarily affected by short-term temperature flux early in the decomposition process, as opposed to long-term accumulated temperature effects as observed in soil chemistry data.

If, as observed for nematodes, thermal limits, or time spent above thermal thresholds prove to inhibit or otherwise affect bacterial and fungal taxa, this has tremendous implications for the construction of microbial models. If high temperature in decomposition is an element only associated with thermogenesis effects, then it is possible that temperatures in these ranges may select for or against particular bacterial or fungal decomposing communities in the soil specifically based upon their adaptations to these temperatures. By extension, high temperatures could also shift transcriptomic and metabolic outputs of these microbial communities in a significant manner. Microbial models based upon accumulated degree-days (ADD) may mask these temperature peaks or sustained thresholds in the calculation of the daily average temperatures, especially if temperature data is used from sources which could not register these localized thermal effects in the first place. Likewise, models built upon data that homogenizes seasonal observations may obscure evidence of these potential thermal signatures.

While magnitude and timing of nematode abundances appears to be at least partially driven by the presence or absence of short-term temperature flux, community diversity appeared to respond instead to decomposition-derived bacterial density in soil, based on the continued presence of large abundances of enrichment-opportunistic bacterial-feeding nematodes. Successional patterns (inclusive of alpha, beta, and functional diversity) in the early portion of both seasonal studies were consistent with those observed in other vertebrate studies, however we did not witness the degree of recovery of either alpha or beta diversity later in time that those same studies show [50, 55]. In the beaver decomposition study from Taylor et al. (2020), changes to trophic composition of nematode communities first shifted during active decay (day 15), to a community largely composed of cp-1/B1 bacterial feeding taxa (Rhabditidae, Diplogastridae, and *Pelodera*) considered to be highly r-selected enrichment opportunists [55]. This population shift lasted through late advanced decay (day 40) in cores and skeletonization (day 110) in interface soils, after which abundances of cp-class 2 taxa, both fungivores and bacterivores had begun to gradually increase in abundance, notably: *Aphelenchoides* (F2), *Boleodorus* (F2), *Ditylenchus* (F2), Tylenchoalimidae (F4), and *Acrobeloides* (B2). *Filenchus* (F2), the fungal feeder most abundant in soil controls, decreased by active decay (day 15) and remained suppressed thereafter. Overall, omnivorous and predaceous taxa of cp-classes 3-5 responded negatively to decomposition, with the exception of *Seinura* (P2) which increased concomitant with increases of *Aphelenchoides.* Of these variously enriched or suppressed taxa, seven passed criteria that suggested their potential utility as indicator taxa for decomposition progression.

Of the cp-1/B1 enrichment taxa shown to be consistently associated with decomposition environments, the family Rhabditidae has appeared with prolonged enrichment in pig and beaver

studies [50, 55], and has been reported as a notable contributor in eukaryotic sequencing, generally associated with early time periods of the various studies [21, 31-33]. Individual genera of prominence within the family of Rhabditidae have occasionally been singled out; Metcalf et al. (2013) described the abundance patterns of *Oscheius tipulae*, Taylor et al. (2020) noted the augmentation of *Pelodera spp*., and this study observed enriched abundances of *Diploscapter*. While this is of ecological and biogeographical interest, the presence of three different dominant taxa within Rhabditidae most likely derives from localized presence or absence of specific genera, and thus strongly underscores the assertion made in Taylor et al. (2020) that cp-1/B1 taxa should be considered at the family level only. As an ecological question, the succession of genera within the family of Rhabditidae has the potential to be quite fascinating, however as a potential forensic tool, a focus on genera would likely lead to both abundance underrepresentation and inaccuracies in timing within Rhabditidae. When considered at the family level, overall cp1/B1 enrichment is consistent with previous reports [21, 31-33, 50, 55].

While the beaver decomposition study outlined in Taylor et al. (2020) showed distinct shifts in contributing taxa, and clear successional progression, these same taxon shifts varied temporally between seasons in the human studies, and successional patterns were indistinct following initial enrichment. As mentioned earlier in this section, initial enrichment patterns of cp-1/B1 taxa during active decay in winter compared favorably to Taylor et al. (2020), whereas spring decomposition patterns more closely resembled those reported by Szelecz et al. (2016) and Steel et al. (2010) regarding the delay in initial abundance increases potentially due to soil heating effects. What is interesting to note is that once the trophic and cp-class shifts toward cp-1/B1 dominance had occurred in both seasons, and cp-2 class taxa began to emerge, a subset of the same diagnostic indicator taxa that appeared in Taylor et al. (2020) appeared here as well,

although their timing was completely different during decomposition progression. For example, *Acrobeloides* (cp-2/B2) and *Aphelenchoides* (cp-2/F2) were found in Taylor et al. (2020) to undergo suppression during the deposition of decomposition products, and enrichment during skeletonization. In the spring human study these two taxa exhibited similar behavior, with suppression evident during active and early advanced decay (day 58) during the period of soil heating, after which point they were both variably enriched throughout the remainder of the study. In the winter study, *Aphelenchoides* was mildly suppressed until the onset of advanced decay (day 75) at which point enrichment was observed, while *Acrobeloides* became enriched with no early suppression at all. In both seasonal studies, the appearance and enrichment of *Seinura* (cp-2/P2), a predator of other nematodes, tracked closely with the enrichment of *Aphelenchoides*, confirming similar observations from Taylor et al. (2020) [55]. In laboratory studies, *Seinura* spp. have been reared on a fairly narrow range of nematode cultures that include *Aphelechus* spp. (cp-2/F2), *Acrobeloides* spp. *Aphelenchoides* spp., and *Ditylenchus* spp. (cp-2/F2), as well as a selected plant-parasitic taxa [128-131]. For some species of *Seinura*, prey specificity has been demonstrated to be very high, limited primarily to the fungal-feeding taxa *Aphelechus* spp., *Aphelenchoides* spp., and *Ditylenchus* spp. [130]. Predatory nematodes typically occupy cp-class 3-5 and reproduce very slowly, however *Seinura* is a cp-class 2 predator. *Seinura paratenuicaudata* has a life cycle of 4-5 days; under optimal conditions it has been observed to feed and reproduce continually, laying up to two eggs per hour, and adult females have been observed to feed on (and kill) 4-6 *Aphelenchus* sp. over the course of a day [130]. In addition, Vats et al. (2004) notes that the optimal temperature for feeding and reproduction is about 30 ^{o}C, while neither occur once temperatures drop to 11-15 ^{o}C. In both the winter and spring studies, *Seinura* was found in soils between June and July, well within feeding

and reproductive temperature optima for *S. paratenuicaudata*. While other *Seinura* spp. temperature-related developmental and reproductive characteristics are not well-described, it is possible that given favorable temperature ranges, the unusually high abundances of this nematode in soils in conjunction with increases in *Aphelenchoides,* a known preferred food source, are coupled in decomposition systems. *Ditylenchus,* another known food source for *Seinura*, was enriched in the winter study during the same timeframe as *Aphelenchoides,* further supporting this enriched coupling between *Seinura* and select fungal-feeding taxa [130]. The presence of *Seinura* is not reported in conjunction with *Aphelenchoides* enrichment in compost studies following the heat peak, suggesting that *Seinura* either was not initially present in these systems, or that the temperatures achieved during the composting process were too high for it to withstand. Given the proliferation of appropriate fungal feeders during the later phases of decomposition in our study, in conjunction with a favorable reproductive temperature range for *Seinura*, it is possible that this constitutes a naturally-occurring predator-prey relationship that has the potential to be harnessed diagnostically. More study is required in order to evaluate the nature of this association; however, this may prove to be an interesting relationship both ecologically and forensically.

Low abundances of *Filenchus* were associated with decomposing buried remains in contrast with abundances found in control soils [53]. In the study reported in Taylor et al. (2020), *Filenchus* abundances decreased during active decay during vertebrate decomposition and remained suppressed thereafter, thus the proposal for its inclusion as an indicator taxon for decomposition progression [55]. This same suppression pattern of *Filenchus* was observed in both seasonal human studies. Here, the suppression effect is larger in the spring in comparison with winter, however in both cases, as soils become impacted, *Filenchus* abundances decrease,

and remain suppressed for the duration of the study. This constitutes the third observation of notable and consistent *Filenchus* suppression in early decomposition. Previously we proposed that *Filenchus* responded negatively to some element of the decomposition process [55], and while this certainly appears to hold true for the spring human decomposition trial, *Filenchus*' moderate response in the winter decomposition trial suggests that the main sensitivity might be to temperature rather than to the chemical environment. This is supported by observations of Tylenchids (which includes *Filenchus*) in compost studies where it was reported that heating of compost to 60 ^{o}C negatively impacted the survival of tylenchids [123]. Taken together, this suggests that *Filenchus*, and perhaps other members of Tylenchidae might be minimally affected in winter decomposition as opposed to warm-weather conditions under which enhanced soil heating can occur. If this is indeed the case, unusually low *Filenchus* abundances might be diagnostic for the presence of heat, however this would require further study in order to verify.

In light of these collective observations, the principal nematode taxa that have proven robust in terms of consistent responses across multiple survey types and biogeographical regions and thus a good candidates as indicators are Rhabditidae [21, 31-33, 50, 53, 55] and Cephalobidae, which includes the genus *Acrobeloides* [10, 32, 53, 55]. *Filenchus* patterns were consistent throughout Keenan et al. (2018), Taylor et al. (2020), and this study, while *Aphelenchoides*, and *Seinura* patterns were consistent throughout this study and Taylor et al. (2020). It should be noted that Szelecz et al. (2018) is a forensic case study in which the bones of a single human were found in a forested area, and thus data do not arise from a longitudinal study [51]. This same is true for results in Keenan et al. 2018, in which a multi-individual grave was exhumed and characterized after a 4-year interment, therefore neither a surface nor longitudinal study [53]. This highlights the fact that indicators either need to be robust across all

studies and regions, or used within the context of their entire community trajectory over time. These taxa alone do not appear to be sufficient to characterize decomposition progression by themselves, since collective changes in functional diversity provides a much better sense of overall community sensitivity, successional trajectory, resilience, and recovery. Also, it is worth noting that responses of cp-1/B1 bacterial feeders as a whole appear to be considerably more diagnostic for degree of soil impaction than do any other trophic group and cp-class; this coupled with no observed relationships between fungal community succession and fungal feeder proliferation suggests that changes in nematode abundance should be viewed from a bacterial biomass context rather than a fungal one.

Conclusions

Environmental impacts stemming from human decomposition are important forensically and ecologically. Short-term, these effects have been described individually in the fields of soil chemistry, microbial ecology, and entomology, however, detailed examination of these effects long-term is poorly characterized, further exacerbated by a lack of union between the three disciplines of study. In this high-resolution study we have demonstrated that environmental and soil chemistry parameters, soil fungal community succession, and free-living soil nematode succession are inextricably interlinked, and that these synergistic processes further vary by season. The relationship between ammonium and nitrate enrichment with measured soil oxygen reduction validates previously proposed models and suggests that the ratio of these N species are robust indicators of decomposition progression. Temporal patterns in fungal community composition revealed two prominent changes of successional trajectory, paralleling major changes across all soil chemical parameters, and specifically corresponded to transitions into and out of reduced-oxygen soil conditions. This evidence of direct linkage between soil chemistry and fungal succession further supports the biogeochemical model proposed by Keenan et al. (2018), and suggests that the magnitudes and timings of fluctuations within soil chemical parameters may function as predictors for successional patterns in microbial ecology. Suppression in nematode abundances observed during the spring trial is likely attributable to increased soil temperatures arising from larval thermogenesis; opposing patterns observed during the winter trial suggests that thermal effects, specifically short-term temperature flux, are likely to drive chemical and biological transformations in the soil resulting from organismal thermal tolerances, enhanced extracellular enzymatic activity, and altered metabolic rates. Short- and long-term cumulative temperature (ADD or ADH) values obtained from soil sensors in

immediate proximity to decomposing remains differed from those of ambient air in the spring trial but not the winter trial, supporting previous reports that decomposition patterns vary seasonally and are strongly affected by the presence of necrophageous insects. These differences in cumulative temperature have implications for not only decomposition modelling, but also for accuracy of PMI calculations when temperature data is obtained from nearest-weather-station data grids, as is currently standard practice. Based upon these collective results, a comprehensive multidisciplinary approach is crucial for the effective study of human decomposition processes in soil. Future work will be needed to assess the nature of seasonal impacts, particularly over multiple climates and soil types, in order to generate robust data sets for the construction of models designed to estimate the PMI.

References

1. Macdonald BCT, Farrell M, Tuomi S, Barton PS, Cunningham SA, Manning AD. Carrion decomposition causes large and lasting effects on soil amino acid and peptide flux. Soil Biology & Biochemistry. 2014;69:132-40. doi: 10.1016/j.soilbio.2013.10.042.

2. Keenan SW, Schaeffer SM, Jin VL, DeBruyn JM. Mortality hotspots: Nitrogen cycling in forest soils during vertebrate decomposition. Soil Biology & Biochemistry. 2018;121:165-76. doi: 10.1016/j.soilbio.2018.03.005.

3. Quaggiotto MM, Evans MJ, Higgins A, Strong C, Barton PS. Dynamic soil nutrient and moisture changes under decomposing vertebrate carcasses. Biogeochemistry. 2019;146(1):71-82. doi: 10.1007/s10533-019-00611-3.

4. Aitkenhead-Peterson JA, Owings CG, Alexander MB, Larison N, Bytheway JA. Mapping the lateral extent of human cadaver decomposition with soil chemistry. Forensic SciInt. 2012;216(1-3):127-34. doi: 10.1016/j.forsciint.2011.09.007.

5. Fancher JP, Aitkenhead-Peterson JA, Farris T, Mix K, Schwab AP, Wescott DJ, et al. An evaluation of soil chemistry in human cadaver decomposition islands: Potential for estimating postmortem interval (PMI). Forensic SciInt. 2017;279:130-9. doi: 10.1016/j.forsciint.2017.08.002.

6. Barton PS, McIntyre S, Evans MJ, Bump JK, Cunningham SA, Manning AD. Substantial long-term effects of carcass addition on soil and plants in a grassy eucalypt woodland. Ecosphere. 2016;7(10). doi: 10.1002/ecs2.1537.

7. Vass AA, Bass WM, Wolt JD, Foss JE, Ammons JT. Time since death determinations of human cadavers using soil solution. Journal of Forensic Sciences. 1992;37(5):1236-53.

8. Towne EG. Prairie vegetation and soil nutrient responses to ungulate carcasses. Oecologia.

2000;122(2):232-9. doi: 10.1007/pl00008851.

9. Benninger LA, Carter DO, Forbes SL. The biochemical alteration of soil beneath a decomposing carcass. Forensic SciInt. 2008;180(2-3):70-5. doi: 10.1016/j.forsciint.2008.07.001.

10. Szelecz I, Koenig I, Seppey CVW, Le Bayon R-C, Mitchell EAD. Soil chemistry changes beneath decomposing cadavers over a one-year period. Forensic Science International. 2018;286:155-65. doi: 10.1016/j.forsciint.2018.02.031.

11. Anderson B, Meyer J, Carter DO. Dynamics of Ninhydrin-Reactive Nitrogen and pH in Gravesoil During the Extended Postmortem Interval. Journal of Forensic Sciences. 2013;58(5):1348-52. doi: 10.1111/1556-4029.12230.

12. Meyer J, Anderson B, Carter DO. Seasonal Variation of Carcass Decomposition and Gravesoil Chemistry in a Cold (Dfa) Climate. Journal of Forensic Sciences. 2013;58(5):1175-82. doi: 10.1111/1556-4029.12169.

13. Perrault KA, Forbes SL. Elemental analysis of soil and vegetation surrounding decomposing human analogues. Canadian Society of Forensic Science Journal. 2016;49(3):138-51. doi: 10.1080/00085030.2016.1184840.

14. Cobaugh KL, Schaeffer SM, DeBruyn JM. Functional and Structural Succession of Soil Microbial Communities below Decomposing Human Cadavers. Plos One. 2015;10(6):20. doi: 10.1371/journal.pone.0130201.

15. Parmenter RR, MacMahon JA. Carrion decomposition and nutrient cycling in a semiarid shrub-steppe ecosystem. Ecological Monographs. 2009;79(4):637-61. doi: 10.1890/08-0972.1.

16. Singh B, Minick KJ, Strickland MS, Wickings KG, Crippen TL, Tarone AM, et al. Temporal

and Spatial Impact of Human Cadaver Decomposition on Soil Bacterial and Arthropod Community Structure and Function. Frontiers in Microbiology. 2018;8:12. doi: 10.3389/fmicb.2017.02616.

17. Dent BB, Forbes SL, Stuart BH. Review of human decomposition processes in soil. Environmental Geology. 2004;45(4):576-85. doi: 10.1007/s00254-003-0913-z.
18. Rath KM, Fierer N, Murphy DV, Rousk J. Linking bacterial community composition to soil salinity along environmental gradients. Isme Journal. 2019;13(3):836-46. doi: 10.1038/s41396-018-0313-8.
19. Rousk J, Baath E, Brookes PC, Lauber CL, Lozupone C, Caporaso JG, et al. Soil bacterial and fungal communities across a pH gradient in an arable soil. Isme Journal. 2010;4(10):1340-51. doi: 10.1038/ismej.2010.58.
20. Hyde ER, Haarmann DP, Petrosino JF, Lynne AM, Bucheli SR. Initial insights into bacterial succession during human decomposition. International Journal of Legal Medicine. 2015;129(3):661-71. doi: 10.1007/s00414-014-1128-4.
21. Carter DO, Metcalf JL, Bibat A, Knight R. Seasonal variation of postmortem microbial communities. Forensic Science Medicine and Pathology. 2015;11(2):202-7. doi: 10.1007/s12024-015-9667-7.
22. Hyde ER, Haarmann DP, Lynne AM, Bucheli SR, Petrosino JF. The Living Dead: Bacterial Community Structure of a Cadaver at the Onset and End of the Bloat Stage of Decomposition. Plos One. 2013;8(10). doi: 10.1371/journal.pone.0077733.
23. Hauther KA, Cobaugh KL, Jantz LM, Sparer TE, DeBruyn JM. Estimating Time Since Death from Postmortem Human Gut Microbial Communities. Journal of Forensic Sciences. 2015;60(5):1234-40. doi: 10.1111/1556-4029.12828.

24. DeBruyn JM, Hauther KA. Postmortem succession of gut microbial communities in deceased human subjects. PeerJ. 2017;5:14. doi: 10.7717/peerj.3437.

25. Pechal JL, Crippen TL, Tarone AM, Lewis AJ, Tomberlin JK, Benbow ME. Microbial Community Functional Change during Vertebrate Carrion Decomposition. PLoS ONE. 2013;8(11):e79035. doi: 10.1371/journal.pone.0079035.

26. Pechal JL, Crippen TL, Benbow ME, Tarone AM, Dowd S, Tomberlin JK. The potential use of bacterial community succession in forensics as described by high throughput metagenomic sequencing. International Journal of Legal Medicine. 2014;128(1):193-205. doi: 10.1007/s00414-013-0872-1.

27. Finley SJ, Pechal JL, Benbow ME, Robertson BK, Javan GT. Microbial Signatures of Cadaver Gravesoil During Decomposition. Microbial Ecology. 2016;71(3):524-9. doi: 10.1007/s00248-015-0725-1.

28. Procopio N, Ghignone S, Williams A, Chamberlain A, Mello A, Buckley M. Metabarcoding to investigate changes in soil microbial communities within forensic burial contexts. Forensic Science International-Genetics. 2019;39:73-85. doi: 10.1016/j.fsigen.2018.12.002.

29. Guo J, Fu X, Liao H, Hu Z, Long L, Yan W, et al. Potential use of bacterial community succession for estimating post-mortem interval as revealed by high-throughput sequencing. Scientific Reports. 2016;6. doi: 10.1038/srep24197.

30. Parkinson RA, Dias K-R, Horswell J, Greenwood P, Banning N, Tibbett M, et al. Microbial Community Analysis of Human Decomposition on Soil. In: Ritz K, Dawson L, Miller D, editors. Criminal and Environmental Soil Forensics. Berlin, Springer; 2009, pp. 379-94.

31. Metcalf JL, Parfrey LW, Gonzalez A, Lauber CL, Knights D, Ackermann G, et al. A microbial clock provides an accurate estimate of the postmortem interval in a mouse model

system. Elife. 2013;2:19. doi: 10.7554/eLife.01104.

32. Metcalf JL, Xu ZZ, Weiss S, Lax S, Van Treuren W, Hyde ER, et al. Microbial community assembly and metabolic function during mammalian corpse decomposition. Science. 2016;351(6269):158-62. doi: 10.1126/science.aad2646.

33. Weiss S, Carter DO, Metcalf JL, Knight R. Carcass mass has little influence on the structure of gravesoil microbial communities. International Journal of Legal Medicine. 2016;130(1):253-63. doi: 10.1007/s00414-015-1206-2.

34. Tomaszewski M, Cema G, Ziembinska-Buczynska A. Influence of temperature and pH on the anammox process: A review and meta-analysis. Chemosphere. 2017;182:203-14. doi: 10.1016/j.chemosphere.2017.05.003.

35. Risch AC, Frossard A, Schuetz M, Frey B, Morris AW, Bump JK. Effects of elk and bison carcasses on soil microbial communities and ecosystem functions in Yellowstone, USA. Functional Ecology. 2020. doi: 10.1111/1365-2435.13611.

36. Procopio N, Ghignone S, Voyron S, Chiapello M, Williams A, Chamberlain A, et al. Soil Fungal Communities Investigated by Metabarcoding Within Simulated Forensic Burial Contexts. Frontiers in Microbiology. 2020;11. doi: 10.3389/fmicb.2020.01686.

37. Fu X, Guo J, Finkelbergs D, He J, Zha L, Guo Y, et al. Fungal succession during mammalian cadaver decomposition and potential forensic implications. Scientific Reports. 2019;9. doi: 10.1038/s41598-019-49361-0.

38. De Boer W, Folman LB, Summerbell RC, Boddy L. Living in a fungal world: impact of fungi on soil bacterial niche development. Fems Microbiology Reviews. 2005;29(4):795-811. doi: 10.1016/j.femsre.2004.11.005.

39. Carter DO, Yellowlees D, Tibbett M. Cadaver decomposition in terrestrial ecosystems.

Naturwissenschaften. 2007;94(1):12-24. doi: 10.1007/s00114-006-0159-1.

40. Carter DO, Tibbett M. Taphonomic mycota: Fungi with forensic potential. Journal of Forensic Sciences. 2003;48(1):168-71.
41. Sagara N, Yamanaka T, Tibbett M. Soil fungi associated with graves and latrines: Toward a forensic mycology. Soil Analysis in Forensic Taphonomy. 2008:67-107. doi: 10.1201/9781420069921.ch4.
42. Tibbett M, Carter DO. Mushrooms and taphonomy: the fungi that mark woodland graves. Mycologist. 2003;17(01):20-4.
43. Findley K, Oh J, Yang J, Conlan S, Deming C, Meyer JA, et al. Topographic diversity of fungal and bacterial communities in human skin. Nature. 2013;498(7454):367-+. doi: 10.1038/nature12171.
44. Grice EA, Segre JA. The skin microbiome. Nature Reviews Microbiology. 2011;9(4):244-53. doi: 10.1038/nrmicro2537.
45. Wu GX, Zhao H, Li CH, Rajapakse MP, Wong WC, Xu J, et al. Genus-Wide Comparative Genomics of Malassezia Delineates Its Phylogeny, Physiology, and Niche Adaptation on Human Skin. Plos Genetics. 2015;11(11):26. doi: 10.1371/journal.pgen.1005614.
46. Belk A, Xu ZZ, Carter DO, Lynne A, Bucheli S, Knight R, et al. Microbiome Data Accurately Predicts the Postmortem Interval Using Random Forest Regression Models. Genes. 2018;9(2). doi: 10.3390/genes9020104.
47. Metcalf JL. Estimating the postmortem interval using microbes: Knowledge gaps and a path to technology adoption. Forensic Science International-Genetics. 2019;38:211-8. doi: 10.1016/j.fsigen.2018.11.004.
48. Seppey CVW, Fournier B, Szelecz I, Singer D, Mitchell EAD, Lara E. Response of forest

soil euglyphid testate amoebae (Rhizaria: Cercozoa) to pig cadavers assessed by high-throughput sequencing. International Journal of Legal Medicine. 2016;130(2):551-62. doi: 10.1007/s00414-015-1149-7.

49. Szelecz I, Fournier B, Seppey C, Amendt J, Mitchell E. Can soil testate amoebae be used for estimating the time since death? A field experiment in a deciduous forest. Forensic Science International. 2014;236:90-8. doi: 10.1016/j.forsciint.2013.12.030.
50. Szelecz I, Sorge F, Seppey CVW, Mulot M, Steel H, Neilson R, et al. Effects of decomposing cadavers on soil nematode communities over a one-year period. Soil Biology & Biochemistry. 2016;103:405-16. doi: 10.1016/j.soilbio.2016.09.011.
51. Szelecz I, Losch S, Seppey CVW, Lara E, Singer D, Sorge F, et al. Comparative analysis of bones, mites, soil chemistry, nematodes and soil micro-eukaryotes from a suspected homicide to estimate the post-mortem interval. Scientific reports. 2018;8(1):25-. doi: 10.1038/s41598-017-18179-z.
52. Braig HR, Perotti MA. Carcases and mites. Experimental and Applied Acarology. 2009;49(1-2):45-84. doi: 10.1007/s10493-009-9287-6.
53. Keenan SW, Emmons AL, Taylor LS, Phillips G, Mason AR, Mundorff AZ, et al. Spatial impacts of a multi-individual grave on microbial and microfaunal communities and soil biogeochemistry. PloS one. 2018;13(12):e0208845. doi: 10.1371/journal.pone.0208845.
54. Taylor LS, Phillips G, Bernard EC, DeBruyn JM. DEPTH STRATIFICATION OF NEMATODE COMMUNITIES ASSOCIATED WITH VERTEBRATE DECOMPOSITION. Journal of Nematology. 2018;50(4):658-9.
55. Taylor LS, Phillips G, Bernard E, DeBruyn J. Soil nematode functional diversity, successional patterns, and indicator taxa associated with vertebrate decomposition hotspots.

PloS one. 2020;15(11):e0241777. doi: 10.1371/journal.pone.0241777.

56. Ferris H, Bongers T. Nematode indicators of organic enrichment. Journal of Nematology. 2006;38(1):3-12.

57. Bernard EC. SOIL NEMATODE BIODIVERSITY. Biology and Fertility of Soils. 1992;14(2):99-103. doi: 10.1007/bf00336257.

58. Bongers T, Bongers M. Functional diversity of nematodes. Applied Soil Ecology. 1998;10(3):239-51. doi: 10.1016/s0929-1393(98)00123-1.

59. Bongers T. The Maturity Index, the evolution of nematode life history traits, adaptive radiation and cp-scaling. Plant and Soil. 1999;212(1):13-22. doi: 10.1023/a:1004571900425.

60. Ettema CH, Bongers T. CHARACTERIZATION OF NEMATODE COLONIZATION AND SUCCESSION IN DISTURBED SOIL USING THE MATURITY INDEX. Biology and Fertility of Soils. 1993;16(2):79-85. doi: 10.1007/bf00369407.

61. Ferris H, Bongers T, de Goede RGM. A framework for soil food web diagnostics: extension of the nematode faunal analysis concept. Applied Soil Ecology. 2001;18(1):13-29. doi: 10.1016/s0929-1393(01)00152-4.

62. Ferris H, Bongers T. Indices Developed Specifically for Analysis of Nematode Assemblages. Nematodes as Environmental Indicators. 2009:124-45. doi: 10.1079/9781845933852.0124.

63. Yeates GW, Bongers T, Degoede RGM, Freckman DW, Georgieva SS. FEEDING-HABITS IN SOIL NEMATODE FAMILIES AND GENERA - AN OUTLINE FOR SOIL ECOLOGISTS. Journal of Nematology. 1993;25(3):315-31.

64. Ferris H, Matute MM. Structural and functional succession in the nematode fauna of a.soil food web. Applied Soil Ecology. 2003;23(2):93-110. doi: 10.1016/s0929-1393(03)00044-1.

65. Ferris H, Griffiths BS, Porazinska DL, Powers TO, Wang K-H, Tenuta M. Reflections on

Plant and Soil Nematode Ecology: Past, Present and Future. Journal of Nematology. 2012;44(2):115-26.

66. Yeates GW. Nematodes as soil indicators: functional and biodiversity aspects. Biology and Fertility of Soils. 2003;37(4):199-210. doi: 10.1007/s00374-003-0586-5.
67. Neher DA. Ecology of Plant and Free-Living Nematodes in Natural and Agricultural Soil. Annual Review of Phytopathology, Vol 48. 2010;48:371-94. doi: 10.1146/annurev-phyto-073009-114439.
68. Suzuki A. Experimental and physiological ecology of ammonia fungi: studies using natural substrates and artificial media. Mycoscience. 2006;47(1):3-17. doi: 10.1007/s10267-005-0270-8.
69. Heaton V, Moffatt C, Simmons T. Quantifying the Temperature of Maggot Masses and its Relationship to Decomposition. Journal of Forensic Sciences. 2014;59(3):676-82. doi: 10.1111/1556-4029.12396.
70. Johnson AP, Mikac KM, Wallman JF. Thermogenesis in decomposing carcasses. Forensic Science International. 2013;231(1-3):271-7. doi: 10.1016/j.forsciint.2013.05.031.
71. Payne JA. A SUMMER CARRION STUDY OF THE BABY PIG SUS-SCROFA LINNAEUS. Ecology. 1965;46(5):592-602. doi: 10.2307/1934999.
72. Damann FE, Tanittaisong A, Carter DO. Potential carcass enrichment of the University of Tennessee Anthropology Research Facility: A baseline survey of edaphic features. Forensic Science International. 2012;222(1-3):4-10. doi: 10.1016/j.forsciint.2012.04.028.
73. Soil Survey Staff. Soil Map: Natural Resources Conservation Service, United States Department of Agriculture; 2018 [cited 2018 16 April]. Available from: https://websoilsurvey.nrcs.usda.gov/app/WebSoilSurvey.aspx.

74. Hartgrove N. Soil Survey of Knox County, Tennessee. United States Department of Agriculture. National Resources Conservation Service; 2006. p. 7, 10, 25-8, 78-9.
75. Megyesi MS, Nawrocki SP, Haskell NH. Using accumulated degree-days to estimate the postmortem interval from decomposed human remains. Journal of Forensic Sciences. 2005;50(3):618-26.
76. Rhine ED, Sims GK, Mulvaney RL, Pratt EJ. Improving the Berthelot reaction for determining ammonium in soil extracts and water. Soil Science Society of America Journal. 1998;62(2):473-80.
77. Doane TA, Horwath WR. Spectrophotometric determination of nitrate with a single reagent. Analytical Letters. 2003;36(12):2713-22. doi: 10.1081/al-120024647.
78. Soukup DA, Buck BJ, Harris W. Chapter 2. Preparing Soils for Mineralogical Analyses. In: Drees ALUaLR, editor. Methods of soil analysis Part 5, Mineralogical methods. Madison, Wisconsin: Soil Science Society of America; 2008. p. 13-31.
79. Cregger MA, Veach AM, Yang ZK, Crouch MJ, Vilgalys R, Tuskan GA, et al. The Populus holobiont: dissecting the effects of plant niches and genotype on the microbiome. Microbiome. 2018;6. doi: 10.1186/s40168-018-0413-8.
80. Schloss PD, Westcott SL, Ryabin T, Hall JR, Hartmann M, Hollister EB, et al. Introducing mothur: Open-Source, Platform-Independent, Community-Supported Software for Describing and Comparing Microbial Communities. Applied and Environmental Microbiology. 2009;75(23):7537-41. doi: 10.1128/aem.01541-09.
81. Abarenkov K, Zirk A, Piirmann T, Pohonen R, Ivanov F, Nilsson RH, et al. Full mothur UNITE+INSD dataset 1. Version 04.02.2020. Community; 2020.
82. Jenkins WR. A rapid centrifugal-flotation technique for separating nematodes from soil.

Plant Dis Rep. 1964;48((9)):692-.

83. R Development Core Team. R: A language and environment for statistical computing. Vienna, Austria: R Foundation for Statistical Computing; 2010.
84. Kolde R. pheatmap: Pretty Heatmaps. 2019.
85. McMurdie PJ, Holmes S. phyloseq: An R Package for Reproducible Interactive Analysis and Graphics of Microbiome Census Data. Plos One. 2013;8(4). doi: 10.1371/journal.pone.0061217.
86. Wickham H. ggplot2: Elegant Graphics for Data Analysis. New York Springer-Verlag; 2016.
87. Wickham H. Easily Install and Load 'Tidyverse' Packages. Comprehensive R Archive Network. 2017.
88. Fox J. Companion to Applied Regression. Comprehensive R Archive Network. 2016.
89. Oksanen J, Blanchet F, Friendly M, Kindt R, Legendre P, McGlinn D, et al. vegan: Community Ecology Package. 2019.
90. Neuwirth E. RColorBrewer: ColorBrewer Palettes. 2014.
91. Essington ME. Soil and water chemistry: an integrative approach. Soil and water chemistry: an integrative approach. 2015;(Ed. 2.):656 pp.- pp.
92. Carroll D. Clay minerals: a guide to their X-ray identification. Spec Pap geol Soc Am. 1970;126:87 pp.- pp.
93. Weatherbee CR, Pechal JL, Benbow ME. The dynamic maggot mass microbiome. Ann Entomol Soc Am. 2017;110(1):45-53. doi: 10.1093/aesa/saw088.
94. Gruner SV, Slone DH, Capinera JL, Turco MP. Volume of Larvae Is the Most Important Single Predictor of Mass Temperatures in the Forensically Important Calliphorid, Chrysomya

megacephala (Diptera: Calliphoridae). Journal of Medical Entomology. 2017;54(1):30-4. doi: 10.1093/jme/tjw139.

95. Charabidze D, Hedouin V. Temperature: the weak point of forensic entomology. International Journal of Legal Medicine. 2019;133(2):633-9. doi: 10.1007/s00414-018-1898-1.

96. Dourel L, Pasquerault T, Gaudry E, Vincent B. Using estimated on-site ambient temperature has uncertain benefit when estimating postmortem interval. Psyche (Cambridge). 2010;2010:1-7.

97. Hofer IMJ, Hart AJ, Martin-Vega D, Hall MJR. Estimating crime scene temperatures from nearby meteorological station data. Forensic Science International. 2020;306. doi: 10.1016/j.forsciint.2019.110028.

98. Noll L, Zhang S, Zheng Q, Hu Y, Wanek W. Wide-spread limitation of soil organic nitrogen transformations by substrate availability and not by extracellular enzyme content. Soil Biology & Biochemistry. 2019;133:37-49. doi: 10.1016/j.soilbio.2019.02.016.

99. FAO. World reference base for soil resources. World Soil Resources Report 106. Rome: Agriculture Organization of the United Nations; 2014.

100. Carter DO, Yellowlees D, Tibbett M. Temperature affects microbial decomposition of cadavers (Rattus rattus) in contrasting soils. Applied Soil Ecology. 2008;40(1):129-37. doi: 10.1016/j.apsoil.2008.03.010.

101. Carter DO, Tibbett M. Microbial decomposition of skeletal muscle tissue (Ovis aries) in a sandy loam soil at different temperatures. Soil Biology & Biochemistry. 2006;38(5):1139-45. doi: 10.1016/j.soilbio.2005.09.014.

102. Haslam TCF, Tibbett M. Soils of Contrasting pH Affect the Decomposition of Buried

Mammalian (Ovis aries) Skeletal Muscle Tissue. Journal of Forensic Sciences. 2009;54(4):900-4. doi: 10.1111/j.1556-4029.2009.01070.x.

103. Carter DO, Yellowlees D, Tibbett M. Moisture can be the dominant environmental parameter governing cadaver decomposition in soil. Forensic Science International. 2010;200(1-3):60-6. doi: 10.1016/j.forsciint.2010.03.031.

104. Dautartas A, Kenyhercz MW, Vidoli GM, Meadows Jantz L, Mundorff A, Steadman DW. Differential Decomposition Among Pig, Rabbit, and Human Remains. Journal of forensic sciences. 2018. doi: 10.1111/1556-4029.13784.

105. Steadman DW, Dautartas A, Kenyhercz MW, Jantz LM, Mundorff A, Vidoli GM. Differential Scavenging Among Pig, Rabbit, and Human Subjects. Journal of forensic sciences. 2018. doi: 10.1111/1556-4029.13786.

106. Notter SJ, Stuart BH, Rowe R, Langlois N. The initial changes of fat deposits during the decomposition of human and pig remains. Journal of Forensic Sciences. 2009;54(1):195-201. doi: 10.1111/j.1556-4029.2008.00911.x.

107. Barton PS, Reboldi A, Dawson BM, Ueland M, Strong C, Wallman JF. Soil chemical markers distinguishing human and pig decomposition islands: a preliminary study. Forensic science, medicine, and pathology. 2020. doi: 10.1007/s12024-020-00297-2.

108. Suh SO, Blackwell M, Kurtzman CP, Lachance MA. Phylogenetics of Saccharomycetales, the ascomycete yeasts. Mycologia. 2006;98(6):1006-17. doi: 10.3852/mycologia.98.6.1006.

109. Zhang N, Castlebury LA, Miller AN, Huhndorf SM, Schoch CL, Seifert KA, et al. An overview of the systematics of the Sordariomycetes based on a four-gene phylogeny. Mycologia. 2006;98(6):1076-87. doi: 10.3852/mycologia.98.6.1076.

110. Sagara N. PRESENCE OF A BURIED MAMMALIAN CARCASS INDICATED BY

FUNGAL FRUITING BODIES. Nature. 1976;262(5571):816-. doi: 10.1038/262816a0.

111. Hawksworth DL, Wiltshire PEJ. Forensic mycology: the use of fungi in criminal investigations. Forensic Science International. 2011;206(1-3):1-11. doi: 10.1016/j.forsciint.2010.06.012.

112. Burcham ZM, Cowick CA, Baugher CN, Pechal JL, Schmidt CJ, Rosch JW, et al. Total RNA Analysis of Bacterial Community Structural and Functional Shifts Throughout Vertebrate Decomposition. Journal of Forensic Sciences. 2019;64(6):1707-19. doi: 10.1111/1556-4029.14083.

113. Briar S, Tenuta M, Barker C, Entz M. SOIL NEMATODE COMMUNITY RESPONSE TO LONG-TERM CROP ROTATION, ORGANIC MANAGEMENT AND PRAIRIE RESTORATION IN THE RED RIVER VALLEY OF CENTRAL NORTH AMERICA. Journal of Nematology. 2009;41(4):313-.

114. Neher DA. Role of nematodes in soil health and their use as indicators. Journal of Nematology. 2001;33(4):161-8.

115. Hoss S, Nguyen HT, Menzel R, Pagel-Wieder S, Miethling-Graf R, Tebbe CC, et al. Assessing the risk posed to free-living soil nematodes by a genetically modified maize expressing the insecticidal Cry3Bb1 protein. Science of the Total Environment. 2011;409(13):2674-84. doi: 10.1016/j.scitotenv.2011.03.041.

116. Ortiz V, Phelan S, Mullins E. A temporal assessment of nematode community structure and diversity in the rhizosphere of cisgenic Phytophthora infestans-resistant potatoes. Bmc Ecology. 2016;16. doi: 10.1186/s12898-016-0109-5.

117. Porazinska DL, McSorley R, Duncan LW, Graham JH, Wheaton TA, Parsons LR. Nematode community composition under various irrigation schemes in a citrus soil

ecosystem. Journal of Nematology. 1998;30(2):170-8.

118. Porazinska DL, Duncan LW, McSorley R, Graham JH. Nematode communities as indicators of status and processes of a soil ecosystem influenced by agricultural management practices. Applied Soil Ecology. 1999;13(1):69-86. doi: 10.1016/s0929-1393(99)00018-9.

119. Ruess L. Nematode soil faunal analysis of decomposition pathways in different ecosystems. Nematology. 2003;5:179-81. doi: 10.1163/156854103767139662.

120. Briar SS, Barker C, Tenuta M, Entz MH. Soil Nematode Responses to Crop Management and Conversion to Native Grasses. Journal of Nematology. 2012;44(3):245-54.

121. Steel H, de la Pena E, Fonderie P, Willekens K, Borgonie G, Bert W. Nematode succession during composting and the potential of the nematode community as an indicator of compost maturity. Pedobiologia. 2010;53(3):181-90. doi: 10.1016/j.pedobi.2009.09.003.

122. Steel H, Buchan D, De Neve S, Couvreur M, Moens T, Bert W. Nematode and microbial communities in a rapidly changing compost environment: How nematode assemblages reflect composting phases. European Journal of Soil Biology. 2013;56:1-10. doi: 10.1016/j.ejsobi.2013.01.003.

123. Steel H, Verdoodt F, Cerevkova A, Couvreur M, Fonderie P, Moens T, et al. Survival and colonization of nematodes in a composting process. Invertebrate Biology. 2013;132(2):108-19. doi: 10.1111/ivb.12020.

124. Felix MA, Ailion M, Hsu JC, Richaud A, Wang J. Pristionchus nematodes occur frequently in diverse rotting vegetal substrates and are not exclusively necromenic, while Panagrellus redivivoides is found specifically in rotting fruits. Plos One. 2018;13(8). doi: 10.1371/journal.pone.0200851.

125. Venette RC, Ferris H. Thermal constraints to population growth of bacterial-feeding

nematodes. Soil Biology & Biochemistry. 1997;29(1):63-74. doi: 10.1016/s0038-0717(96)00259-3.

126. Anderson RV, Coleman DC. NEMATODE TEMPERATURE RESPONSES - A NICHE DIMENSION IN POPULATIONS OF BACTERIAL-FEEDING NEMATODES. Journal of Nematology. 1982;14(1):69-76.

127. Bakonyi G, Nagy P, Kovacs-Lang E, Kovacs E, Barabas S, Repasi V, et al. Soil nematode community structure as affected by temperature and moisture in a temperate semiarid shrubland. Applied Soil Ecology. 2007;37(1-2):31-40. doi: 10.1016/j.apsoil.2007.03.008.

128. Wood FH. BIOLOGY OF SEINURA-DEMANI (NEMATODA-APHELENCHOIDIDAE). Nematologica. 1974;20(3):347-&. doi: 10.1163/187529274x00384.

129. Hechler HC, Taylor DP. LIFE HISTORIES OF SEINURA CELERIS S OLIVEIRAE S OXURA AND S STEINERI (NEMATODA - APHELENCHOIDIDAE). Proceedings of the Helminthological Society of Washington. 1966;33(1):71-.

130. Vats R, Kanwar RS, Bajaj HK. Biology of Seinura paratenuicaudata Geraert. Nematologia Mediterranea. 2004;32(1):117-21.

131. Hechler HC. DESCRIPTION, DEVELOPMENTAL BIOLOGY, AND FEEDING HABITS OF SEINURA TENUICAUDATA (DE MAN) JB GOODEY, 1960 (NEMATODA-APHELENCHOIDIDAE), A NEMATODE PREDATOR. Proceedings of the Helminthological Society of Washington. 1963;30(2):182-.

Appendix 3

Table 3.1: Spring 2018 donor sampling. Date of sampling, associated study day, ADH calculated from ambient air, internal donor, and soil temperatures are shown, along with morphological decomposition stage. Decomposition stages that include more than one sampling time point are numbered sequentially. Beginning in advanced decay, sampling occurred at approximately 8400 ADH intervals based off ambient air temperatures.

Study Day	Study Date	ADH ambient	ADH internal	ADH donor soil	ADH soil control	Morphological Decomposition stage
0	2 May 18	0	0	0	0	Initial
8	10 May 18	3801	2457	2703	3525	Bloat
12	14 May 18	6036	5352	5362	5578	Active decay
16	18 May 18	8180	8528	8360	7648	Advanced 1
27	29 May 18	14,213	17,814	18,289	13,501	Advanced 2
43	14 June 18	23,070	29,967	30,771	22,104	Advanced 3
58	29 June 18	31,864	40,296	41,581	30,707	Advanced 4
72	13 July 18	40,428	50,757	51,922	38,979	Advanced 5
86	27 July 18	48,562	60,190	61,203	46,965	Advanced 6
103	13 Aug 18	58,224	70,875	71,557	56,530	Advanced 7
117	27 Aug 18	66,125	79,316	79,553	64,310	Advanced 8
132	11 Sep 18	75,002	88,381	88,547	73,013	Advanced 9
150	29 Sep 18	85,018	98,590	98,759	82,971	Advanced 10
168	17 Oct 18	93,873	107,592	107,850	91,879	Advanced 11
201	19 Nov 18	101,688	115,703	116,954	100,777	Advanced 12
254	11 Jan 19	110,453	124,074	127,477	110,492	Advanced 13
303	1 Mar 19	118,303	131,326	135,944	118,509	Skeletonization 1
340	7 Apr 19	127,298	140,320	144,538	127,166	Skeletonization 2
357	24 Apr 19	134,033	147,055	151,096	133,676	Skeletonization 3
376	13 May 19	143,017	156,039	159,517	142,144	Skeletonization 4

Table 3.2: Winter 2019 donor sampling. Date of sampling, associated study day, ADH calculated from ambient air, internal donor, and soil temperatures are shown, along with morphological decomposition stage. Decomposition stages that include more than one sampling time point are numbered sequentially. Beginning in advanced decay, sampling occurred at approximately 8400 ADH intervals based off ambient air temperatures.

Study Day	Study Date	ADH ambient	ADH internal	ADH donor soil	ADH soil control	Morphological Decomposition stage
0	8 Feb 19	0	0	0	0	Initial
21	1 Mar 19	3992	3319	3826	4010	Bloat
38	18 Mar 19	7485	6968	7594	7453	Active decay
55	4 Apr 19	11,787	11,662	12,127	11,595	Active/Advanced
75	24 Apr 19	19,721	20,608	22,782	18,981	Advanced 1
94	13 May 19	28,704	30,224	33,575	27,346	Advanced 2
110	29 May 19	37,257	39,027	43,005	35,304	Advanced 3
126	14 June 19	45,759	48,411	52,404	43,466	Advanced 4
140	28 June 19	53,497	56,443	60,714	50,813	Advanced 5
158	16 July 19	64,369	67,393	71,952	61,169	Skeletonization 1
172	30 July 19	72,485	75,351	79,891	68,939	Skeletonization 2
186	13 Aug 19	80,716	83,391	87,883	76,821	Skeletonization 3
201	28 Aug 19	89,633	92,077	96,552	85,440	Skeletonization 4
216	11 Sep 19	98,414	100,397	104,845	93,794	Skeletonization 5
234	30 Sep 19	109,169	110,724	115,079	104,141	Skeletonization 6
252	18 Oct 19	117,660	119,031	123,576	112,587	Skeletonization 7
290	25 Nov 19	126,679	128,883	134,019	122,428	Skeletonization 8
335	9 Jan 20	134,894	136,943	142,473	130,809	Skeletonization 9
384	27 Feb 20	143,609	144,965	151,104	139,403	Skeletonization 10

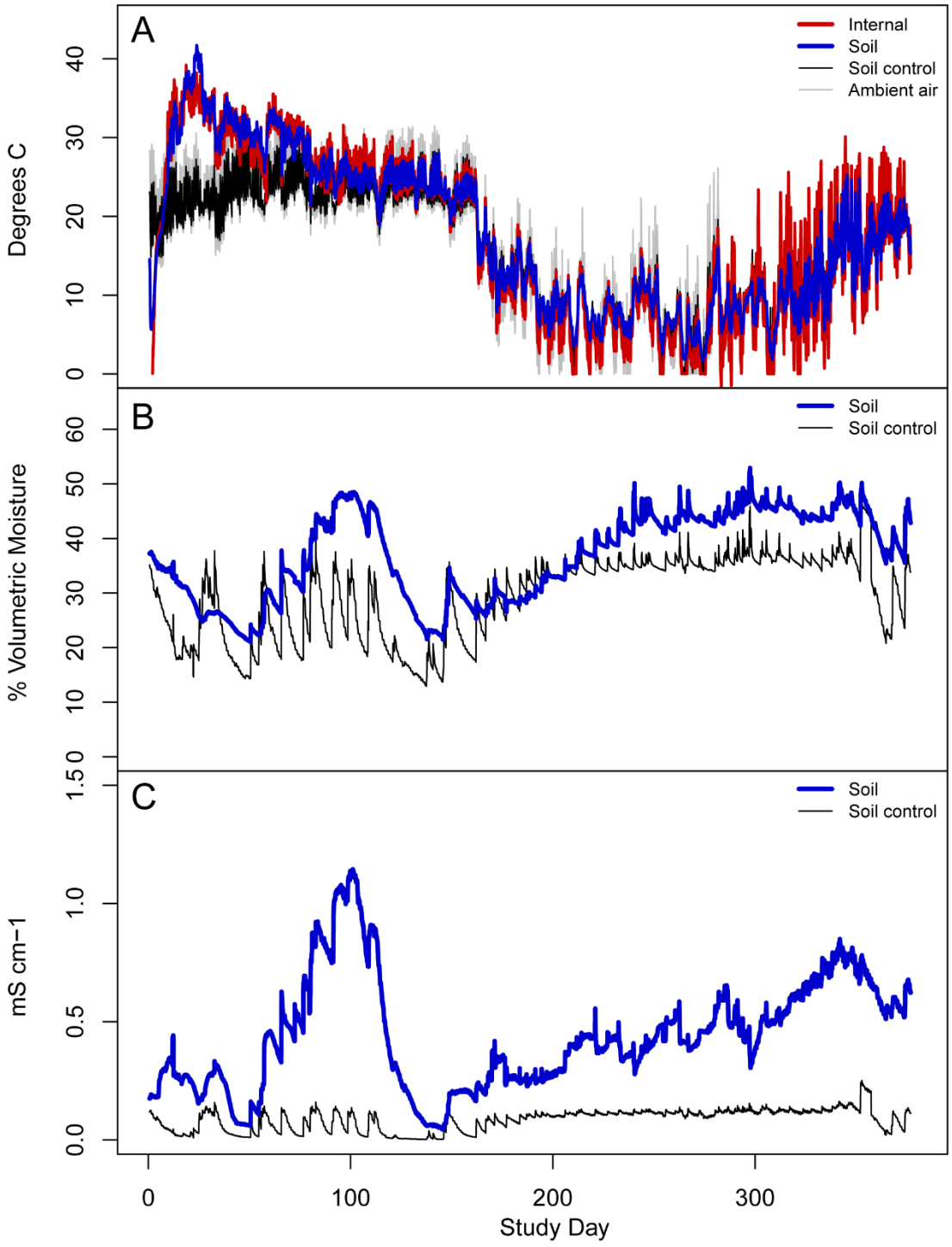

Figure 3.1: Soil sensor data from spring donor series. Temperature (A), soil moisture (B), and soil electrical conductivity (C) are shown by study day. Controls are shown in black and soil data shown in blue. For temperature data, ambient air is shown in grey, and donor internal temperatures are shown in red.

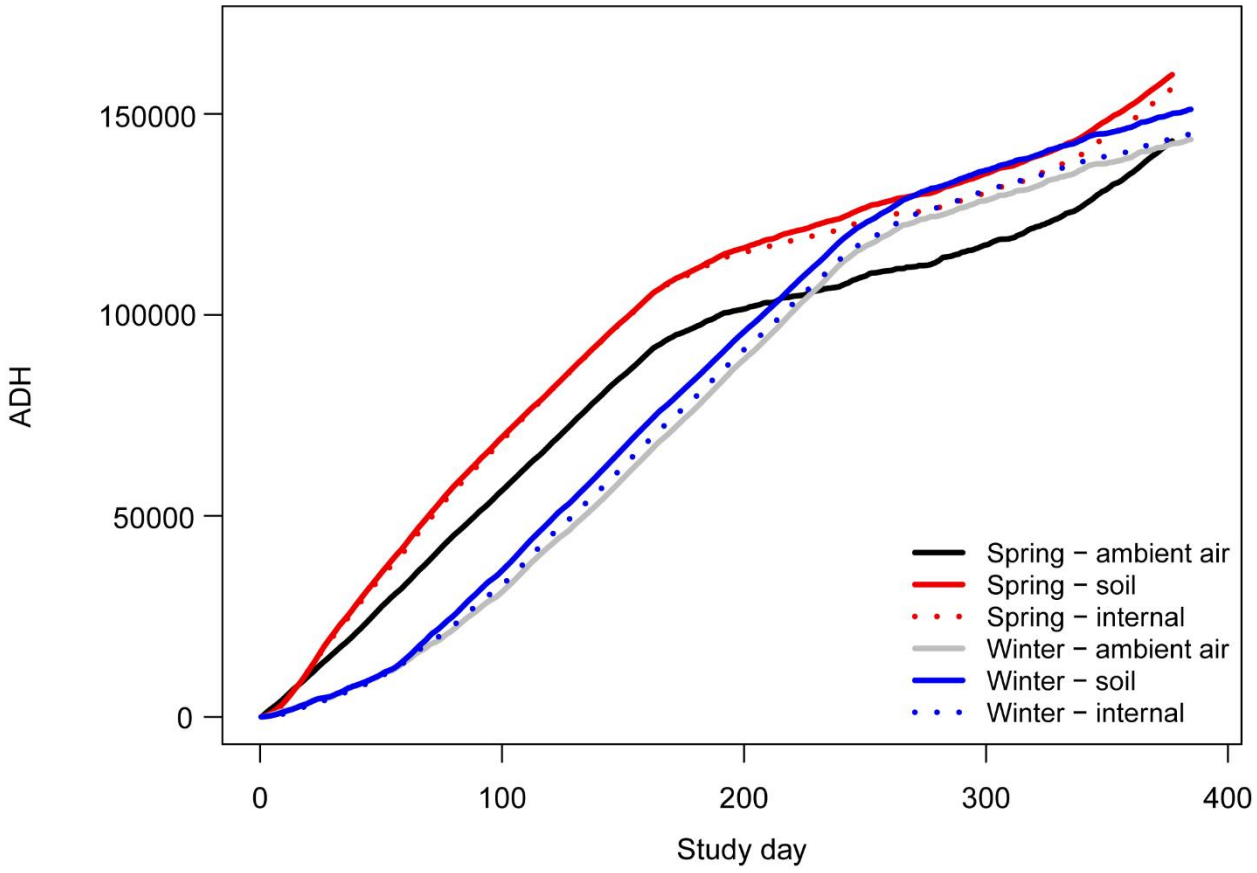

Figure 3.2. Accumulated degree hours (ADH) for environmental temperature probes shown by study day for spring and winter donor trials. Cumulative temperatures for internal and soil probes diverged from cumulative ambient air temperatures during the spring study partially due to insect-thermogenesis (red and black lines). In the absence of insect activity, this trend was reduced in the winter study**.**

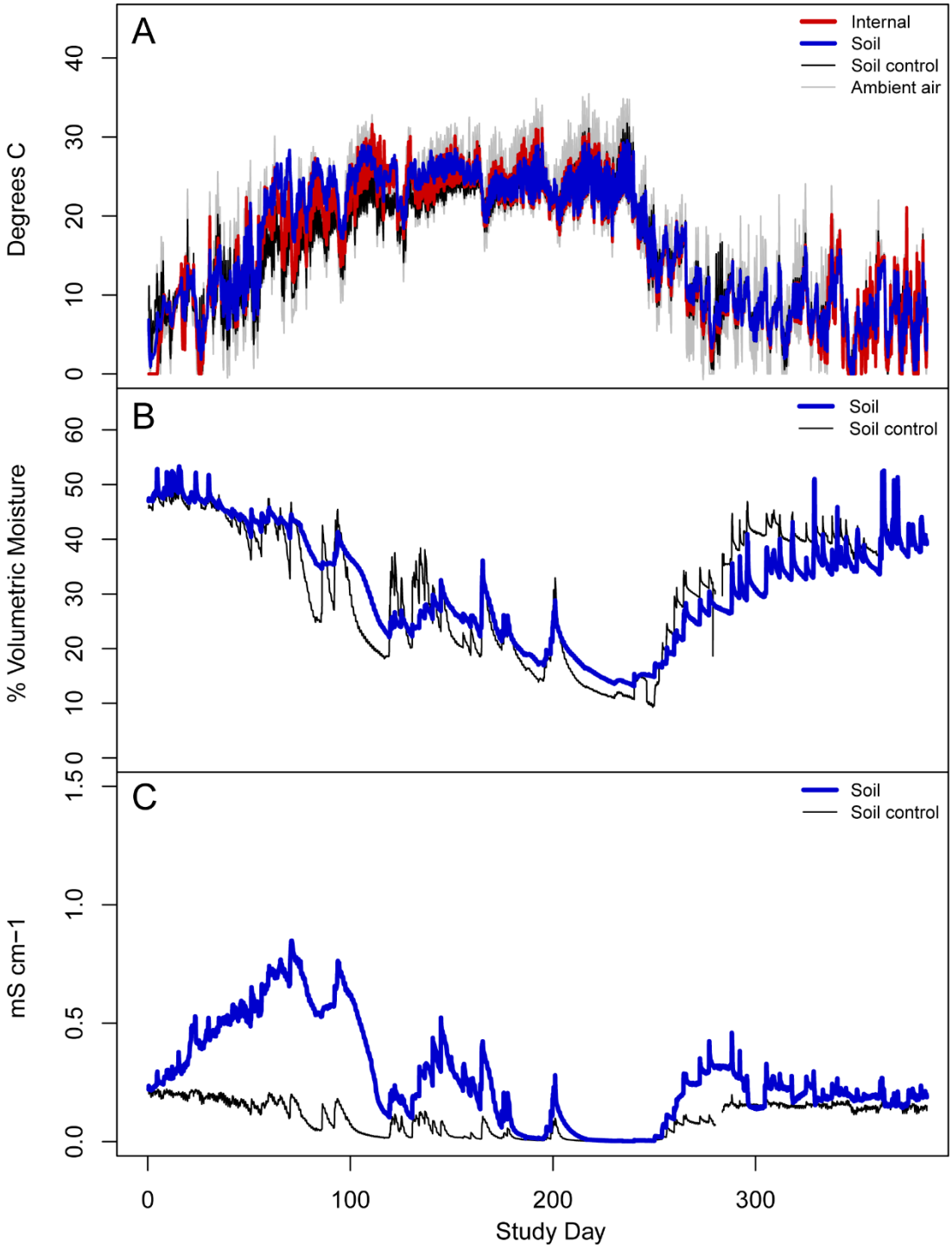

Figure 3.3: Soil sensor data from winter donor series. Temperature (A), soil moisture (B), and soil electrical conductivity (C) are shown by study day. Controls are shown in black and soil data shown in blue. For temperature data, ambient air is shown in grey, and donor internal temperatures are shown in red.

Table 3.3: Spring 2018: Effects of decomposition-impacted soils and time on soil chemical parameters. Results of two-way ANOVAs comparing impacted soils (Treatment) and study date (Day), as well as interaction effects.

		Treatment		Day		Treatment*Day	
		F	p	F	p	F	p
Cores (0-1 cm)	**pH**	302.9634	**<0.001*** **	4.223	**<0.001*** **	1.6918	0.055
	Conductivity (EC)	124.4799	**<0.001*** **	2.6503	**0.001** **	2.2834	**0.006** **
	Dissolved Oxygen	89.075	**<0.001*** **	4.989	**<0.001*** **	5.1319	**<0.001*** **
	Respiration (CO_2)	212.7239	**<0.001*** **	6.2403	**<0.001*** **	6.4309	**<0.001*** **
	NH_4^+-N	43.8043	**<0.001*** **	1.8054	**0.036***	1.7851	**0.039***
	NO_3^--N	35.4101	**<0.001*** **	2.4144	**0.003** **	2.0896	**0.012***
Interfaces (1-16 cm)	**pH**	99.5135	**<0.001*** **	2.8683	**<0.001*** **	1.4287	0.137
	Conductivity (EC)	43.9451	**<0.001*** **	0.7595	0.746	0.6823	0.825
	Respiration (CO_2)	269.4217	**<0.001*** **	7.1957	**<0.001*** **	7.7097	**<0.001*** **
	NH_4^+-N	102.2633	**<0.001*** **	8.1918	**<0.001*** **	8.1696	**<0.001*** **
	NO_3^--N	43.367	**<0.001*** **	2.2847	**0.006** **	2.3146	**0.005** **

Significant differences based upon $p < 0.05$ are presented in bold type. Asterisks indicate levels of significance: * $p < 0.05$, ** $p < 0.01$, *** $p < 0.001$

Table 3.4: Spring 2018 soil chemical parameters in core soils (1-16 cm). Means (n=3) and standard deviations are shown.

Study day	Location	pH	Conductivity (µS cm^{-1})	Percent Dissolved Oxygen	Respiration (µmol CO_2 gdw^{-1} day^{-1})	Ammonium (µg gdw^{-1})	Nitrate (µg gdw^{-1})
0	Donor	7.4 ± 0.2	39.7 ± 19.6	97.3 ± 0.7	2.5 ± 0.5	8.94 ± 1.75	8.11 ± 1.77
	Control	7.4 ± 0.3	31.3 ± 11.9	97.8 ± 0.9	3 ± 0.9	9.03 ± 2.31	7.26 ± 1.41
8	Donor	6.6 ± 0.4	131.7 ± 3.7	59.7 ± 43.2	17.4 ± 7.4	31.18 ± 5.82	7.2 ± 5.09
	Control	7.3 ± 0.2	81.4 ± 6.8	98.6 ± 0.8	3 ± 0.8	8.61 ± 1.22	6.31 ± 1.33
12	Donor	6.4 ± 0.3	404.4 ± 217.7	38.9 ± 10	44.6 ± 4.5	357.44 ± 211.99	3.06 ± 1.74
	Control	7.3 ± 0.3	48 ± 3.9	100.1 ± 0.9	2.2 ± 0.5	9.99 ± 2.71	7.77 ± 0.68
16	Donor	5.9 ± 0.0	568.7 ± 232.3	47.3 ± 7.7	51.5 ± 3.4	665.17 ± 375.55	1.12 ± 0.68
	Control	7.3 ± 0.1	87.9 ± 65.9	98.3 ± 1	1.9 ± 0.2	9.01 ± 1.94	6.12 ± 2.31
27	Donor	5.8 ± 0.2	413.8 ± 46.5	56.6 ± 17	57.9 ± 2.5	368.02 ± 443.14	5.01 ± 6.84
	Control	7.1 ± 0.1	42.4 ± 2.3	98.1 ± 0.3	2.4 ± 0.3	9.79 ± 1.03	6.21 ± 1.01
43	Donor	5.7 ± 0.2	533.1 ± 142	73.3 ± 8	49 ± 5.7	314.71 ± 239.18	6.88 ± 4.37
	Control	7.1 ± 0.1	66.8 ± 11.7	99.1 ± 0.3	2.2 ± 0.2	10.35 ± 2.25	6.67 ± 2.45
58	Donor	6.4 ± 0.1	397.4 ± 181.1	73.9 ± 12.2	60 ± 10	282.85 ± 371.14	3.53 ± 3.09
	Control	7.3 ± 0.0	38.8 ± 14.9	96.8 ± 1.3	2.7 ± 0.4	3.82 ± 3.85	8.28 ± 2.91
72	Donor	6.6 ± 0.6	557.3 ± 429	70 ± 17.4	31.5 ± 17.8	414.59 ± 417.15	7.5 ± 4.19
	Control	7.4 ± 0.1	53.8 ± 22.6	96.8 ± 0.8	1.8 ± 0.1	5.69 ± 1.14	4.12 ± 2.21
86	Donor	6.5 ± 0.3	314.2 ± 160.5	84.8 ± 11.5	31.2 ± 24	304.09 ± 275.72	22.19 ± 16.85
	Control	7.2 ± 0.3	40.4 ± 17.9	97.8 ± 1.1	1.9 ± 0.4	6.81 ± 3.09	7.89 ± 2.89
103	Donor	6.0 ± 0.4	392.7 ± 169.2	84 ± 11.1	28 ± 21.4	140.66 ± 132.17	44.35 ± 37.95
	Control	7.3 ± 0.2	56.7 ± 15.8	97.2 ± 1.7	2.2 ± 0.6	6.7 ± 1.09	5.89 ± 2.26
117	Donor	6.0 ± 0.5	395.9 ± 244.5	92.8 ± 5.6	29.8 ± 24	198.55 ± 199.37	72.62 ± 56.16
	Control	7.2 ± 0.1	55.5 ± 18	98.6 ± 0.4	2 ± 0.3	7.44 ± 1.01	10.79 ± 2.9
132	Donor	6.0 ± 0.2	373.6 ± 237.8	96 ± 4.6	26.3 ± 20.4	107.48 ± 110.87	59.43 ± 64.05
	Control	6.9 ± 0.2	51.2 ± 14.8	99 ± 0.6	1.3 ± 0	2.57 ± 0.68	3.61 ± 2.2
150	Donor	6.4 ± 0.1	277.3 ± 104.5	92.9 ± 6.5	19.7 ± 14.3	124.91 ± 153.72	36.7 ± 19.55
	Control	7.2 ± 0.1	51.4 ± 12	97 ± 2.1	2.8 ± 0.5	7.58 ± 0.78	6.49 ± 1.84
168	Donor	6.3 ± 0.2	229.1 ± 107	99.6 ± 3.1	7.7 ± 4.4	52.79 ± 47.74	57.5 ± 29.91
	Control	7.2 ± 0.1	48.8 ± 13.1	100.5 ± 0.2	1.8 ± 0.1	5.98 ± 0.58	8.9 ± 1.21
201	Donor	6.3 ± 0.6	275.2 ± 184.9		4.6 ± 2.1	50.51 ± 31.44	60.28 ± 46.38
	Control	7.2 ± 0.1	44.6 ± 5.7		2.4 ± 0.5	8.13 ± 0.81	8.79 ± 2.67
254	Donor	6.6 ± 0.2	183.7 ± 16.5		9.1 ± 4.8	132.74 ± 62.12	40.21 ± 5.4
	Control	7.6 ± 0.2	74.4 ± 26.5		2.2 ± 0.9	8.45 ± 3.14	10.28 ± 3.84
303	Donor	6.7 ± 0.2	111 ± 15.1		15.4 ± 12.4	96.79 ± 66.29	35.23 ± 7.57
	Control	7.5 ± 0.1	42.2 ± 6.7		2 ± 0.5	7.07 ± 1.43	6.32 ± 0.49
340	Donor	6.2 ± 0.7	282.8 ± 173.1		15.9 ± 10.3	125.2 ± 116.16	101.22 ± 85.15
	Control	7.3 ± 0.1	75.6 ± 16.8		3.3 ± 0.9	8.48 ± 1.89	11.08 ± 0.7
357	Donor	6.2 ± 0.3	112.8 ± 42.5		9.9 ± 7.2	41.34 ± 29.47	41.52 ± 16.18
	Control	7.0 ± 0.1	34.7 ± 7.6		3.7 ± 0.9	7.7 ± 3.27	8.05 ± 2.17
376	Donor	6.6 ± 0.8	106.2 ± 64.9		7.8 ± 3.9	53.07 ± 55.74	28.81 ± 26.42
	Control	7.4 ± 0.2	33.1 ± 3.7		2 ± 0.4	4.24 ± 1.17	4.68 ± 2.3

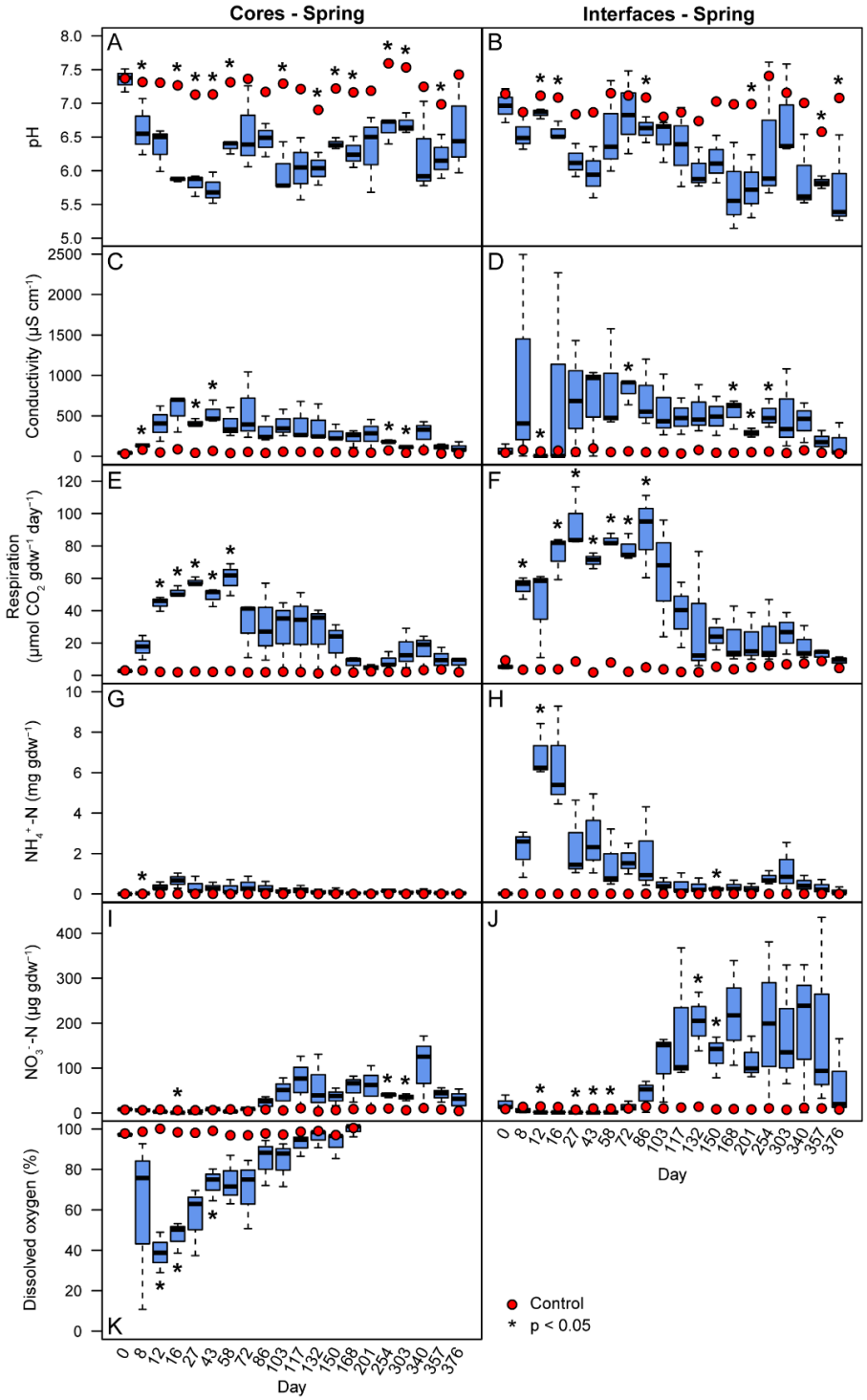

Figure 3.4. Spring 2018 soil chemistry data in core (1-16 cm) and interface (0-1 cm) soils. pH (A-B), electrical conductivity (C-D), respiration (E-F), ammonium-N (G-H), nitrate-N (I-J), and dissolved oxygen (K), are shown by study day. Boxes (n=3) display 25th and 75th quartiles and medians, and whiskers display ± 1.5 quartiles. Control means (n=3) are represented by red dots. Asterisks denote significance ($p < 0.05$) based upon paired Student's T-tests conducted at each sampling time point.

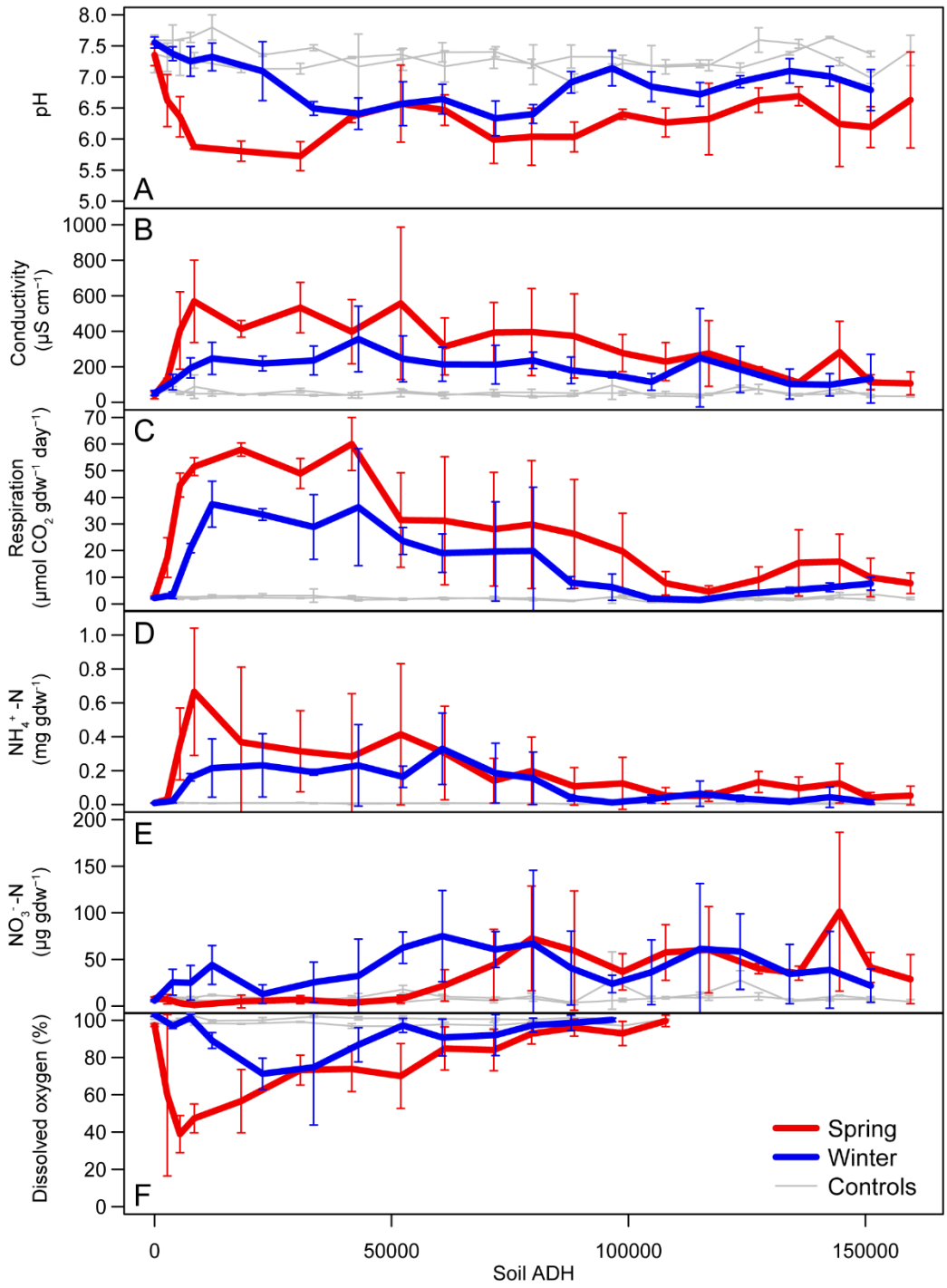

Figure 3.5: Seasonal comparisons between soil pH, conductivity, CO_2, NH_4^+-N, NO_3^--N, and dissolved oxygen in core (1-15 cm) soils. The magnitude and timing of changes in pH (A), conductivity (B), CO_2 (C), NH_4^+-N (D), NO_3^--N (E), and dissolved oxygen (F) are shown in units of equivalent thermal units. In all cases the magnitude of effect is larger in spring. Error bars reflect one standard deviation from means.

Table 3.5: Effects of decomposition on soil chemical parameters for Spring 2018 soils. Paired sample T-tests were conducted at each sampling time point in order to compare changes between impacted soils and controls. P-values are shown.

Day	Location	pH	EC	DO	CO_2	NH_4^+-N	NO_3^--N
0	**Core**	0.901	0.668	0.635	0.560	0.912	0.561
	Interface	0.281	0.511		0.150	0.781	0.372
8	**Core**	**0.038***	**0.003****	0.265	0.094	**0.029***	0.727
	Interface	0.170	0.372		**0.005****	0.088	0.199
12	**Core**	0.075	0.103	**0.01***	**0.003****	0.103	0.069
	Interface	**0.047***	**0.048***		0.147	**0.012***	**0.036***
16	**Core**	**0.004****	0.052	**0.008****	**0.002****	0.094	**0.047***
	Interface	**0.027***	0.461		**0.011***	0.050	0.079
27	**Core**	**0.008****	**0.005****	0.052	**<0.001*****	0.297	0.756
	Interface	0.060	0.254		**0.016***	0.173	**0.010***
43	**Core**	**0.012***	**0.025***	**0.033***	**0.005****	0.159	0.903
	Interface	0.147	0.225		**0.002****	0.138	**0.014***
58	**Core**	**0.005****	0.065	0.069	**0.010***	0.324	0.087
	Interface	0.284	0.180		**<0.001*****	0.228	**0.028***
72	**Core**	0.153	0.165	0.113	0.102	0.232	0.183
	Interface	0.523	**0.013***		**0.003****	0.064	0.754
86	**Core**	0.114	0.082	0.188	0.167	0.205	0.248
	Interface	**0.019***	0.100		**0.029***	0.261	0.399
103	**Core**	**0.032***	0.076	0.138	0.179	0.223	0.206
	Interface	0.490	0.143		0.112	0.114	0.144
117	**Core**	0.057	0.121	0.190	0.187	0.240	0.182
	Interface	0.415	0.073		0.088	0.304	0.198
132	**Core**	**0.036***	0.130	0.330	0.168	0.243	0.258
	Interface	0.117	0.089		0.324	0.230	**0.034***
150	**Core**	**0.005****	0.052	0.265	0.186	0.320	0.102
	Interface	0.062	0.086		0.055	**0.027***	**0.045***
168	**Core**	**0.025***	0.096	0.679	0.145	0.230	0.102
	Interface	0.114	**0.047***		0.214	0.144	0.087
201	**Core**	0.149	0.158		0.175	0.141	0.182
	Interface	**0.038***	**0.016***		0.195	0.145	0.059
254	**Core**	**0.014***	**0.015***		0.175	0.074	**0.007****
	Interface	0.207	**0.046***		0.292	0.058	0.227
303	**Core**	**0.**003**	**0.014***		0.214	0.144	**0.022***
	Interface	0.442	0.242		0.143	0.231	0.165
340	**Core**	0.108	0.167		0.178	0.224	0.210
	Interface	0.079	0.131		0.283	0.189	0.213
357	**Core**	**0.030***	0.113		0.306	0.215	0.068
	Interface	**<0.001*****	0.193		0.193	0.282	0.294
376	**Core**	0.179	0.205		0.111	0.273	0.261
	Interface	**0.024***	0.409		0.123	0.355	0.393

Significant differences based upon $p < 0.05$ are presented in bold type. Asterisks indicate levels of significance: * $p < 0.05$, ** $p < 0.01$, *** $p < 0.001$

This resource was prepared by the author(s) using Federal funds provided by the U.S. Department of Justice. Opinions or points of view expressed are those of the author(s) and do not necessarily reflect the official position or policies of the U.S. Department of Justice.

Table 3.6: Spring 2018 soil chemical parameters in interface soils (0-1 cm). Means (n=3) and standard deviations are shown.

Study day	Location	pH	Conductivity ($\mu S\ cm^{-1}$)	Respiration ($\mu mol\ CO_2\ gdw^{-1}\ day^{-1}$)	Ammonium ($\mu g\ gdw^{-1}$)	Nitrate ($\mu g\ gdw^{-1}$)
0	**Donor**	7.1 ± 0.3	73.7 ± 68.9	5.4 ± 1.3	22.75 ± 17.3	20.4 ± 16.8
	Control	7.3 ± 0.3	43.8 ± 3.8	9.3 ± 1.7	19.44 ± 3.37	8.25 ± 1.75
8	**Donor**	6.7 ± 0.3	969.1 ± 1336.7	54.7 ± 6.7	2158.82 ± 1179.64	6.32 ± 7.52
	Control	7.0 ± 0.0	80.2 ± 35.4	3.5 ± 0.9	13.02 ± 3.06	13.15 ± 1.53
12	**Donor**	7.0 ± 0.1	4 ± 0.9	43.5 ± 28.2	6905.52 ± 1325.29	1.62 ± 1.27
	Control	7.3 ± 0.2	60.3 ± 21.7	3.6 ± 2	13.78 ± 4.94	14.04 ± 5.44
16	**Donor**	6.7 ± 0.2	759.1 ± 1307.7	75 ± 13.7	6377.71 ± 2563.33	1.43 ± 0.81
	Control	7.3 ± 0.0	69.3 ± 16.1	3.8 ± 1	11.09 ± 1	12.94 ± 5.91
27	**Donor**	6.2 ± 0.3	706.1 ± 714.1	94.2 ± 19.3	2376.81 ± 1965.27	1.2 ± 0.66
	Control	7.0 ± 0.1	53.2 ± 1.9	8.6 ± 0.9	15.95 ± 2.91	6.95 ± 0.46
43	**Donor**	6.1 ± 0.4	669.4 ± 577.8	71 ± 4.8	2775.12 ± 1992.18	0.77 ± 0.4
	Control	7.0 ± 0.4	98.7 ± 8.5	1.8 ± 0.6	27.4 ± 11.73	9.73 ± 2.17
58	**Donor**	6.7 ± 0.8	826.9 ± 650.1	83.6 ± 3.7	1492.05 ± 1492.52	1.95 ± 2.5
	Control	7.3 ± 0.0	52.1 ± 21.1	7.9 ± 0.5	12.19 ± 2.09	9.21 ± 0.43
72	**Donor**	7.0 ± 0.7	826 ± 162.2	78.2 ± 8.2	1679.07 ± 770.68	12.92 ± 11.71
	Control	7.3 ± 0.1	61.8 ± 11.4	2.2 ± 1.3	8.38 ± 2.09	9.64 ± 4.36
86	**Donor**	6.8 ± 0.2	720.7 ± 422.9	88.9 ± 26	1895.22 ± 2108.34	40.95 ± 35.87
	Control	7.3 ± 0.1	50.5 ± 26.3	4.9 ± 1.5	11.61 ± 4.67	13.67 ± 8.59
103	**Donor**	6.6 ± 0.4	572.9 ± 393.8	62.6 ± 36.3	470.7 ± 294.5	112.42 ± 77.16
	Control	7.0 ± 0.4	49.7 ± 8.9	3.7 ± 1	10.74 ± 1.75	9.76 ± 3.35
117	**Donor**	6.5 ± 0.6	488.5 ± 225	38.4 ± 20.3	431.06 ± 534.01	186.05 ± 156.84
	Control	7.0 ± 0.3	35 ± 14.5	2.1 ± 0.6	12.63 ± 6.07	11.72 ± 3.85
132	**Donor**	6.1 ± 0.3	552.5 ± 297	31.6 ± 39	366.91 ± 367.38	203.55 ± 65.24
	Control	6.9 ± 0.2	78.4 ± 34.9	2 ± 0.7	5.63 ± 0.66	13.53 ± 3.31
150	**Donor**	6.3 ± 0.4	497.3 ± 240.6	24.9 ± 9.6	267.05 ± 77.16	129.59 ± 46.38
	Control	7.2 ± 0.1	44.3 ± 11	5.3 ± 1.9	10.06 ± 3.23	7.86 ± 0.67
168	**Donor**	5.8 ± 0.7	547.7 ± 183.3	22.3 ± 17.9	371.92 ± 271.59	220.5 ± 116.54
	Control	7.2 ± 0.2	44.5 ± 14	3.8 ± 0.2	9.43 ± 3.29	8.36 ± 2.53
201	**Donor**	5.8 ± 0.5	289.6 ± 54.8	21.2 ± 15.4	282.74 ± 205.12	116.46 ± 47.43
	Control	7.2 ± 0.1	50.4 ± 9.5	5 ± 1	8.62 ± 1.2	7.4 ± 0.9
254	**Donor**	6.5 ± 1.2	514.7 ± 178.7	23.6 ± 20.3	775.82 ± 331.51	195.65 ± 186.36
	Control	7.6 ± 0.1	58.6 ± 22.2	6.3 ± 2.2	9.87 ± 2.06	10 ± 0.98
303	**Donor**	6.9 ± 0.8	516.5 ± 499.7	26.2 ± 12.9	1202.03 ± 1211.54	176.27 ± 136.92
	Control	7.3 ± 0.1	40.2 ± 5.3	6.9 ± 1.7	9 ± 1.19	6.86 ± 0.55
340	**Donor**	6.0 ± 0.6	431.3 ± 245.6	18.5 ± 10.7	476.46 ± 413.99	189.27 ± 169.92
	Control	7.2 ± 0.0	75.4 ± 6.2	7.4 ± 2.8	10.02 ± 3.67	11.13 ± 1.4
357	**Donor**	5.9 ± 0.1	187.3 ± 126.4	12.8 ± 4	314.78 ± 362.68	186.82 ± 216.91
	Control	6.7 ± 0.1	42.9 ± 5.8	8.9 ± 1.6	10.44 ± 1.84	9.93 ± 0.73
376	**Donor**	5.8 ± 0.8	165.6 ± 215.8	8.9 ± 3.1	132.64 ± 183.6	63.26 ± 88.3
	Control	7.3 ± 0.4	34.5 ± 3.6	4.5 ± 1.5	6.71 ± 1.04	7.36 ± 2.26

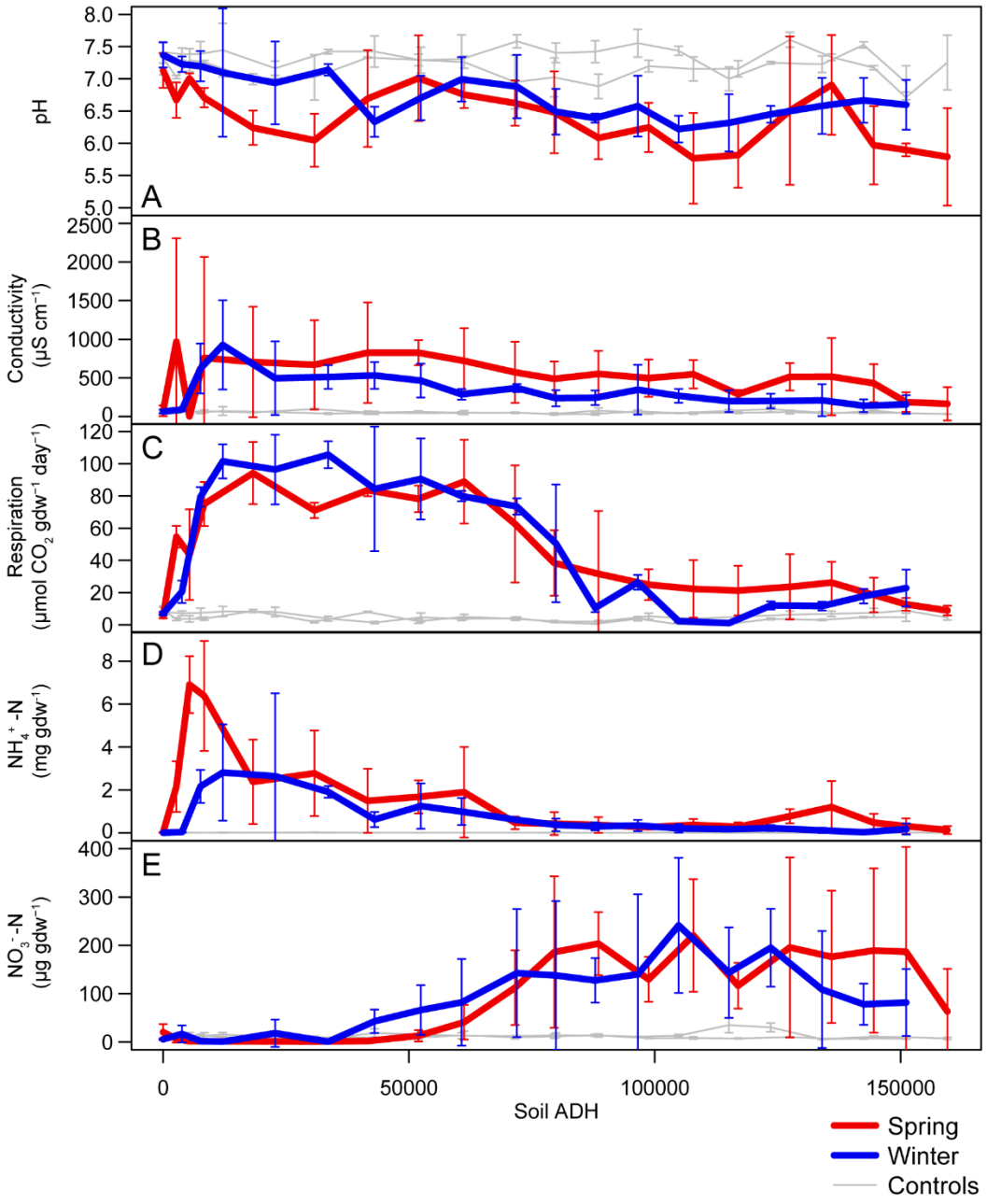

Figure 3.6: Seasonal comparisons between soil pH, conductivity, CO_2, NH_4^+-N, NO_3^--N, and dissolved oxygen in interface (0-1 cm) soils. The magnitude and timing of changes in pH (A), conductivity (B), CO_2 (C), NH_4^+-N (D), NO_3^--N (E), and dissolved oxygen (F) are shown in units of equivalent thermal units. In all cases the magnitude of effect is larger in spring. Error bars reflect one standard deviation from means.

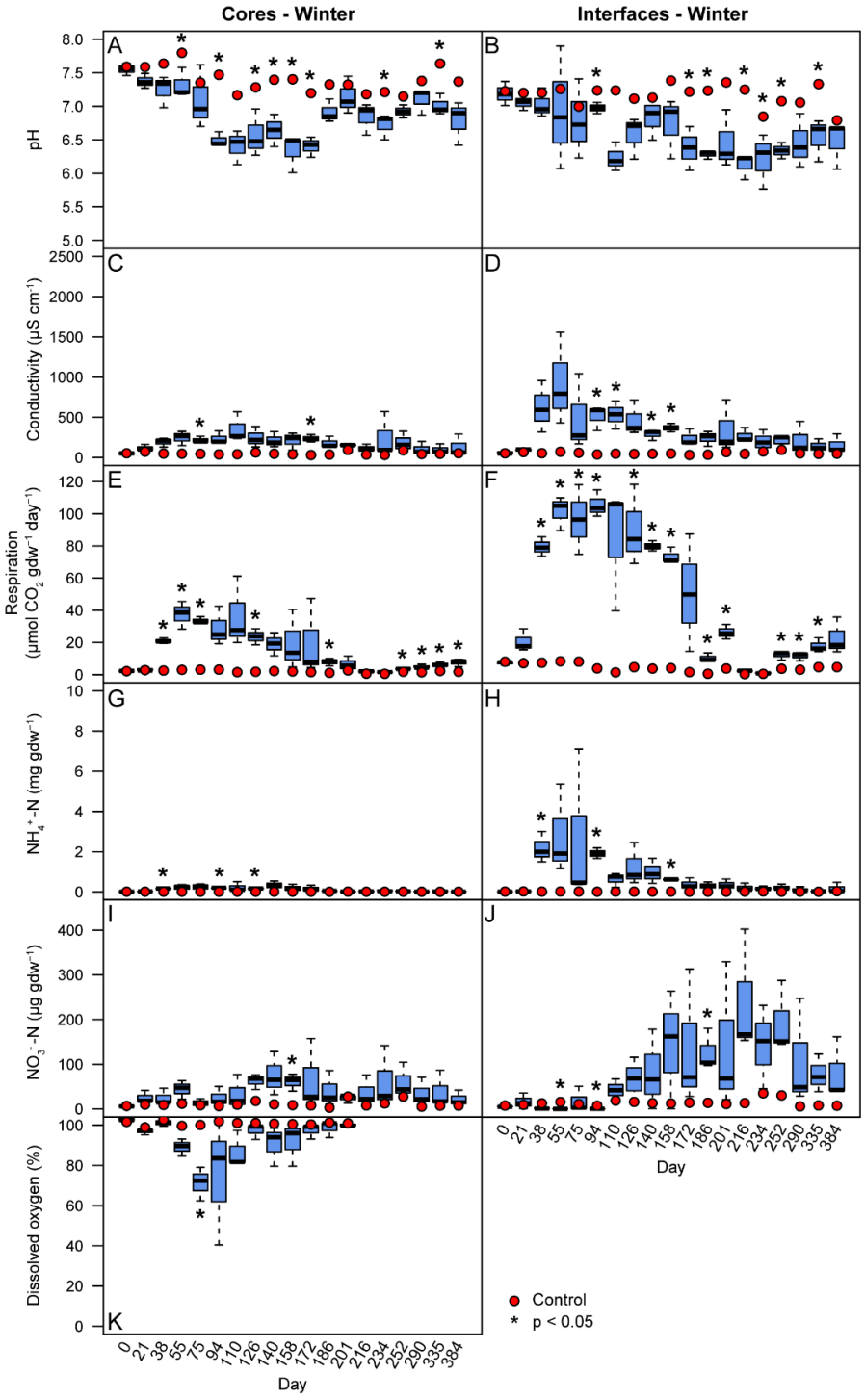

Figure 3.7 Winter 2019 soil chemistry data in core (1-16 cm) and interface (0-1 cm) soils. pH (A-B), electrical conductivity (C-D), respiration (E-F), ammonium-N (G-H), nitrate-N (I-J), and dissolved oxygen (K), are shown by study day. Boxes (n=3) display 25th and 75th quartiles and medians, and whiskers display ± 1.5 quartiles. Control means (n=3) are represented by red dots. Asterisks denote significance ($p < 0.05$) based upon paired Student's T-tests conducted at each sampling time point.

This resource was prepared by the author(s) using Federal funds provided by the U.S. Department of Justice. Opinions or points of view expressed are those of the author(s) and do not necessarily reflect the official position or policies of the U.S. Department of Justice.

Table. 3.7: Winter 2019 effects of decomposition-impacted soils and time on soil chemical parameters. Results of two-way ANOVAs comparing impacted soils (Treatment) and study date (Day), as well as interaction effects.

		Treatment		Day		Treatment*Day	
		F	p	F	p	F	p
Cores	pH	151.3049	**<0.001*** **	7.5879	**<0.001*** **	2.5476	**0.002****
	Conductivity (EC)	84.6112	**<0.001*** **	1.1882	0.292	1.4979	0.114
	Dissolved Oxygen	26.4818	**<0.001*** **	2.7934	**0.005****	2.6212	**0.008****
	Respiration (CO_2)	104.3606	**<0.001*** **	5.3561	**<0.001*** **	4.7664	**<0.001*** **
	NH_4^+-N	51.3889	**<0.001*** **	2.3796	**0.005****	2.3274	**0.006****
	NO_3^--N	34.9852	**<0.001*** **	1.0777	0.390	0.821	0.670
Interfaces	pH	101.2533	**<0.001*** **	2.6083	**0.002****	1.8893	**0.029***
	Conductivity (EC)	85.4386	**<0.001*** **	2.6334	**0.002****	2.6000	**0.002****
	Respiration (CO_2)	442.883	**<0.001*** **	20.109	**<0.001*** **	18.207	**<0.001*** **
	NH_4^+-N	28.9167	**<0.001*** **	2.1315	**0.012***	2.1341	**0.012***
	NO_3^--N	40.3386	**<0.001*** **	2.2397	**0.008****	1.8862	**0.030***

Significant differences based upon $p < 0.05$ are presented in bold type. Asterisks indicate levels of significance: * $p < 0.05$, ** $p < 0.01$, *** $p < 0.001$

Table 3.8: Winter 2019 soil chemical parameters in core soils (1-16 cm). Means (n=3) and standard deviations are shown.

Study day	Location	pH	Conductivity (uS cm^{-1})	Percent Dissolved Oxygen	Respiration (umol CO_2 gdw^{-1} day^{-1})	Ammonium (µg gdw^{-1})	Nitrate (µg gdw^{-1})
0	Donor	7.6 ± 0.1	52.4 ± 14.4	103 ± 1	2.2 ± 0.3	9.24 ± 0.85	5.92 ± 0.95
	Control	7.6 ± 0.1	53.2 ± 8.6	101.6 ± 1.2	2.1 ± 0.6	8.98 ± 0.42	6.63 ± 2.14
21	Donor	7.4 ± 0.1	114.6 ± 43.9	97 ± 1.5	3.2 ± 1.3	21.19 ± 11.95	25.61 ± 13.9
	Control	7.6 ± 0.2	73.1 ± 16	98.9 ± 0.7	2.8 ± 0.4	9.03 ± 1.37	9.59 ± 0.64
38	Donor	7.3 ± 0.2	193.2 ± 56.7	101.3 ± 1.9	20.9 ± 1.7	160.74 ± 22.09	24.9 ± 18.57
	Control	7.6 ± 0.1	49.1 ± 9.9	102.8 ± 0.8	2.5 ± 0.1	9.12 ± 1.24	8.88 ± 1.42
55	Donor	7.3 ± 0.2	246.9 ± 90.5	89.1 ± 4.3	37.4 ± 8.6	215.26 ± 171.67	44.07 ± 20.81
	Control	7.8 ± 0.2	47.8 ± 13	99.6 ± 0.6	3 ± 0.5	7.26 ± 2.1	11.72 ± 0.9
75	Donor	7.1 ± 0.5	218.4 ± 41.3	71.3 ± 8.4	33.5 ± 2.2	231.37 ± 186.35	12.73 ± 10.14
	Control	7.4 ± 0	45.8 ± 5.4	100.1 ± 1.3	3 ± 0.8	7.4 ± 0.43	8.32 ± 2.87
94	Donor	6.5 ± 0.1	235.4 ± 81.8	74.8 ± 30.9	28.9 ± 12.1	190.86 ± 17.48	25.44 ± 21.6
	Control	7.5 ± 0	39.4 ± 4.4	101.9 ± 0.5	3.1 ± 2.5	7.72 ± 3.32	6.34 ± 1.19
110	Donor	6.4 ± 0.3	356.4 ± 184.9	86.8 ± 9.2	36.3 ± 21.9	230.78 ± 240.34	32.33 ± 39.45
	Control	7.2 ± 0.5	41.4 ± 17.9	101.1 ± 0.9	1.5 ± 0.3	7.34 ± 0.84	9.44 ± 4.1
126	Donor	6.6 ± 0.4	245.4 ± 129.4	97.2 ± 3.8	23.6 ± 5	163.93 ± 62.87	62.59 ± 16.91
	Control	7.3 ± 0.2	62.6 ± 6.3	101.1 ± 1.1	1.7 ± 0.4	7.85 ± 0.94	17.79 ± 4.27
140	Donor	6.6 ± 0.2	214 ± 96	90.7 ± 9.9	19 ± 7.2	329.38 ± 210.54	75.07 ± 48.93
	Control	7.4 ± 0.2	46.7 ± 10	100.7 ± 0.5	2.2 ± 0.2	9.27 ± 1.19	10.21 ± 2.36
158	Donor	6.3 ± 0.3	211.9 ± 109.1	92 ± 11	19.6 ± 18.6	185.48 ± 175.95	60.65 ± 19.28
	Control	7.4 ± 0.1	40.5 ± 8.5	100.5 ± 0.5	2 ± 0.5	7.55 ± 2.14	8.51 ± 1.21
172	Donor	6.4 ± 0.2	236 ± 46.6	97.4 ± 3.7	19.9 ± 23.8	155.02 ± 155.21	67.01 ± 78.68
	Control	7.2 ± 0.3	31.3 ± 4.7	100.3 ± 0.7	1.5 ± 0.3	7.33 ± 1.66	7.83 ± 2.53
186	Donor	6.9 ± 0.2	180 ± 74.8	98.6 ± 4.1	7.9 ± 2.3	39.76 ± 18.63	40.71 ± 39.63
	Control	7.3 ± 0.2	36.4 ± 3.7	101.3 ± 0.2	1.1 ± 0.2	4.84 ± 0.83	2.67 ± 1.2
201	Donor	7.1 ± 0.3	154.7 ± 17.4	100.2 ± 1	6.3 ± 4.9	12.2 ± 6.86	23.82 ± 9.41
	Control	7.3 ± 0.1	95.6 ± 80	100.9 ± 0.1	2.6 ± 2.4	10.6 ± 10.08	27.39 ± 30.73
216	Donor	6.8 ± 0.2	114.7 ± 47.3		2 ± 0.9	32.74 ± 24.49	36.28 ± 34.75
	Control	7.2 ± 0.3	36.2 ± 9.8		0.6 ± 0.1	6.09 ± 0.68	7.64 ± 2.74
234	Donor	6.7 ± 0.2	250.7 ± 276.9		1.5 ± 0.6	64.25 ± 74.88	61.36 ± 69.89
	Control	7.2 ± 0.1	32 ± 6.3		0.5 ± 0	6.49 ± 1.8	12.27 ± 2.56
252	Donor	6.9 ± 0.1	185.1 ± 130.2		3.6 ± 0.3	36.91 ± 18.88	58.56 ± 40.54
	Control	7.1 ± 0.1	90.7 ± 7.1		1.8 ± 0.4	6.55 ± 2.29	27.57 ± 10.42
290	Donor	7.1 ± 0.2	103.3 ± 84.2		5.1 ± 1.2	16.82 ± 12.47	34.35 ± 31.92
	Control	7.4 ± 0	43.1 ± 3.5		1.4 ± 0.1	4.75 ± 0.58	5.06 ± 2.69
335	Donor	7 ± 0.2	98.7 ± 63		6.2 ± 1.6	43.81 ± 60.41	38.83 ± 41.18
	Control	7.6 ± 0	46.5 ± 3.8		2.2 ± 0.6	3.64 ± 0.92	7.19 ± 1.73
384	Donor	6.8 ± 0.3	133.3 ± 137		7.6 ± 2.4	13.85 ± 13.16	21.81 ± 17.92
	Control	7.4 ± 0	53.6 ± 22		1.7 ± 0.4	5.62 ± 1.05	7.26 ± 1.23

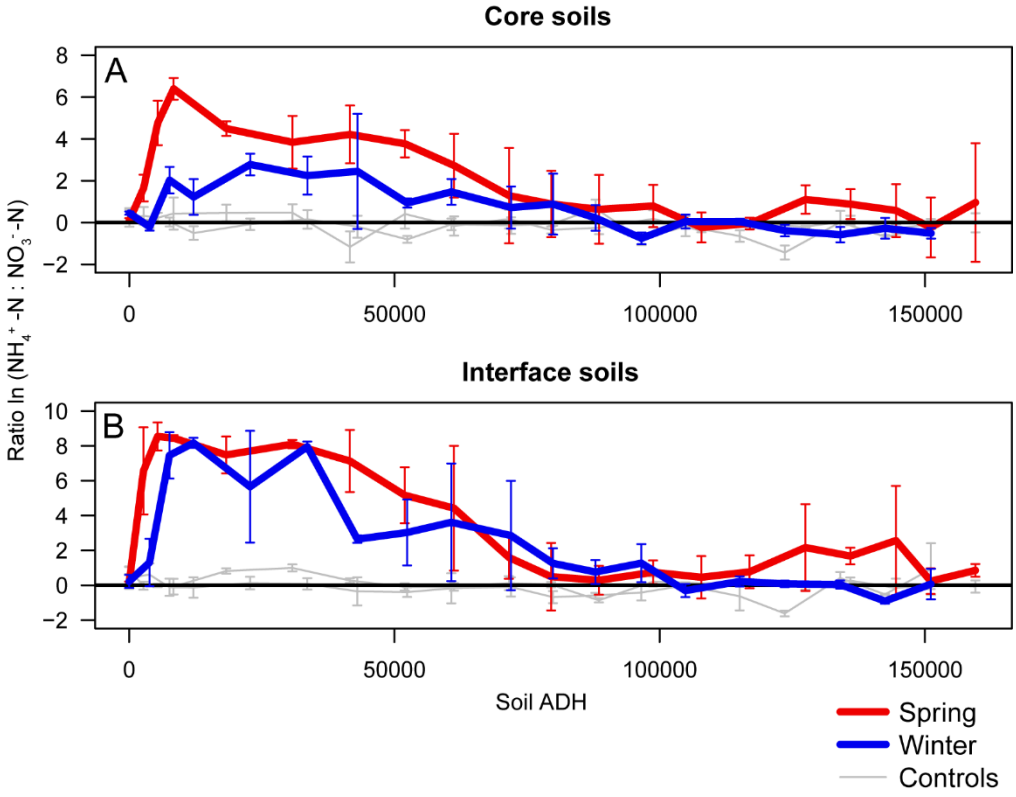

Figure 3.8: Ratio of ammonium and nitrate in soil. The natural log of the ratio of ammonium to nitrate in both spring and winter series decomposition soils is elevated until just after 100,000 ADH, commensurate with reduced oxygen in the soil. Error bars reflect one standard deviation from means.

Table 3.9: Effects of decomposition on soil chemical parameters for Winter 2019 soils. Paired sample T-tests were conducted at each sampling time point in order to compare changes between impacted soils and controls. P-values are shown.

Study Day	Location	pH	EC	DO	CO_2	NH_4^+-N	NO_3^-N
0	**Core**	0.267	0.957	0.395	0.904	0.570	0.447
	Interface	0.647	0.453		0.671	0.473	0.116
21	**Core**	0.409	0.296	0.263	0.554	0.248	0.171
	Interface	0.334	0.206		0.084	0.598	0.555
38	**Core**	0.168	0.064	0.401	**0.003****	**0.006****	0.253
	Interface	0.485	0.088		**<0.001*****	**0.04***	0.062
55	**Core**	**<0.001*****	0.063	0.059	**0.021***	0.169	0.115
	Interface	0.669	0.130		**0.007****	0.164	**0.032***
75	**Core**	0.459	**0.023***	**0.021***	**0.003****	0.173	0.608
	Interface	0.646	0.247		**0.016***	0.359	0.695
94	**Core**	**0.002****	0.053	0.267	0.072	**0.004****	0.266
	Interface	**0.012***	**0.036***		**0.002****	**0.006****	**0.007****
110	**Core**	0.074	0.107	0.096	0.113	0.248	0.429
	Interface	0.054	**0.047***		0.067	0.095	0.304
126	**Core**	**0.041***	0.127	0.258	**0.015***	**0.049***	0.050
	Interface	0.155	0.078		**0.023***	0.179	0.237
140	**Core**	**0.004****	0.106	0.234	0.060	0.120	0.139
	Interface	0.158	**0.021***		**<0.001*****	0.113	0.290
158	**Core**	**0.011***	0.106	0.328	0.243	0.219	**0.038***
	Interface	0.104	**0.008****		**0.002****	**0.002****	0.228
172	**Core**	**0.015***	**0.014***	0.263	0.317	0.240	0.311
	Interface	**0.023***	0.072		0.146	0.160	0.287
186	**Core**	0.130	0.075	0.363	**0.039***	0.089	0.235
	Interface	**0.016***	0.080		**0.019***	0.108	**0.047***
201	**Core**	0.469	0.348	0.297	0.461	0.884	0.891
	Interface	0.095	0.286		**0.017***	0.161	0.312
216	**Core**	0.315	0.134		0.105	0.208	0.270
	Interface	**0.015***	0.054		0.052	0.222	0.103
234	**Core**	**0.032***	0.297		0.113	0.320	0.344
	Interface	**0.046***	0.275		0.096	0.143	0.154
252	**Core**	0.065	0.322		**0.005****	0.127	0.328
	Interface	**0.006****	0.300		**0.024***	0.113	0.073
290	**Core**	0.151	0.326		**0.026***	0.243	0.226
	Interface	0.179	0.325		**0.039***	0.301	0.277
335	**Core**	**0.021***	0.276		**0.042***	0.368	0.308
	Interface	**0.046***	0.206		**0.044***	0.084	0.108
384	**Core**	0.107	0.453		**0.041***	0.375	0.284
	Interface	0.416	0.271		0.145	0.369	0.207

Significant differences based upon $p < 0.05$ are presented in bold type. Asterisks indicate levels of significance: * $p < 0.05$, ** $p < 0.01$, *** $p < 0.001$

Table 3.10: Winter 2019 soil chemical parameters in interface soils (0-1 cm).
Means (n=3) and standard deviations are shown.

Study day	Location	pH	Conductivity (uS cm^{-1})	Respiration (umol CO_2 gdw^{-1} day^{-1})	Ammonium (µg gdw^{-1})	Nitrate (µg gdw^{-1})
0	**Donor**	7.4 ± 0.2	64.5 ± 25.1	7 ± 1.1	7.21 ± 1.62	5.73 ± 0.95
	Control	7.4 ± 0.2	52.8 ± 4.1	8 ± 3.7	13.24 ± 10.42	7.27 ± 1.56
21	**Donor**	7.2 ± 0.1	90.9 ± 19	20.5 ± 7	35.55 ± 27.43	16.71 ± 17.7
	Control	7.4 ± 0.1	67.6 ± 7.5	7.1 ± 1.5	21.28 ± 18.91	9.13 ± 1.9
38	**Donor**	7.2 ± 0.2	621.8 ± 321.6	79.4 ± 6.1	2162.16 ± 769.9	1.78 ± 1.8
	Control	7.4 ± 0.2	54.2 ± 14.7	7.4 ± 2.9	11.49 ± 5.04	12.4 ± 3.07
55	**Donor**	7.1 ± 1	926.8 ± 576.7	101.5 ± 10.6	2811.16 ± 2241.18	0.7 ± 0.36
	Control	7.4 ± 0.4	72 ± 55.7	8.3 ± 3.2	16.67 ± 14.37	15.5 ± 4.42
75	**Donor**	6.9 ± 0.6	496.1 ± 476.6	96.4 ± 21.6	2639.81 ± 3859.39	18.19 ± 28.49
	Control	7.2 ± 0.1	59.2 ± 12.7	8 ± 2.9	12.49 ± 3.81	10.71 ± 0.99
94	**Donor**	7.1 ± 0.1	512.6 ± 153.1	105.6 ± 8.3	1910.24 ± 268.16	0.71 ± 0.28
	Control	7.4 ± 0	38.3 ± 9.8	3.8 ± 1.5	7.73 ± 2.21	7 ± 1.09
110	**Donor**	6.3 ± 0.2	532.1 ± 172.6	84.4 ± 38.7	623.95 ± 354.4	42.86 ± 24.39
	Control	7.4 ± 0.2	47.7 ± 19.6	1.4 ± 0.7	12.72 ± 4.04	18.68 ± 8.68
126	**Donor**	6.7 ± 0.3	465.6 ± 218.9	90.5 ± 25.2	1250.68 ± 1058.94	66.06 ± 51.35
	Control	7.3 ± 0.2	44 ± 1.4	4.6 ± 2.7	10.97 ± 4.33	15.71 ± 3.04
140	**Donor**	7 ± 0.3	288.6 ± 67.8	79.9 ± 3.2	992.33 ± 628.7	82.03 ± 89.83
	Control	7.3 ± 0.4	46.6 ± 15.8	3.7 ± 1.1	10.76 ± 4.64	12.86 ± 5.84
158	**Donor**	6.9 ± 0.5	369.7 ± 52.5	73.4 ± 5.1	607.06 ± 42.56	142.51 ± 132.53
	Control	7.6 ± 0.1	49 ± 2.7	4 ± 0.9	11.72 ± 4.68	12.17 ± 1.35
172	**Donor**	6.5 ± 0.4	237.6 ± 104.7	50.5 ± 36.5	371.77 ± 288.88	137.77 ± 153.66
	Control	7.4 ± 0.2	31.5 ± 3.4	1.5 ± 0.1	6.77 ± 0.22	13.94 ± 4.83
186	**Donor**	6.4 ± 0.1	243.3 ± 94.6	10.5 ± 2.5	301.98 ± 182.93	127.42 ± 46.19
	Control	7.4 ± 0.2	34.6 ± 14.5	0.5 ± 0.1	7.71 ± 1.44	13.72 ± 1.96
201	**Donor**	6.6 ± 0.5	347.2 ± 322.8	26.3 ± 4.6	345.4 ± 264.82	140 ± 166.09
	Control	7.6 ± 0.2	67.9 ± 16.6	3.8 ± 1.3	7.85 ± 4.05	10.95 ± 0.42
216	**Donor**	6.2 ± 0.2	268.9 ± 89.3	2.3 ± 0.8	211.65 ± 196.72	241.32 ± 139.96
	Control	7.4 ± 0.1	45.2 ± 4.8	0.3 ± 0	12.81 ± 0.29	13.04 ± 2.54
234	**Donor**	6.3 ± 0.4	199.5 ± 140.7	1 ± 0.5	168.54 ± 107.76	143.52 ± 93.72
	Control	7 ± 0.2	75 ± 14.1	0.5 ± 0.2	18.44 ± 7.97	34.97 ± 16.03
252	**Donor**	6.5 ± 0.1	201.4 ± 95	12 ± 2.5	225.6 ± 139.55	195.04 ± 80.66
	Control	7.3 ± 0	96.1 ± 36.7	3.6 ± 0.6	5.95 ± 1.55	30.25 ± 9.14
290	**Donor**	6.6 ± 0.4	211.1 ± 207.6	11.6 ± 2.7	113.83 ± 129.35	108.68 ± 121
	Control	7.2 ± 0.1	51.2 ± 12.4	3 ± 0.4	8.79 ± 2.62	5.62 ± 0.49
335	**Donor**	6.7 ± 0.3	140.5 ± 82.5	17.8 ± 4.5	30.21 ± 13.2	78.06 ± 42.56
	Control	7.5 ± 0	45.9 ± 9.7	4.7 ± 0.4	4.53 ± 0.88	7.69 ± 1.78
384	**Donor**	6.6 ± 0.4	156.9 ± 120	22.8 ± 11.4	176.94 ± 259.72	81.75 ± 69.44
	Control	6.9 ± 0.3	47.8 ± 6.7	4.7 ± 2.5	34.19 ± 44.64	0.01 ± 0

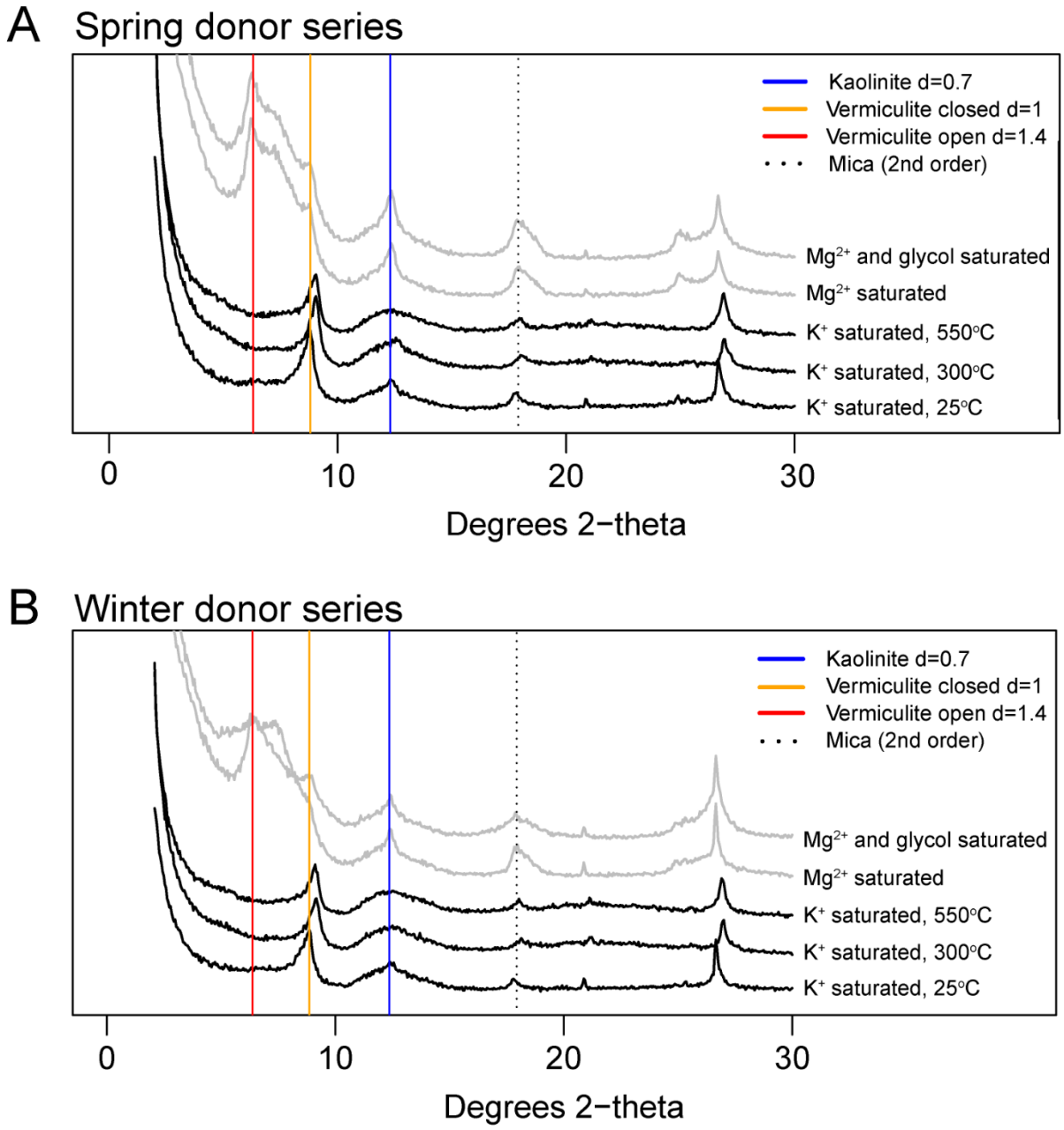

Figure 3.9: X-ray diffractograms of clay minerals in spring and winter donor series soils. Treatments (K^+ saturated at 25 °C, K^+ saturated at 300 °C, K^+ saturated at 550 °C, Mg^{2+} saturated, and Mg^{2+} with glycol) are shown for both (A) spring donor soils and (B) winter donor soils. Clay minerals are identified by d-spacing in nm.

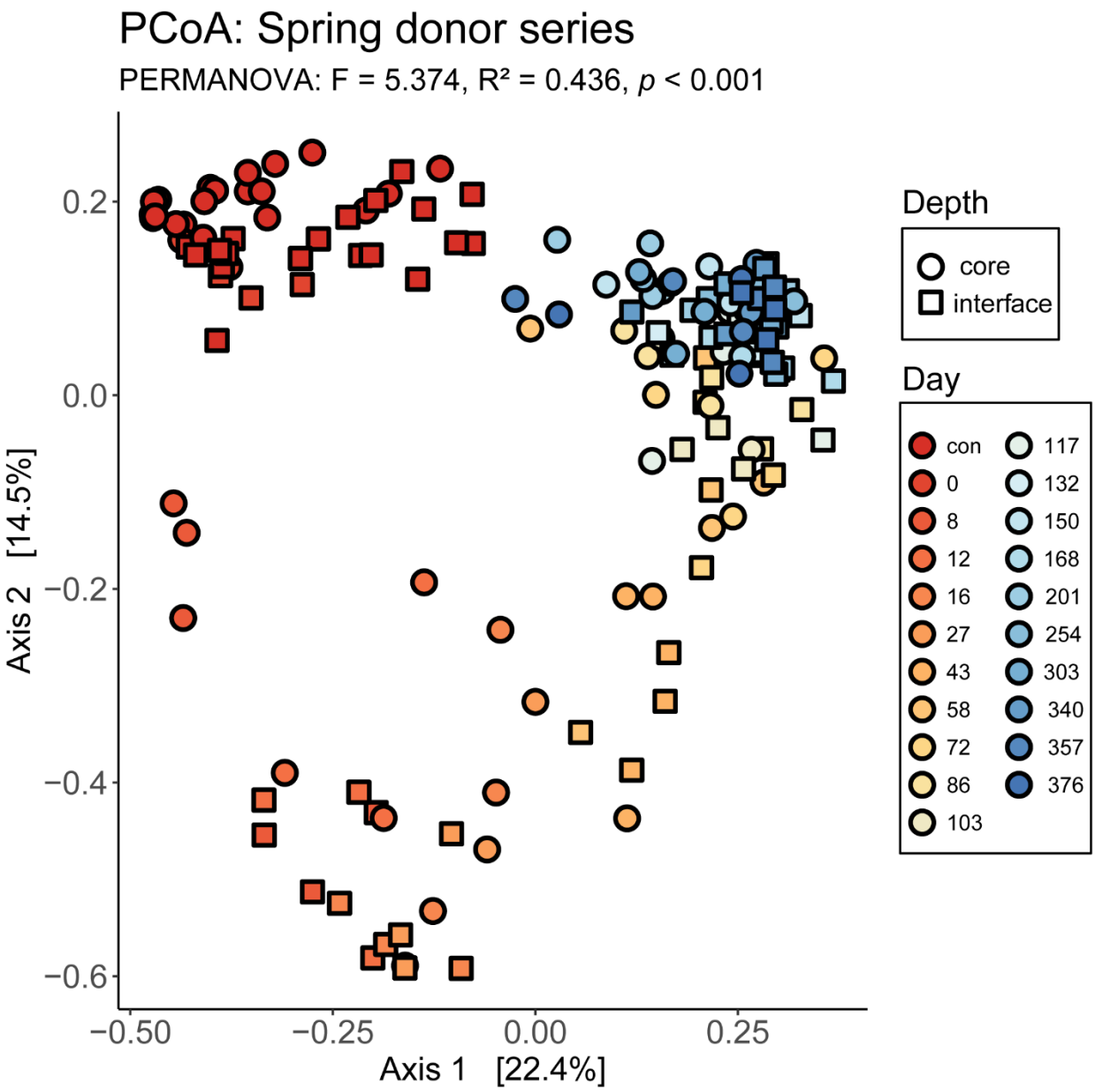

Figure 3.10: Principal coordinates analysis of spring donor series fungal communities by study day. PCoA plot of Bray-Curtis dissimilarities shows changes in fungal beta diversity between study days. Community recovery does not occur after one year. Soil depths are shown by circles (cores) and squares (interfaces). Statistical significance of changes by study day is evaluated by PERMANOVA.

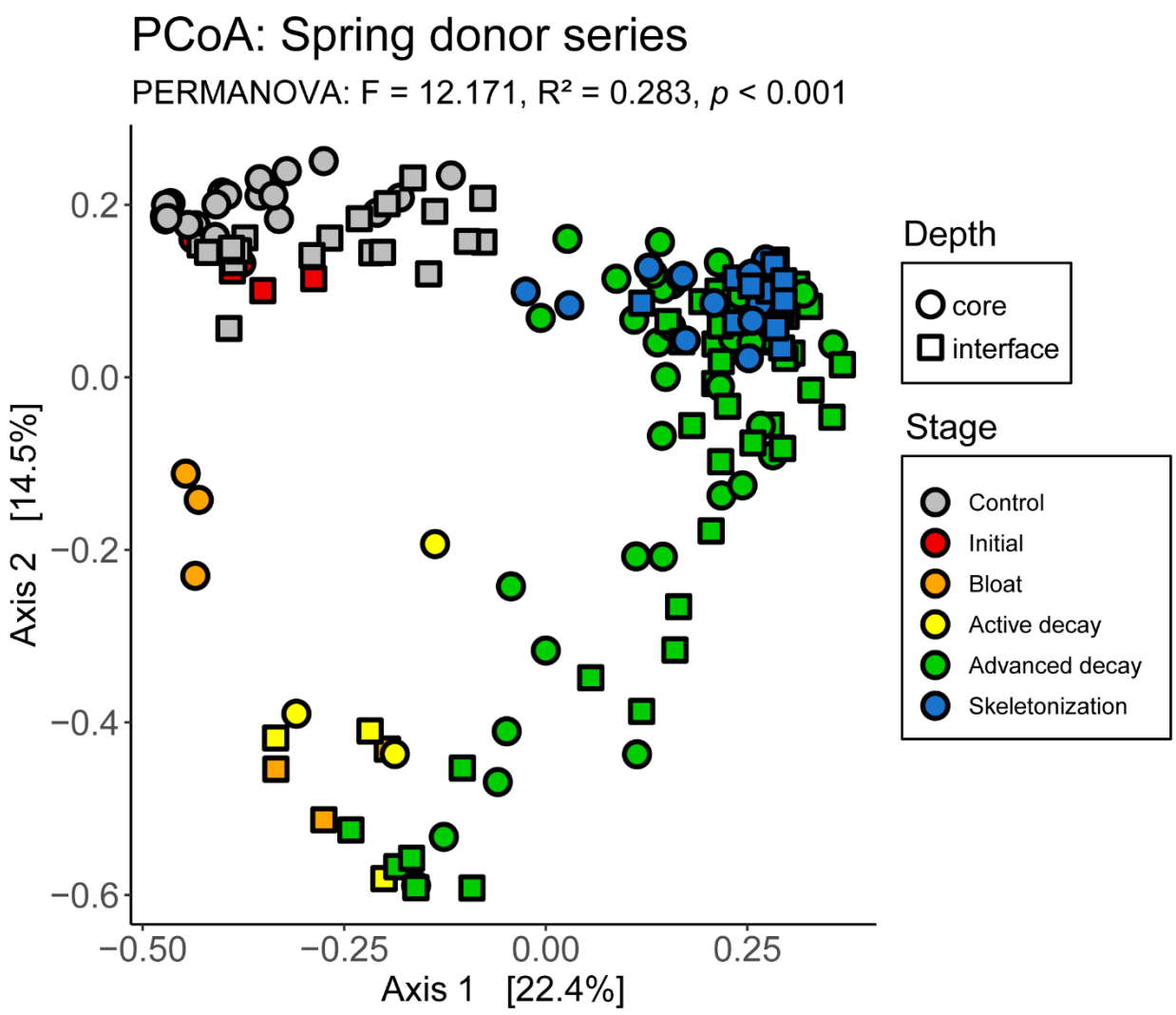

Figure 3.11: Principal coordinates analysis of spring donor series fungal communities by morphological stage. PCoA plot of Bray-Curtis dissimilarities shows changes in fungal beta diversity between decomposition stages. Community recovery does not occur after one year. Soil depths are shown by circles (cores) and squares (interfaces), and morphological decomposition stages are shown by color. Statistical significance of changes by morphological stage is evaluated by PERMANOVA.

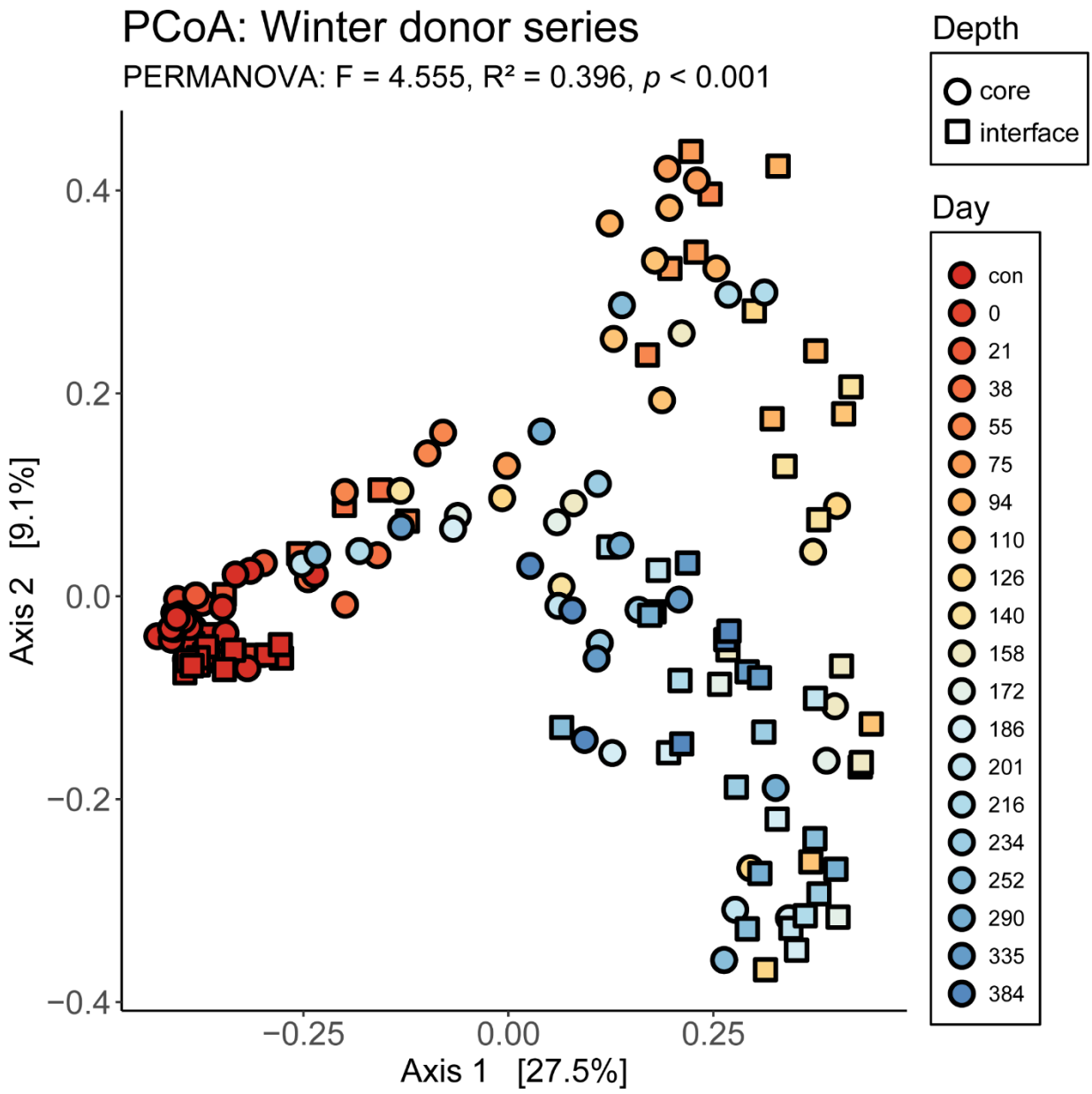

Figure 3.12: Principal coordinates analysis of winter donor series fungal communities by study day. PCoA plot of Bray-Curtis dissimilarities shows changes in fungal beta diversity between study days. Community recovery does not occur after one year. Soil depths are shown by circles (cores) and squares (interfaces). Statistical significance of changes by study day is evaluated by PERMANOVA.

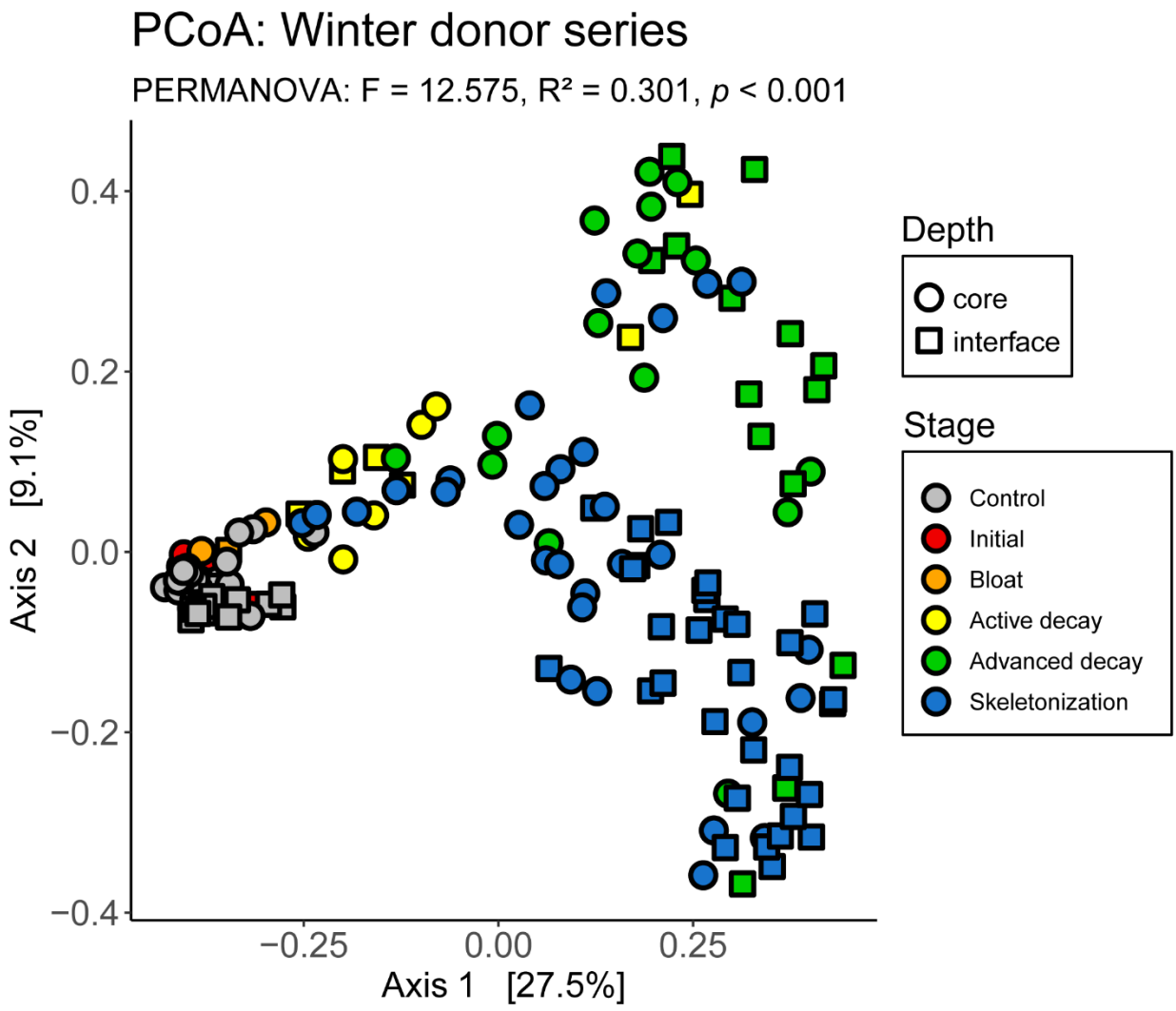

Figure 3.13: Principal coordinates analysis of winter donor series fungal communities by morphological stage. PCoA plot of Bray-Curtis dissimilarities shows changes in fungal beta diversity between decomposition stages. Community recovery does not occur after one year. Soil depths are shown by circles (cores) and squares (interfaces), and morphological decomposition stages are shown by color. Statistical significance of changes by morphological stage is evaluated by PERMANOVA.

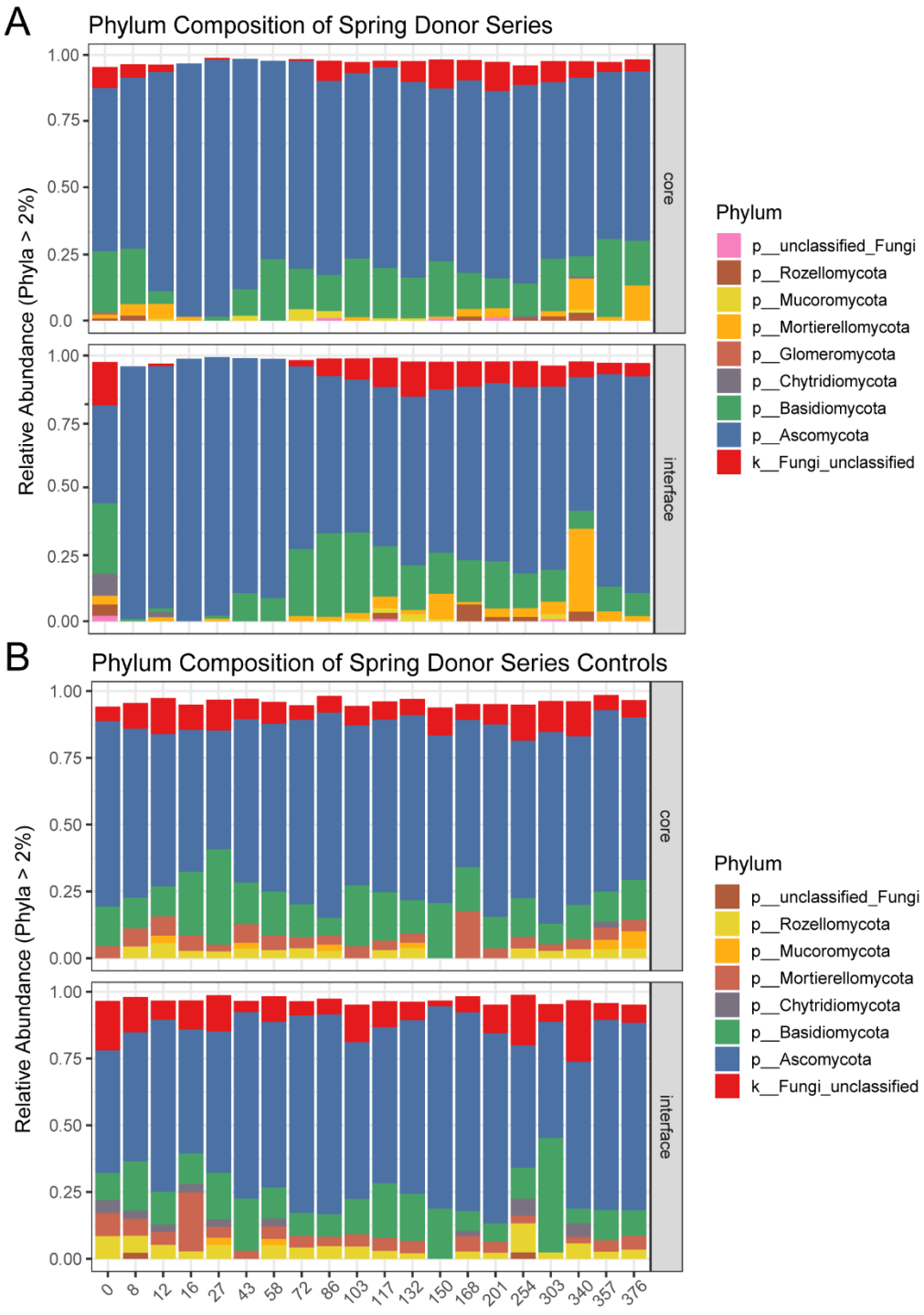

Figure 3.14: Phylum composition of spring trial soils. Relative abundances of phyla in cores and interfaces are shown for (A) impacted soils and (B) controls.

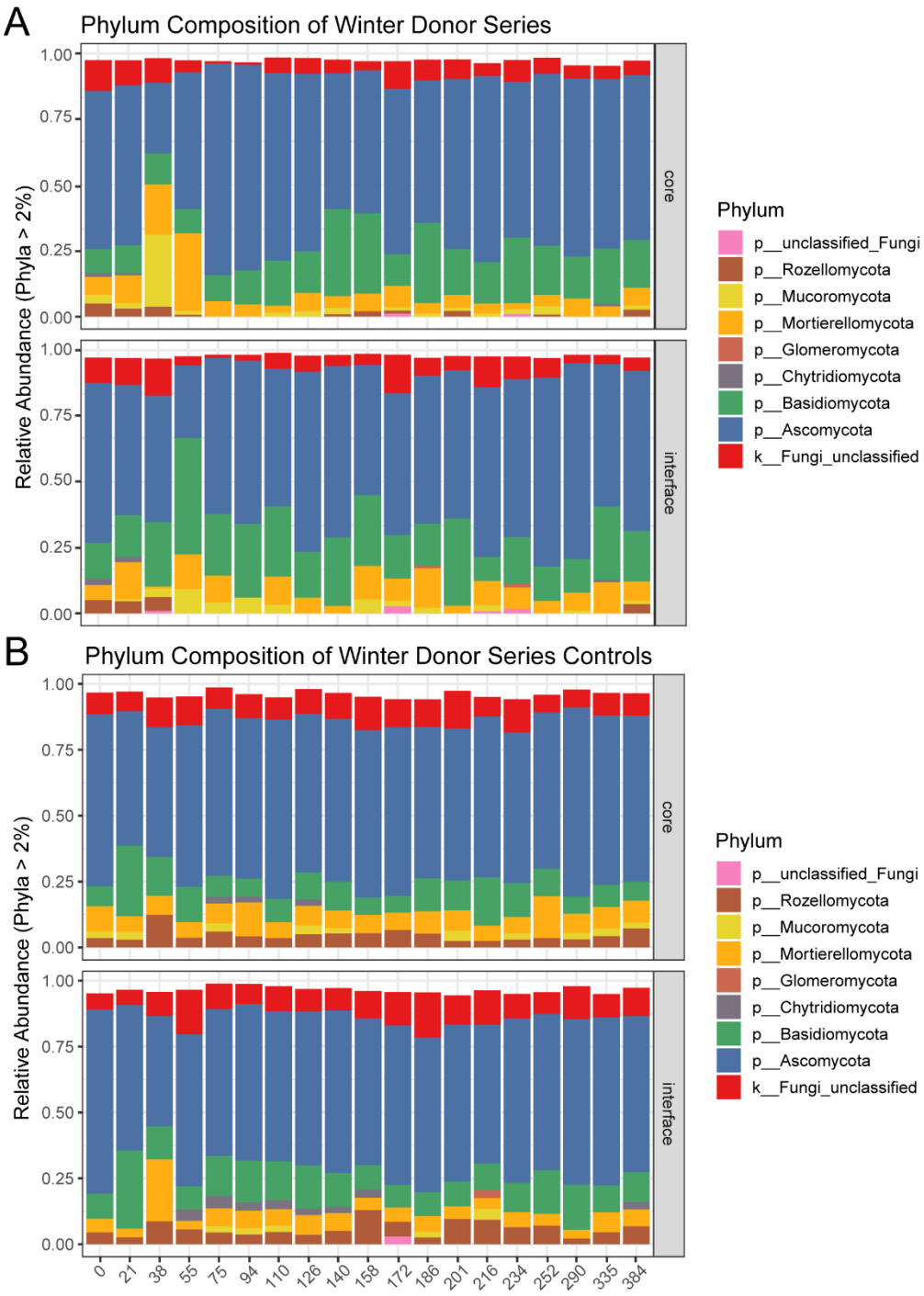

Figure 3.15: Phylum composition of winter trial soils. Relative abundances of phyla in cores and interfaces are shown for (A) impacted soils and (B) controls.

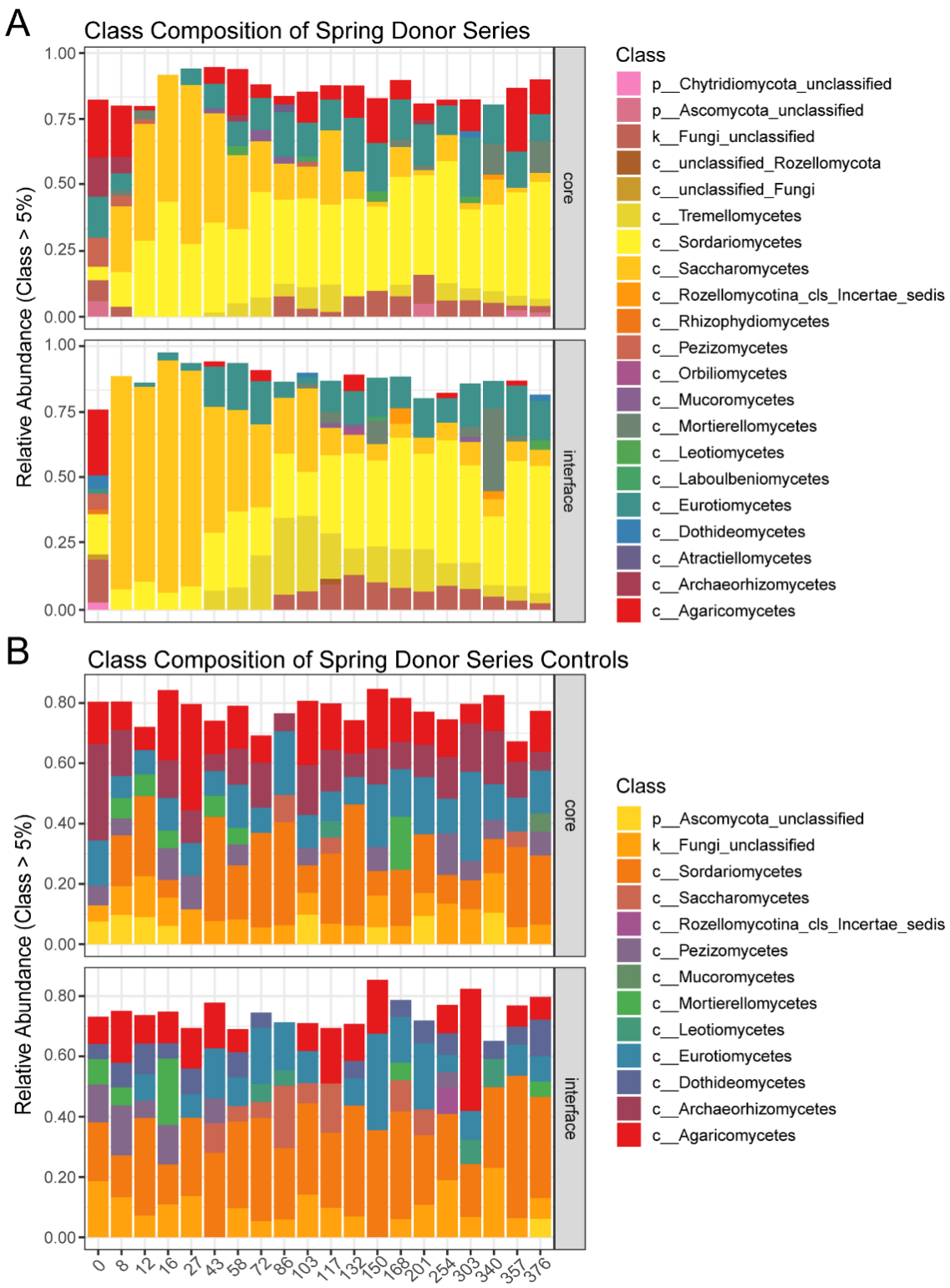

Figure 3.16: Class composition of spring trial soils. Relative abundances of classes in cores and interfaces are shown for (A) impacted soils and (B) controls.

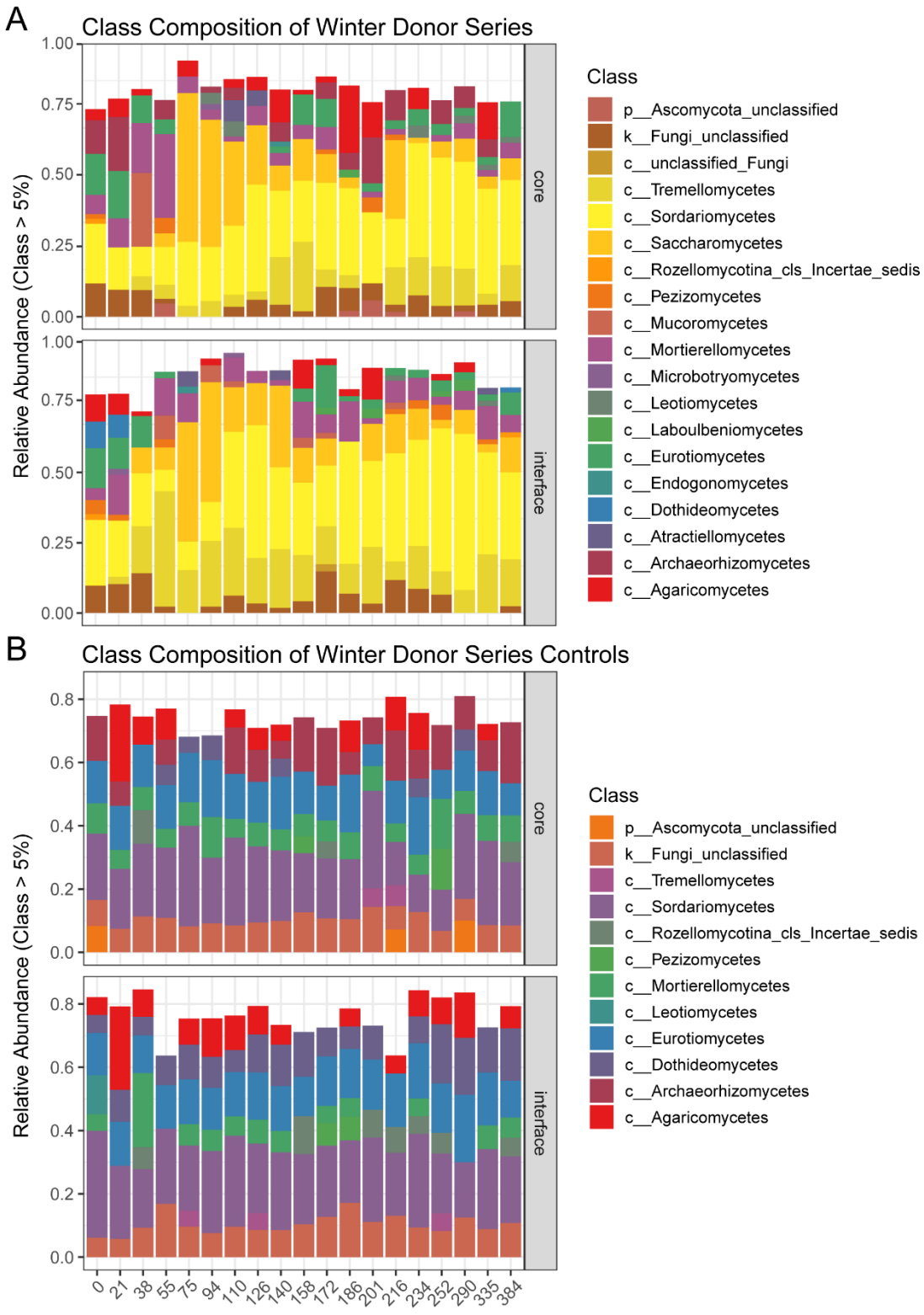

Figure 3.17: Class composition of winter trial soils. Relative abundances of classes in cores and interfaces are shown for (A) impacted soils and (B) controls.

This resource was prepared by the author(s) using Federal funds provided by the U.S. Department of Justice. Opinions or points of view expressed are those of the author(s) and do not necessarily reflect the official position or policies of the U.S. Department of Justice.

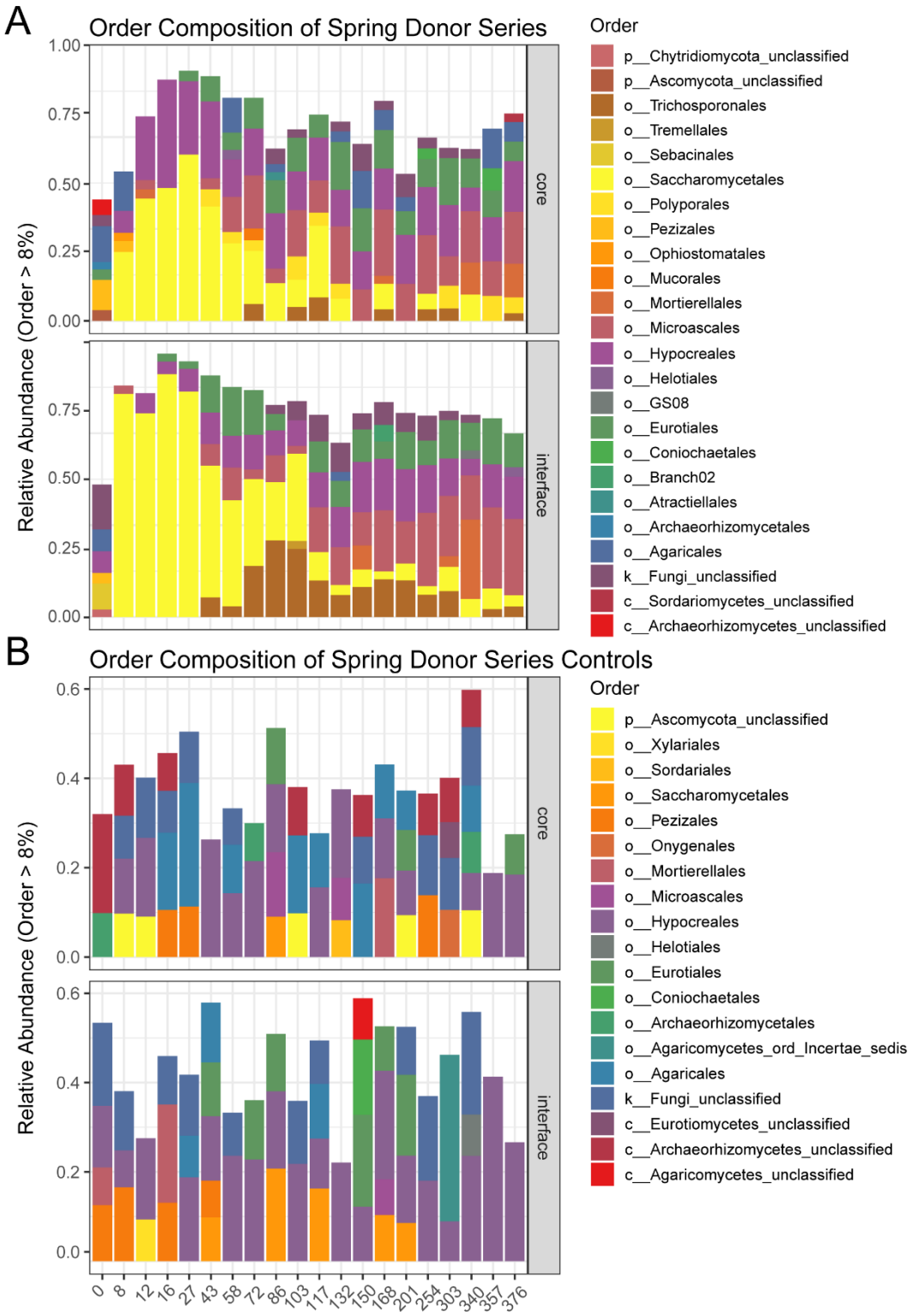

Figure 3.18: Order composition of spring trial soils. Relative abundances of orders in cores and interfaces are shown for (A) impacted soils and (B) controls.

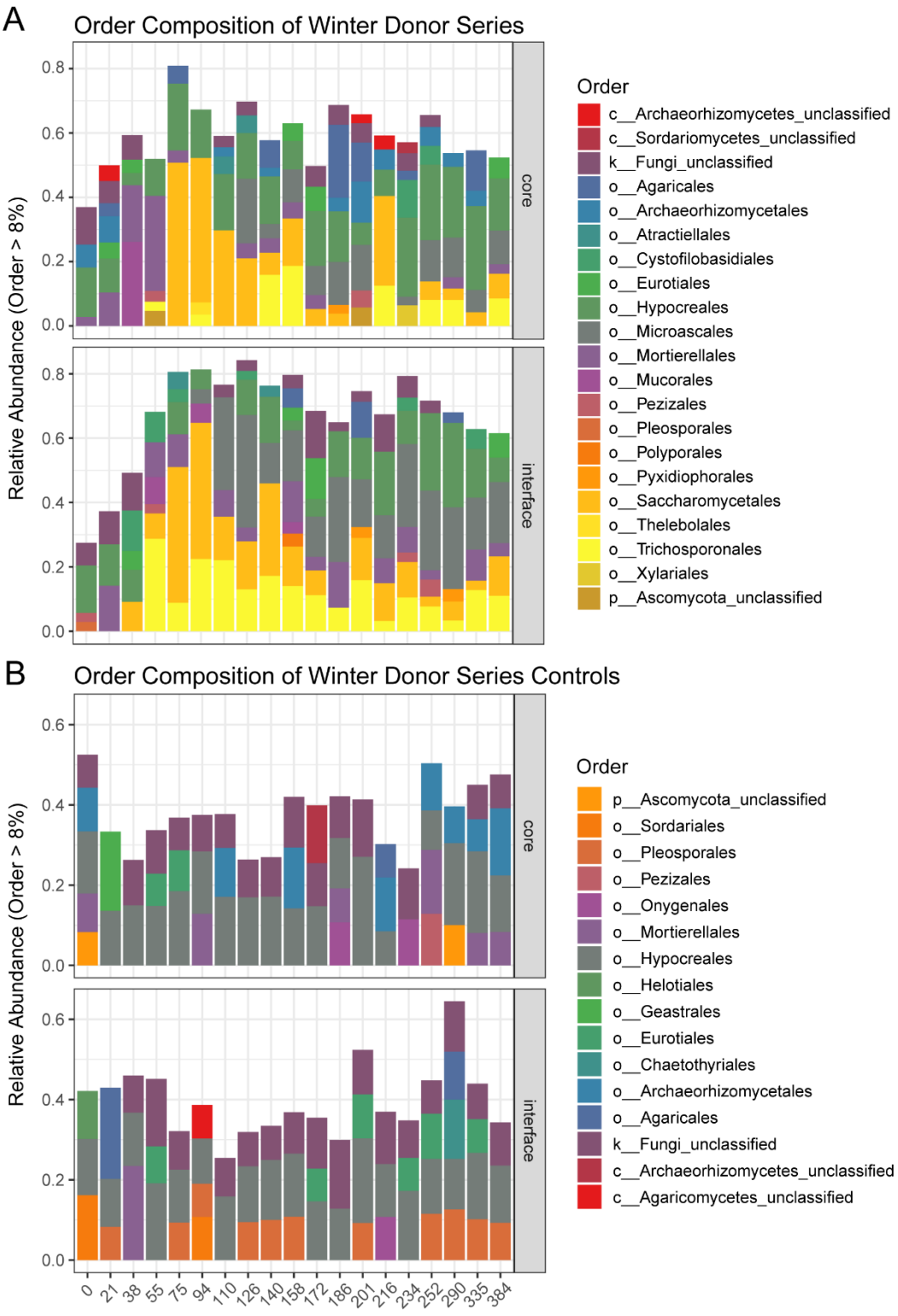

Figure 3.19: Order composition of winter trial soils. Relative abundances of orders in cores and interfaces are shown for (A) impacted soils and (B) controls.

Table 3.11: Spring 2018: Effects of decomposition-impacted soils and time on nematode abundance and alpha diversity. Results of two-way ANOVAs comparing impacted soils (Treatment) and study date (Day), as well as interaction effects.

		Treatment		Day		Treatment*Day	
		F	p	F	p	F	p
Cores (0-1 cm)	**Abundance**	19.2745	**<0.001*** **	1.9027	**0.025***	1.2659	0.230
	Richness	284.252	**<0.001*** **	5.3539	**<0.001*** **	2.1765	**0.009** **
	Shannon diversity	158.6997	**<0.001*** **	2.0693	**0.013***	1.0414	0.426
Interfaces (1-16 cm)	**Abundance**	27.6987	**<0.001*** **	1.4585	0.125	1.385	0.159
	Richness	753.8462	**<0.001*** **	6.3632	**<0.001*** **	1.8938	**0.026***
	Shannon diversity	592.2146	**<0.001*** **	4.5712	**<0.001*** **	3.0703	**<0.001*** **

Significant differences based upon $p < 0.05$ are presented in bold type. Asterisks indicate levels of significance: * $p < 0.05$, ** $p < 0.01$, *** $p < 0.001$

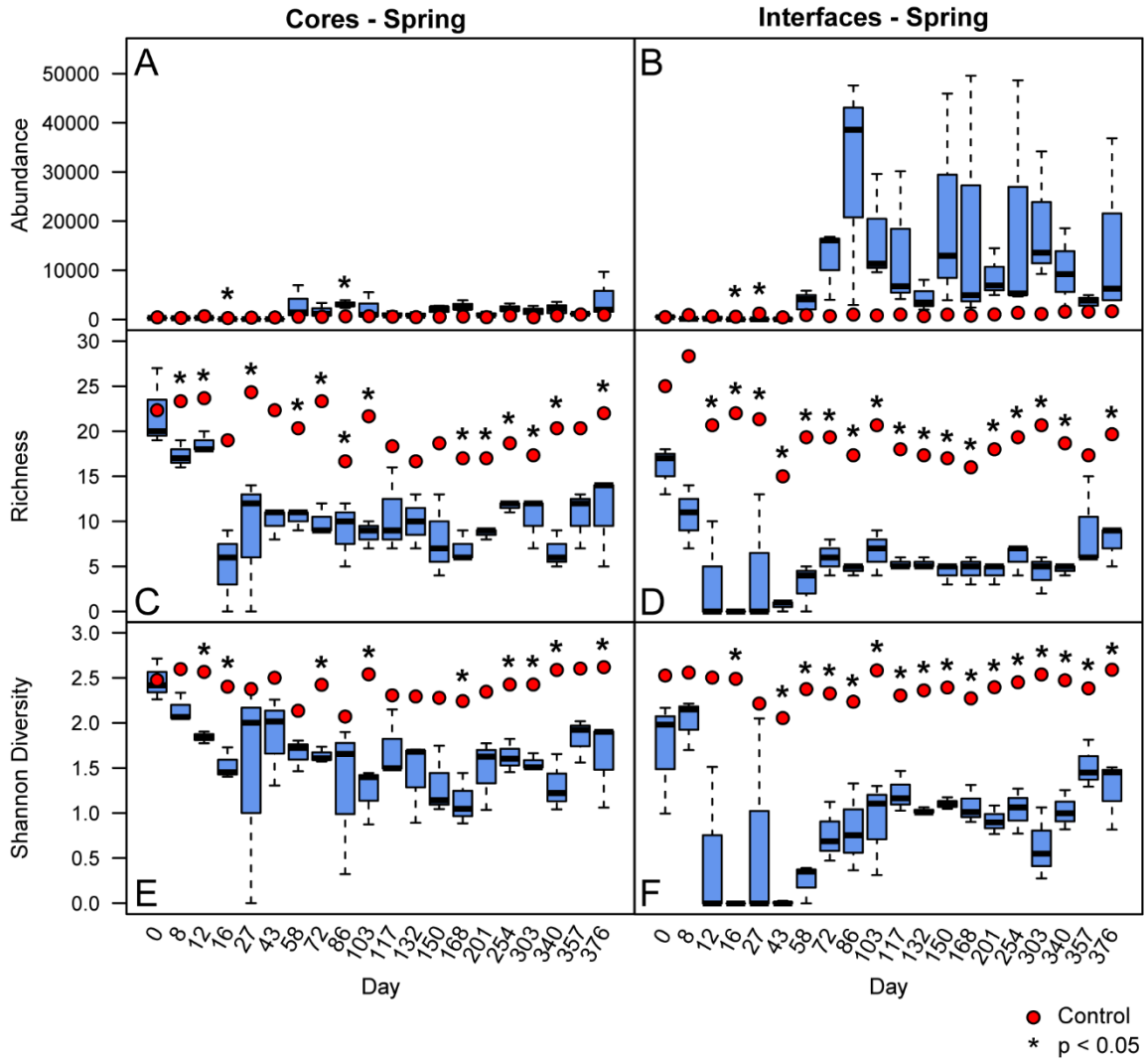

Figure 3.20. Spring 2018 nematode abundances and alpha diversity. Abundances (A-B), richness (C-D), and Shannon diversity (E-F) are shown by study day for core and interface soils. Boxes (n=3) display 25th and 75th quartiles and medians, and whiskers display ± 1.5 quartiles. Control means (n=3) are represented by red dots. Asterisks denote significance ($p < 0.05$) based upon paired Student's T-tests conducted at each sampling time point.

This resource was prepared by the author(s) using Federal funds provided by the U.S. Department of Justice. Opinions or points of view expressed are those of the author(s) and do not necessarily reflect the official position or policies of the U.S. Department of Justice.

Table 3.12: Summary table of nematode abundances and alpha diversity in Spring 2018 core (1-16 cm) soils. Means (n=3) and standard deviations are shown.

Study day	Location	Abundances per 100 gwd soil	Richness per 100 gdw soil	Shannon Diversity
0	**Donor**	284 ± 92	22 ± 4.4	2.5 ± 0.2
	Control	423 ± 123	22.3 ± 0.6	2.5 ± 0.2
8	**Donor**	261 ± 133	17.3 ± 1.5	2.1 ± 0.2
	Control	305 ± 88	23.3 ± 2.1	2.6 ± 0.1
12	**Donor**	360 ± 126	18.7 ± 1.2	1.8 ± 0.1
	Control	655 ± 20	23.7 ± 0.6	2.6 ± 0.1
16	**Donor**	81 ± 23	5 ± 4.6	1.5 ± 0.2
	Control	277 ± 46	19 ± 4	2.4 ± 0.1
27	**Donor**	71 ± 69	8.7 ± 7.6	1.4 ± 1.3
	Control	365 ± 71	24.3 ± 2.1	2.4 ± 0.2
43	**Donor**	92 ± 33	10 ± 1.7	1.9 ± 0.5
	Control	400 ± 144	22.3 ± 4.7	2.5 ± 0.3
58	**Donor**	2897 ± 3555	10.3 ± 1.2	1.7 ± 0.2
	Control	543 ± 289	20.3 ± 0.6	2.1 ± 0.2
72	**Donor**	1662 ± 1516	10 ± 1.7	1.6 ± 0.1
	Control	527 ± 308	23.3 ± 0.6	2.4 ± 0.2
86	**Donor**	3094 ± 777	9 ± 3.6	1.3 ± 0.8
	Control	633 ± 238	16.7 ± 5.9	2.1 ± 0.5
103	**Donor**	2298 ± 2802	8.7 ± 1.5	1.2 ± 0.3
	Control	669 ± 209	21.7 ± 2.5	2.5 ± 0.2
117	**Donor**	1039 ± 538	10.7 ± 4.7	1.7 ± 0.4
	Control	566 ± 400	18.3 ± 1.5	2.3 ± 0.2
132	**Donor**	944 ± 490	10 ± 3	1.4 ± 0.5
	Control	460 ± 204	16.7 ± 4.5	2.3 ± 0.2
150	**Donor**	1951 ± 1079	8 ± 4.6	1.3 ± 0.4
	Control	528 ± 172	18.7 ± 3.5	2.3 ± 0.1
168	**Donor**	2665 ± 1122	7 ± 1.7	1.1 ± 0.3
	Control	595 ± 106	17 ± 0	2.2 ± 0.2
201	**Donor**	1012 ± 500	8.7 ± 0.6	1.5 ± 0.4
	Control	452 ± 126	17 ± 2	2.3 ± 0.2
254	**Donor**	2276 ± 887	11.7 ± 0.6	1.6 ± 0.2
	Control	804 ± 210	18.7 ± 0.6	2.4 ± 0.1
303	**Donor**	1646 ± 1070	10.3 ± 2.9	1.6 ± 0.1
	Control	433 ± 50	17.3 ± 1.2	2.4 ± 0.1
340	**Donor**	2052 ± 1585	6.7 ± 2.1	1.3 ± 0.3
	Control	793 ± 200	20.3 ± 3.2	2.6 ± 0.2
357	**Donor**	1115 ± 190	10.7 ± 3.2	1.8 ± 0.2
	Control	1008 ± 435	20.3 ± 2.1	2.6 ± 0.2
376	**Donor**	4263 ± 4725	11 ± 5.2	1.6 ± 0.5
	Control	933 ± 274	22 ± 1.7	2.6 ± 0.2

Table 3.13: Effects of decomposition on nematode abundances and alpha diversity for Spring 2018 soils. Paired sample T-tests were conducted at each sampling time point in order to compare changes between impacted soils and controls. P-values are shown.

Study Day	Location	Abundances	Richness	Shannon Diversity
0	**Core**	0.378	0.914	0.968
	Interface	0.646	0.130	0.180
8	**Core**	0.687	**0.009****	0.078
	Interface	0.079	**0.050**	0.186
12	**Core**	0.055	**0.013***	**0.013***
	Interface	0.607	**0.032***	0.056
16	**Core**	**0.005**	0.074	**0.032***
	Interface	**0.035***	**<0.001*****	**<0.001*****
27	**Core**	0.057	**0.039***	0.378
	Interface	**0.019***	**0.042***	0.168
43	**Core**	0.093	0.061	0.269
	Interface	0.295	**0.010***	**0.003****
58	**Core**	0.389	**0.010***	0.164
	Interface	0.308	**0.015***	**<0.001*****
72	**Core**	0.379	**0.008****	**0.032***
	Interface	0.121	**0.019***	**0.015***
86	**Core**	**0.016***	**0.029***	0.073
	Interface	0.177	**0.013***	**0.035***
103	**Core**	0.392	**0.014***	**0.024***
	Interface	0.120	**0.002****	**0.026***
117	**Core**	0.474	0.137	0.187
	Interface	0.256	**0.025***	**0.004****
132	**Core**	0.311	0.109	0.088
	Interface	0.161	**0.029***	**0.006****
150	**Core**	0.155	0.055	0.061
	Interface	0.254	**0.005****	**0.005****
168	**Core**	0.995	**0.010***	**0.009****
	Interface	0.357	**0.006****	**0.020***
201	**Core**	0.227	**0.011***	0.060
	Interface	0.099	**0.016***	**0.003****
254	**Core**	0.146	**<0.001*****	**0.008****
	Interface	0.341	**0.008****	**0.032***
303	**Core**	0.191	**0.020***	**0.021***
	Interface	0.145	**0.013***	**0.018***
340	**Core**	0.341	**0.004****	**0.008****
	Interface	0.245	**0.002****	**0.003****
357	**Core**	0.723	0.054	0.072
	Interface	0.251	0.151	**0.027***
376	**Core**	0.359	**0.032***	**0.031***
	Interface	0.362	**0.016***	**0.043***

Significant differences based upon $p < 0.05$ are presented in bold type. Asterisks indicate levels of significance: * $p < 0.05$, ** $p < 0.01$, *** $p < 0.001$

Table 3.14: Summary table of nematode abundances and alpha diversity in Spring 2018 interface (0-1 cm) soils. Means (n=3) and standard deviations are shown.

Study day	Location	Abundances per 100 gwd soil	Richness per 100 gdw soil	Shannon Diversity
0	**Donor**	579 ± 200	16 ± 2.6	1.7 ± 0.6
	Control	466 ± 173	25 ± 4	2.5 ± 0.2
8	**Donor**	136 ± 63	10.7 ± 3.5	2 ± 0.3
	Control	895 ± 334	28.3 ± 3.8	2.6 ± 0.2
12	**Donor**	387 ± 524	3.3 ± 5.8	0.5 ± 0.9
	Control	612 ± 191	20.7 ± 3.2	2.5 ± 0.1
16	**Donor**	29 ± 51	0 ± 0	0 ± 0
	Control	550 ± 156	22 ± 1	2.5 ± 0
27	**Donor**	67 ± 115	4.3 ± 7.5	0.7 ± 1.2
	Control	1201 ± 176	21.3 ± 2.1	2.2 ± 0.1
43	**Donor**	155 ± 258	0.7 ± 0.6	0 ± 0
	Control	428 ± 153	15 ± 3	2.1 ± 0.2
58	**Donor**	3318 ± 2989	3 ± 2.6	0.2 ± 0.2
	Control	878 ± 177	19.3 ± 1.2	2.4 ± 0.1
72	**Donor**	12282 ± 7197	6 ± 2	0.8 ± 0.3
	Control	687 ± 529	19.3 ± 1.5	2.3 ± 0.1
86	**Donor**	29708 ± 23622	4.7 ± 0.6	0.8 ± 0.5
	Control	993 ± 709	17.3 ± 3.1	2.2 ± 0.1
103	**Donor**	16850 ± 11075	6.7 ± 2.5	0.9 ± 0.5
	Control	813 ± 475	20.7 ± 2.1	2.6 ± 0
117	**Donor**	13682 ± 14320	5.3 ± 0.6	1.2 ± 0.2
	Control	1001 ± 414	18 ± 4	2.3 ± 0.2
132	**Donor**	4505 ± 3163	5.3 ± 0.6	1 ± 0
	Control	671 ± 262	17.3 ± 3.2	2.4 ± 0.2
150	**Donor**	20938 ± 22136	4.3 ± 1.2	1.1 ± 0.1
	Control	989 ± 450	17 ± 2.6	2.4 ± 0.2
168	**Donor**	18983 ± 26526	4.7 ± 1.5	1.1 ± 0.2
	Control	765 ± 107	16 ± 2.6	2.3 ± 0.2
201	**Donor**	8783 ± 5040	4.3 ± 1.2	0.9 ± 0.2
	Control	1022 ± 490	18 ± 4	2.4 ± 0.3
254	**Donor**	19539 ± 25207	6 ± 1.7	1 ± 0.3
	Control	1356 ± 237	19.3 ± 2.3	2.5 ± 0.2
303	**Donor**	18995 ± 13318	4.3 ± 2.1	0.6 ± 0.4
	Control	1123 ± 136	20.7 ± 1.2	2.5 ± 0.1
340	**Donor**	9907 ± 8317	4.7 ± 0.6	1 ± 0.2
	Control	1578 ± 747	18.7 ± 1.5	2.5 ± 0.1
357	**Donor**	3524 ± 1599	9 ± 5.2	1.5 ± 0.3
	Control	1601 ± 490	17.3 ± 1.2	2.4 ± 0
376	**Donor**	14904 ± 19152	7.7 ± 2.3	1.3 ± 0.4
	Control	1678 ± 491	19.7 ± 0.6	2.6 ± 0.1

Table 3.15: Winter 2019 effects of decomposition-impacted soils and time on nematode abundance and alpha diversity. Results of two-way ANOVAs comparing impacted soils (Treatment) and study date (Day), as well as interaction effects.

		Treatment		Day		Treatment*Day	
		F	p	F	p	F	p
Cores (0-1 cm)	**Abundance**	39.8673	**<0.001*** **	1.8067	**0.040***	1.6859	0.061
	Richness	230.4011	**<0.001*** **	3.2206	**<0.001*** **	3.0984	**<0.001*** **
	Shannon diversity	107.4298	**<0.001*** **	2.8648	**<0.001*** **	2.8292	**<0.001*** **
Interfaces (1-16 cm)	**Abundance**	77.1223	**<0.001*** **	5.2158	**<0.001*** **	5.116	**<0.001*** **
	Richness	523.9174	**<0.001*** **	4.2357	**<0.001*** **	5.5493	**<0.001*** **
	Shannon diversity	697.1161	**<0.001*** **	4.3376	**<0.001*** **	8.0479	**<0.001*** **

Significant differences based upon $p < 0.05$ are presented in bold type. Asterisks indicate levels of significance: * $p < 0.05$, ** $p < 0.01$, *** $p < 0.001$

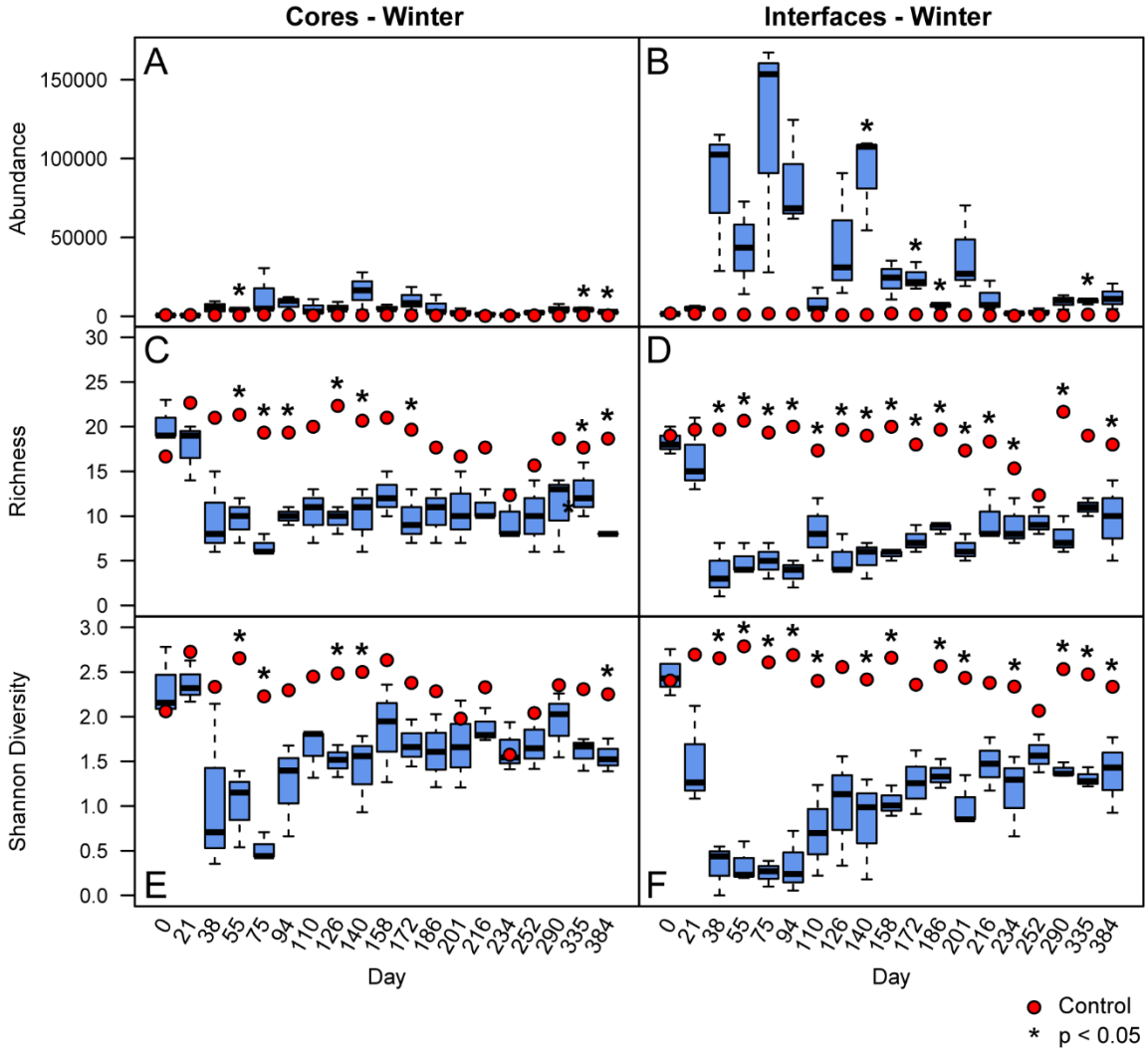

Figure 3.21. Winter 2019 nematode abundances and alpha diversity. Abundances (A-B), richness (C-D), and Shannon diversity (E-F) are shown by study day for core and interface soils. Boxes (n=3) display 25th and 75th quartiles and medians, and whiskers display $\pm$ 1.5 quartiles. Control means (n=3) are represented by red dots. Asterisks denote significance ($p < 0.05$) based upon paired Student's T-tests conducted at each sampling time point.

This resource was prepared by the author(s) using Federal funds provided by the U.S. Department of Justice. Opinions or points of view expressed are those of the author(s) and do not necessarily reflect the official position or policies of the U.S. Department of Justice.

Table 3.16: Summary table of nematode abundances and alpha diversity in Winter 2019 core (1-16 cm) soils. Means (n=3) and standard deviations are shown.

Study day	Location	Abundances per 100 gwd soil	Richness per 100 gdw soil	Shannon Diversity
0	**Donor**	753 ± 351	20.3 ± 2.3	2.3 ± 0.4
	Control	828 ± 34	16.7 ± 0.6	2.1 ± 0.2
21	**Donor**	994 ± 802	17.7 ± 3.2	2.4 ± 0.2
	Control	828 ± 315	22.7 ± 2.3	2.7 ± 0
38	**Donor**	5330 ± 4520	9.7 ± 4.7	1.1 ± 0.9
	Control	778 ± 288	21 ± 1	2.3 ± 0.2
55	**Donor**	4107 ± 1070	9.7 ± 2.5	1 ± 0.4
	Control	610 ± 106	21.3 ± 1.2	2.7 ± 0.3
75	**Donor**	13204 ± 15051	6.7 ± 1.2	0.5 ± 0.2
	Control	1128 ± 350	19.3 ± 2.5	2.2 ± 0.4
94	**Donor**	8071 ± 5147	10 ± 1	1.2 ± 0.5
	Control	914 ± 30	19.3 ± 2.1	2.3 ± 0.4
110	**Donor**	4959 ± 5196	10.3 ± 3.1	1.6 ± 0.3
	Control	614 ± 54	20 ± 1.7	2.4 ± 0.3
126	**Donor**	5886 ± 2788	9.7 ± 1.5	1.5 ± 0.2
	Control	711 ± 57	22.3 ± 2.1	2.5 ± 0.3
140	**Donor**	16155 ± 11950	10 ± 3.6	1.4 ± 0.4
	Control	720 ± 160	20.7 ± 2.9	2.5 ± 0.4
158	**Donor**	5287 ± 1797	12.3 ± 2.5	1.9 ± 0.6
	Control	804 ± 253	21 ± 2.6	2.6 ± 0.2
172	**Donor**	10317 ± 7501	9.7 ± 3.1	1.7 ± 0.3
	Control	589 ± 180	19.7 ± 0.6	2.4 ± 0.2
186	**Donor**	6249 ± 6390	10.3 ± 3.1	1.6 ± 0.4
	Control	511 ± 85	17.7 ± 2.3	2.3 ± 0.3
201	**Donor**	2485 ± 2280	10.7 ± 4	1.7 ± 0.5
	Control	971 ± 577	16.7 ± 3.8	2 ± 0.3
216	**Donor**	1540 ± 1036	11 ± 1.7	1.9 ± 0.2
	Control	247 ± 76	17.7 ± 2.1	2.3 ± 0.1
234	**Donor**	877 ± 470	9.7 ± 2.9	1.6 ± 0.3
	Control	440 ± 196	12.3 ± 5.5	1.6 ± 0.8
252	**Donor**	2431 ± 1065	10 ± 4	1.7 ± 0.3
	Control	553 ± 39	15.7 ± 3.2	2 ± 0.2
290	**Donor**	4786 ± 2689	11 ± 4.4	1.9 ± 0.4
	Control	425 ± 130	18.7 ± 1.2	2.4 ± 0.1
335	**Donor**	4213 ± 1409	12.7 ± 3.1	1.6 ± 0.2
	Control	739 ± 120	17.7 ± 2.5	2.3 ± 0.3
384	**Donor**	2480 ± 746	8 ± 0	1.6 ± 0.2
	Control	564 ± 191	18.7 ± 3.1	2.3 ± 0.2

Table 3.17: Summary table of nematode abundances and alpha diversity in Winter 2019 interface (0-1 cm) soils. Means (n=3) and standard deviations are shown.

Study day	Location	Abundances per 100 gwd soil	Richness per 100 gdw soil	Shannon Diversity
0	**Donor**	1569 ± 88	18.3 ± 1.5	2.5 ± 0.3
	Control	1853 ± 611	19 ± 1.7	2.4 ± 0.2
21	**Donor**	4926 ± 1808	16.3 ± 4.2	1.5 ± 0.6
	Control	1671 ± 276	19.7 ± 3.2	2.7 ± 0.1
38	**Donor**	82090 ± 46670	3.7 ± 3.1	0.3 ± 0.3
	Control	1304 ± 416	19.7 ± 3.5	2.7 ± 0.2
55	**Donor**	43473 ± 29369	5 ± 1.7	0.3 ± 0.2
	Control	1114 ± 452	20.7 ± 2.3	2.8 ± 0.1
75	**Donor**	116248 ± 76810	5 ± 2	0.3 ± 0.1
	Control	1726 ± 417	19.3 ± 1.5	2.6 ± 0.2
94	**Donor**	84978 ± 34480	3.7 ± 1.5	0.3 ± 0.3
	Control	1454 ± 274	20 ± 1	2.7 ± 0.1
110	**Donor**	9223 ± 7692	8.3 ± 3.5	0.7 ± 0.5
	Control	745 ± 190	17.3 ± 2.1	2.4 ± 0.2
126	**Donor**	45499 ± 40001	5.3 ± 2.3	1 ± 0.6
	Control	739 ± 267	19.7 ± 2.1	2.6 ± 0.2
140	**Donor**	90554 ± 31245	5.3 ± 2.1	0.8 ± 0.6
	Control	979 ± 411	19 ± 3.6	2.4 ± 0.2
158	**Donor**	23527 ± 12363	5.7 ± 0.6	1 ± 0.2
	Control	1789 ± 153	20 ± 2	2.7 ± 0.1
172	**Donor**	24545 ± 8768	7.3 ± 1.5	1.3 ± 0.4
	Control	1209 ± 524	18 ± 3.6	2.4 ± 0.2
186	**Donor**	6654 ± 1517	8.7 ± 0.6	1.4 ± 0.2
	Control	802 ± 288	19.7 ± 2.3	2.6 ± 0.2
201	**Donor**	38822 ± 27614	6.3 ± 1.5	1 ± 0.3
	Control	837 ± 102	17.3 ± 2.9	2.4 ± 0.4
216	**Donor**	11498 ± 9660	9.7 ± 2.9	1.5 ± 0.3
	Control	478 ± 79	18.3 ± 0.6	2.4 ± 0.1
234	**Donor**	1684 ± 983	9 ± 2.6	1.2 ± 0.5
	Control	378 ± 114	15.3 ± 2.3	2.3 ± 0.2
252	**Donor**	2857 ± 1910	9.3 ± 1.5	1.6 ± 0.2
	Control	564 ± 99	12.3 ± 0.6	2.1 ± 0.2
290	**Donor**	9218 ± 4568	7.7 ± 2.1	1.4 ± 0.1
	Control	504 ± 122	21.7 ± 3.8	2.5 ± 0.2
335	**Donor**	9444 ± 1728	11 ± 1	1.3 ± 0.1
	Control	1138 ± 238	19 ± 2.6	2.5 ± 0.1
384	**Donor**	12085 ± 8125	9.7 ± 4.5	1.4 ± 0.4
	Control	712 ± 65	18 ± 1.7	2.3 ± 0.1

Table 3.18: Effects of decomposition on nematode abundances and alpha diversity for Winter 2019 soils. Paired sample T-tests were conducted at each sampling time point in order to compare changes between impacted soils and controls. P-values are shown.

Study Day	Location	Abundances	Richness	Shannon Diversity
0	Core	0.766	0.093	0.285
	Interface	0.533	0.184	0.511
21	Core	0.696	0.225	0.159
	Interface	0.067	0.362	0.056
38	Core	0.234	0.051	0.194
	Interface	0.095	**0.045**	**0.010**
55	Core	**0.026**	**0.020**	**0.049**
	Interface	0.127	**0.006**	**0.003**
75	Core	0.292	**0.017**	**0.020**
	Interface	0.123	**<0.001**	**<0.001**
94	Core	0.139	**0.023**	0.096
	Interface	0.052	**0.005**	**0.005**
110	Core	0.281	0.065	0.097
	Interface	0.191	**0.028**	**0.008**
126	Core	0.082	**0.021**	**0.022**
	Interface	0.191	**0.025**	0.064
140	Core	0.153	**0.018**	**0.005**
	Interface	**0.039**	**0.042**	**0.049**
158	Core	0.051	0.058	0.117
	Interface	0.091	**0.010**	**0.009**
172	Core	0.157	**0.022**	0.053
	Interface	**0.041**	**0.029**	0.062
186	Core	0.258	0.092	0.119
	Interface	**0.018**	**0.019**	**0.017**
201	Core	0.442	0.203	0.537
	Interface	0.140	**0.011**	**0.017**
216	Core	0.152	0.063	0.077
	Interface	0.185	**0.043**	0.054
234	Core	0.114	0.287	0.885
	Interface	0.125	**0.003**	**0.021**
252	Core	0.097	0.286	0.402
	Interface	0.183	0.122	0.162
290	Core	0.115	0.073	0.195
	Interface	0.081	**0.034**	**0.014**
335	Core	**0.048**	**0.013**	0.080
	Interface	**0.015**	0.062	**0.007**
384	Core	**0.027**	**0.026**	**0.048**
	Interface	0.138	**0.046**	**0.031**

Significant differences based upon $p < 0.05$ are presented in bold type. Asterisks indicate levels of significance: * $p < 0.05$, ** $p < 0.01$, *** $p < 0.001$

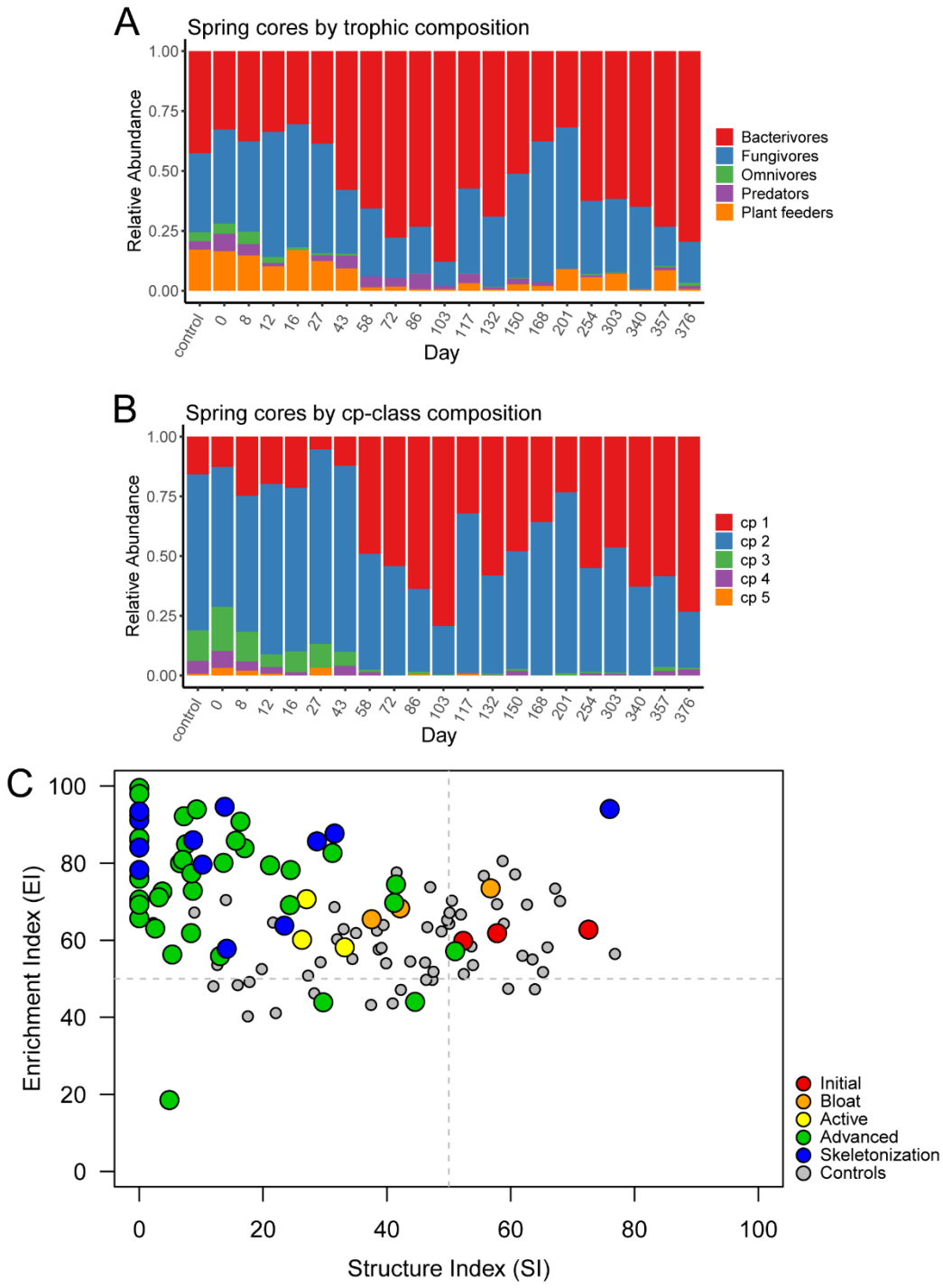

Figure 3.22: Temporal changes in nematode community composition and functional diversity in Spring core (1-16 cm) soils. Relative abundances of (A) trophic groups, (B) cp-classes, and (C) functional diversity are shown in core soils by study date.

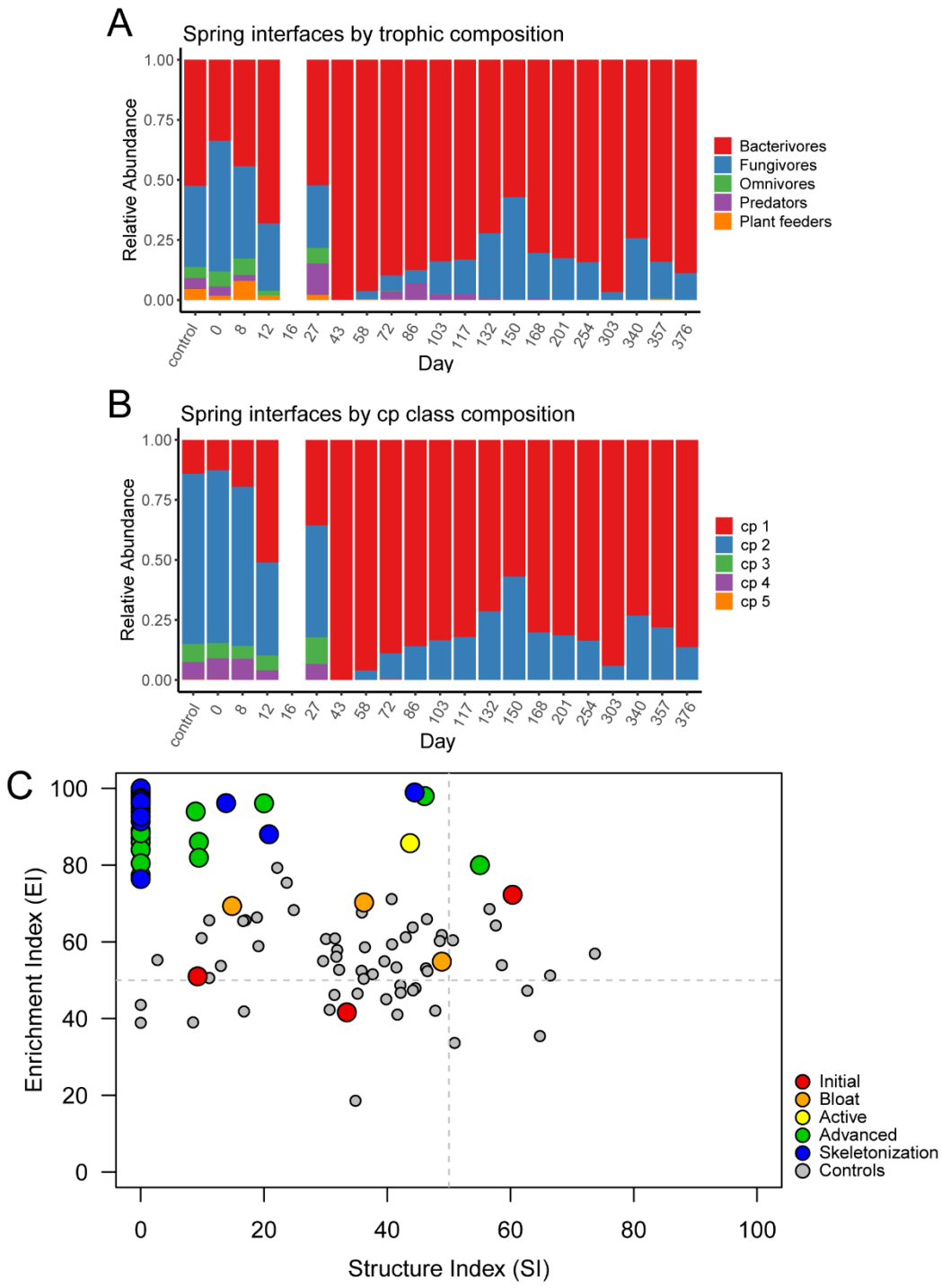

Figure 3.23: Temporal changes in nematode community composition and functional diversity in Spring interface (0-1 cm) soils. Relative abundances of (A) trophic groups, (B) cp-classes, and (C) functional diversity are shown in core soils by study date.

This resource was prepared by the author(s) using Federal funds provided by the U.S. Department of Justice. Opinions or points of view expressed are those of the author(s) and do not necessarily reflect the official position or policies of the U.S. Department of Justice.

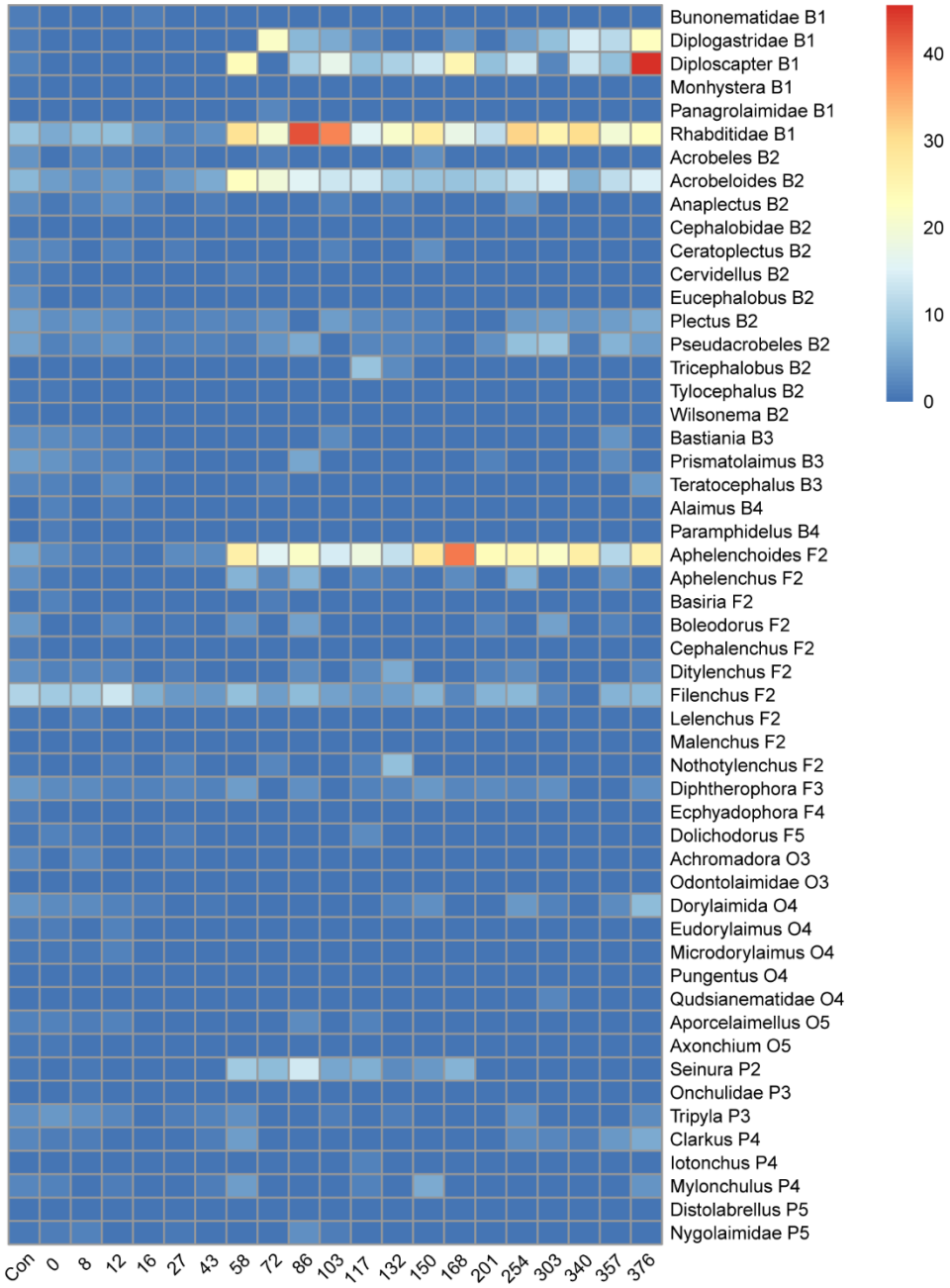

Figure 3.24: Heatmap showing changes in individual nematode abundances by study day in spring core (1-16 cm) soils. Data shows that abundances sharply increase beginning on day 58 for Diplogastridae, *Diploscapter*, Rhabditidae, *Acrobeloides*, *Aphelenchoides*, and *Seinura*. *Filenchus* abundances decreased. Nematodes are listed by trophic groups and further delineated by increasing cp-class. Data are square-root transformed means of each taxon.

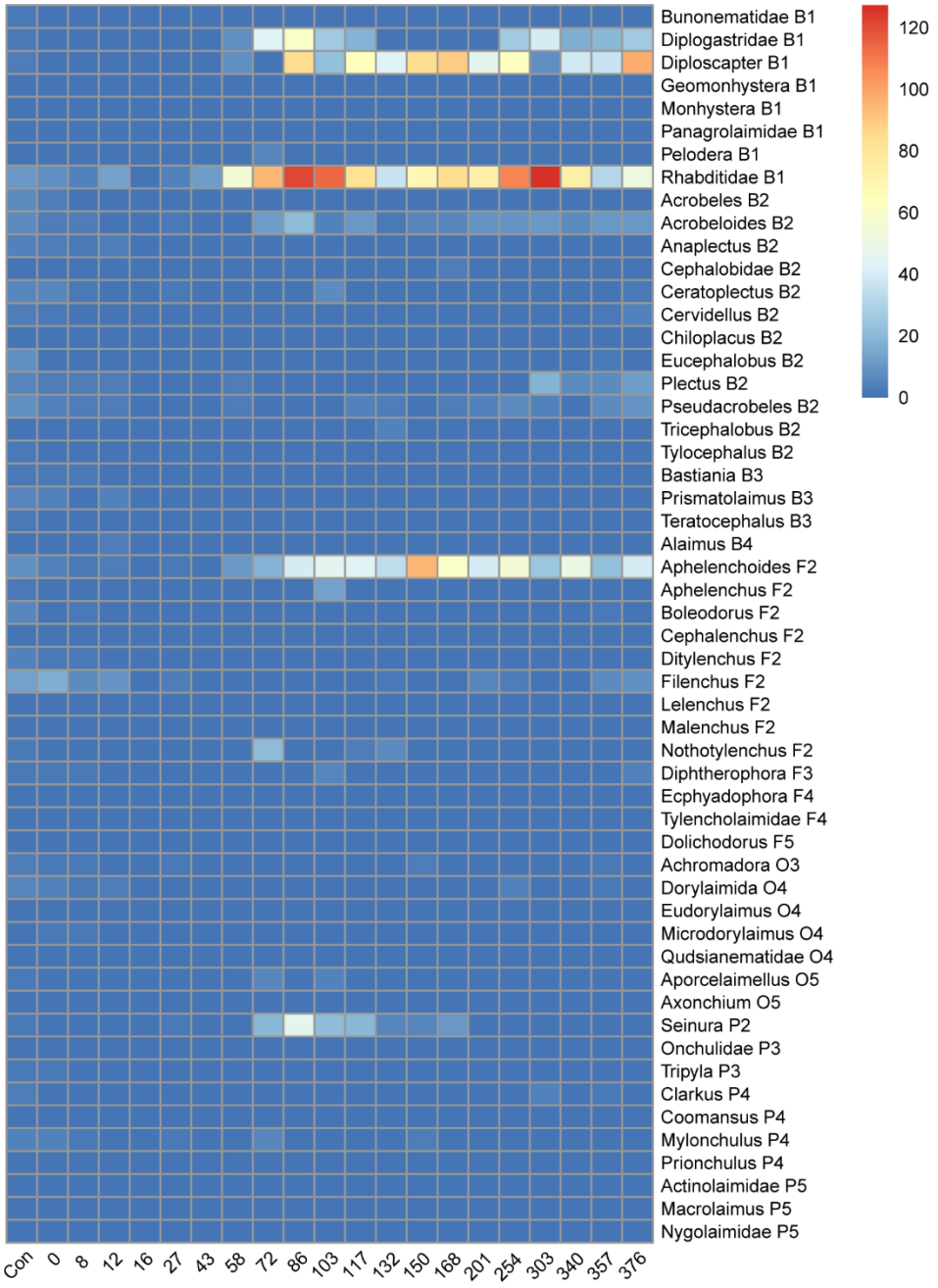

Figure 3.25: Heatmap showing changes in individual nematode abundances by study day in spring interface (0-1 cm) soils. Data shows that abundances sharply increase beginning on day 58 for Diplogastridae, *Diploscapter*, Rhabditidae, *Aphelenchoides*, and *Seinura*. *Filenchus* abundances decreased. Nematodes are listed by trophic groups and further delineated by increasing cp-class. Data are square-root transformed means of each taxon.

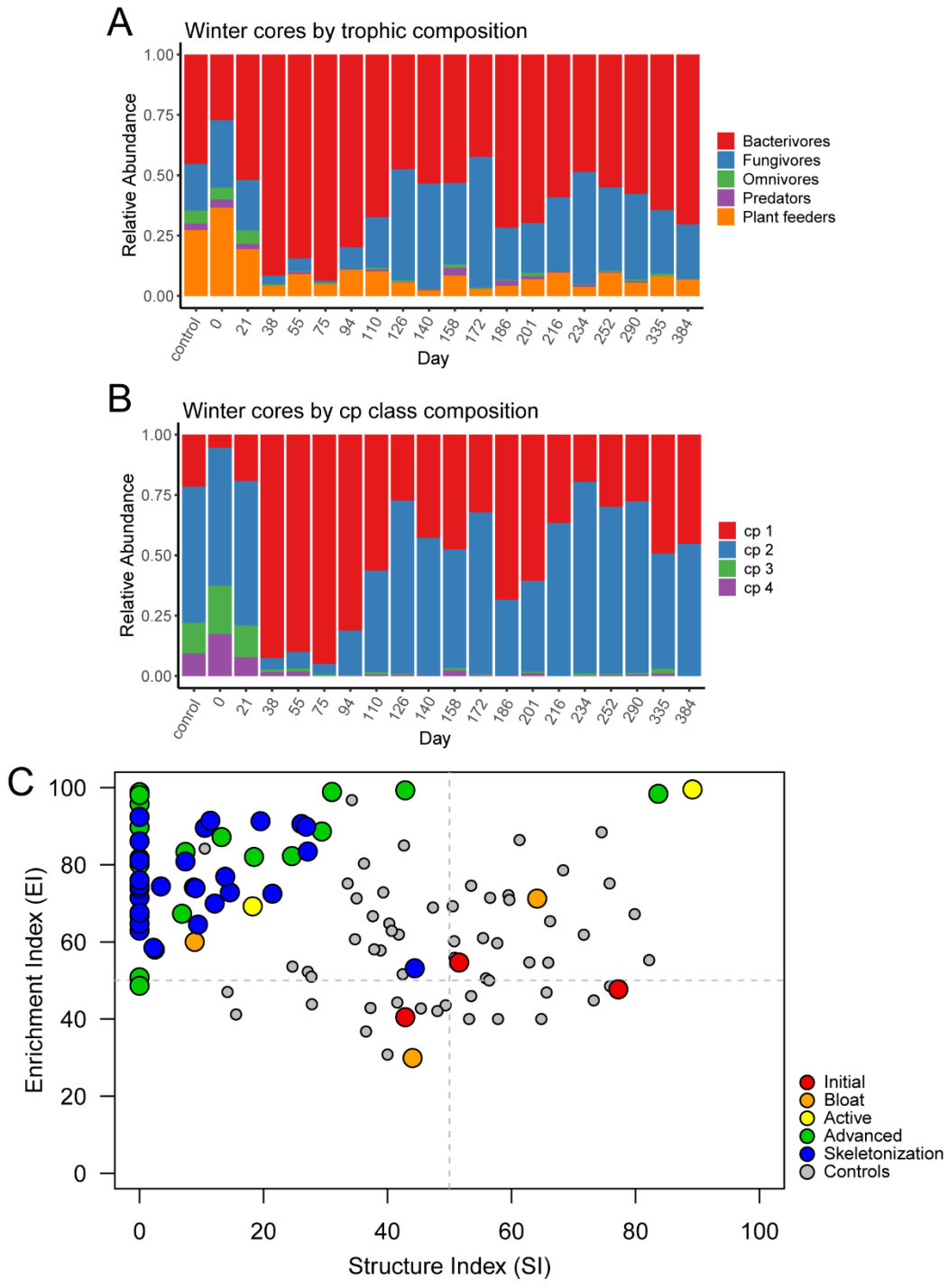

Figure 3.26: Temporal changes in nematode community composition and functional diversity in Winter core (1-16 cm) soils. Relative abundances of (A) trophic groups, (B) cp-classes, and (C) functional diversity are shown in core soils by study date.

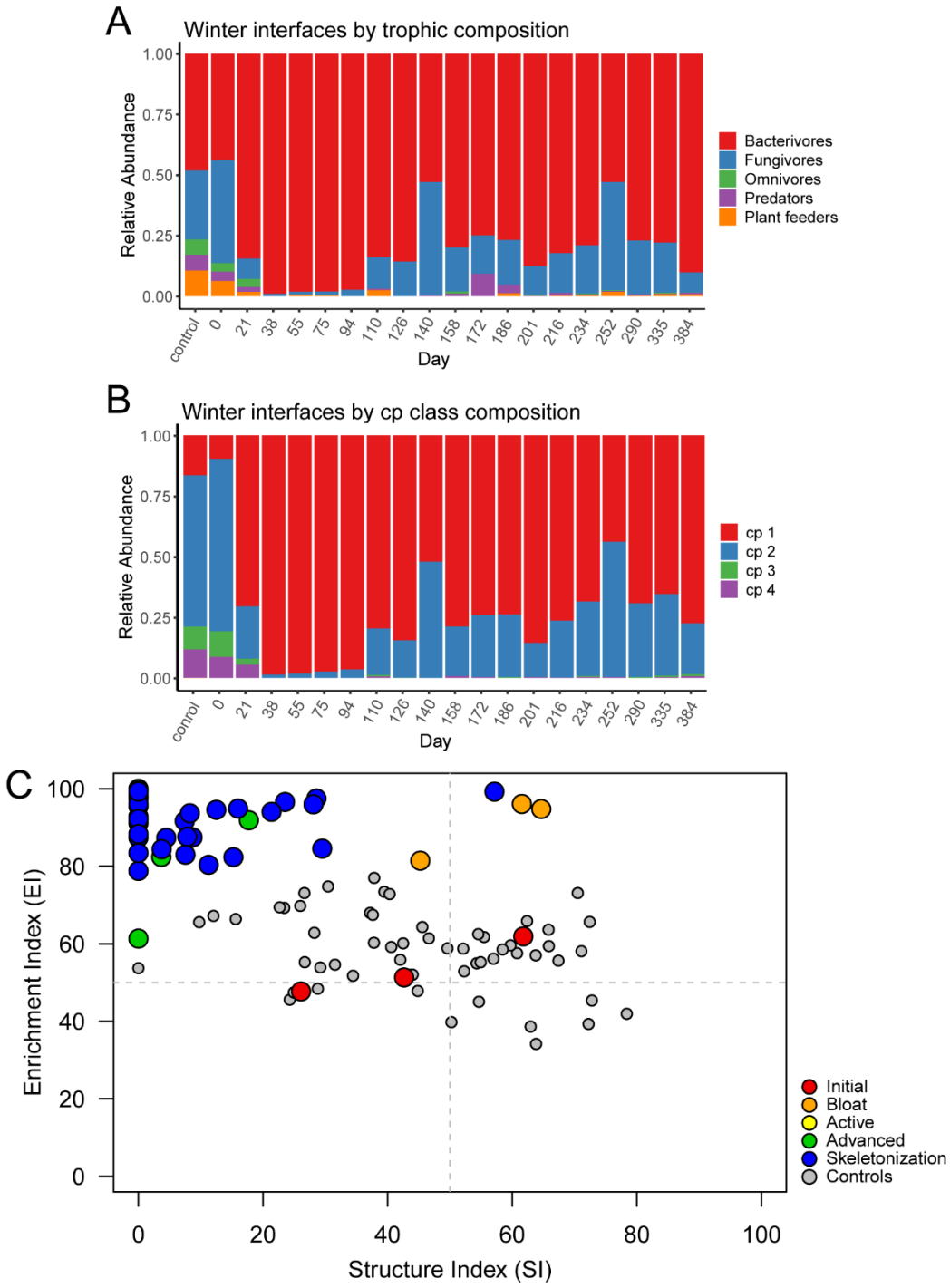

Figure 3.27: Temporal changes in nematode community composition and functional diversity in Winter interface (0-1 cm) soils. Relative abundances of (A) trophic groups, (B) cp-classes, and (C) functional diversity are shown in core soils by study date.

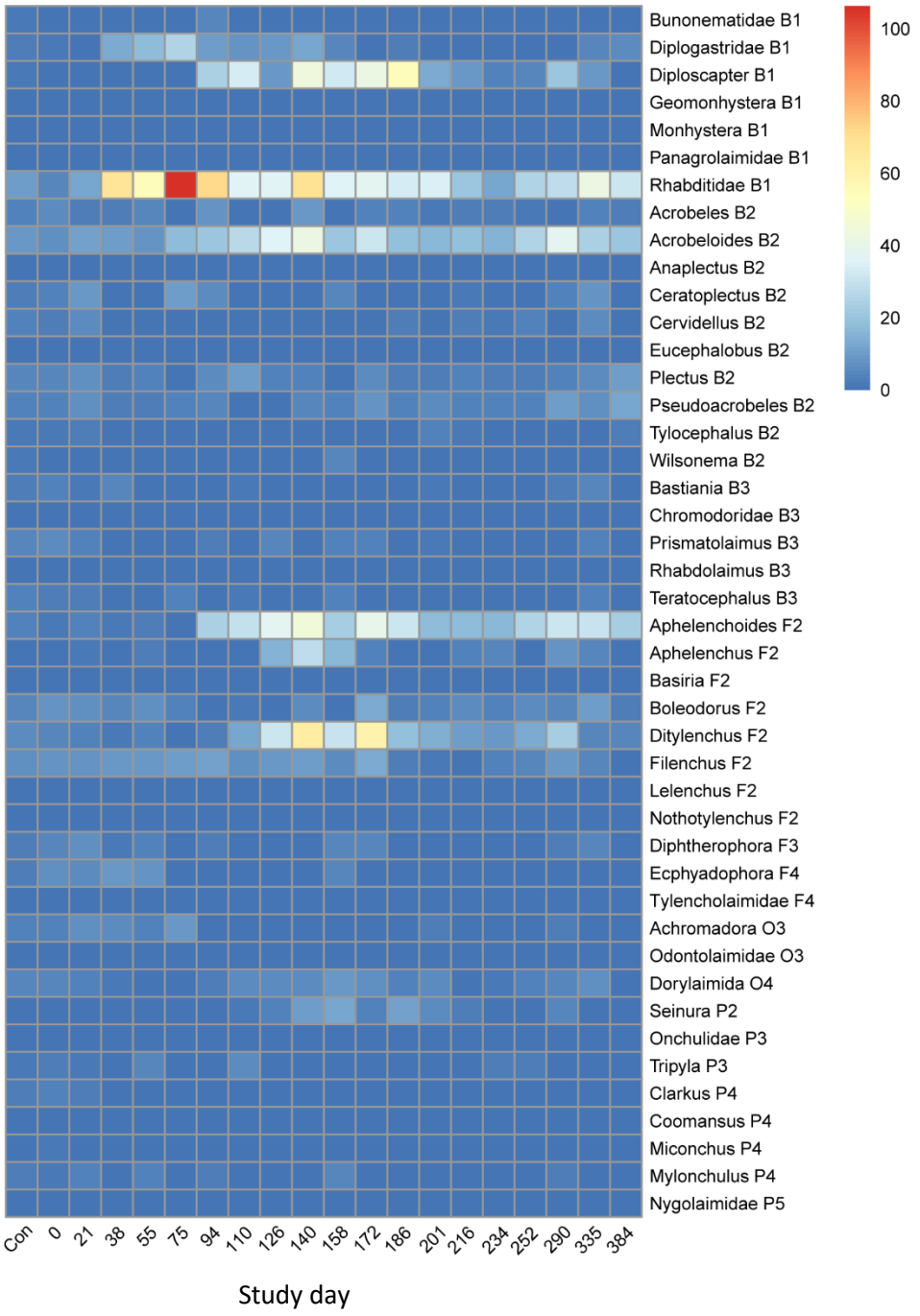

Figure 3.28: Heatmap showing changes in individual nematode abundances by study day in winter core (1-16 cm) soils. Data shows that abundances increase during active decay (day 38) for Diplogastridae and Rhabditidae. *Diploscapter*, *Acrobeloides*, *Aphelenchoides*, *Ditylenchus*, and *Seinura* increase during advanced decay (after day 75). *Filenchus* abundances decreased. Nematodes are listed by trophic groups and further delineated by increasing cp-class. Data are square-root transformed means of each taxon.

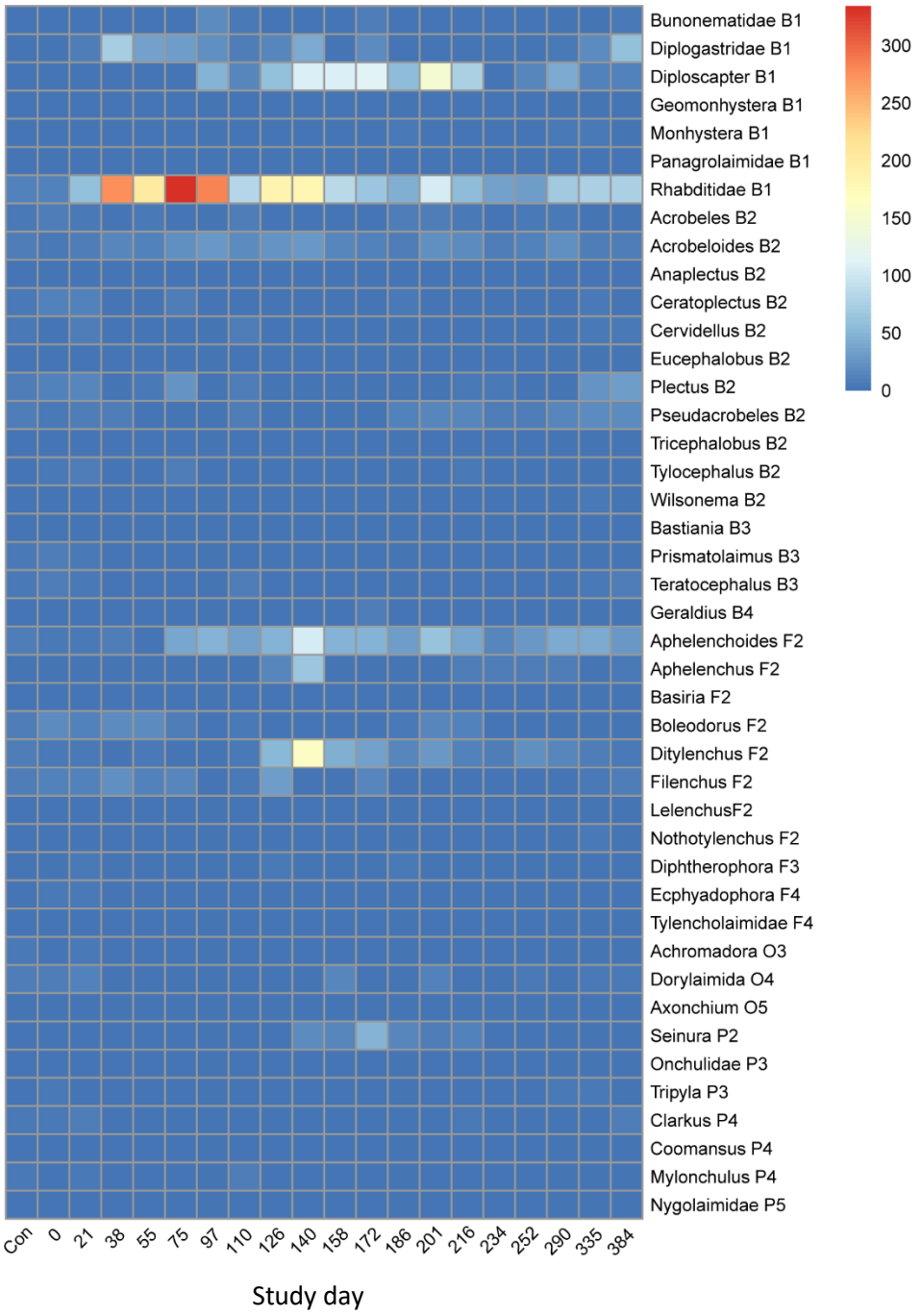

Figure 3.29: Heatmap showing changes in individual nematode abundances by study day in winter interface (0-1 cm) soils. Data shows that abundances increase during bloat through active decay (days 21-38) for Diplogastridae and Rhabditidae. *Diploscapter*, *Aphelenchoides*, *Ditylenchus*, and *Seinura* increase during advanced decay (after day 75). *Filenchus* abundances decreased. Nematodes are listed by trophic groups and further delineated by increasing cp-class. Data are square-root transformed means of each taxon.

Conclusion

The effects of vertebrate decomposition are wide-ranging across multiple foodwebs, and these impacts have been shown to persist in the environment, however there is a lack of systematic assessment of these changes over long periods of time or in sufficiently high resolution as to resolve seasonal flux patterns. Furthermore, current study has largely remained restricted to the individual disciplines of soil chemistry and microbial ecology, and thus has neglected the integration between these two fields of decomposition research, let alone explored their impacts on higher levels of the soil foodweb. The ultimate aim of this body of research was to explore nematode systematics in decomposition environments, culminating in a pair of long-term human decomposition seasonal trials, in high resolution, with the specific intent of integrating the fields of soil chemistry, microbial ecology, and nematology in order to assess the relationships of cross-disciplinary impacts. Of these three fields, soil chemistry has the largest body of literature dedicated to its study. Molecular microbial ecology, for forensic purposes, is still an emerging field, and primarily focuses on bacterial successional characteristics in the early phases of decomposition. Nematology as a forensic tool has had very little study dedicated to it, however initial results are promising. Therefore, prior to performing a fully integrated study, further examination of nematode community systematics was required in order to ascertain the nature of their responses to the decomposition environment. Our body of work consisted of three objectives: evaluation of nematode communities in a multi-individual grave, evaluation of longitudinal patterns in nematode diversity in an animal model system, and finally, a seasonal human decomposition study that integrated the three disciplines of soil chemistry, microbial ecology, and nematology.

In the first objective, nematode community composition was examined in association with interred human remains, which demonstrated that communities within a gravesoil vertical

profile differed from those found in soils unimpacted by decomposition. The nematodes *Filenchus* and *Plectus* emerged as possible taxa of interest. In the second objective, a long-term vertebrate model system was used to ascertain patterns in nematode alpha, beta, and functional diversity throughout decomposition, and to identify candidate taxa that could be used as indicators of decomposition progression. Increases in the abundances of bacterial-feeding taxa of the family Rhabditidae were found to correspond to the morphological stages of active and advanced decay, and following these elevated abundances successional patterns became apparent, consistent with findings in the literature from both decomposition systems and general nematode ecology. Members of the family Rhabditidae, and genera *Acrobeloides*, *Aphelenchoides*, and *Filenchus* were found to be robust indicators not only in this study, but across other successional studies in the literature that included findings from both visual observations (microscopic) and amplicon sequencing studies. These data and this study design were then used as the basis for the construction of the comprehensive human decomposition trials. In the third objective, two seasonal human decomposition trials were conducted, designed to integrate nematology results with those from soil chemistry and fungal ecology in order to capture a comprehensive view of decomposition-induced soil responses across all three disciplines simultaneously. Changes in all three disciplines were shown to occur concurrently, however, distinct differences were observed between the two seasonal studies, primarily with respect to timing and magnitude of response patterns.

We found that soil temperature increased during the spring trial in conjunction with larval thermogenesis and active decay, an effect that was not observed in the winter trial. This soil heating was of sufficient degree that nematode populations in the soil were adversely affected for a period of 50 days. Given that changes in soil heating has implications for extracellular

enzymatic activity, microbial metabolic and growth rates, as well as N and C cycling within the soil, we propose that changes in soil temperature during larval thermogenesis must be considered in the construction of models that include these phenomena. Conversely, the lack of soil heating and attendant effects upon soil chemistry and microbial ecology must be taken into account for cooler seasons or other circumstances in which insect activity is not present. This temperature effect alone highlights the difficulties in modelling decomposition systems and determining whether universal modelling is of sufficient resolution to capture realistic error rates, or whether numerous models are necessary in order to capture environmental and seasonal nuances. Additionally, long-term differences between cumulative soil and ambient temperatures demonstrates the likelihood for considerable error associated with current methods for PMI calculations when temperature values are obtained from nearest-neighbor weather stations. We have shown that the differences in these respective temperatures over the course of a year can introduce error rates of between 15-30 days.

We have shown that soil chemistry, when used in high resolution, is a sensitive methodology for determining decomposition progression. Here, we report that in contravention to a large part of the vertebrate decomposition literature, pH does not necessarily increase during human decomposition, and that in fact it is one of the least consistent and understood soil chemical parameters. We have demonstrated that soil respiration mirrors measured oxygen reduction in the soil, validating previous assumptions that increased microbial activity results in reduced soil oxygen, and confirming results from Keenan et al. (2018). We demonstrated that the ratio of inorganic nitrogen pools followed the same patterns between seasons, and that these ratios were linked to changes in oxygen availability, further validating proposed biogeochemical models.

We reported successional patterns in fungal communities during the early phases of decomposition, notably at the class taxonomic level, however we discovered that there was not sufficient or robust variation between individual taxa to be of utility in describing later stages of decomposition except in terms of ecological interest. Changes in beta diversity were more revealing; here we identified highly distinctive patterns of decomposition progression corresponding to the onset of chemical changes within the soil, the reduction and recovery of soil oxygen levels, and changes in nitrogen speciation, and these collective changes were consistent across seasons. The co-occurrence of patterns in fungal beta diversity and soil chemistry, and the robustness of these observations across seasons makes a compelling argument that microbial ecology should not be studied independently of soil chemistry, particularly when data is to be used for model construction. However, we would be remiss without emphasizing one caveat; taxon-based amplicon studies cannot distinguish between live or dead organisms, and absolute abundances can only be inferred without additional assays specifically designed to quantify them. Based upon these collective data, and acknowledging their constraints, we strongly recommend that future studies employ taxon-independent techniques (i.e. transcriptomics, or metabolomics) in conjunction with a comprehensive soil chemistry panel; we feel that this may prove to be a more appropriate and sensitive indicator of decomposition progression simply by shifting the focus to changes in community responses arising from environmental pressures, rather than the ambiguous shifts in specific taxa. Furthermore, this would eliminate the controversial practice of utilizing predictive metabolic models that are often applied to taxon-based data in an attempt to create precisely this explanatory power.

We found that in human trials nematode communities were of themselves not diagnostic for decomposition progression; changes in their alpha, beta, and functional diversity only

mirrored changes observed in soil chemistry to a limited extent in the early phases of each seasonal trial. This was not an expected result in comparison with the extent of successional patterns observed in the Chapter 2 vertebrate study, however, given that humans are larger organisms, it is reasonable that longer-lasting impacts could be observed. Considering size of impact, this could easily account for the soil impaction observed in Chapter 1, which originated from 3 comingled humans. While long-term successional patterns may not have been identified in the Chapter 3 study, nematodes were singularly instructive in identifying the contributions of temperature to the decomposition process. Their continued community disturbance at the conclusion of each trial, exemplified by high abundances of enrichment-opportunistic bacterial feeders, poses important questions about the nature of the perceived recovery of respiration rates at the end of the study; respiration is typically considered indicative of microbial activity, however substantial bacterial biomass must be present in order to stimulate these types of nematodes. Therefore, we conclude that nematology is an important accompanying discipline to forensic soil study.

In summation, this body of work describes a detailed view of nematology associated with a variety of decomposition environments. This work also tracks decomposition progression simultaneously across the fields of soil chemistry, fungal ecology, and nematology. We report that soil chemistry and fungal beta diversity are inextricably interlinked, as are nematode abundances and thermal effects, and that all three fields mirror seasonal rates of change in decomposition progression. This suite of simultaneous changes is sufficiently compelling for us to recommend that it is absolutely crucial to broaden decomposition soil research into an interdisciplinary study in order to fully and accurately contextualize these processes in future work. Furthermore, based upon these collective data, and in conjunction with materials available

in the literature at this current date, we question whether there is currently adequate and robust data in order to construct accurate or appropriately representative PMI models at this time. It is our recommendation that considerably more data be amassed originating from multiple environments and seasons, prior to the development and construction of PMI models.

Vita

Lois Stacy Taylor graduated with a B.Sc. degree in Physics from Southwest Missouri State University (now Missouri State University), Springfield, MO. She received a M.Sc. degree in Molecular Biophysics and M.M. in orchestral conducting from the University of Tennessee, Knoxville, TN. After working as the Director of Operations for the Knoxville Symphony Orchestra, she was accepted in the PhD program at the University of Tennessee, Knoxville, in the department of Biosystems Engineering and Soil Science, and joined the laboratory of Dr. Jennifer DeBruyn. She received her PhD in 2020.